論文 / 著書情報
Article / Book Information

題目(和文)	
Title(English)	Geotectonic Evolution of England made by Pacific-type orogeny from Neoproterozoic to Cambrian
著者(和文)	岡田吉弘
Author(English)	Yoshihiro Okada
出典(和文)	学位:博士(理学), 学位授与機関:東京工業大学, 報告番号:甲第9393号, 授与年月日:2014年3月26日, 学位の種別:課程博士, 審査員:丸山　茂徳,綱川　秀夫,横山　哲也,上野　雄一郎,小川　康雄
Citation(English)	Degree:Doctor (Science), Conferring organization: Tokyo Institute of Technology, Report number:甲第9393号, Conferred date:2014/3/26, Degree Type:Course doctor, Examiner:,,,,
学位種別(和文)	博士論文
Type(English)	Doctoral Thesis

Geotectonic Evolution of England made by Pacific-type orogeny from Neoproterozoic to Cambrian

Department of Earth and Planetary Sciences, Tokyo Institute of Technology

Yoshihiro Okada

Contents

Chapter 1 General Geology of British Isles and Adjacent areas…..…. .9

Abstract…….. ….. ….. ….. ….. ….. …..….. ……. . ... ….. ….. ….. …..…. 9
1-1. Geological Outline and paleocontinental framework of the British Isles…….. ….. ….. ….. ….. ….. …..….. ……... ….. ….. ….. …. 10
1-2. Geological background of British Isles…….. ..…... ….. ……. ….. …. 15
1-3. Two types of orogeny……. ….... ….. ….. …..……. ….. ….. ….. …..…..23
1-4. This study…….. ….. ...…... ….. ….. ….. ….. ….. ….. ….. ….. ….. ….. ….24
References…….. ….. ….. ….. ….. ….. ….. …..….. ….. ….. ….. ….. …..….26

Chapter 2 Geology of the Lleyn Peninsula; Ediacaran-Cambrian accretionary complex……29

Abstract……..29
2-1 Introduction……30
2-1-1 Areal distribution of the Gwna Supergroup in the Lleyn Peninsula..34
2-1-2 Stratigraphy of Gwna Group and related units……35
2-1-3 Demonstration of accretionary complex (OPS)…….37
2-2 Geology of the Lleyn Peninsula…….….38
2-2-1 Geological outline…….….39
2-2-2 Detailed geological map in key areas along the coast of the Lleyn Peninsula……..…..41
2-2-2-1 Porth Felen Southwest Coast……42
2-2-2-2 Braich y Pwll (Lighthouse and its western cost……...49
2-2-2-3 Mynydd Carreg (Red chert Quarry……...57
2-2-2-4 Porthorion..……..62
2-2-2-5 Porth Oer……...72
2-2-2-6 South Porth Lago……..76
2-2-2-7 North Porth Lago……..80
2-2-2-8 Penrhyn Nefyn peninsula

(BS and Gwna Group to the west)……..…..82
2-3 Lithology, Geochronology and OPS…….82
2-3-1 Method of geochronology……..82
2-3-2 Result…….85
2-3-2-1 U-Pb ages of tuff zircon grains in Lleyn……85
2-3-2-2 Age spectrum of detrital zircon grains from sandstone in Lleyn…….86
2-3-3 Reconstructed geological columns and depositional age……...90
2-3-3-1 Porth Felen…….….90
2-3-3-2 Braich y Pwll (Lighthouse and its western cost)……93
2-3-3-3 Mynydd Carreg (Red chert Quarry): Intermediate between Middle and South……...97
2-3-3-4 Porthorion…….……..98
2-3-3-5 Porth Oer…….……..100
2-3-3-6 Porth Lago……...…….102
2-3-3-7 Penrhyn Nefyn Peninsula…….105
2-4 Discussion…….106
2-4-1 Type of ACs and formed age of the Gwna Group in Lleyn……..106
2-4-2 Demonstration of ACs and the type…….....109
2-4-3 Travel history of accreted oceanic materials……....110
2-4-3-1 Travel history of Type I Gwna ACs…….....112
2-4-3-2 Travel history of Type 2 Gwna Group……..114
2-4-3-3 Travel history of Type 3 Gwna Group……..116
2-4-4 Geotectonic implications in England-Wales; role of Pacific-type orogeny…….……...117
2-5 Conclusion…….118
References……...120
Table…….....124

Chapter 3 Geology of Anglesey Island 129

Abstract……129
3-1. Introduction…….....130
3-2. Geologic outline……...……131

3-2-1 BS-EA regional metamorphic belt……...……133
3-2-2 Gwna Group structurally below the BS-EA unit; Llanddwyn Island as a type locality... ……..……133
3-2-3 Central Shear Zone, renamed as the Central regional metamorphic belt…….....134
3-2-4 Coedana Granite-Gneiss Complex (CGGC) and associated rocks (hornfels) and overlying unit of CGGC with unconformity; the Ordovician to Early Silurian units……..135
3-2-5 New Harbour Group schist belt……...……135
3-2-6 New Harbour Ophiolite belt…….135
3-2-7 South Stack Group ……..……136
3-2-8 Parys Mountain hydrothermal ore at 430Ma……..…….138
3-3 Zircon chronology…….138
3-3-1 Method…….……139
3-3-2 Result……...……140
3-4 Description of each unit t……...……...140
3-4-1 Menai BS-EA facies regional metamorphic belt
(1) Zircon ages of host metagreywackes from BS-EA unit…….…...142
(2) Zoning of mineral distribution……...143
(3) P-T conditions of each metamorphic zone in Menai Blueschist...147
(4) Characteristic occurrence of Menai Blueschist…….149
3-4-2 Gwna Group observed on the Llanddwyn Island……..…..150
3-4-3 Gwna Group observed on central Anglesey……..…...156
3-4-4 Central Shear Zone (renamed as the Central regional metamorphic belt)……..157
(1) Protoliths of CSZ……...157
(2) Progressive metamorphism of CSZ in the Cambrian age...……...159
(3) Regional isograds of the Central Shear Zone……160
(4) Metamorphic reactions……..……162
(5) Internal P-T structure……...…..162
3-4-5 New Harbour Schist belt…….……...……..……163
3-4-6 New Harbour Ophiolite belt……..……...165
3-4-7 Church Bay Tuff (465Ma): 436Ma acidic tuff Unit (Skerrie island equivalents)…….167
3-4-8 South Stack group……167
3-4-9 Klippe associated with post-Devonian overthrust……...169

3-4-10 Mid-Paleozoic graven sediments……...172
3-5Discussion……173
3-5-1 Geochronological relation of the Gwna, New Harbour and South Stack Group……...173
3-5-2 Provenance area for ACs during the Neoproterozoic to Paleozoic..175
3-5-3 New Harbour Schist Belt……176
3-5-4 Three regional metamorphic belts in the Anglesey Island……...177
3-5-5 A summary of geochronology for the Wales-Anglesey Island…….178
3-5-6 Structural relationship between all units in Anglesey Island……...180
3-6 Conclusion……...182
References……..……...183
Table……..186

Chapter 4 Geotectonic Evolution of England-Wales made by Pacific-type orogeny from Neoproterozoic to Cambrian……..190

Abstract……190
4-1 Introduction……...191
4-2 Recognition of pacific-type orogeny in Anglesey island to LlyenPeninsula, England –Wales…….....193
4-3 Pacific-type Orogeny through time……...196
4-3-1 Pacific-type orogeny in British Islands. ……..196
4-3-2 Crustal growth of British Islands by Pacific-type orogeny…..198
4-3-3 Comparison to Japanese Islands...……...…198
4-4 Discussion……199
4-4-1Paleogeographic Reconstruction……...199
4-4-2 When Iapetus Ocean was born?.....204
4-4-3 Birth of Rheic Ocean……...205
4-5 Summary Whole scenario: Geotectonic evolution of England-Wales…..205
(1) Stage I: Initiation of pacific-type orogeny...……....206
(2) Stage II (630Ma): Formation of the oldest ACs……..…206
(3) Stage III (600-570Ma): Accretion of type 2 Gwna Group……...207
(3)Stage IV (560Ma): Exhumation of BS-EA unit (Pacific-type orogeny 1)…….…...207

(3) Stage VI (540Ma): Formation of Gwna Type 3 ACs……...208
(4) Stage IV (Pacific-type Orogeny 2, 530Ma): Exhumation of regional metamorphic belt CSZ……...210
(5)Stage VII (Pacific-type Orogeny 3, 520-510Ma): Exhumation of regional metamorphic belt, NHS……..…211
(6) Stage VIII (Collision-type Orogeny at 520-490Ma): South Stack Group……..…….....212
(7) Stage IX (Overthrusting and large-scale gravity slides): Formation of olistostrome in Ordovician time……..…213
(8) Stage X (Parys Mountain and Church Bay acidic volcanism)……..…….……213
References…...……215

Chapter 5 Discovery of deep-sea sediments formed during the Marinoan Superanoxia…….219

Abstract……219
5-1 Introduction……...220
5-2 Geological Outline……222
5-3 Ocean plate stratigraphy in Porth Felen southwest coast……..……255
5-4 Zircon……231
5-5 Discussion……232
5-1 Marinoan Snowball Earth and "Superanoxia"…….233
5-2 Significance of deep-sea sediments…….235
References……...239

Chapter 6 New chronological constraints for Cryogenian to Cambrian rocks in the Three Gorges, Weng'an and Chengjiang areas, South China…….240

Abstract……240
6-1. Introduction……..242
6-2 Geology…….247
6-2-1 Three Gorges area……247

6-2-2 Weng'an area……..……..250
6-2-3 Chengjiang area (Maotianshan)…….251
6-2-4 Pre Cryogenian Rocks in the Yangtze craton…….252
6-3 Method…….254
6-3-1 Sample preparation and cathodoluminescence images of zircons……..254
6-3-2 Analytical methods with LA-ICP-MS and Nano-SIMS instruments……255
6-4 Results……..257
6-4-1 Zircon U-Pb ages from the Cambrian tuff beds……..257
6-4-2 Age spectrum of detrital zircon grains from the Cryogenian to Ediacaran sandstones……...…260
6-5 Discussion……268
6-5-1 Chronological constraints from tuff beds……268
6-5-2 Comparison of carbon isotope excursions……..271
6-5-3 Provenance of sediments in the Nanhua and Kangdian rift basins……272
6-6 Conclusions…….275
References……..286

Acknowledgements…….287

Chapter 1 General Geology of British Isles and Adjacent areas

Abstract

Geology of England is briefly reviewed. The British Isles and adjacent regions are composed of four units, (1) Late Archean to Early Proterozoic basement rocks with Neoproterozoic cover sequence, (2) metamorphosed cover sequence deposited on the Laurentian passive continental margin from Neoproterozoic to Cambrian sequence called Barrovian Metamorphism, intruded by Siluro-Devonian TTG plutons, (3) Accretionary complex from Ordovician to Silurian, CA volcanic sequence of Lake District, and Anglesey Island to England which was formed by a series of Pacific-type orogens. (4) On the western end of England Lizard ultramafic ophiolitic unit is exposed to mark the Variscan suture of Rheic Ocean which corresponds to the collisional site of Gondwana against Laurentia.

Since Dewey (1969), most British geologists have long considered that two orogenies by continental collision made major structure of British Isles, although minor modifications were performed. It was Leggett et al. (1979) who insisted the Pacific-type accretionary complex was formed along the southern margin of Scotland during the Silurian age, and more recently Sawaki et al. (2010).

On the other hand, England-Wales have not been fully investigated because of thick cover sequence of normal deposits ranging from Cambrian to Tertiary age. We, Japanese Group, have long worked in this region to demonstrate the ubiquitous occurrence of ACs and contemporaneous TTG formation at continental side, originally

along the margin of W. Africa and separated since Cambrian time as same as Japanese islands of post-Japan Sea.

Keywords: Pacific-type orogeny, Iapetus, Avalonia, W Africa, Accretionary complex

1-1 Geological Outline and paleocontinental framework of the British Isles

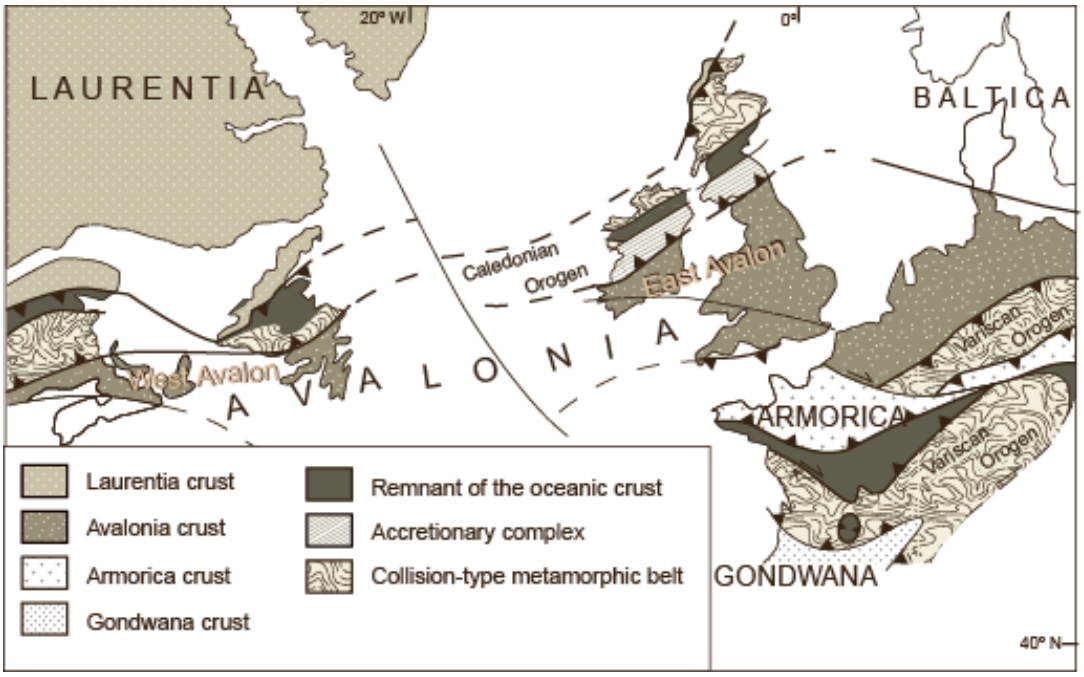

Fig.1-1 Simplified geologic map of Western Europe and eastern Canada.
Possible basement configuration of Western Europe and Eastern Canada, showing the main structures of the Laurentia, Avalonia and Armorica continental plates and Collision-type metamorphic belts of Caledonian and Variscan orogens. (e.g. Matte, 1991, 2001)

The simplified geologic map of Western Europe and eastern Canada is shown in Fig. 1-1. And, Fig. 1-2 shows the main tectonic units and geologic cross section of the

British Islands and Ireland. The geology of British Isles are mainly composed of Caledonian orogen and Avalonia micro-continent. The Scottish Caledonide mainly consists of the Collision-type metamorphic belt, Cambro-Ordovician oceanic crust and Southern Upland accretionary complex (Fig. 1-2). The micro-continent Avalonia occupies about 60% of British Isles, and mostly covered by Phanerozoic stratigraphic sediments (Fig 1-3). On the southern side of Avalonia the other collision type metamorphic belt which was created by the Variscan orogeny are extending in the Western Europe (Fig1-2). The Variscan orogen is formed by the closure of Rheic ocean and Galicia-Southern Brittany Ocean (eg. Matte, 1991, 2001). On the other hand, the closure of Iapetus Ocean led to the Caledonian Orogen. Avalonia is composed of the west Avalon and east Avalon (Fig. 1-1). The west Avalon of North America is named after its type locality on the Avalon Peninsula of eastern Newfoundland, it also includes a coastal strip in eastern New Brunswick and Novascotia and Boston Basin. Paleo-magnetic results have been summarized by Van de Voo (1993). The east Avalon includes the southern part of England, Wales, and Ireland. Paleo-magnetic data from east Avalon have been reviewed by Trench and Torsvic (1991), Van de Voo (1993), and Torsvik et al. (1993). The paleo-latitude determined from the east and west Avalon terrains during the Paleozoic are compared with those expected if there terrains were part of Laurentia or Gondwana (McElhinly and McFaddem, 1999). Fig 1-4 shows the map of 480-420Ma reconstructions on the basis of faunal and paleo-magnetic data (Cocks and Torsvic, 2002) for the West and East Avalon terrains. The observed paleo-latitudes show the agreement with those predicted from Gondwana in early Cambrian time throughout the Ordovician, the Rheic Ocean widened at the expense of Iapetus as Avalonia drifted northward toward Baltica and Laurentia (Fig. 1-4). The

endemic fauna of Avalonia were progressively replaced by those of Baltica and Laurentia affinities in the Llandeilo-Ashgill (Fortey and Cocks, 2003), suggesting increasingly proximity to those continents and widening gap with Gondwana by the mid Ordovician (ca. 465Ma) (Nance and Linnemann (2008)). Similarly, paleo-magnetic data indicates that by 460Ma Avalonia lay at 41°S (Hamilton and Myrphy, 2004), some 1700-2000km south of Laurentia (at about 20°S; McMiocaill and Somethrust (1994)) and about 2100km north of Gondwana (at about 60°S; Cocks and Torsvic,2002). This requires Avalonia to have drifted northward at the relatively rapid rate of 8-10cm per year (Nance and Linnemann, 2008).

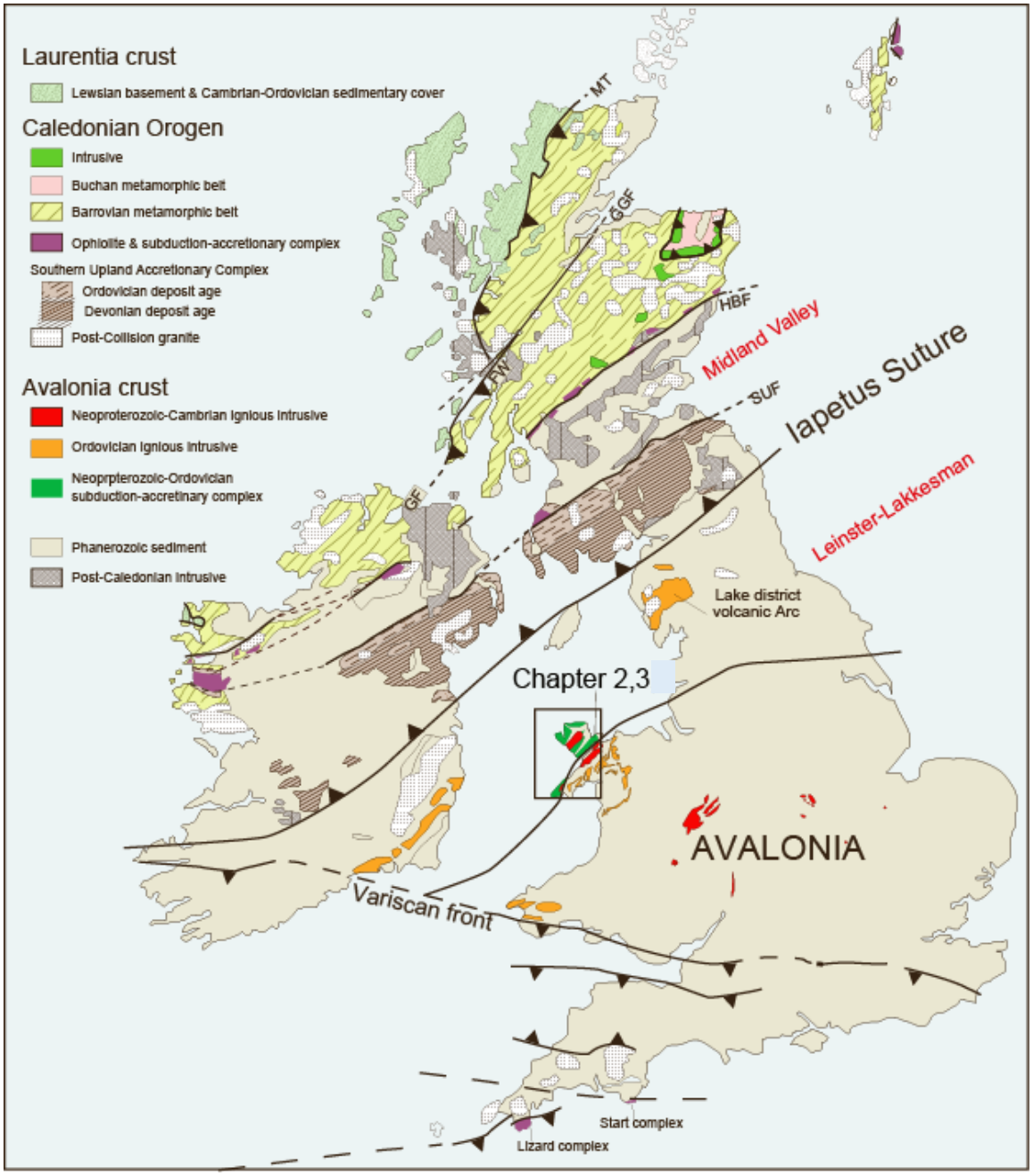

Fig. 1-2 Simplified geological map of British Isles and Ireland. (British geological survey 1980)

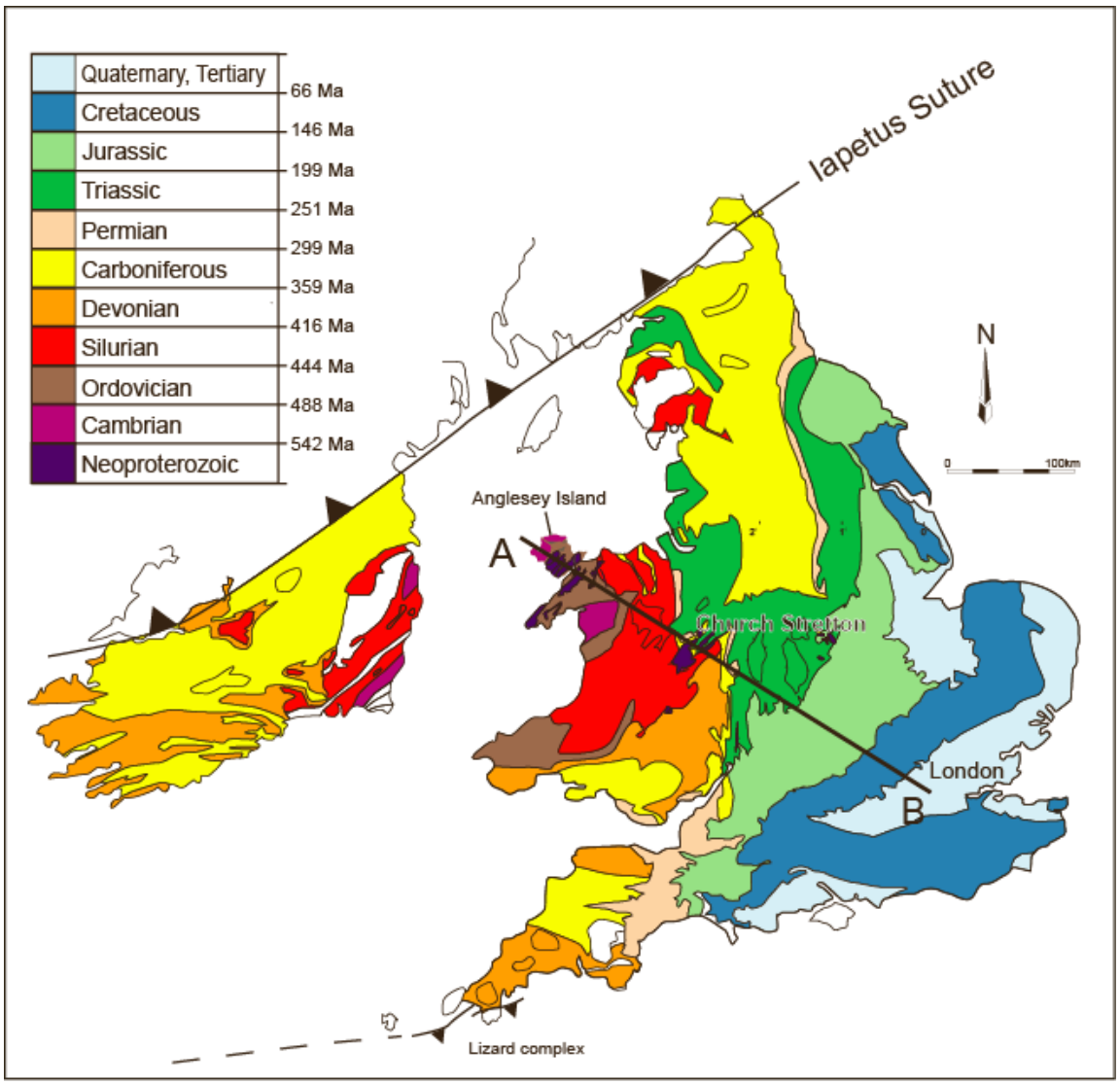

Fig. 1-3 Geological map of England and adjacent regions after British Geological Survey map.

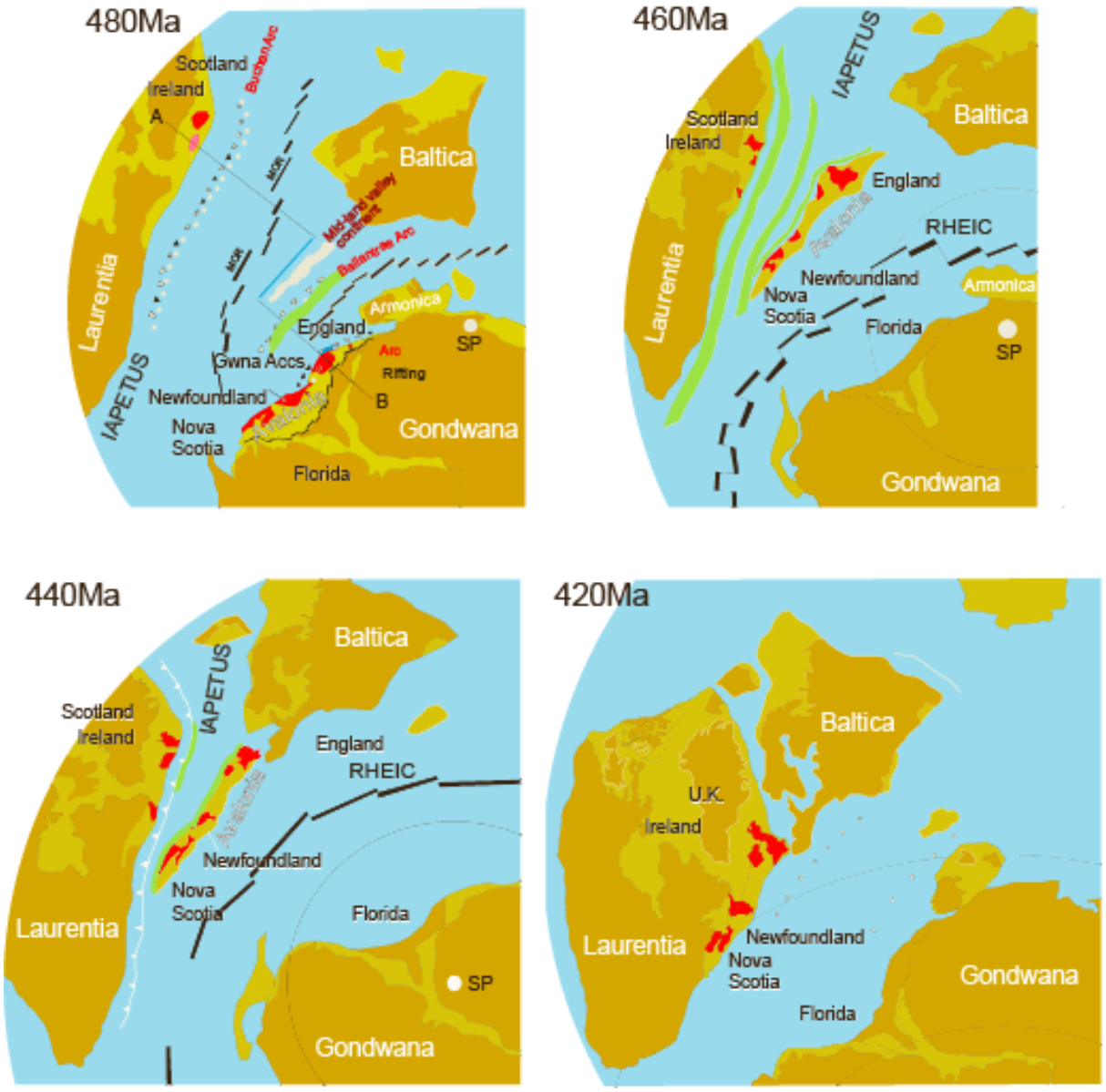

Fig. 1-4 Paleogeographic maps of 480-420 Ma after Cocks and Torsvik (2002)

1-2 Geological background of British Isles

Academically, geology started from British Isles, and it provided innovating idea to assess the geological phenomena during last 2 centuries. According to the Woodcock and Strachan (2002), James Hutten was persuaded, by uniformities that mark both the longevity and cyclicity of geological events seen in Britains major tectonic

phases. His *Theory of the Earth (1795)* and its development by John Playfair and Charles Lyell marked the beginning of the modern historical geology. The foundation of the world's first Geological Society in London (1807) provided a forum in which Britain's geological history was rapidly pieced together. William Smith soon published his geological map of England and Wales (1815) based on the principles of correlating strata and fossils, that have become modern stratigraphy. The geological survey of Great Britain was formed (1835) to produce a more detailed geological map of the country, and a few years later came Richard Griffiths, geological map of Ireland at about the same time begun the collaboration and later confrontation, between Rodelick Marchson and Adam Sedgwick, which resulted in the establishment of Cambrian (1835), Silurian (1835) and Devonian (1839) Systems and through Charles Laowarth's eventual mediation (1879), the Ordovician system.

As described above, Phanerozoic sedimentary rocks in southern British Isles provided fundamental ideas of geology; in contrast, the basement complex (Avalonia basement) has not been evaluated enough because of extremely lesser outcrop than those Phanerozoic sedimentary cover. In the west Wales, Precambrian blueschist belt, which are the basement rock of Avalonia, are exposed along the NW-SE high-angle faults on Anglesey Island. First description of this schist belt was done by Henslow (1822) who mapped this belt. After that, Blake (1888) discovered glaucophane in this schist and Greenly (1919) mapped and documented the geology of Anglesey in more detail. After long period of inactivity, Wood (1974) put the blueschists into the framework of a Pacific-type orogen containing mélanges and ophiolitic relics, and made a comparative study of rocks in California. Gibbons (1983) suggested that the evidence in Anglesey for subduction of the time including the blueschists was weak, and Gibbons

(1989) interpreted the tectonic belts in Anglesey in terms of suspect terrains. At about the same time, Dallmeyer and Gibbons (1987) reported an $^{40}Ar/^{39}Ar$ mineral age on glaucophane of 560-550Ma for the blueschists which they interpreted as the metamorphic recrystallization age. However, in spite of all these studies, the Anglesey blueschists have never been interpreted in the light of modern understanding of comparative blueschists belts in Pacific-type orogens such as Japan and California. Therefore, their role in the geotectonic development of Avalonia basement has never been fully appreciated. There are two other localities of blueschists in British Isles at Ballantrae Ophiolite (Balsillie, 1937), southern Scotland, and at Clew Bay Ophiolite (Chew et al., 2003). However, in the British Isles the significance of those blueschists is also scarcely evaluated.

Study of geology of Scotland also played a key role to develop the fundamental ideas of metamorphic petrology. George Barrow (1893) showed the metamorphic zones in Scottish Highland for the first time. After this work of Barrow, progressive metamorphism was named as Barrovian metamorphism. 25 years later, Harker (1918, 1932) tried to explain the meaning of the Barrovian metamorphism for the first time. In his concept of metamorphism, independent parameters which controlled the metamorphic assemblages are metamorphic temperature (or pressure), sheering stress, and metamorphic pressure and temperature have functional dependency. However this concept was denied by later experimental studies (e.g. Miyashiro (1951, 1953). Instead, Escola (1920, 1939) proposed another concept of metamorphism in which the independent parameters are temperature and pressure. He provided the concept of metamorphic facies now widely accepted as nature of metamorphism. After that, Miyashiro (1961) proposed the concept of three types of metamorphic facies series

(high P/T, medium P/T and low P/T types). The metamorphic belt in Scottish Highland was treated as type locality of medium P/T metamorphic facies series. In addition, J. F. Dewy (1969) explained geology of Scotland using plate tectonics for the first time and Leggett et al. (1979, 1982) introduced the idea of accretionary prism to the Europe by assessing in the Southern Uplands accretionary complex in the south Scotland.

Fig 1-5 shows the model of geotectonic evolution of the Scottish Caledonian Orogen after Oliver (2001). In this model, the oceanic crust of Highland Border ophiolite is firstly emplaced at the Laurentia continental margin by obduction, and then the continent marginal sediments were metamorphosed by the compression and arc magma heating. Subsequent collision occurred between Cambrian-Ordovician arc complex and Avalonia micro-continent (Fig 1-5, F-G). Hence, they did not think that the collision type metamorphic belt is formed along the plate boundary such as suture zone. This tectonic model has quite inconsistent with the tectonic model of Irish Caledonian orogeny (Fig 1-6; Clift et al, 2004). Insist that the collision of oceanic Lough Nafooey Island arc with the passive margin of Laurentia in western Ireland resulted in the deformation, magmatism and metamorphism of Irish Caledonian Orogeny. The metamorphosed Laurentia marginal sediments (Dalradian Supergroup) now exposed in Connemara and North Mayo, were exhumed to the surface along the subduction zone. They proposed that this exhumation occurred mainly as a result of an ocean ward collapse of the colliding arc southward, probably aided by subduction rollback, into the new trench formed after subduction polarity reversal following collision. As mentioned above, there are two different evolutional models of metamorphic belt of Scottish and Irish Caledonian orogeny. In those models, main orogeny should appear at geotectonic structure of metamorphic belt; although their orogenic structure has never been fully

evaluated.

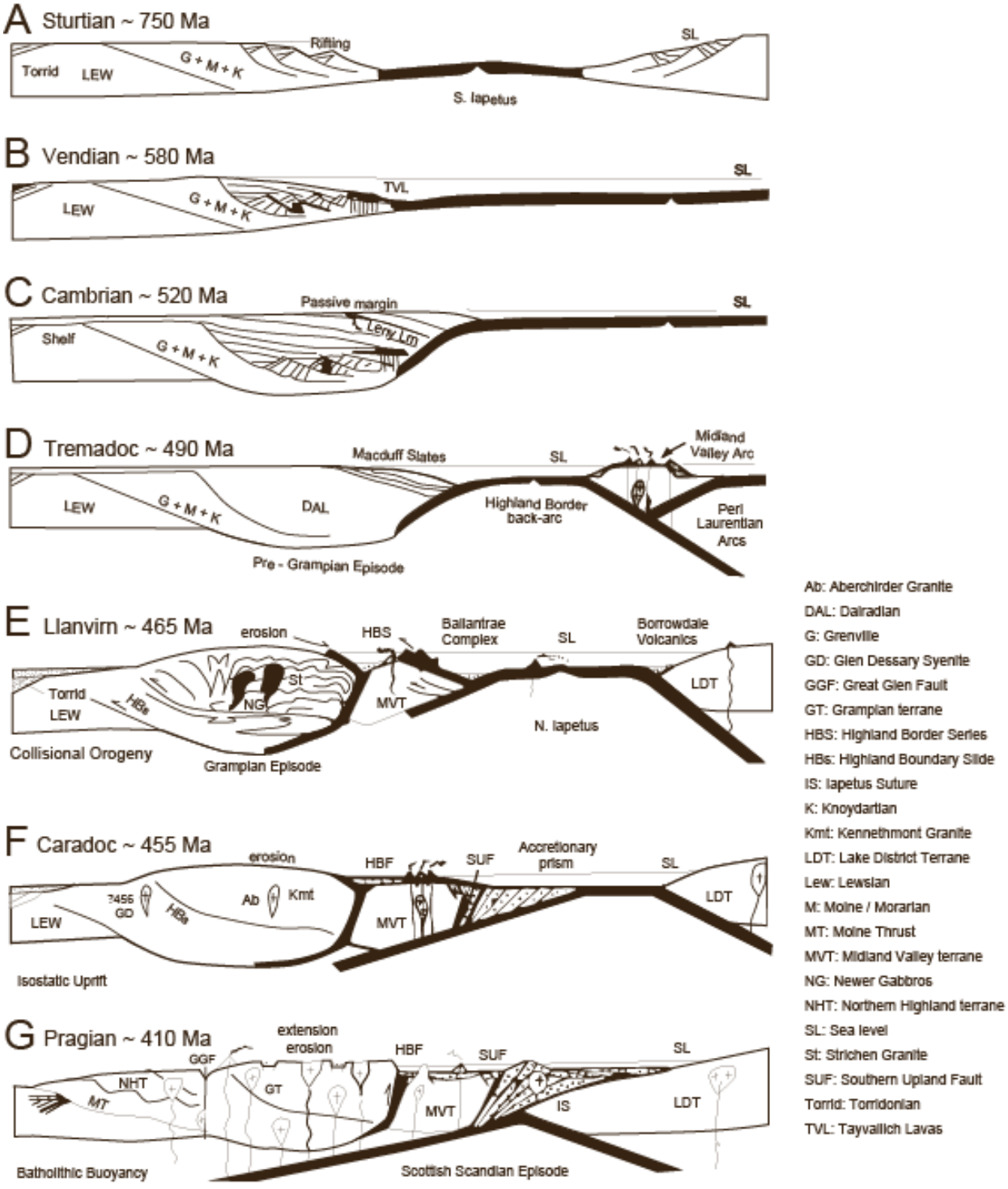

Fig. 1-5 Schematic sections illustrating evolution of the Scottish Caledonian orogen after Oliver

(2001).

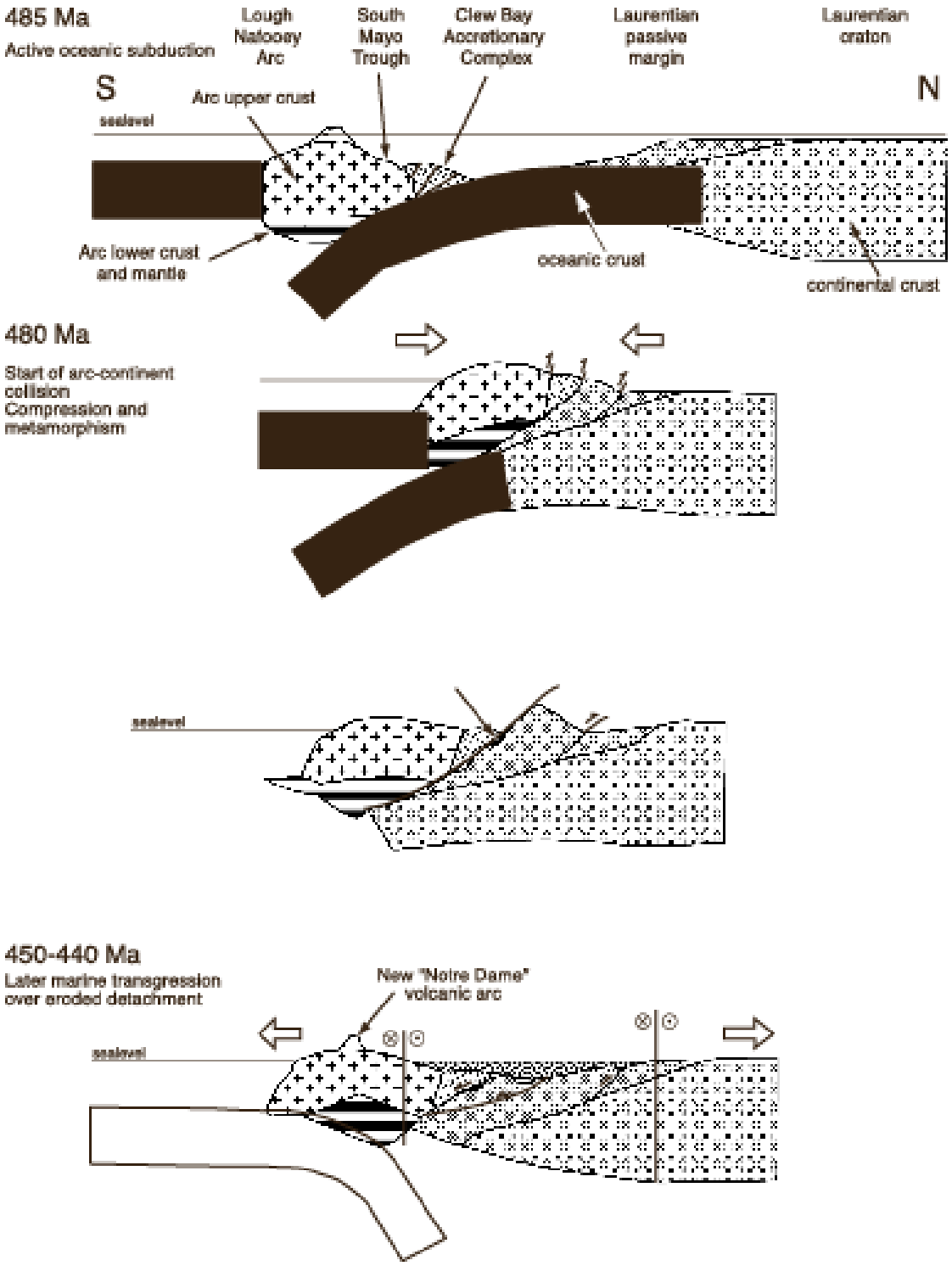

Fig. 1-6 Schematic sections illustrating evolution of the Irish Caledonian orogen after Clift et al., 2004.

Therefore till latter half of the 20th century, geology of British Isles had been providing a referential region for global geological history; however now we need to attempt reviewing regional geological history with most updated understanding of orogeny.

1-3 Two types of orogeny

Orogeny is the term which means a geological phenomenon occurring at the convergent plate margins including magmatism, metamorphism and major reconstruction of geological structures. In terms of plate tectonic paradigm, the Phanerozoic history of the Earth is regarded as a repetition of active orogenic period and less active inter-orogenic period. One of the most remarkable findings of the early plate tectonic studies in 1970-1980s, is to figure out the two different type of orogeny throughout the Earth's history; Collision-type and Pacific-type. The former is formed by the collision of two continents. The type localities of this type of orogen are Alps, Himalaya and Scotland (e.g. Dewy, 1969; Dewy and Bird, 1970; Kaneko, 1997) (Fig. 1-7A). The latter, which is also termed as accretionary-type of Cordilleran-type orogeny, occurs at the convergent plate margins under which an oceanic plate subducted (e.g. Dewy and Bird, 1970; Isozaki, 1996; Maruyama, 1997). The type localities of this type of orogen are circum-Pacific regions as its name represents. Representative structures of these two types of orogens are shown in Fig. 1.7. SW-Japan are chose as type localities of Pacific-type (Fig. 1-7B) orogens. Table 1-1 summarizes the comparison of their orogenic features such as 1) dimension, 2) protolith, 3) metamorphic facies series, 4) presence or absence of granitic batholith, and 5) type of orogenic belt type after

Maruyama et al., (1996). The most important similarity is their large-scale structure. Both types of orogens have subhorizontal structure which is asymmetry with oceanward vergency. The most remarkable difference is the dimension. The total width of Pacific-type orogen is a few km to tens of kilometer, whereas the Collision-type is ten times as large as that. In terms of component of the orogen, the largest difference is the presence of huge batholith belts as wide as 300km in the pacific-type orogens. These batholith belts are composed of granitoids characteristically of tonalite-trogjemite-granodiolite (TTG) compositions. The Collision-type is associated only with a small amount of granitic intrusions which often refers as leucogranite. Hence the pacific-type orogeny contributes to the continental growth, whereas the collision type only reconstructs the distribution of continent, and makes no contribution to their growth. Both the collision- and pacific- orogens have regional metamorphic belt in their core parts called as orogenic routes. Although its dimension is very different by the orogen type, regional metamorphic belt occurs as a flat-lying thin sheet in both types of orogens. The formation and the exhumation of the regional metamorphic belt is the most essential event in orogenic processes. Therefore, to clarify the geotectonic structure of metamorphic belt is of first importance to understand the orogeny.

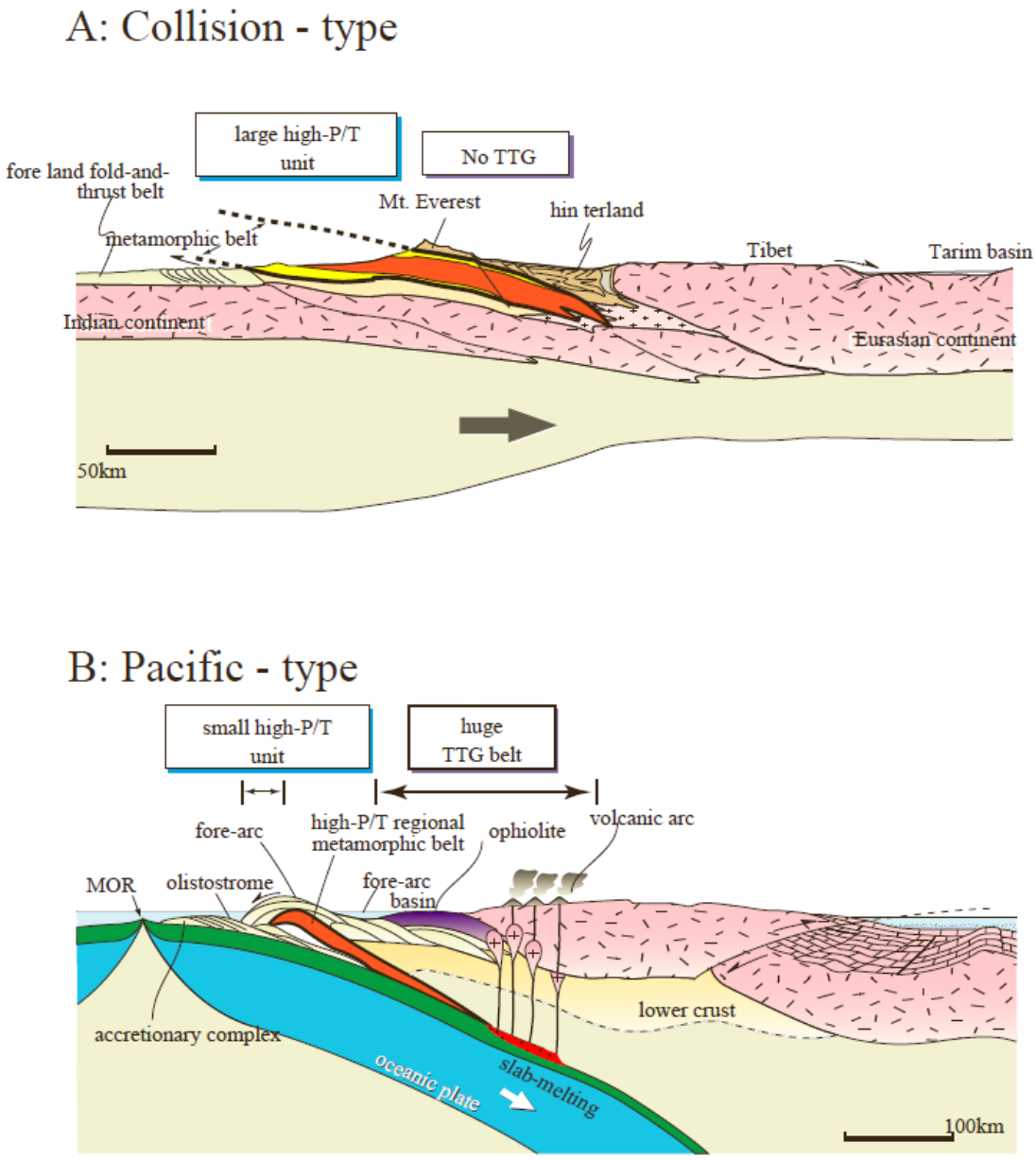

Fig.1-7 Large-scale structure of two types of orogen. A: Collision-type orogen. Type locality of this type of orogen is Himalaya. B: Pacific-type orogen. Type locality of this type of orogen is SW-Japan. MOR: mid-ocean ridge.

	Collision - type	**Pacific-type**
Dimention	Width: a few 10 km	Width: a few km
	Length: a few 1000 km	Length: a few 100 km
	Thickness: a few km	Thickness: a few 100 m
Protolith	Platform sediments, granite, bimodal volcanics (basalt and dasite)	Deep sea sediments (chert, mudstone), trench turbidite, MORB-type
Metamorphic facies series	medium-*P* type	high-*P* type
Granitic batholith	rare or absent	Huge
Orogenic peridotite	Grt, Sp-peridotite	Sp, Pl-peridotite

Table 1-1 Comparison of the specifications of Collision-type and Pacific-type orogens after Maruyama et al. (1996).

1-4 This study

The aim of this thesis is to demonstrate the geotectonic development of England-Wales and summarize research results given through my doctoral course since 2011. This thesis has 2 parts consisting of 6 chapters.

Part 1 is demonstration of the geotectonic development of England-Wales which starts from the general introduction of this Thesis in Chapter 1, and followed by descriptive work of regional geology of the Lleyn Peninsula (Chapter 2) and the Anglesey Island (Chapter 3). Key works are the reconstruction of Ocean Plate Stratigraphy (OPS) based on the detailed field mapping along the coast of the Lleyn Peninsula and the Anglesey Island. Another key point is the zircon chronology separated from inter-layering tuff layers and sandstones cap rocks of trench-turbidite. At the last of the Part 1, Chapter 4 demonstrates the geotectonic history of England-Wales based on detailed systematic investigation given in Chapter 2 and 3 with application of new

methodology of accretionary complex geology and zircon chronology. Fig.1-8 guides the study areas of each chapter.

Part 2 is study results derived through application of zircon chronology, which contains 2 chapters. Chapter 5 discusses Snowball Earth state looking at the abundances of platinum group elements in deep-sea sediments, and the cause of Snowball Earth. And Chapter 6 describes to unfold the surface environment around the Cambrian explosion based on zircon chronological analysis, using samples from the Three Gourges in Weng'an and Chengjian areas in South China. Geographical area is totally different from England-Wales of British Isles as titled as this thesis, however, I include this chapter as remarkable result based on zircon chronology through my research in the doctoral course.

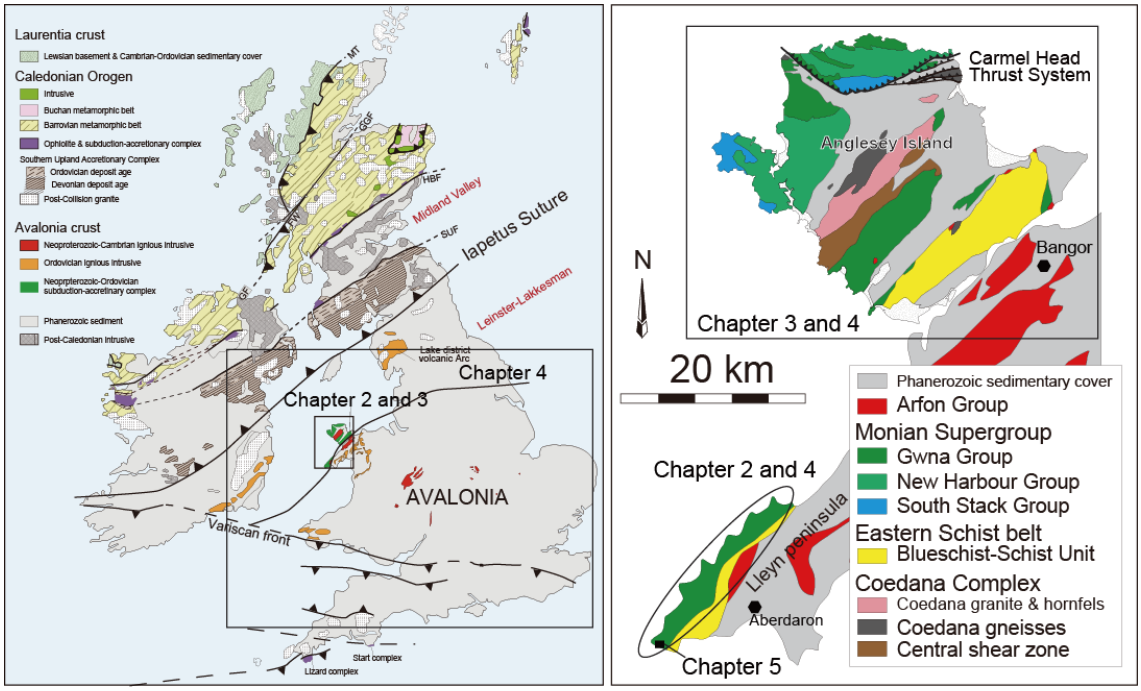

Fig. 1-8 This study areas of each chapter.

References

Balsillie, D. 1937. Further observations on the Ballantrae igneous complex, South Ayrshire. Geological Magazine, 74, 20-33.

Barrow, G. 1893. On an intrusion of muscovite-biotite gneiss in the southeastern Highlands of Scotland, and its accompanying metamorphism. Quarterly Journal of the Geological Society London, 49, 330-358.

Blake, J.F. 1888. The occurrence of glaucophane-bearing rocks in Anglesey. Geological Magazine, 5, 125-127.

Chew, D.M., Daly, J.S., Page, L.M., Kennedy, M.J. 2003. Grampian orogenesis and the development of blueschist-facies metamorphism in western Ireland. Journal of the Geological Society, London, 160, 911-924.

Clift, P.D., Dewey, J.F., Draut, A.E., Chew, D.M., Mange, M., Ryan, P.D. 2004. Rapid tectonic exhumation, detachment faulting and orogenic collapse in the Caledonides of western Ireland. Tectonophysics, 384, 91-113.

Cocks, L.R.M., Torsvik, T.H., 2002. Earth geography from 500 to 400 million years ago: a faunal and palaeomagnetic review. Journal of Geological Society, London, 159, 631-644.

Collins, A.S., Buchan, C. 2004. Provenance and age constraints of the South Stack Group, Anglesey, UK: U-Pb SIMS detrital zircon data. Journal of the Geological Society, London, 161, 743-746.

Dallmeyer, R.D., Gibbons, W. 1987. The age of blueschist metamorphism on Anglesey, North Wales: evidence from 40Ar/39Ar mineral dates of the Penmynydd schists. Journal of the Geological Society, London, 144, 843-850.

Dewey, J.F. 1969. Evolution of the Appalachian/Caledonian Orogen. Nature, 222, 124-129.

Dewey, J. F., Bird, J. M. 1970. Mountain belts and the new global tectonics. Journal of Geophysical Research, 75, 2625-2647.

Eskola, P. 1920. The mineral facies of rocks. Norsk Geologisk Tidsskr, 6, 143-194.

Eskola, P. 1939. Die metamorphen Gesteine. In: Barth, T.F.W, Correns, C.W., Eskola, P. (Eds.) Die Entstehung der Gesteine, 263-407. Julius Springer, Berlin. (Reprinted in 1960 and 1970)

Fortey, R.A., Cocks, L.R.M., 2003. Palaeontological evidence bearing on global Ordovician-Silurian continental reconstructions: Earth-Science Reviews, 61, 245-307.

Barrow, G. (1893). On an intrusion of muscovite-biotite gneiss in the south-eastern Highlands of Scotland, and its accompanying metamorphism. Quarterly Journal of the Geological Society, 49(1-4), 330-358.

Gibbons, W. 1983. The Monian 'Penmynydd Zone of Metamorphism' in Llŷn, North Wales. Geological Journal, 18, 21-41.

Gibbons, W. 1989. Suspect terrane definition in Anglesey, North Wales. Geological Society of America, Special Papers, 230, 59-65.

Greenly, E. 1919. The Geology of Anglesey, Memoir Geological Survey of Great Britain, (2 vols.), HMSO, London, 980 pp.

Hamilton, M.A., Murphy, J.B., 2004. Tectonic significance of a Llanvirn age for the Dunn Point volcanic rocks, Avalon terrane, Nova Scotia, Canada: Imprecations for the evolution of the Iapetus and Rheic Oceans. Tectonophysics, 379, 199-209.

Harker, A. 1918. The present position and outlook of the study of metamorphism in rock masses. Quarterly Journal Geological Society of London, 74, 1i-1xxx.

Harker, A. 1932. Metamorphism. A study of the transformations of rock-masses. Methuen, London.

Henslow, J.S. 1822. Geological description of Anglesea, Transactions of the Cambridge Philiosophical Society, 1, 359-452.

Hutton, J. 1795. Theory of the Earth.

Isozaki,Y., 1996. Anatomy and genesis of a subduction-related orogen: a new view of geotectonic subdivision and evolution of the Japanese Islands. Isl. Arc 5, 289–325.

Kaneko, Y. 1997. Two-step exhumation model of the Himalayan metamorphic belt, Central Nepal. Journal of the Geological Society of Japan, 103, 203-226.

Leggett, J. K., McKerrow, W.S., Casey, D. M. 1982. The anatomy of a Lower Palaeozoic accretionary forearc: The Southern Uplands of Scotland. In: Leggett, J.K. (Eds.) Trench-Forearc Geology. Geological Society, London, Special Publications, 10, 494-520.

Leggett, J.K., McKerrow, W.S., Eales, M.H. 1979. The Southern Uplands of Scotland: a Lower Palaeozoic accretionary prism. Journal of the Geological Society, London, 136, 755-770.

Matte, P. 1991. Accretionary history and crustal evolution of the Variscan Belt in western Europe. Tectonophysics, 196, 309-339.

Matte, P. 2001. The Variscan collage and orogeny (480-290 Ma) and the tectonic definition of the Armorica microplate: a review. Terra Nova, 13, 122-128.

Mac Niocaill, C., Smethrust, M.A. 1994. Palaeozoic palaeogeography of Laurentia and its margins: a reassessment of palaeomagnetic data. Geophysical Journal International, 116, 715-725.

Maruyama, S., 1997. Whole-Earth dynamics (in Japanese). Iwanami-shoten, Tokyo.

Maruyama, S., Liou, J.G., Terabayashi, M., 1996. Blueschists and Eclogites of the World and their Exhumation. International Geology Review 38, 485-594.

McElhinny, M.W., McFadden, P.L. 1999. Paleomagnetism: continents and oceans. In: Dmowska, R., Holton, J.R., Rossby, H.T. (Eds.). International Geophysics Series, 73.

Miyashiro, A. 1951.Kyanites in druses in Kyanite-quartz veins from Saiho-ri in the Fukushinzan district, Korea. Journal of Geological Society of Japan, 57, 59-63.

Miyashiro, A. 1953. Calcium-poor garnet in relation to metamorphism. Geochimica et Cosmochimica Acta, 4, 179-208.

Miyashiro, A. 1961. Evolution of metamorphic belts. Journal of Petrology, 2, 277-311.

Nance, R. D., Linnemann, U., 2008. The Rheic Ocean: Origin, Evolution, and Significance. GSA today. 18, 4-12.

Oliver, G.J.H. 2001. Reconstruction of the Grampian episode in Scotland: its place in the Caledonian orogeny. Tectonophysics, 332, 23-49.

Sawaki, Y., Shibuya, T., Kawai, T., Komiya, T., Omori, S., Iizuka, T., Hirata, T., Windley, B.F., Maruyama, S., 2010. Imbricated ocean-plate stratigraphy and U-Pb zircon ages from tuff beds in cherts in the Ballantrae complex, SW Scotland. Geological Society of America Bulletin 122, 454-464.

Soper, N.J., England, R.W., Snyder, D.B., Ryan, P.D. 1992. The Iapetus suture zone in England, Scotland and eastern Ireland: a reconciliation of geological and deep seismic data. Journal of the Geological Society, London, 149, 697-700.

Torsvik, T.H., Trench, A.T., Svensson, I., Walderhaugh, H.J. 1993. Palaeogeographic significance of mid-Silurian palaeomagnetic results from southern Britain-major revision of the apparent polar wander path for eastern Avalonia. Geophysical Journal International, 113, 651-668.

Trench, A., Torsvik, T.H. 1991. A revised Palaeozoic apparent polar wander path for Southern Britain (Eastern Avalonia). Geophysical Journal Society, London, 148, 949-957.

Van der Voo, R. 1993. Paleomagnetism of the Atlantic, Tethys and Iapetus Oceans. Cambridge University Press, Cambridge.

Van Staal, C., R., Dewey, J., F., Mac Niocaill, C., McKerrow, W., S., 1998. The Cambrian-Silurian tectonic evolution of the northern Appalachians and British Caledonides: history of a complex, west and southwest Pacific-type segment of Iapetus. Geological Society, London, Special Publications, 143, 197-242.

Wood, D.S. 1974. Ophiolites, mélanges, blueschists, and ignimbrites: early Caledonian
21 subduction in Wales? In: Dott, R.H. and Shaver, R.H. (Eds.) Modern and Ancient Geosynclinal Sedimentation. Society of Economic Paleontologists and Mineralogists, Special Publication, 19, 334-344.

Woodcock, N., Strachan, R. 2002. Regional geological history: why and how. In Woodcock, N., Strachan, R. (Eds.) Geological History of Britain and Ireland. 3-18.

Chapter 2 Geology of the Lleyn Peninsula; Ediacaran-Cambrian accretionary complex

Abstract

The chaotic unit called the Gwna Group has been investigated in detail along the coastline of the Lleyn Peninsula. Oceanic plate stratigraphy (MORB, chert, claystone, carbonate and turbidite) is observed and two-type structures in these areas were found in this study. These are the typical accretionary complex (AC), tectonically mixed with oceanic materials of MORB, OIB, bedded chert and/or red claystone, with trench turbidite. Some of them are derived from two-step mixing. The one (duplex-type) is tectonic mixing at shallow depth by underplating of duplex-type ACs, and the other (olistostrome-type) is recycled ACs which had once underplated and been pushed up tectonically upward, then gravitationally collapsed. The collapsed ACs were redeposited at trench to be incorporated again into accretionary wedge. This type of ACs is apparently remarkably different in appearance (olistostrome), but the entity is two-fold mixing at trench. In these two-types of ACs, the critical characteristics are, common occurrence of layer-parallel faults, mixed lithology of oceanic materials with continental arkosic sandstone/mudstone, variation of ages of their formation with a systematic order called Ocean Plate Stratigraphy (OPS).

OPS for each individual ACs has been established by zircon chronology, and classified them into three-types, Type 1 is 630-600 Ma ACs (Early Ediacaran), Type 2 600-560Ma (Early Ediacaran) and the Type 3 is 570-540Ma (Middle Ediacaran). Braich y Pwll area with the structure of olistostrome-type shows Type 3. On the other hand,

another areas with Duplex-type have Type 1 or Type 2 by zircon chronology. Therefore, it indicates that the olistostrome of olistostrome-type was caused after duplex structure of duplex-type.

In addition, a reasonable interpretation to the Gwna group in Lleyn Peninsula with 637Ma to 541Ma is obtained and shown in a three travel history diagrams. Type1) Gwna Group 1 deposited from continental margin to mid-ocean ridge in ca. 630 Ma and appended to West Africa continent in ca. 610 Ma. Type2) Gwna Group 2 deposited from continental margin to mid-ocean ridge in ca. 610 Ma and appended to West Africa continent in ca. 570 Ma. Type 3) Gwna Group 3 deposited at deep-sea sediment in ca. 590-540 Ma and appended to the continent after formed blue schist (ca. 560 Ma).

The large-scale structure of these three ACs and tectonically interlayered ca.560Ma BS belt clearly indicates the (1) nearly subhorizontal thrusts with downward younger polarity, (2) BS belt is tectonically inserted between Type 2 and 3 with NW-ward vergency, and (3) Late-stage (presumably Late Cambrian or Ordovician) vertical faulting modified the subhorizontal tectonic juxtaposition. The large-scale NS-trending displacement caused the apparent juxtaposition of ACs, ranging over 110 m.y. (630-520Ma).

Keywords: accretionary complex, olistostrome, Gwna complex, OPS, layer-parallel faults

2-1. Introduction

The Lleyn Peninsula is especially known for the numerous coastal exposures of Precambrian and Lower Paleozoic rocks, giving unusual rocks from the normal

sequence deposited on the shallow marine continental platform. The sediments have been called the Gwna Group (Greenly, 1919).

The term, mélange, was applied to the Gwna Group in Wales, and its interpretation was first tried by Greenly (1919) who mentioned the possible large-scale gravitational deposition. Since plate tectonics synthesis has become available in 1968-1970, British geologist J. F. Dewey tried to speculate the geotectonic development of the British Isles by continental collision happened twice with assumption that ophiolite belt marks the presence of vast oceans before the final closure of intervening ocean. Melange unit has not been regarded to be an index rock unit to remark the ancient trench at consuming plate boundary.

However, Thorpe (1972), in his argument of plate tectonic convergence of oceanic plate under the Cambrian England, insisted the Pacific-type subduction to make accretionary complex with accretion of MORB-type greenstones. To incorporate MORB-like greenstones into arkosic sandstone unit, subduction of oceanic slab capped by deep-sea sediments is an inevitable process. Although Maltman (1977) argued against Thorpe (1972), the structural investigation of Gwna Supergroup has stopped over long time with an exception by Leggett (1979) who mapped the Southern Highland of Scotland where a series of Ordovician ACs are exposed, not a part of the Gwna Supergroup, and speculated it as ACs, although no MORB and deep-sea sediments are mapped.

Geology of Anglesey Island and adjacent regions of Snowdonian Mountains (Lleyn Peninsula) has long been well-investigated back to Greenly (1919), and later by Shackleton (1969) and his students. They have been puzzled by its unusual stratigraphy.

The apparent stratigraphic top is the oldest rock unit of Latest Proterozoic

Coedana granite, gneiss and some supra-crustal sedimentary rocks. They proposed a nearly sub-horizontal thrust called Carmel Head Thrust to the north of Anglesey Island (Fig. 2-1), and it occurred after Ordovician because of the presence of Ordovician rocks in the overriding unit.

After the boom of terrane theory mentioning small-scale continents as small as a few hundreds of km, Gibbons (1987) interpreted BS-bearing units and surrounding Gwna Group could have been derived as strike-slip juxtaposition of terranes, along the Cambrian strike-slip boundaries.

Kawai et al. (2006) have mapped the BS-bearing units in Anglesey Island and related rock units in the Lleyn Peninsula, and succeeded in drawing mineral isograds to estimate high-P/T subduction zone geotherm. They have concluded that it must have been formed at deep in subduction zone, and tectonically juxtaposed at shallow depth with the Gwna ACs at 550-560Ma by ridge subduction which enabled the tectonic extrusion process. Maruyama et al. (2010) have also demonstrated the presence of ACs at Llanddwyn island, a small island NW off Anglesey Island, and showed the methods how to demonstrate ACs in origin.

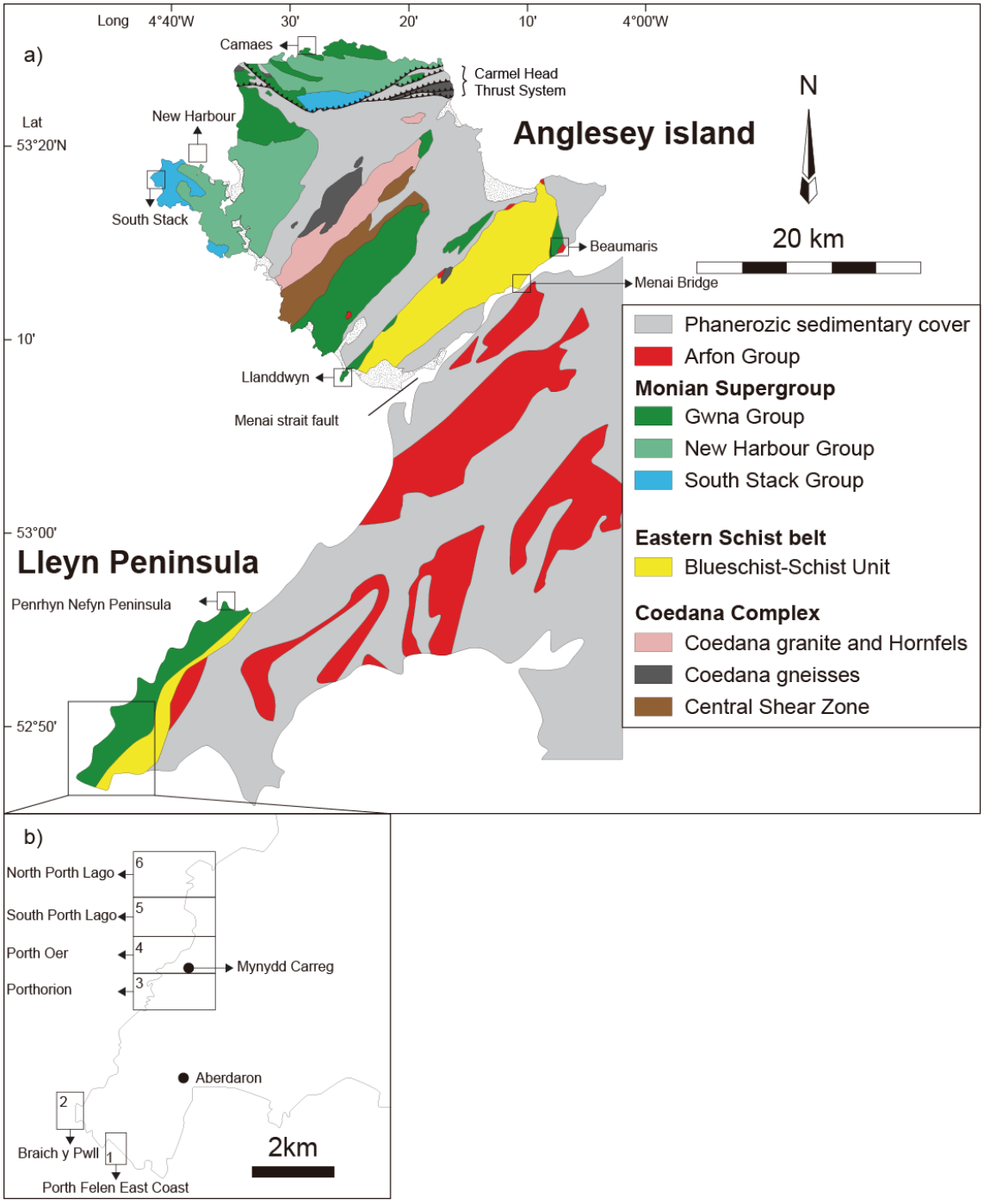

Fig. 2-1 Geological sketch map of the Anglesey Island and the Lleyn Peninsula (adapted by Greenly (1919) and Shackleton (1969)). (b) close-up topographic map in south Lleyn Peninsula. The seven geological regions are described in great details from southern to northern area, (1) Porth Felen Southwest Coast (Fig. 2-5), (2) Braich y Pwll (Fig. 2-8), (3) Mynydd Carreg (Fig. 2-10), (4) Porthorion (Fig. 2-12), (5) Porth Oer (Fig. 2-16), (6) South Porth Lago (Fig. 2-18), and (7) North Porth Lago (Fig. 2-20).

The most difficult and critical point to identify ACs in origin was chronology. The fossil identification is not yet available for those Ediacaran-Cambrian type rock units. In this paper, the zircon chronology was introduced extensively. If the age is introduced combined with ACs geology, a series of new information is led, (1) the formation age of ACs at trench, (2) subduction polarity, (3) birth and annihilation date of oceanic lithosphere, and (4) geotectonic environment where AC was formed, either active continental margin or immature intra-oceanic arc, (5) mechanism to form the ACs, and finally (6) the separation of England from West African craton.

2-1-1. Areal distribution of the Gwna Supergroup in the Lleyn Peninsula

The Gwna Supergroup is widely distributed not only in Lleyn Peninsula but also, Anglesey Island from south to the north (Fig.2-1). The definition of the Gwna is lithology and its chaotic mode of occurrence. The rock unit is composed of greenstone (metabasalt in composition), chert, claystone and alternating greywacke sandstone and mudstone. The unit exhibits chaotic occurrence called mélange and/or olistostrome with frequent occurrence of layer-parallel thrusts. By these modes of occurrence, Barber and Max (1979) suspected to be ACs, and proposed the model to form mélange as mud-diapirism with a suggestion of on-going modern example in the forearc region of Indonesia. It should be noted that the modern example, however, is the example of post-accretion at trench. It is not certain whether mud-diapirism plays a critical role of making mélange at initial stage of accretion.

Also it should be noted that the bedded chert has not yet determined to be deep-sea sediments in Precambrian time, because there was no data available for sedimentation rate.

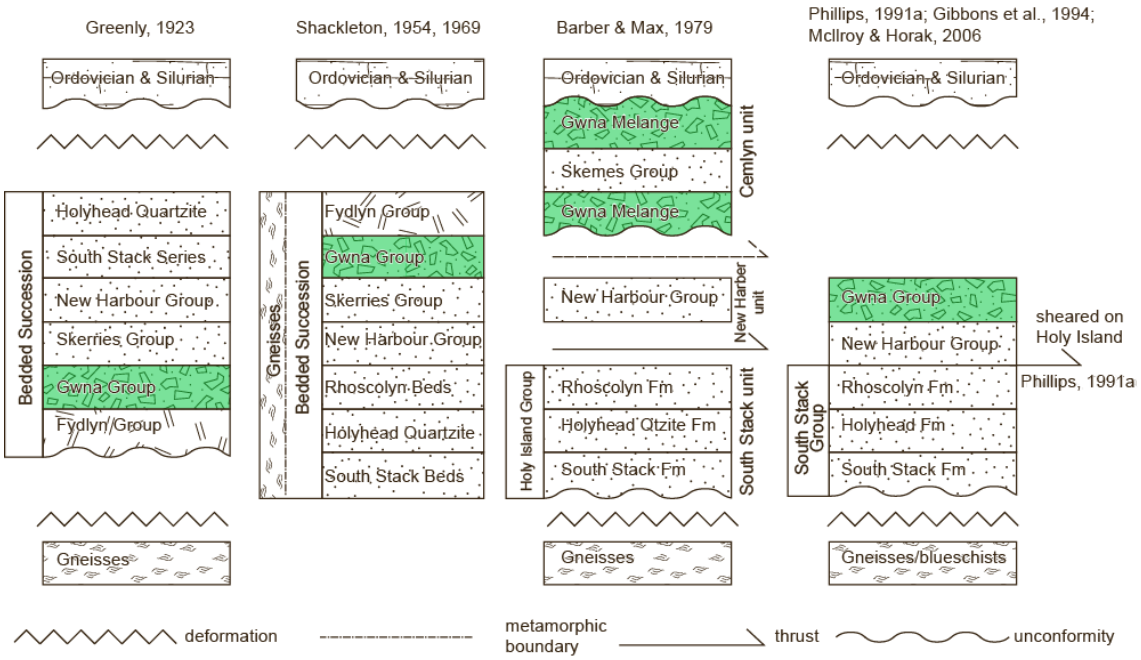

Fig. 2-2 Stratigraphic columns of Gwna Group and related units after Greenly (1919). The green band shows the Gwna Group. Later stratigraphic columns in Anglesey to the right.

2-1-2. Stratigraphy of Gwna Group and related units

Geological sketch map of the Anglesey Island and the Lleyn Peninsula is shown in Fig. 2-1. Modified after Greenly (1923) and Shackleton (1969). Stratigraphy of this region has been modified several times since the first standard model by Greenly (1919). Based on his first detailed geologic mapping, major three units separated by faults (three major deformation events, were defined, (1) the Coedana Gneiss and associated metamorphic rocks as the oldest basement rocks, (2) Bedded Successions of Fydlyn Group, Gwna Group, Skerries Group, New Harbour Group, South Stack Series, and Holyhead Quartzite in ascending order, and (3) the cap Ordovician & Silurian (Fig. 2-2).

40 years later, Shackleton (1954; 1969) modified the stratigraphy as below; (1)

Coedana gneiss was overthrust above the Bedded Succession with a sharp tectonic boundary against the Bedded Succession, and (2) the sequence of Bedded Succession. The stratigraphic bottom is the South Stack, followed by Holyhead Quartzite, Rhoscolyn Beds, New Harbour Group, Skerries Group, Gwna group and Fydlyn Group in ascending order (Fig. 2-2), which was upside-down model against Greenly (1923).

Appearances of plate tectonics in Earth Sciences, geological interpretations were drastically changed, specifically by the presence of index rock types such as ophiolite, blueschist, and mélange (Dewey, 1969). First recognition of blueschist in UK was by Blake in 1888, but his interpretation as a marker of consuming plate boundary has long been delayed until Kawai et al. (2006). Because of the presence of ophiolite, the first documentation by Thorpe (1972) which mainly remained as geochemical analysis of MORB with resembling its composition to MORB (Thorpe, 1972) has not been well-followed by later workers.

On the other hands, Barber and Max (1979) remarked the Gwna Group as mélange unit which may indicate the ancient subduction zone, similar to the Californian mélange (Cowan and Page, 1975; Hamilton, 1969). They have proposed the revised stratigraphy which has been extensively modified (Fig. 2-2). They have speculated the Gwna mélanges which sandwiched the Skerries Group to form the Cemlyn unit which unconformably overlain by the Ordovician and Silurian units. The New Harbour Group includes ophiolite unit, hence it was regarded as an allochthonous unit separated by two faults below and above. The South Stack Unit is present at the bottom as same as by Shackleton (1969).

Phillips (1991), Gibbons et al. (1994), and Mcllroy and Horak (2006) have simplified the lithostratigraphy. The basement unit includes blueschist, and the

stratigraphic intermediate is continuous without gap and the Gwna Group is the youngest below the unconformity under the Ordovician and Silurian units.

Thus, the interpretation of the Gwna Group has not yet settled, and highly variable in interpretation and geologic ages, ranging from the nearly oldest to the youngest right below the Ordovician unconformity.

2-1-3. Demonstration of accretionary complex (OPS)

First of all, here introduce the concept and methodology of Accretionary Complex Geology. Accretionary complex is found in general from Pacific type orogens. The accretionary complex is a mixture of oceanic materials with trench turbidites as typically shown in a cross section in Fig. 2-3 at left-bottom. The typical example is listed up in the enlarged small inset diagram between the top boundary and bottom boundary, several horses are developed separated each other by link thrusts. Within the link-thrusts, several horses are defined. Within each horse, there is a coherent succession of MORB capped by chert and trench turbidite is observed. The right bottom figure illustrates the mechanism how to make accretionary complex from the bottom to upward in sequence, through the step-wise jumping of plate boundary fault. See the details more in the figure.

The reconstructed scenario of mechanism is shown on the top figure. From the mid-oceanic ridge to trench, a series of developing OPS is illustrated. From the birth place of MORB crust to the trench, deep-sea sediment gradually accumulates on the ocean-floor. Red claystone deposits extremely slow speed ca. 1m per 1 m.y. Two orders of magnitude were slower than that of Phanerozoic cherts (Matsuda and Isozaki, 1991). Frequently, OIB magmatism occurs between MOR and the trench (Fig. 2-3).

Above the deep-sea sediments or pelagic bedded chert layers, hemipelagic sediments usually mudstones rest on the deep-sea sediments, and finally trench turbidite accumulate right above hemipelagites. Age of lowermost deep-sea sediments defines the time of birth of plate, whereas the age of hemipelagite indicate the age of arrival time to trench. Subducting bottom age from top age of deep-sea sediments, the age of annihilated slab is obtained (top figure of Fig. 2-3).

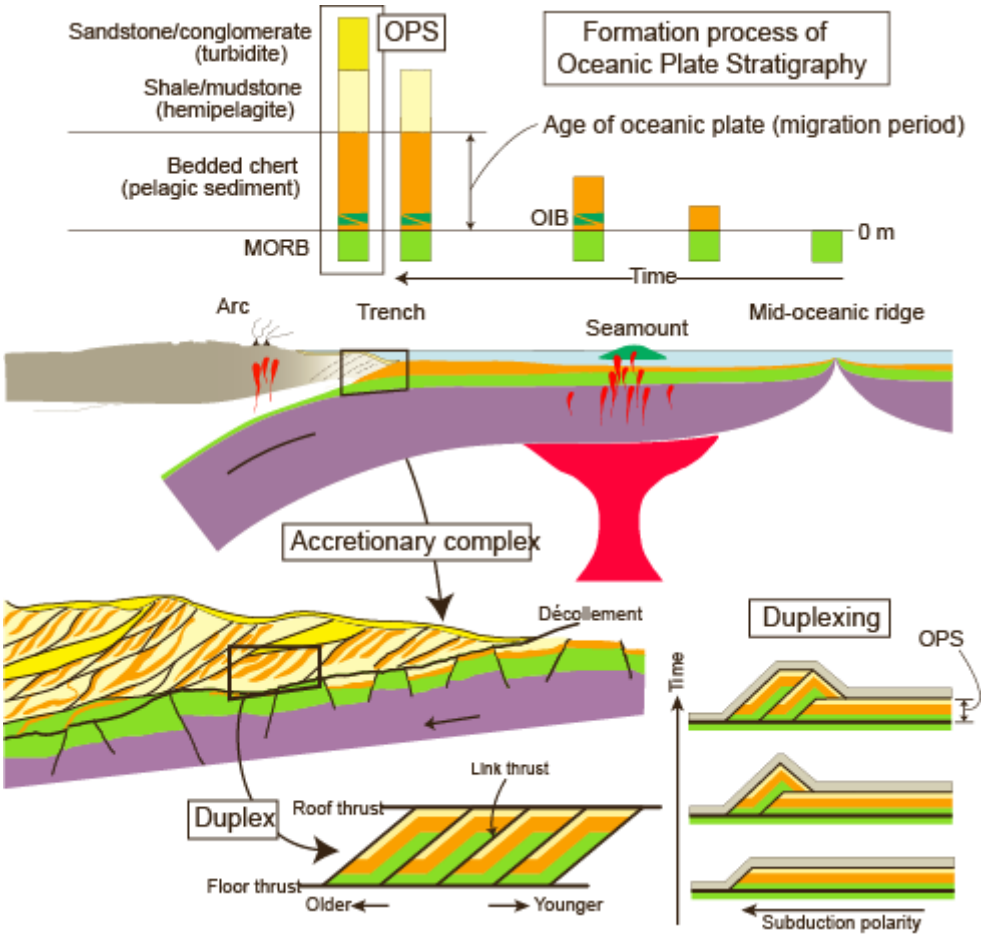

Fig. 2-3 Formation process of ocean plate stratigraphy and accretionary complex. (Modified after Matsuda and Isozaki, 1991).

2-2. Geology of the Lleyn Peninsula

In this paper, I introduce the method of detailed mapping to clarify structural

relationships along the coastline which has nearly continuous exposures, combined with zircon chronology, which is different from microfossils like radiolarians and conodonts (Matsuda and Isozaki, 1991). Applied skills and method was established by Japanese previous workers and adjusted to the Gwna group.

On the other hand, Google maps were excellent to conduct the field survey with high-resolution and colors reflecting rock-types and lineaments to follow precise fault lineaments.

2-2-1. Geological outline

The Porth Felen SW Coast area and Braich y Pwll regions are shown in Fig. 2-4. There are nearly perfect continuous exposures at the south head of the Lleyn Peninsula. In this region, the Gwna Group composed of basalt (greenstone), bedded chert-claystone, and sandstone-mudstone units are present, together with Na-amphibole-schist units of strongly penetrative fabrics. In addition, the post-orogenic coarse-grained sedimentary units dominated by sandstone and mudstone with conglomerates with presumably Ordovician age are present with high-angle fault contacts against the Gwna Group, schist unit and ACs.

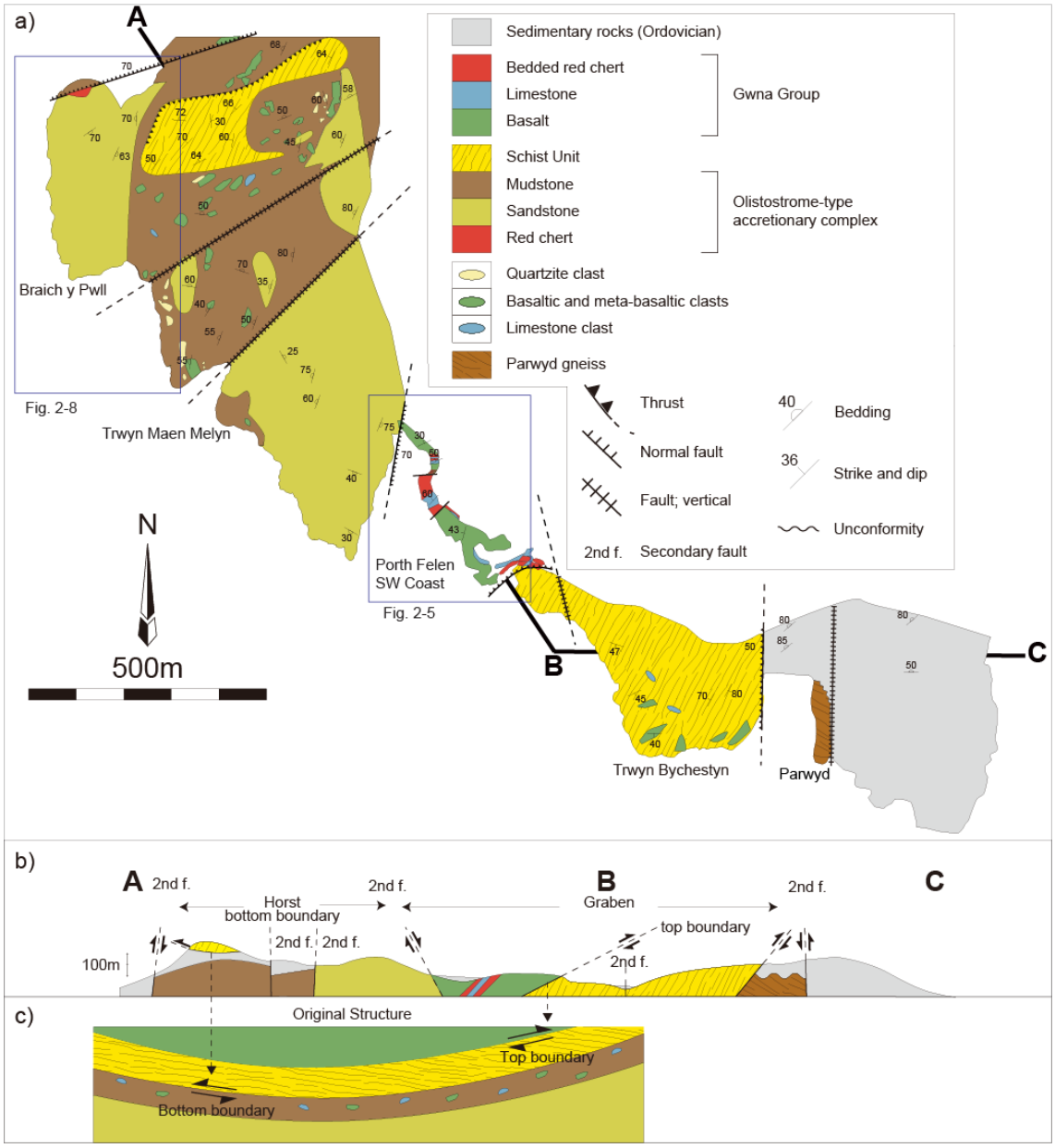

Fig. 2-4 Index map of Lleyn Peninsula to show the detailed mapping regions. B); along the cross section A-B-C, c); the original relationship among the all units is also shown (Kawai et al., 2007).

The olistostrome-type ACs is distinguished from the Gwna Group ACs, because of remarkable and spectacular occurrence of huge olistoliths both oceanic, such as greenstone, chert and mudstone which must have once formed ACs and later mixed with younger ACs at consuming plate boundary, and continental affinities such as

quartzite and platform impure carbonates with stromatolite structure.

Along the southernmost region in the mapped area, Parwyd gneiss equivalent to Coedana gneiss is exposed (Fig. 2-4). Along the cross section A-B-C, the structural relationship is shown, and the original cross section before the secondary normal faulting is reconstructed at the bottom figure of Fig. 2-4. The structural top is the MORB-carbonate-bedded chert which is underlain by the BS unit with deformation fabrics of normal faulting with an upward sense to the east (Kawai et al., 2007). Below the BS unit, the olistostrome-type ACs is present. The shear sense between the BS unit and the underlying unit is a reverse fault with an upward sense to the west, showing a paired fault to indicate the northwestward wedge extrusion of BS unit.

2-2-2. Detailed geological map in key areas along the coast of the Lleyn Peninsula

It is necessary to observe detailed geology in Lleyn and systematic collection of rock samples to reconstruct ACs. However, outcrops are poor on-land because of plants and buildings covering the surface. Therefore, we focused the detailed mapping at a scale 1:5000 with further detailed sketch work at 1:2500 scale, along the coastline over 4km of the Lleyn Peninsula (Fig. 2-1(b)).

In following sections, seven geological regions are described in great details from southern to northern area, (1) Porth Felen SW Coast, (2) Braich y Pwll, (3) Mynydd Carreg, (4) Porthorion, (5) Porth Oer, (6) South Porth Lago, and (7) North Porth Lago.

Also there are several excellent outcrops area to further north along the coast such as Penrhyn Nefyn Peninsula showing Gwna Group with minor chert with turbidites and ACs (Fig. 2-4).

2-2-2-1. Porth Felen Southwest Coast

Porth Felen SW Coast locates about 3.5 km to the southwest from Aberdaron. The detailed description was yet available, except the geologic map published in 2001 from Geological Survey of London.

Kawai et al (2007) found that the top boundary of the schist unit of regional metamorphic belt was exposed in this area (Fig.2-4). This area consists of pillow basalt, red claystone, dolostone, turbidite, tuff, black mudstone and white chert (Fig.2-5). Although there is about 50 m thick MORB-like pillow basalt with quartz vein from the western end point to the east, highly sheared basalt with brown color is observed in eastside because of alteration and deforming by shear. This layer is equivalent to a structural bottom. The eastside basalt shows pillow structure with 2-3 cm chilled margin, and the facing direction (stratigraphic top) is eastside. The basalt is covered by 7m thick red-colored claystone (Fig.2-5). Thick dolostone layers with ca. 10m are found on red claystone. The boundary of red claystone and dolostone is layer-parallel thrust. The dolostone lies on a reddish pillow basalt with inter-pillow red chert and dolostone, and there is a few meter thick red claystone and dolostone alternation on the dolostone layer. Generally, this structure means ocean plate stratigraphy (OPS).

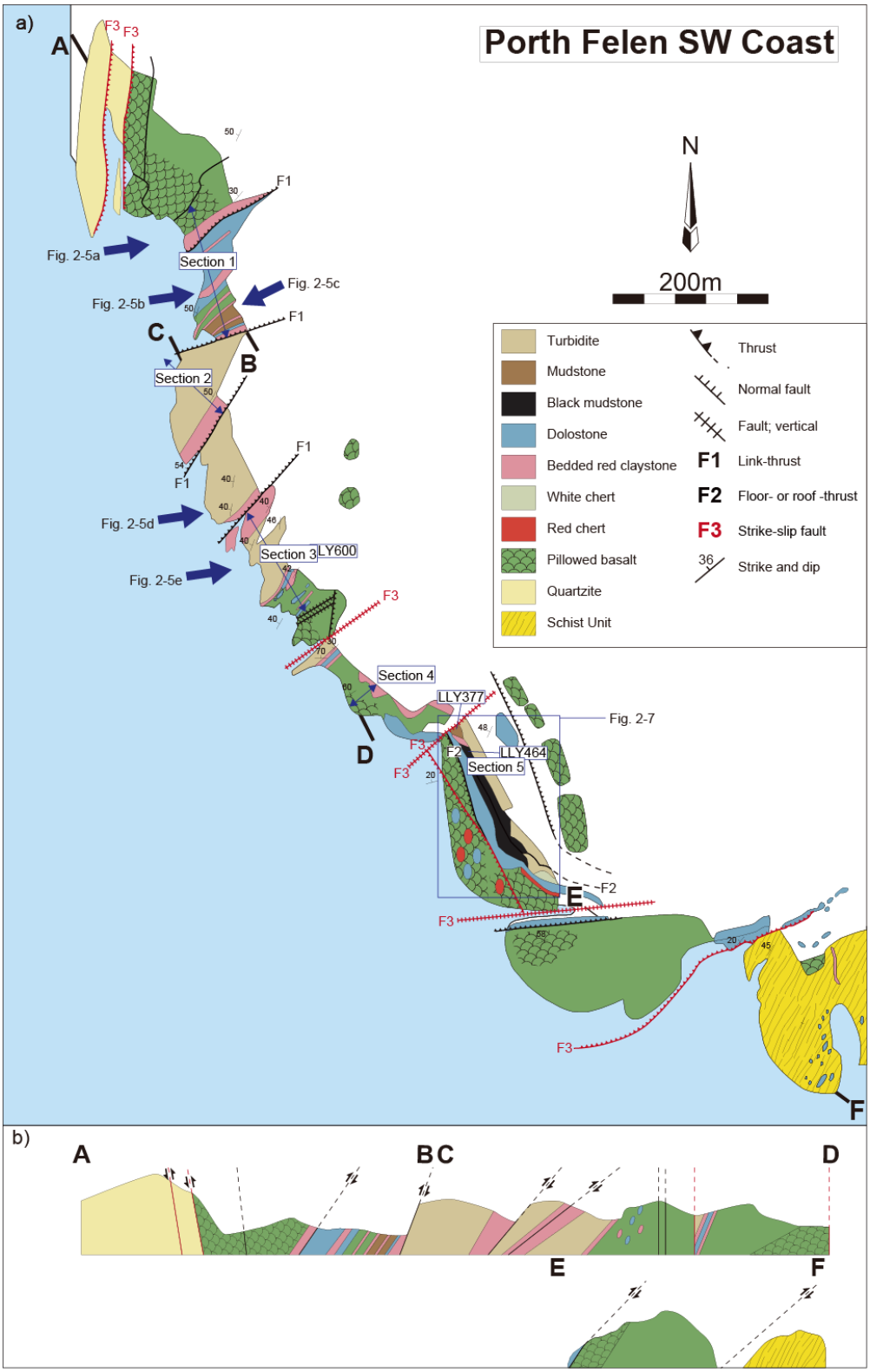

Fig. 2-5. Geologic sketch map along the coast at Porth Felen SW Coast. Note the faulted blocks of oceanic rocks such as greenstone (MORB), chert, black mudstone. All of these are highly deformed by layer-parallel thrusting and high-angle faults at later stage. Cross section along A-B-C-D-E-F is

shown on the bottom. Location of field photos is also shown on the map (see Fig, 2-6). From section 1 to 5 were reconstructed geological column in Fig. 2-25.

(a)

(b)

(c)

(d)

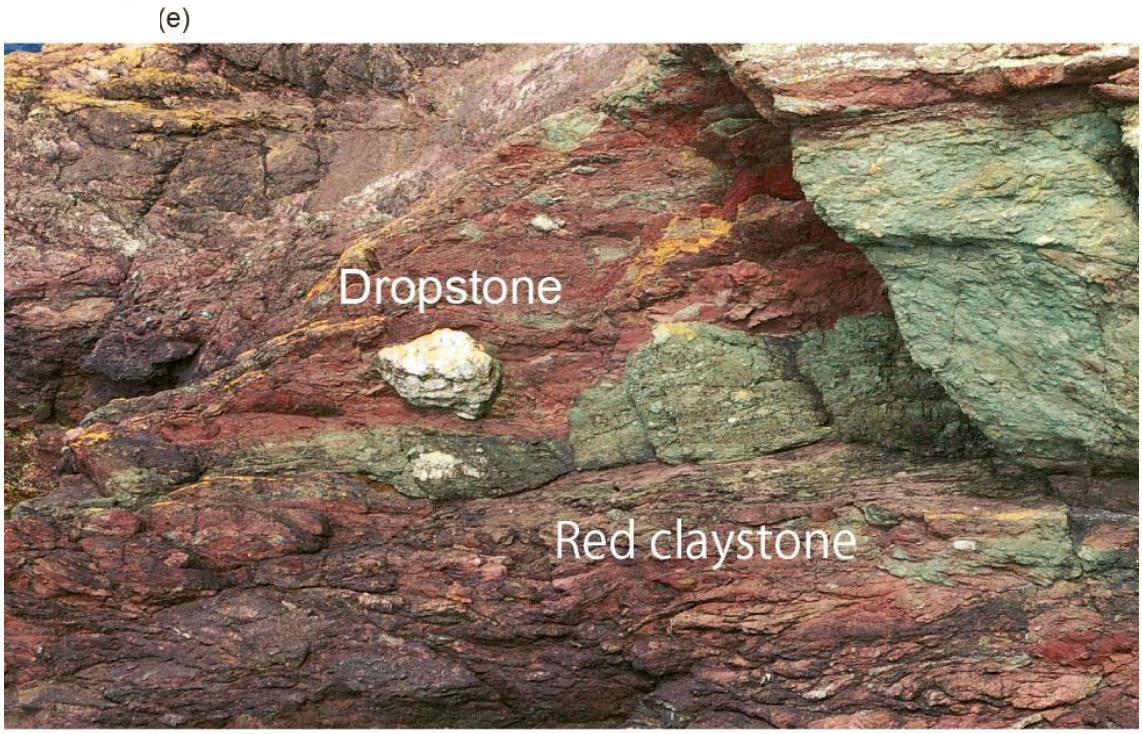

Fig. 2-6 Field photos. Note the locations shown on Fig. 2-5. 2-6(a) shows extensively and hydrothermally altered and sheared pillow basalts with epidote, chlorite, carbonate and network quartz veins, 2-6(b) exhibits the overlying red claystones interlayered with finely altered bedded chert (1-2mm thick), 2-6(c) Stratigraphic top unit with conglomeratic volcanic breccias, 2-6(d) layer-parallel thrust between bed claystone and turbidite, 2-6(e) Granitic dropstone inserted in the red claystone on the cliff, indicating glacial period corresponding to Marinoan snowball Earth.

The center of Porth Felen SW Coast mainly consists of turbidite, red claystone and basalt (Fig. 2-5). The thickness of turbidite and red claystone has ca. 30m and 5-15 m, respectively. 1 m size quartz- rich sandstone block resembles dropstone and is observed in the hemipelagic claystone and turbidite (Fig. 2-6 (e)). Moreover, there are 2 cm – 5cm thick tuff layer and bedded mudstone with about 50cm thick in turbidite. In basalt, there is dolostone with ca. 1 m thick lens structure. On the other hand, there are thrusts and high-angle secondary fault in this area. The structures show parallel to several sedimentary layers with about 45 degrees dip to northwest. Therefore, the fault

and sedimentary layers are formed at the same time. Unlike the several sedimentary layers, the most of red claystone and turbidite has north-northeast strike, dipping 40 degree to the north.

The southern area consists almost of pillow basalts with over 20 m thick, overlain by dolostone or red claystone (Fig.2-5). At Windley point shown in Fig. 2-5, an excellent succession of Ocean Plate Stratigraphy is observed along the continuous cliff.

Fig. 2-7 is the close-up sketch of the outcrop in the Windley point. The exposure is composed of complexly deformed and faulted blocks by numbers of faults, some are layer-parallel and another is cut by high-angle normal faults. However, the structural bottom is MORB-type pillow basalt overlain by dolostones. The 20-50m thick MORB-type pillow basalts overlain by dolostone (10m) interlayered finely with black mudstone (10m), white-colored bedded chert sequence (8m), and finally by hemipelagic claystones with dropstones and sandy to conglomeratic turbidite (east side in Fig. 2-7). All of these are cut by faults, typically a series of duplex-type deformation is observed (Fig. 2-7). F1 means either top- and/or floor-thrust, and develops parallel to the stratigraphic boundaries, hence layer-parallel. Within the unit separated by two faults of F1, numbers of link thrust is developed, each link thrust termed as F1 is shown in the figure to define each horse. F3 was formed at latest stage, presumably during the stage of dome-up after the exhumation of BS unit at mid-crustal depth (Kawai et al., 2006; 2007).

Yet, in some points, original stratigraphic relations are preserved. Based on those detailed stratigraphic observations, the reconstructed OPS is shown in Fig. 2-25. It consists of basalt, dolostone, black mudstone, white chert and turbidite, respectively from the bottom. In this area, the black mudstone and the turbidite show duplex

structure. These structures mean ocean plate stratigraphy

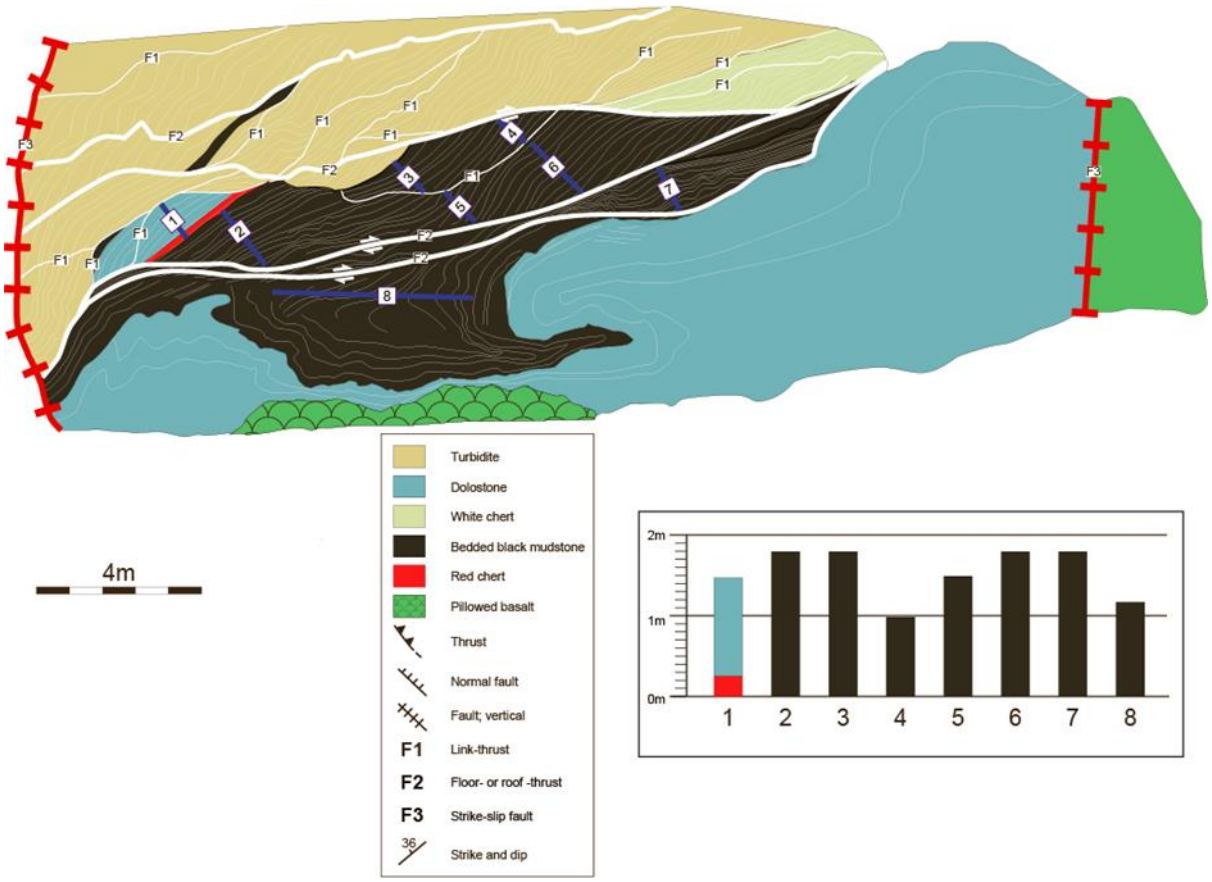

Fig. 2-7 Sketch map of Windley Point to show the OPS in details. Note the excellent exposure of duplex-type accretionary complex to preserve the original OPS shown at right hand side. F1 means layer-parallel top and floor thrusts, F1 means link thrust within accretionary prism. F3 means the youngest high-angle fault. Systematic sample collection is shown in great details below. Geological columns in 8 sections are figured by observing detailed faults.

Five geological columns in this area are figured by this detailed geological survey, especially detailed faults. Section 1-5 point from north (Fig. 2-5). In the most north of section 1, pillow basalt, bedded chert, dolostone and turbidite are found and suggest oceanic plate stratigraphy. Section 2 shows thick turbidite at the south of section 1. Section 3 in center of Porth Felen SW Coast consists of pillow basalt and turbidite with

large sandstone boulders. In section 4, basalt and red claystone are found (Fig. 2-25). Section 5 is observed in the northwest of Windley point and has black mudstone (Fig. 2-5 and 25). The detailed lithofacies are mentioned in section 3-2-3.1. The geological columns indicate OPS. Moreover, tuff layers in turbidite are observed in section 3. The tuff (LLY600) is collected to analyze depositional age by U-Pb dating of zircons. In section 5 (Windley Point), sandstones (LLY377 and LLY464) in two layers, the mudstone and the top turbidite layer, are collected to discuss depositional age of the black mudstone.

2-2-2-2. Braich y Pwll (Lighthouse and its western cost)

The Braich y Pwll region belongs to the ACs with olistostrome-type former ACs, collapsed presumably by the gravity flows on the trench-slope break, as estimated by their mode of occurrence. The nearly perfect and continuous exposures are observed along the coastal line with 50-60m height. Units A, B and C are differentiated by its lithology (Fig. 2-8). Type A contains oceanic blocks as olistoliths such as red bedded chert and MORB-type greenstones, whereas B is composed of rhythmically alternating mudstone and sandstone with or without highly deformed with manner of penetrative fabrics, often accompanied with red claystones (hemipelagite). The southernmost unit is termed as C that is coarse-grained sedimentary unit presumably deposited at latest stage on the continental shelf, and tectonically juxtaposed at latest high-angle normal fault (Fig. 2-8).

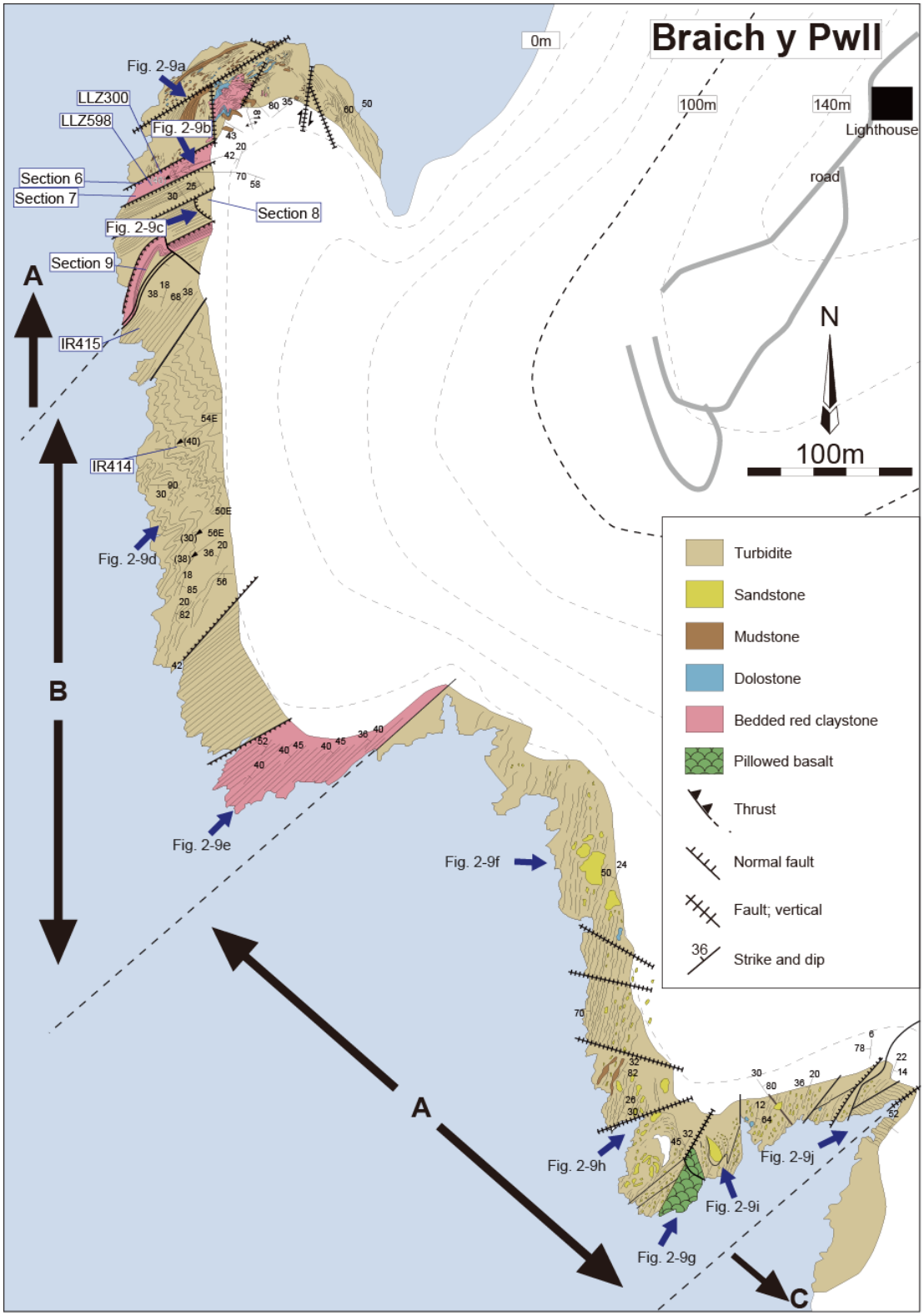

Fig. 2-8. Geologic sketch map along the coastline from Lighthouse of Braich y Pwll to the south. A typical olistostrome-type mélange unit is observed. Units, A, B and C are distinguished. Cross section along N-S profile is also shown. From section 6 to 9 were reconstructed geological column

in Fig. 2-26.

(a)

(b)

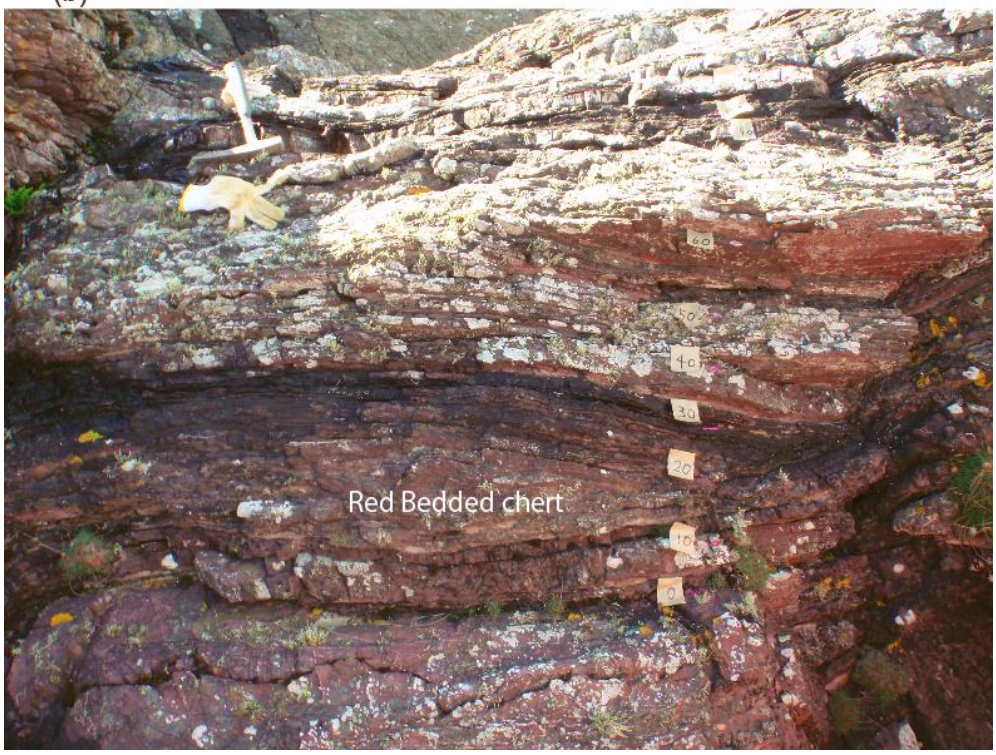

(c)

(d)

(e)

(f)

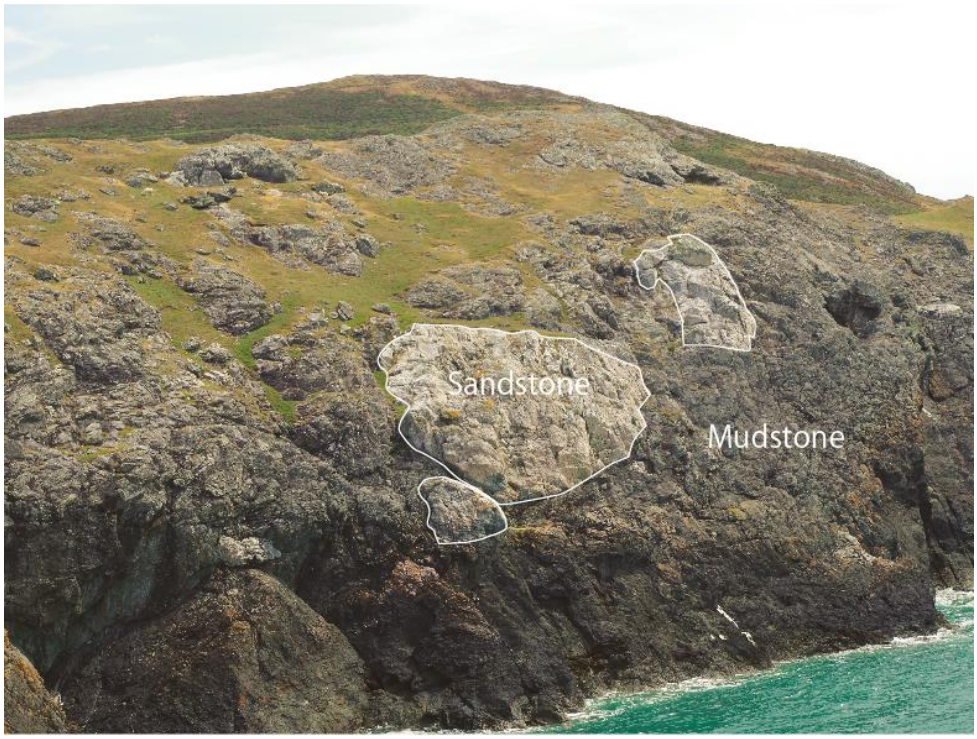

(g)

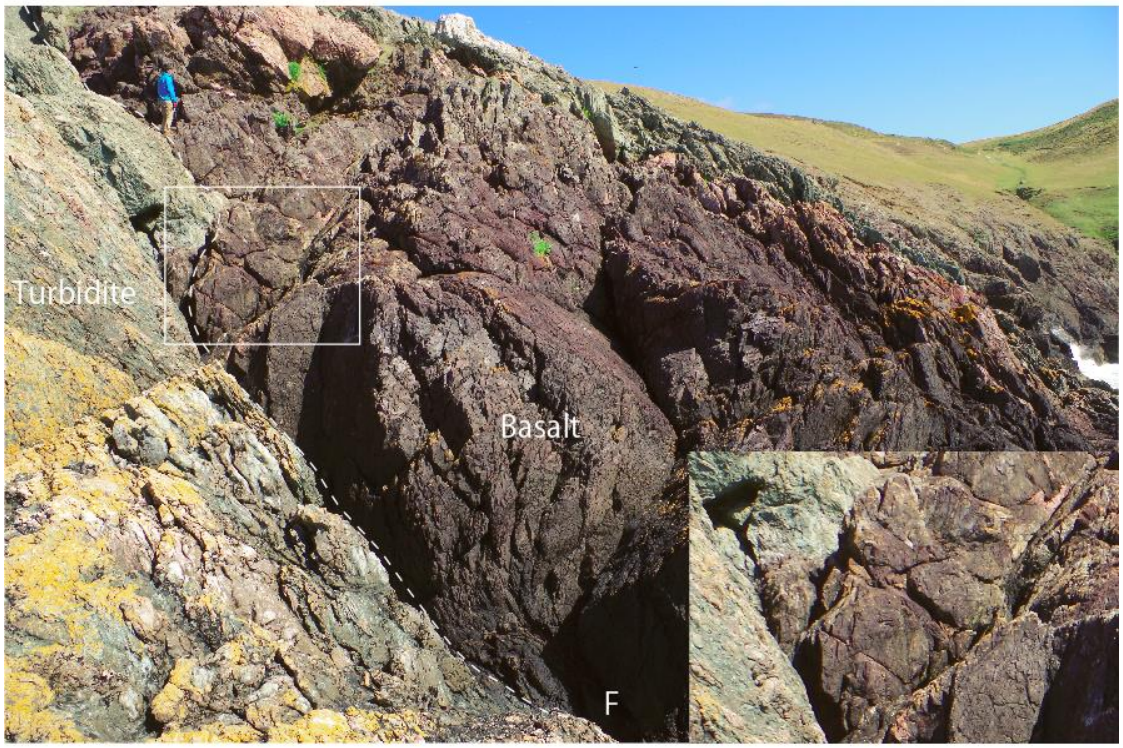

(h)

(i)

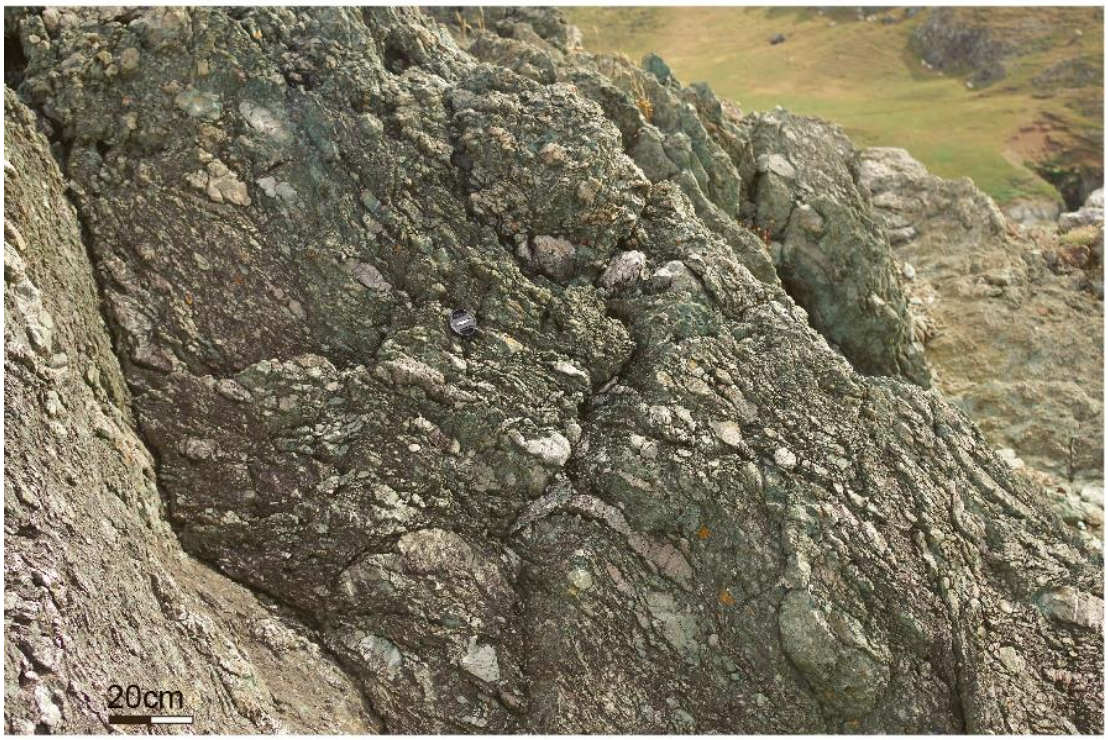

(j)

Fig. 2-9. 2-9(a): 2 x 10m lens of dolostone olistolith within muddy matrix, 2-9(b): tectonic lens of red bedded chert sequence, 2-9(c): Red bedded chert and overlying sandy turbidite, 2-9(d):

Crenulation fold of hemipelagic sediments, 2-9(e): Alternating hemipelagites alternation and fine-grained black shale, 2-9(f): three large olistoliths of granite set in the muddy matrix, 2-9(g): 20 x 50 m block of MORB-type pillow basalts set in the highly sheared matrix and faults on the left, 2-9(h, i) Alternating quartzite and conglomerate with trench turbidite origin, , 2-9(j): High-angle normal fault dividing the Ordovician shelf deposit on the right-hand side.

At north side in Fig. 2-8, some faults show northeast stripe and high angle dipping. In addition, sandstone and dolostone is observed in mudstone matrix, and this structure indicates olistostrome. The dolostone layers have 0.5 to 2 m thickness and bounding structure. On the other hand, the sandstone and mudstone layers have 0.1 to 50 m thickness and show olistoliths. Moreover, the difference of grain size between upper side (sandstone) and lower side (red clay) is observed in the olistolith layers, transition fine to coarse grain (Fig2-8).

In the north side of unit A, there are about 30 × 60 m size red claystone and sandstone with olistolith. The olistolith of red claystone have alternation of gray shale with ca. 5 mm thick and red claystone with 1 – 5 cm, and shows totally about 20 m (Fig. 2-9 a,b and c). In addition, almost faults dipping high angle of parallel strike with bedding plane are observed in this area, while there are some faults of vertical strike with bedding plane. The olistolith in north and south side of unit A shows different size and exposure, but the olistolith in north and south side of unit A shows similar structure such as transition of grain size. Thus, we suggest that the olistolith is provided by same events. We consider that the northern side olistolith was derived from southern side by active tectonic event like slide. On the other hand, we figure lithostratigraphies in four sections (section 6-9) of south area (Fig. 2-8, 26) to find chert, red claystone and turbidite. However, it is difficult to find lithostratigraphies in north area, because the area with olistostrome, corresponding accretionaly complex, has too small in scale. The

geological columns have 2-8 m thickness, section 9 shows thickest column. Moreover, we corrected shale (LLZ300 and LLZ298) in section 2 to analyze U-Pb age of zircons (section 3-2-3.2).

In the B area, sandstone and mudstone mainly expose (Fig.2-8). The north side in this area shows coherent folding and has ca. 150 m thickness in total, composed by alternation of 1-10 cm thick sandstone and 1-2 mm thick mudstone (Fig. 2-9 d and e). The folding axis shows about northeast strike and about 40 degree dipping to south. In the southern part of this area, there is coherent exposed alternation of 3 – 10 cm thick sandstone and 2-10mm thick mudstone and totally thickness shows 60 m. Toward the south from southern side of B area, there is alternation of 1 – 5 cm thick siltstone or red shale and 2-10 mm mudstone, and the layers have northeast strike and 40 degree dipping to the north.

In the south of the area, olistostrome-type sediments are exposed (Fig. 2-9 f-j). The olistolith has from 5 cm to 50 m, especially more than 10 m olistoliths show quartzite or sandstone and the number of olistolith shows less than that in west. In addition, there are mainly sandstone and dolostone in this area other than the olistolith. The olistolith has slope to the west side. Although some faults have parallel strike with the mudstone layers, secondarily faults in this area have east-west strike and high angle dipping. Sandstone layers with muddy matrix in this area show many slips by the crack which is deformed structure caused by redeposition. On the other hand, pillow basalt with inter-pillow chert and dolostone is exposed in southern side. This structure is also observed in north side of Porth Felen SW Coast.

2-2-2-3. Mynydd Carreg (Red chert Quarry)

The Mynydd Carreg area is 7 km to the north from Aberdaron, a rare inland exposure standing 1km inside from the coastline. More than 50 exposures are available on this hill, but most of them are MORB-like greenstones. One of the five red chert outcrops is called Mynydd Carreg Quarry. This outcrop was observed red chert, white chert, black mudstone, dolomitic marble, dolostone and bedded mudstone. Moreover, about 50 m western side of this outcrop exposed greenstone. Thus, the lithological feature of the Mynydd Carreg is similar to the Porth Felen SW Coast. The north-facing small outcrop is investigated in great details, and the result is shown in Fig. 2-10. Five N-S trending vertical faults develop in this 10m high quarry. The original stratigraphy is well-documented as seen along the cross section of A-B on the bottom figure.

Extremely graphite-enriched black mudstone is also crop out at Windley point in Porth Felen SW Coast, occurs at the stratigraphical bottom (Fig. 2-11c, d). Bedded mudstone covers black mudstone. Red chert is observed at the stratigraphical top and does not have bedded structure (Fig. 2-11 a, b). The massive red cherts were not observed in other area of Lleyn peninsula. On the other hand, white chert has bedded structure, which observed in at Windley point in Porth Felen SW Coast. Bedded mudstone in the east side of this area is highly weathering. The lithostratigraphical relation of this site and Windley point in Porth Felen SW Coast is very similar. So, basalt and dolostone would lay under the black mudstone. Geological column (section 10) in this area is reconstructed in Fig. 2-27. The column consists of pillow basalt, dolostone, black mudstone and turbidite in ascending order (section 3-2-3.3). The lithostratigraphy indicates oceanic plate stratigraphy. In addition, acidic tuff layer is present between gray mudstone in center of this area (Fig. 2-10). We corrected rocks to analyze U-Pb age (UKY20: Section 3-2-3.3).

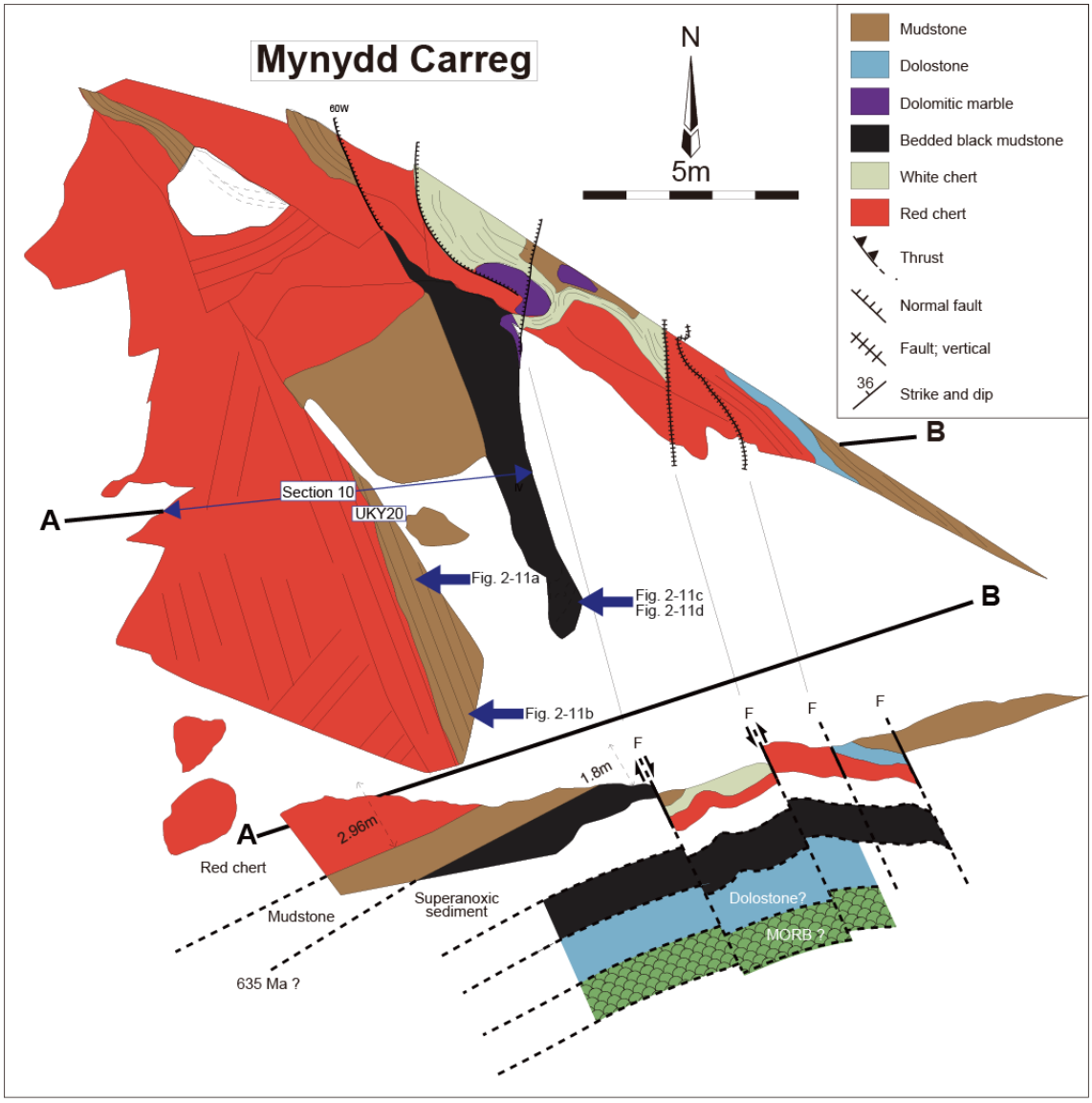

Fig. 2-10. Geologic sketch map of Mynydd Carreg outcrop. Cross section along A-B is shown below. The Marinoan super-anoxia is interlayered red chert layers and MORB or dolostone on the bottom. Also note the location of photos in Fig. 2-11.

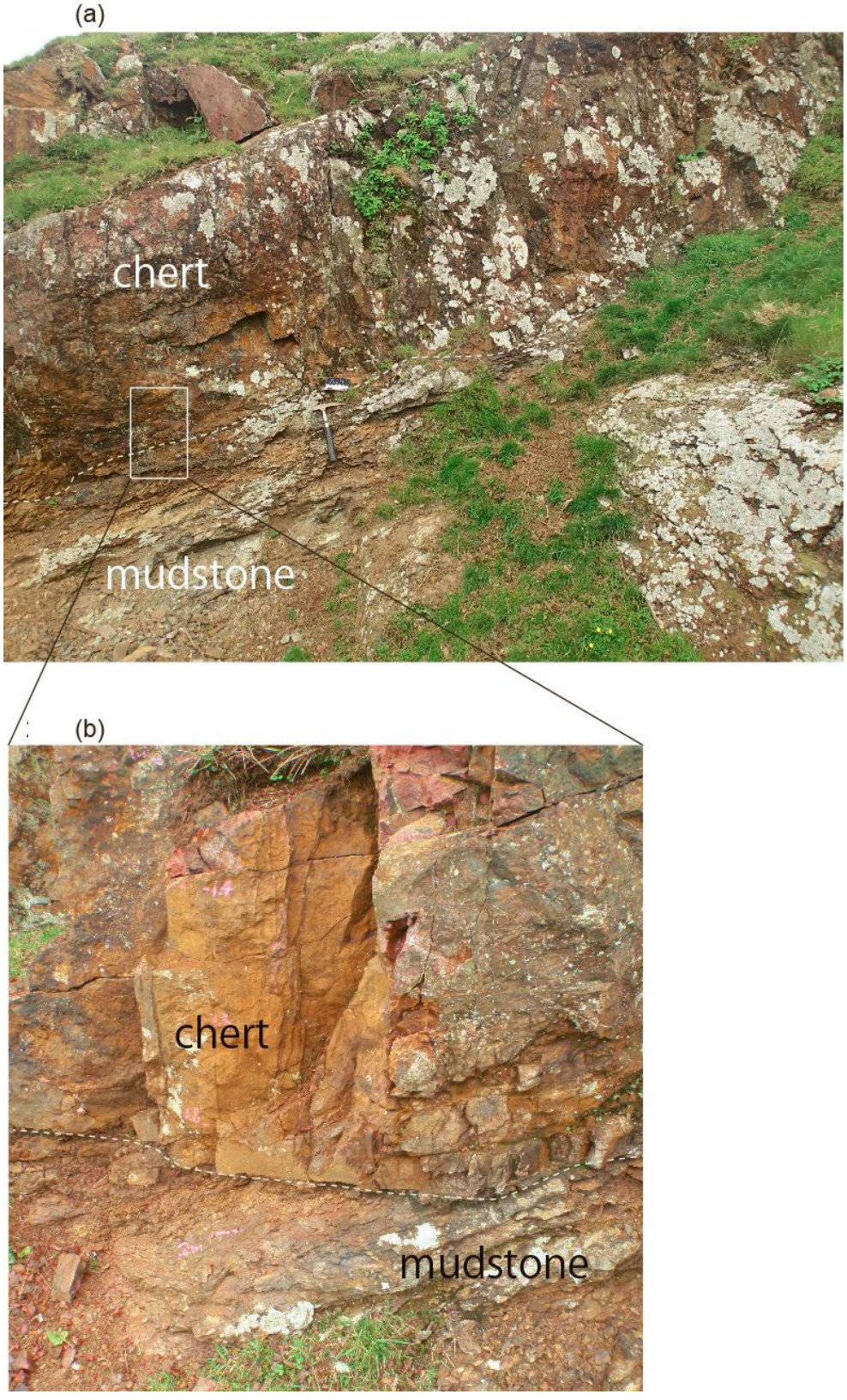
(a)
chert
mudstone
(b)
chert
mudstone

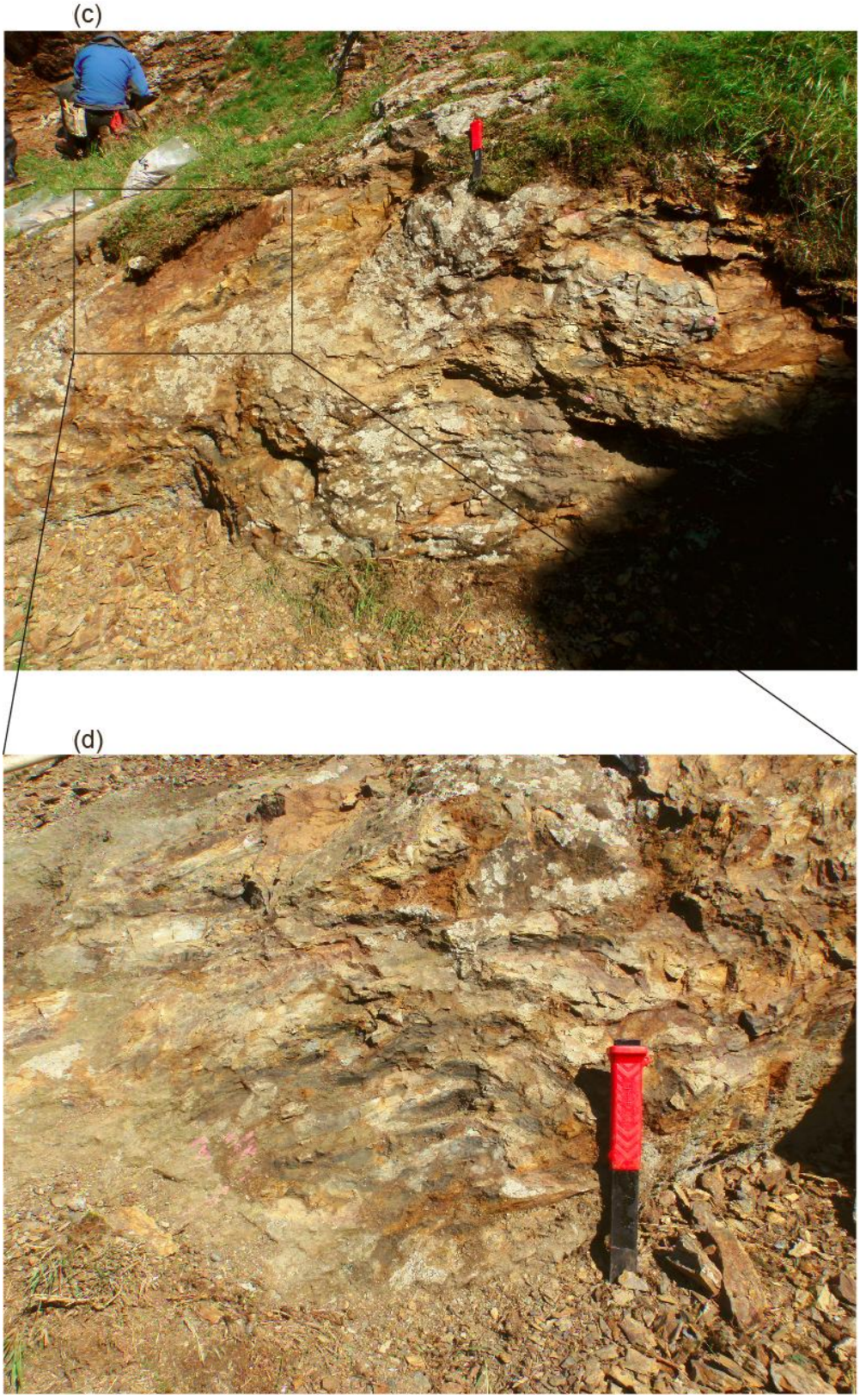

Fig. 2-11. Field photos, 2-11(a): Boundary between the lower mudstone and upper red chert, 2-11(b): Close-up view of the boundary between chert and mudstone, 2-11(c): Bottom of black mudstone,

2-11(d): Close-up view of the boundary of the black mudstone in (c).

2-2-2-4. Porthorion

Figure 2-12 is the geological map in the northeast area of Porthorion. The northern half of the area is the southern extension of Porth Oer (see next section), and is composed dominantly of pillow basalts, red claystones, dolostones, sandstones and turbidites. Several strike-slip faults (F3) cross cut the original duplex domains. Especially, the Aberdaron fault cross cut the Lleyn peninsula. More than 20 horses are present, although the reconstruction of the original structure and the sense of subduction seems to be difficult.

The southern half of the area is dominated by sandstones with intercalated mudstones. Layer-parallel faults are also present. Lithologically, this unit is similar to the northern North Porth Lago. F3 faults obliterate the original duplex structure.

The center of this area is mainly composed of pillow basalts (Fig2-13 (c)). This area has several vertical faults to east-west strike. The basalts between faults are sheared and do not maintain pillow or sheet structures.

The northern half of the area composed pillow basalts, bedded red claystones and dolostones. Dolostones in the middle area crop out as 20–50 m size olistoliths in the red claystones and turbidites. And, red claystones around olistoliths have dolomite or calcite vein like mesh structure (Fig. 2-13 (b)). On the other hand, red bedded claystones including red cherts crop out in north side. The detailed field sketch in this area is shown in Fig. 2-14. Pillow basalts in northern side have southern top structure and include some dolomitic lenses with 2-5 m thickness. Moreover, in the north end, limestone matrix fills between basaltic fragments (Fig. 2-13 (a)).

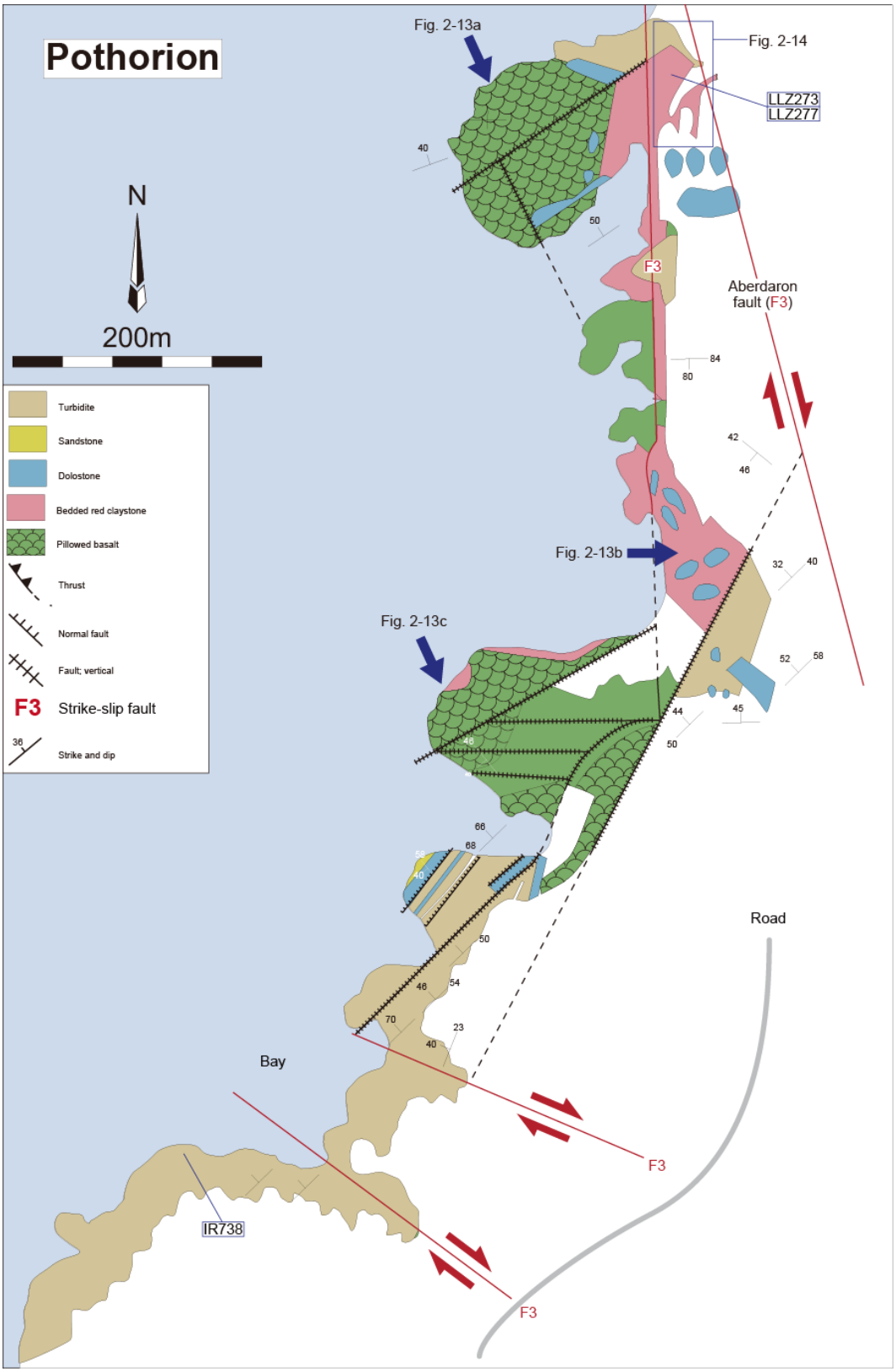

Fig. 2-12. Field sketch map of Gwna group along the coast line. Field photos of sampling locations are shown in Fig. 2-13. F3 represents strike-slip fault with high-angle. The box in the upper-right has

close-up sketch shown in Fig. 2-14.

(a)

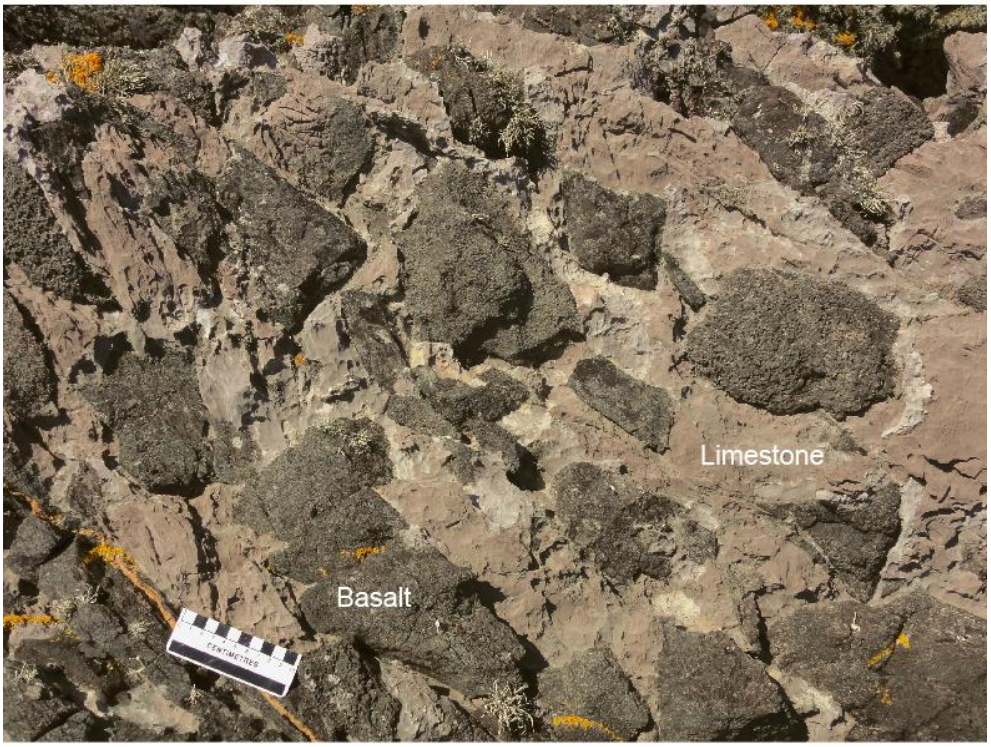

(b)

(c)

Fig.2-13. 2-13(a): Limestone filling in between basalt blocks in north Porthorion, 2-13(b): filling gaps of red claystone with limestone, 2-13(c): pillow basalts indicating stratigraphic top.

Figure 2-14 shows geological map in northeast area of Porthorion. Basalts, red claystones, green claystones, mudstones, sandstones and dolostones are observed in this area. The strike-slip fault (F3) has north strike and high angle dipping and is occurred later than the other faults in this area (Fig. 2-15a, b). The floor or roof thrusts show southwest strike, separate 5 horses (Fig. 2-15d, e, f, g). The horse 1-3 consists of ca. 10-30 m thick red claystone with intercalated ca. 2-5 cm thick siliceous claystones, 1-4 mm thick claystones and sandstones. About 30 m thick red claystones include green claystones and 10 m sandstones exposed in the horse 4. The horse 4 includes several faults that may have been caused by floor or roof thrust; it is difficult to clarify the lithological structures, such as thickness or sense of strike and dipping, in east and west

sides from the fault. The most of red claystone and sandstone layers have east-west strike and high angle dipping in the house 4. The house 5 consists of basalt, red claystone and green claystone. The basalts are clearly altered and sheared. The red claystones overlie the basalts and clearly show higher deformed and altered than the other horses.

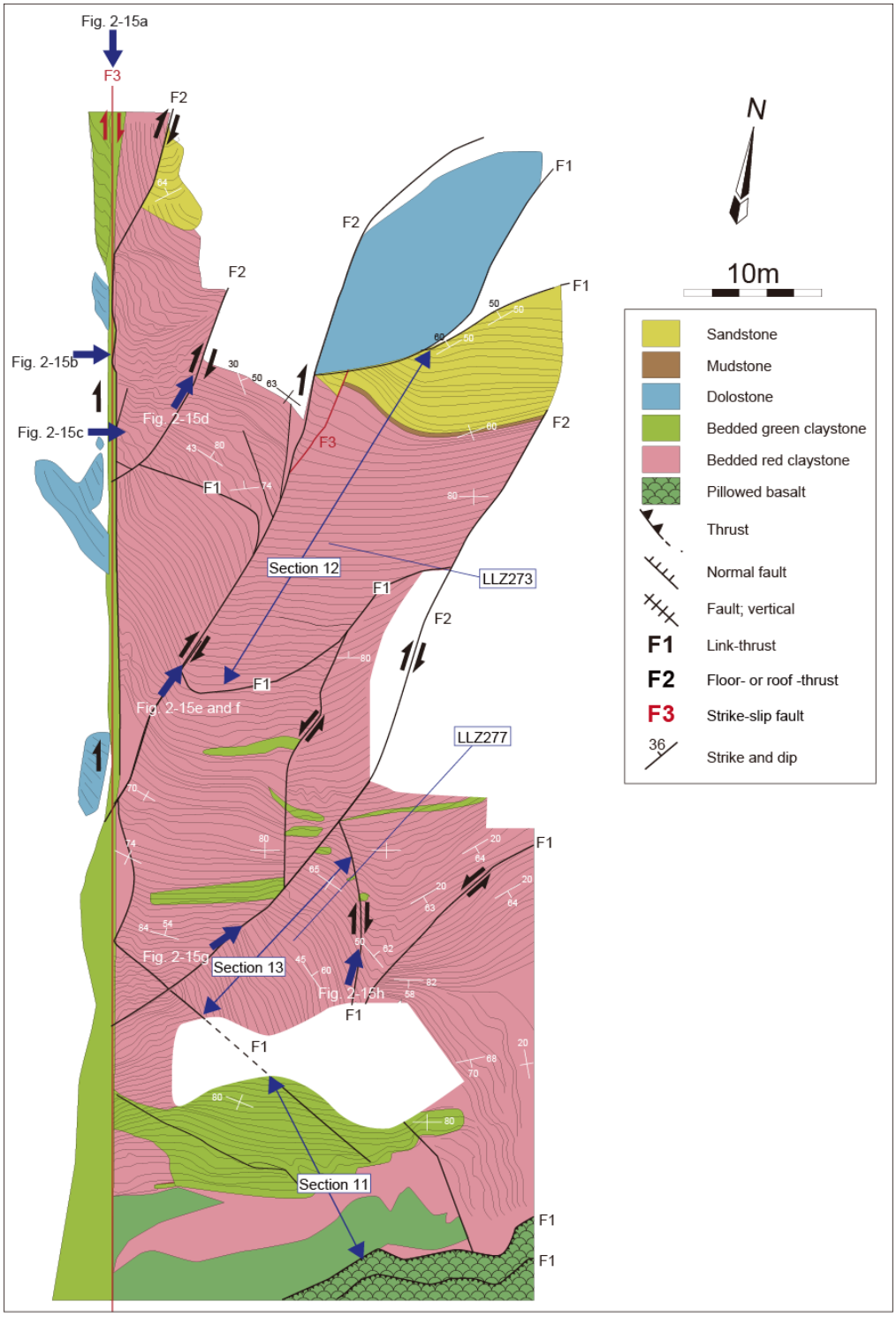

Fig. 2-14. Enlarged sketch map of pillow basalt, red claystone and hemipelagic to trench sandstone in Porthorion. Although numbers of faults, formed at different stages, are present, original ocean plate stratigraphy can be reconstructed (see inset figure on the right). Locations of the outcrop photos (Fig. 2-15) are also shown. Stratigraphic columns of the section 11 to 13 were reconstructed (Fig. 2-28).

(a)

(b)

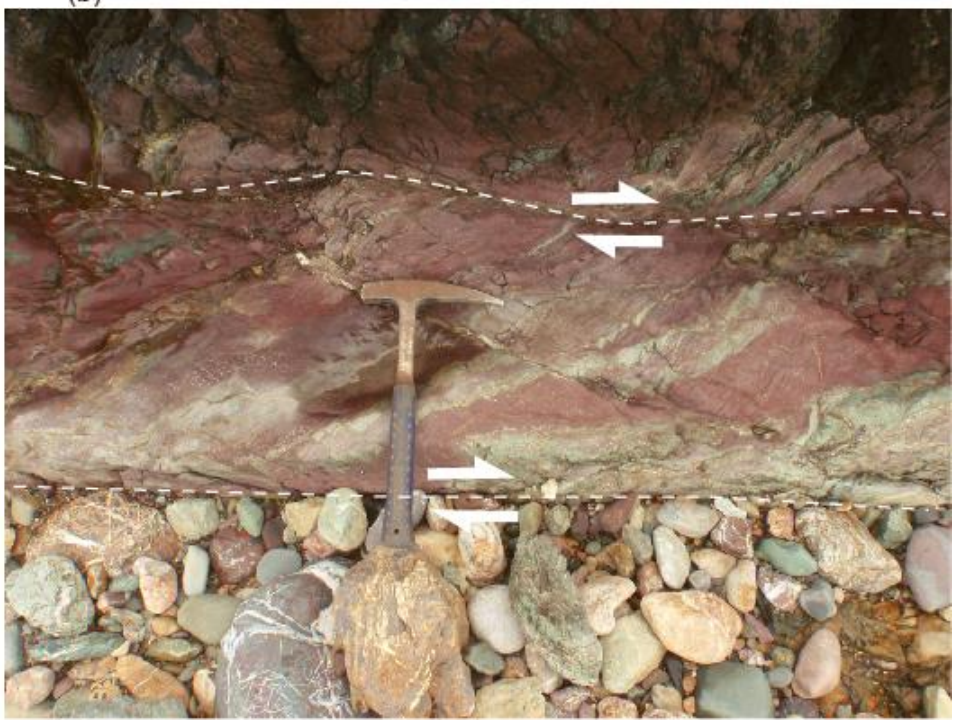

(c)

(d)

(e)

(f)

(g)

(h)

Fig. 2-15 2-15(a): High-angle fault F3 in pillow basalts, 2-15(b): F3 is a right-lateral strike slip fault, 2-15(c): banded red claystone and chert layer, 2-15(d, e, g): Right lateral F2 fault in red claystone,

2-15(f, h): duplex fault (F1) in bedded red claystone.

2-2-2-5. Porth Oer

Figure 2-16 is the geological map in the northeast area of Porth Oer. Most of Porth Oer is covered by red claystones and basalts with minor turbidites and dolostones. The reconstructed lithostratigraphy shows OPS. Lithofacies in the southern side of Ystum Fault have different characteristic from the northern side, mainly composed of basalt. Most of basalts in the southern side were altered and deformed; however, some part of basalts maintain pillow or sheet structures. There are many faults in this area. The faults can be divided into three; 1) Northwest faults (F3). 2) East strike faults (F1). The area of Fig 2-16b probably shows reworked duplex structure. The layers between the northwest faults consists of basalts, red claystones and dolostones, showing repeated lithologies (section 14, 15, 16). In addition, these three sections have layer-parallel thrusts (F1) and pillow basalts with southern top structure. These trends suggest duplex structure. It is difficult to find red claystones maintaining clear depositional structure because of alteration, recrystallization or weathering (Fig. 2-17 (c)). In the northern area, calcite veins with net-like structure in red claystones are present, just like the red claystones in Porthorion (Fig 2-17 (b)). The massive dolostone blocks (Fig. 2-16), that crop out across 50×50m area, involve in the red claystones with net-like calcite veins. On the other hand, dolostones with 1-2 m thickness crop out in section 14, 15 and 16. The turbidites in the northern side consist of alternated sandstone and mudstone (Fig. 2-17 (a)).

The 2 m thick red claystone overlies the basalt in the west side (section 17). The acidic tuff with 3 cm thickness is observed in lower part of red claystone. So, I collected

tuff sample to analyze the U-Pb zircon age (LLY38).

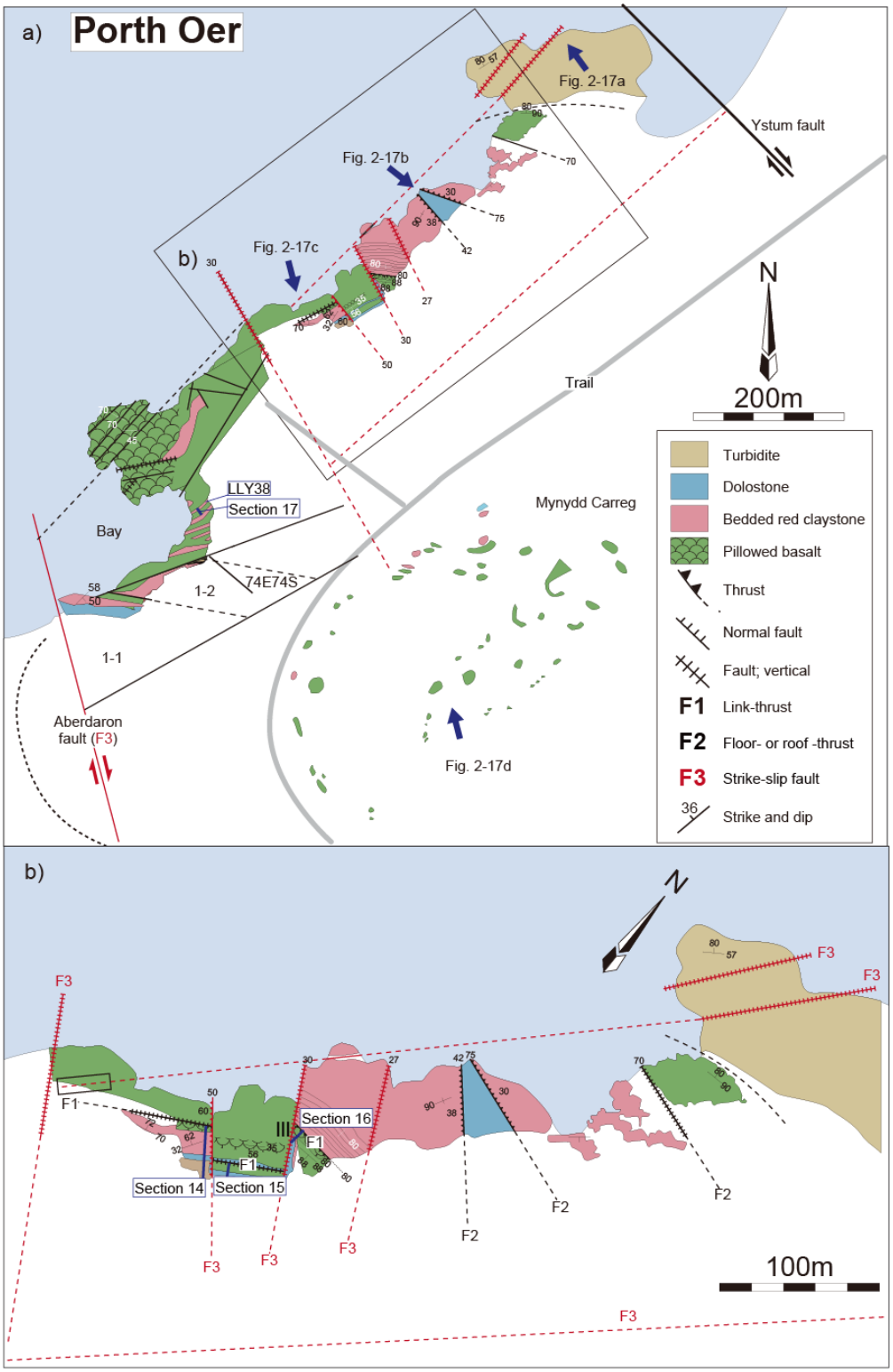

Fig. 2-16 Geologic sketch map of Porth Oer. (a) Upper figure shows the geology along the coast and on-land hill with Mynydd Carreg. (b) Lower figure is the enlarged portion of box in (a). The locations of field photo in Fig. 2-17 are shown. Stratigraphic columns in section 14 to 17 are

reconstructed (Fig. 2-29).

(a)

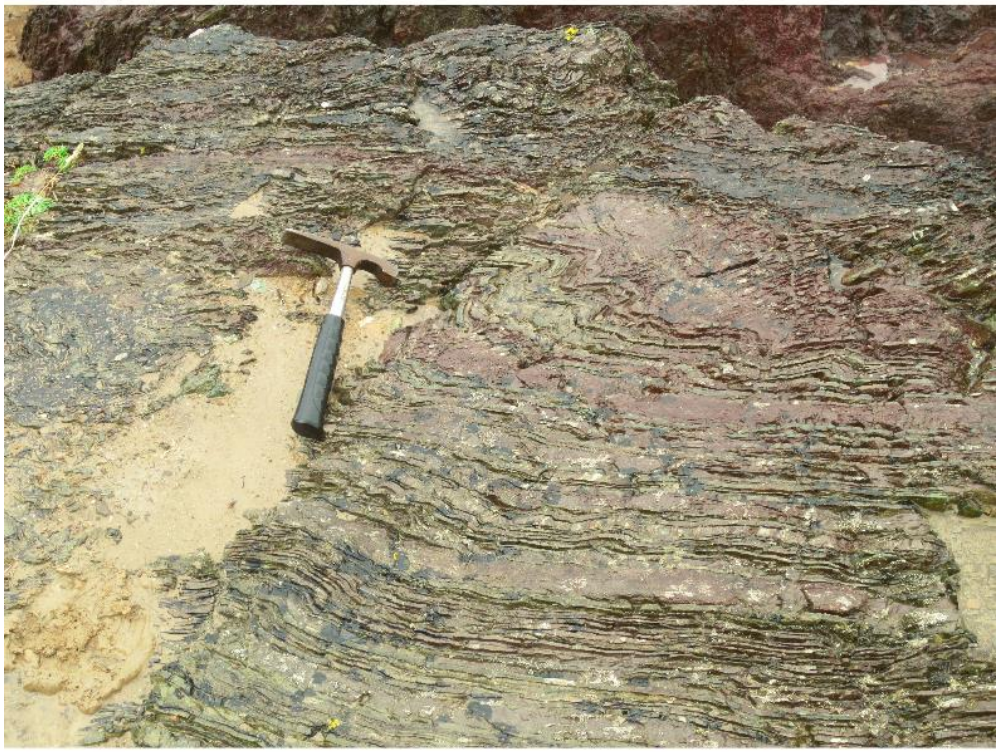

(b)

(c)

(d)

Fig.2-17 Field photos 2-17(a): bedded chert in north Porth Oer (Fig. 2-16), turbidite area, 2-17(b): boundary of weathered dolostone and red claystone, 2-17(c): bedded chert on the right and turbidite

on the left 2-17(d): highly weathered pillow lava pile on the hill. The shape of pillow remains well.

2-2-2-6. South Porth Lago

Figure 2-18 is geological map and cross section in the northeast area of South Porth Lago. There is ca. 500 m thick greenstone with pillow and sheet flow structure in south from east-west fault (Fig.2-18). The most of faults in this area have northeast strike and high angle dipping, but some of the faults show north-south strike. In addition, syncline is observed in middle of this area (Fig. 2-19 (a)). In the northern area, ca. 10 m thick red bedded claystone is weathered. Pillow structures of basalts represent north-top direction in the northern area, but south-top in the middle and southern areas.

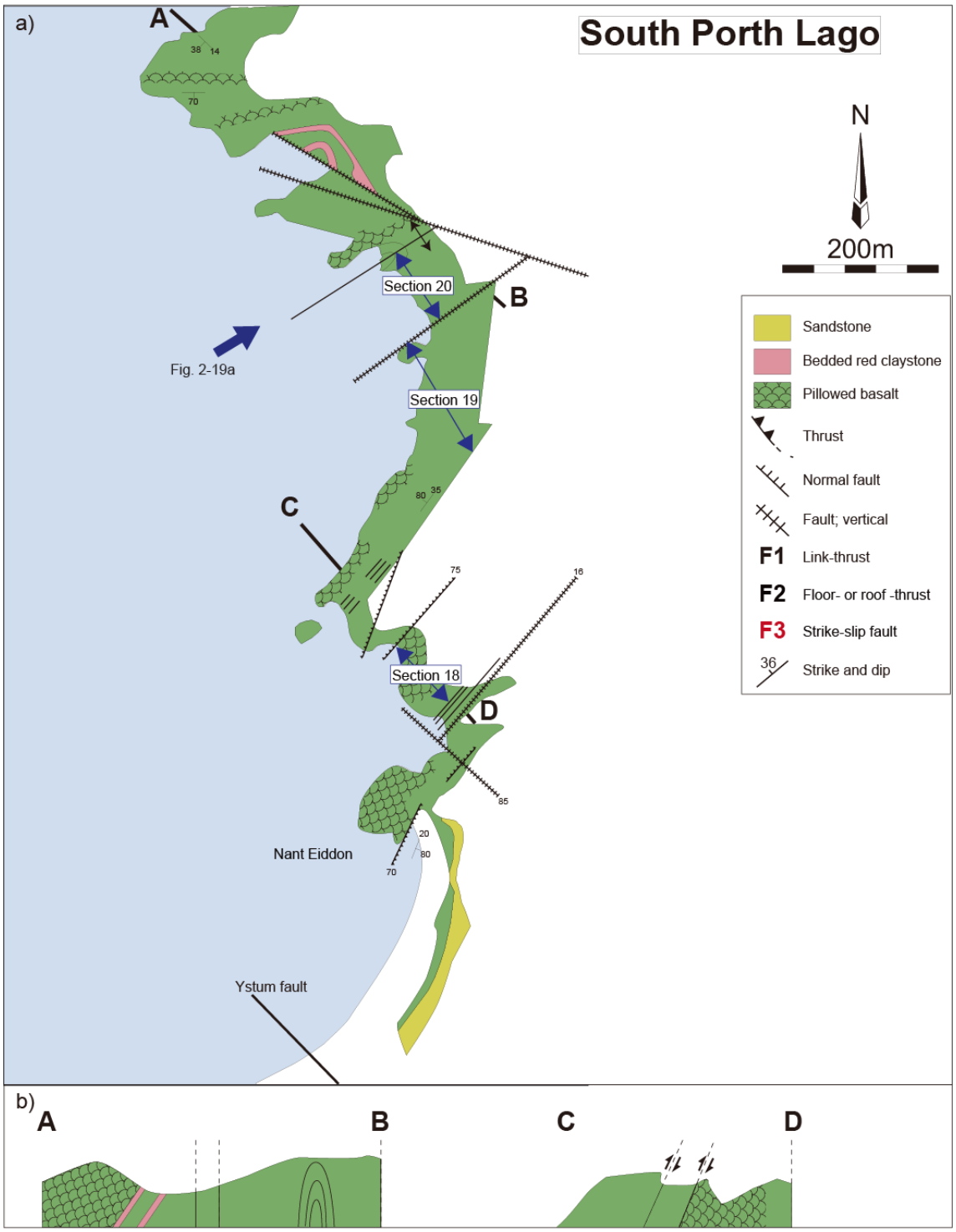

Fig. 2-18. Geologic sketch map of South Porth Lago. Note the reconstructed OPS in the middle right inset figure. Location of field photos is shown (Fig. 2-19 a). The cross section along A-B-C-D is also shown. Stratigraphic columns of section 18 to 20 are reconstructed (Fig. 2-30).

(a)

(b)

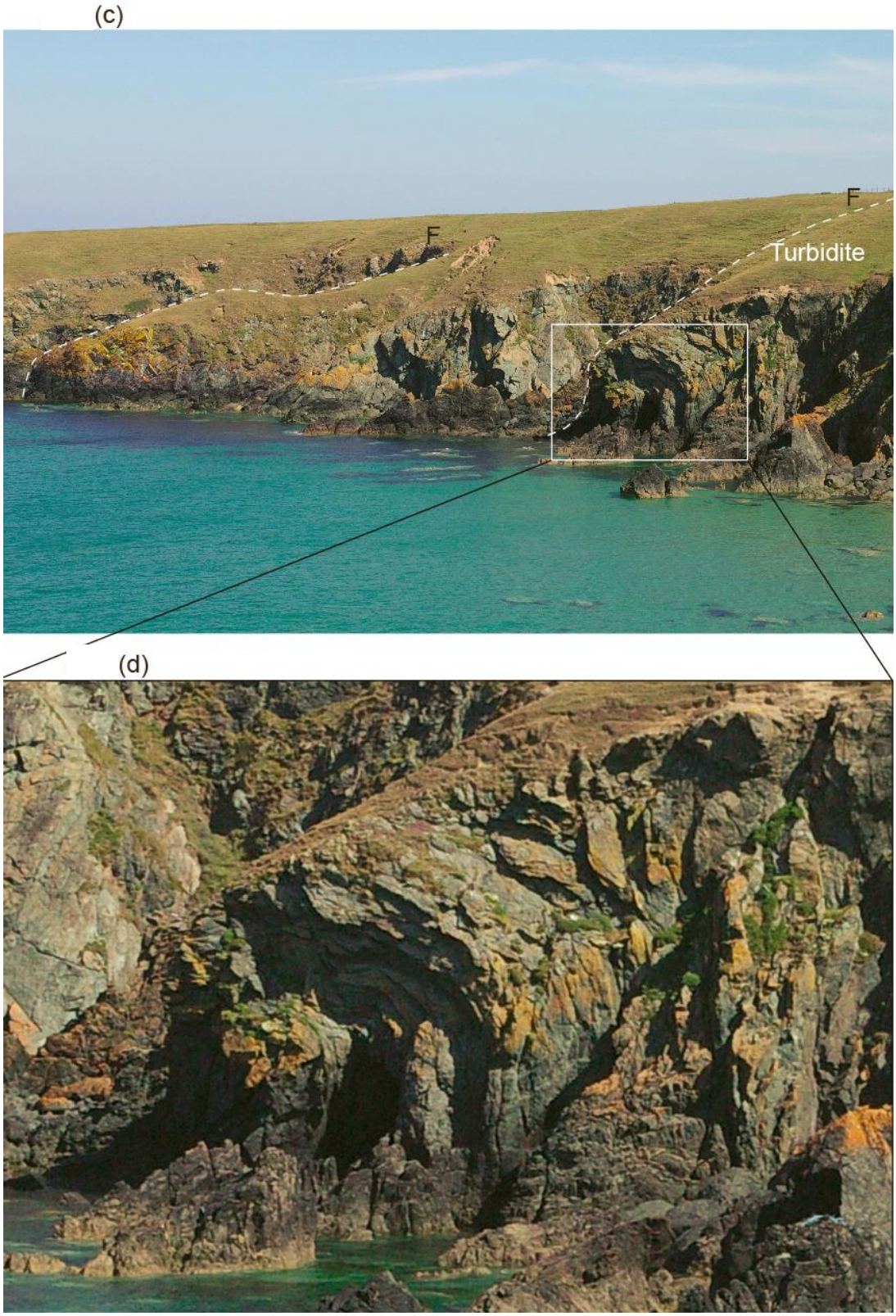

Fig. 2-19. Outcrop photos of the North and South Porth Lago. 2-19(a): Subhorizontal clastic unit of alternating sandstone and mudstone. 2-19(b): Mudstone-dominated turbidite with intercalated

sandstone. 2-19(c, d); vertical fault and synclinal structure of pillow basalts.

2-2-2-7. North Porth Lago

Figure 2-20 is the geological map and cross section in North Porth Lago. Layer-parallel thrusts have 50-70E strike (F1). The north area consists of turbidite, silicious sandstone, gray mudstone and dolostone. Turbidite layers have parallel strike to the faults with 50-70E strike and dipping to the north about 60-70 degree. The turbidite consists of sandstone with 1-10 cm thickness and thin mudstone with 0.2-1 cm thickness (Fig. 2-19 (b)). In addition, there are some silicious sandstone layers or lenses with 0.1-3 m thickness in the turbidite (Fig. 2-19 (a)). These lithological features are similar to the southern area in Porthorion.

The south side of the beach mainly consists of turbidite with smaller amount of red claystone and basalt (section 21, 22). The strike and dipping of these rocks and layer-parallel thrusts are similar to the northern area. The red-purple claystone has clear bedding and 20 m thickness. In the section 21, the turbidite layers have 20 m thickness in maximum, and a part of the turbidite changes to green-gray color by alteration. Basalts in Section 21 and the southern end have north-top pillow structure, such as basalts of the northern area in South Porth Lago. Stratigraphic columns of section 21 to 24 were reconstructed (Fig. 2-31). And, I collected the sandstone samples for the U-Pb zircon dating (IR731, LLY154b).

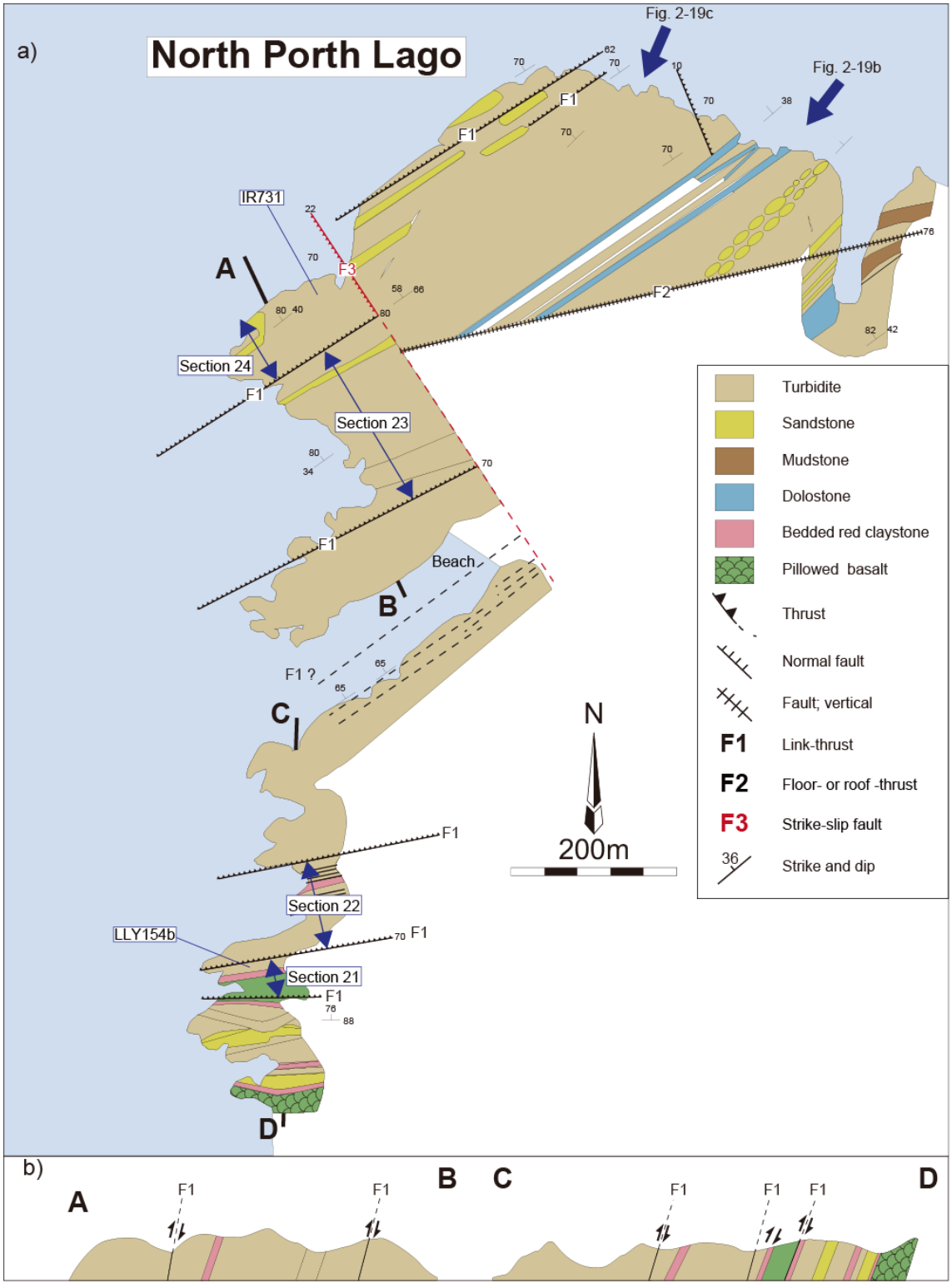

Fig. 2-20. Geologic map along the coastline of North Porth Lago. The reconstructed OPS is shown in the middle right inset figure. Cross section along A-B-C-D is shown on the bottom. Also note the location of field photos (Fig. 2-19 b, c). Stratigraphic columns of section 21 to 24 were reconstructed (Fig. 2-31).

2-2-2-8. Penrhyn Nefyn Peninsula (BS and Gwna Group to the west)

Penrhyn Nefyn Peninsula is a small Peninsula at the NE of Lleyn Peninsula where BS unit occurs close to the Gwna group. The protoliths of the blueschist facies metamorphic rocks on Penrhyn Nefyn Peninsula are basic greenschist (basalt), chert, carbonate and mafic mudstone (phengite schist). The OPS reconstructed by the stratigraphic sequence of pillow basalt, red claystone and turbidite was described by Kawai et al. (2007). The zircons separated from turbidite sandstone LLZ595 showed the youngest age.

2-3. Lithology, Geochronology and OPS

Through detailed field mapping in Lleyn, I collected rock samples systematically and analyzed the geological age of each groups to unfold the tectonic history of Lleyn. On the basis of the dating results, I will describe the evolutionary process of this area.

2-3-1. Method of geochronology

We separated zircons from the tuffs and sandstones. The zircons were extracted using a mineral separation system at the Tokyo Institute of Technology, and were then mounted on 10 mm epoxy discs. The zircons were polished until the midsections of the grains were exposed. Final polishing was performed with a 0.25 μm diamond paste. Cathodoluminescence (CL) images were obtained using a JEOL JSM-5310 scanning electron microprobe combined with an Oxford cathodoluminescence system at the Tokyo Institute of Technology. The detailed analytical method is described elsewhere (Iizuka et al., 2005, 2007). The zircons display various internal structures; oscillatory

zonation, inherited cores, dull structures, mottled structure and overgrowths. The internal structures are empirically used to identify the igneous origin and to evaluate the influence of alteration and late-stage thermal modification. The CL images show that ca. 30 % of zircons from the tuff beds have oscillatory rims and inherited cores with white dusty structures or dull structures and ca. 70 % of the zircons display no zonation or mottled structure. Although some magmatic zircons also display dull structures, metamorphic or re-crystallized zircons commonly show these textures. In addition, many zircons contain mineral inclusions, which we checked under a microscope, and thus were able to avoid mineral inclusions during the U-Pb isotope analyses. We analyzed U-Pb ratios of the oscillatory rims to determine the igneous age of the individual grains from the tuffs and sandstones.

In situ zircon U-Pb dating was carried out using a Nu AtttoM single-collector ICP-MS (Nu instruments, Wrexham, UK) coupled to a NWR-193 laser-ablation system (ESI, Portland, US), that utilizes a 193 nm ArF excimer laser, at Department of Geology and Mineralogy, Kyoto University. The laser was operated with an output energy of ~4.4 mJ per pulse, repetition rate of 8 Hz and laser spot size of 15-25 μm in diameter, providing an estimated power density of the sample of < 3.0 Jcm^{-2}. The pulse count was 140 shots. The ablation occurs in helium gas within the micro cell of < 1ml, and then the ablated sample aerosol and helium gas were mixed with argon gas downstream of the cell. The helium minimizes redeposition of ejecta or condensates while argon provides efficient sample transport to the ICP-MS (Eggins et al., 1998; Gunther and Heinrich, 1999; Jackson et al., 2004). The signal-smoothing device was applied to minimize the introduction of large aerosols into the ICP, reducing signal spikes (Tunheng and Hirata, 2004).

The ICP-MS is optimized using continuous ablation of a 91500 zircon standard (Wiedenbeck et al., 1995, 2004) and NIST SRM 610 to provide maximum sensitivity while maintaining low oxide formation (ThO/Th < 3-5%). Data were acquired on seven isotopes, ^{202}Hg, ^{204}Pb, ^{206}Pb, ^{207}Pb, ^{208}Pb, ^{232}Th, and ^{238}U using a low-resolution deflector jump mode, which measures the signal intensity at the peak top.

Background and ablation data for each analysis were collected over ~100 and ~10 seconds, respectively. Backgrounds were measured with the laser shutter closed and employing identical settings and gas flows to those used during ablation. Data were acquired consisting of multiple groups of 10 sample unknowns bracketed by quartets of 91500 zircon standard (Wiedenbeck et al., 1995, 2004) following single background analysis.

^{202}Hg was monitored to correct the isobaric interference of ^{204}Hg on ^{204}Pb. To reduce the isobaric interference, an Hg-trap device with an activated charcoal filter was applied to the Ar make-up gas before mixing with He carrier gas (Hirata et al., 2005). Prior to each individual analysis, regions of interest were pre-ablated using a few pulses of the laser with laser spot size of xx μm in diameter to remove potential surface contamination, dramatically reducing common Pb contamination (Iizuka and Hirata, 2004). 204 intensities of background and samples are 250 cps and 800 cps, respectively. Most of 204 intensity for background is Hg, as indicated by a background ^{202}Hg/^{204}Pb ratio indistinguishable form natural Hg, ^{202}Hg/^{204}Hg=29.863/6.865 (*confirm it*). When ^{204}Pb data for unknown sample was obtained and a sample has a discordant age without common Pb correction, common Pb correction was applied to the sample following the two-stage model of Stacey and Kramers (1975). The maximum level of the correction was fourth time. If the sample required more than the maximum level of correction, the

age of sample was discarded. The effect of the common Pb correction was factored into the analytical errors on the ages.

All data reduction including the common Pb correction was conducted off-line using in-housed excel spreadsheet. Background intensities were interpolated using an averaged value among two background data acquired before and after each unknown sample groups. The mean and standard error of the measured ratios among each eight 91500 zircon standard data bracketing unknown sample groups were calculated, and the mean and standard error measured for 91500 zircon standard were applied for age estimate and uncertainty propagation. All uncertainties are quoted at the 2 sigma level. ^{235}U was calculated from ^{238}U using a $^{238}U/^{235}U$ ratio of 137.88 (Jaffey et al., 1971).

2-3-2. Result

2-3-2-1. U-Pb ages of tuff zircon grains in Lleyn

All analytical data with LA-ICP-MS are summarized in Tables 2-1 and 2, respectively. The U-Pb Concordia diagrams ($^{207}Pb/^{235}U$ versus $^{206}Pb/^{238}U$) of zircons are presented in Figure 2-21. We monitored ^{204}Pb during the analyses by LA-ICP-MS and excluded zircons with detectable ^{204}Pb from Table 2-1, since the ^{204}Pb is not radioactive in origin. The results of zircons plot on the concordia curve within analytical 2σ error represent the true igneous age of the tuff bed (Fig. 2-21). The zircons of LLY600 in Porth Felen SW Coast show 630 ± 8 Ma (MSWD = 4.6) and 632 ± 11 Ma (MSWD = 1.4) using weighted mean $^{206}Pb/^{238}U$ and $^{207}Pb/^{235}U$ ages, respectively. On the other hand, the zircons of LLY38 in Porth Felen SW Coast show 619 ± 7 Ma (MSWD = 1.5) and 617 ± 6Ma (MSWD = 9.2) using weighted mean $^{206}Pb/^{238}U$ and $^{207}Pb/^{235}U$ ages, respectively. Therefore, the results of tuff zircons in Porth Felen SW Coast indicate ca.

630 Ma in agreement within an error. Moreover, the zircons of UKY20 in Mynydd Carreg show 635 ± 16 Ma (MSWD = 6.7) and 640 ± 12 Ma (MSWD = 0.8) using weighted mean $^{206}Pb/^{238}U$ and $^{207}Pb/^{235}U$ ages, respectively. The ages mean similar with the zircons in Porth Felen SW Coast.

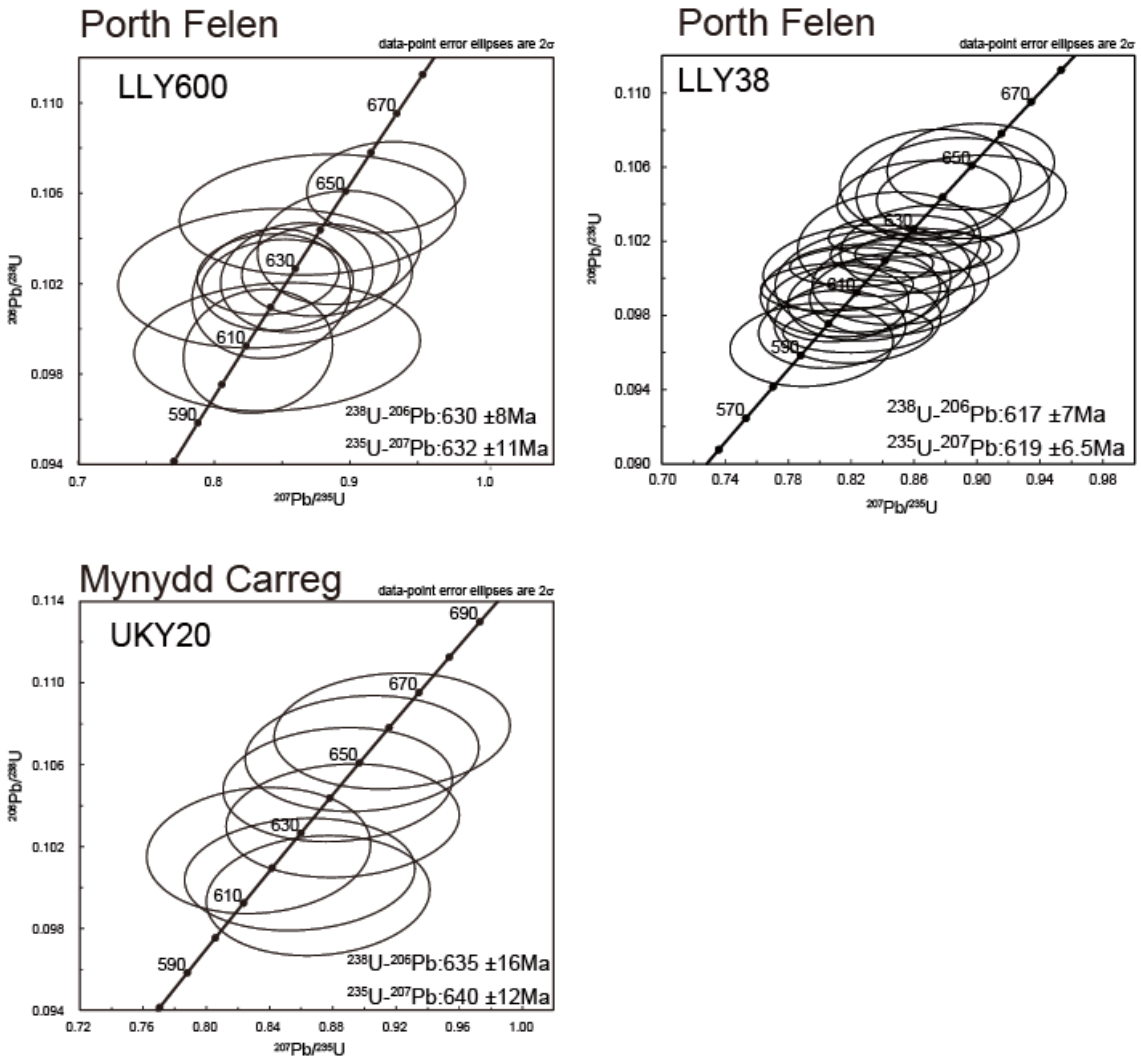

Fig. 2-21. The U-Pb concordia diagrams from tuff layer in Lleyn.

2-3-2-2. Age spectrum of detrital zircon grains from sandstone in Lleyn

The results of U-Pb dating of detrital zircons from sandstones and igneous zircons from tuffs by LA-ICP-MS are listed in Table 2-2. Most zircons from the sandstones are

rounded and show oscillatory zoning under CL images. Some zircons contain an inherited core. However, no systematic differences of the CL images and shapes of zircons were detected in each age population.

In eight samples of Lleyn (LLZ595 50, LLY154b, IR731, LLY377, LLY464, LLZ273, LLZ277 20 and LLZ298), age of zircons from sandstone is analyzed. The nine samples consist of Gwna Group. The results of zircons from nine samples plotted on a Concordia curve within 2σ error show 59, 94, 60, 81, 16, 9, 28, 40 and 13 grains, respectively. The number of disconcordance in IR731, IR738, LLY377, LLY464 and LLZ298 shows more than 10 % of all analysis of zircons, indicating a possibility of Pb loss. Moreover, the youngest ages of LLZ595 50, LLY154b, IR731, LLY377, LLY464, LLZ273, LLZ277 20 and LLZ298 are 628 ± 29, 572 ± 11, 608 ± 16, 610 ± 10, 637 ± 13, 558 ± 13, 541 ± 16 and 549 ± 14 Ma (Fig.2-22, 23, 24). Therefore, the youngest ages in the results show three distinct ages, ca. 630, 610, 550 Ma. The youngest age suggest later deposition. The Gwna Group in Lleyn was deposited during ca. 630- 540 Ma.

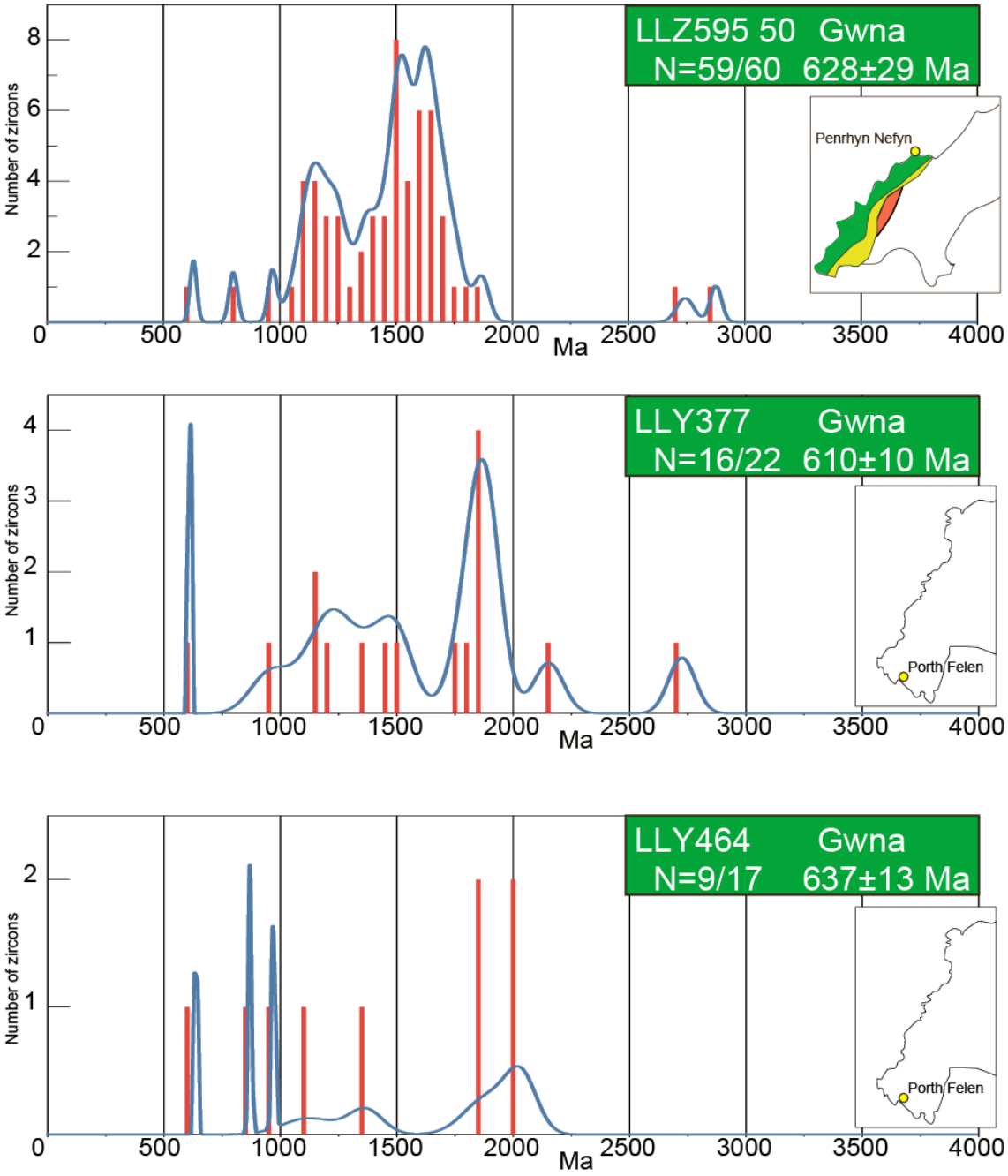

Fig. 2-22. Age distributions of detrital zircons from sandstones in Lleyn, Gwna Group.

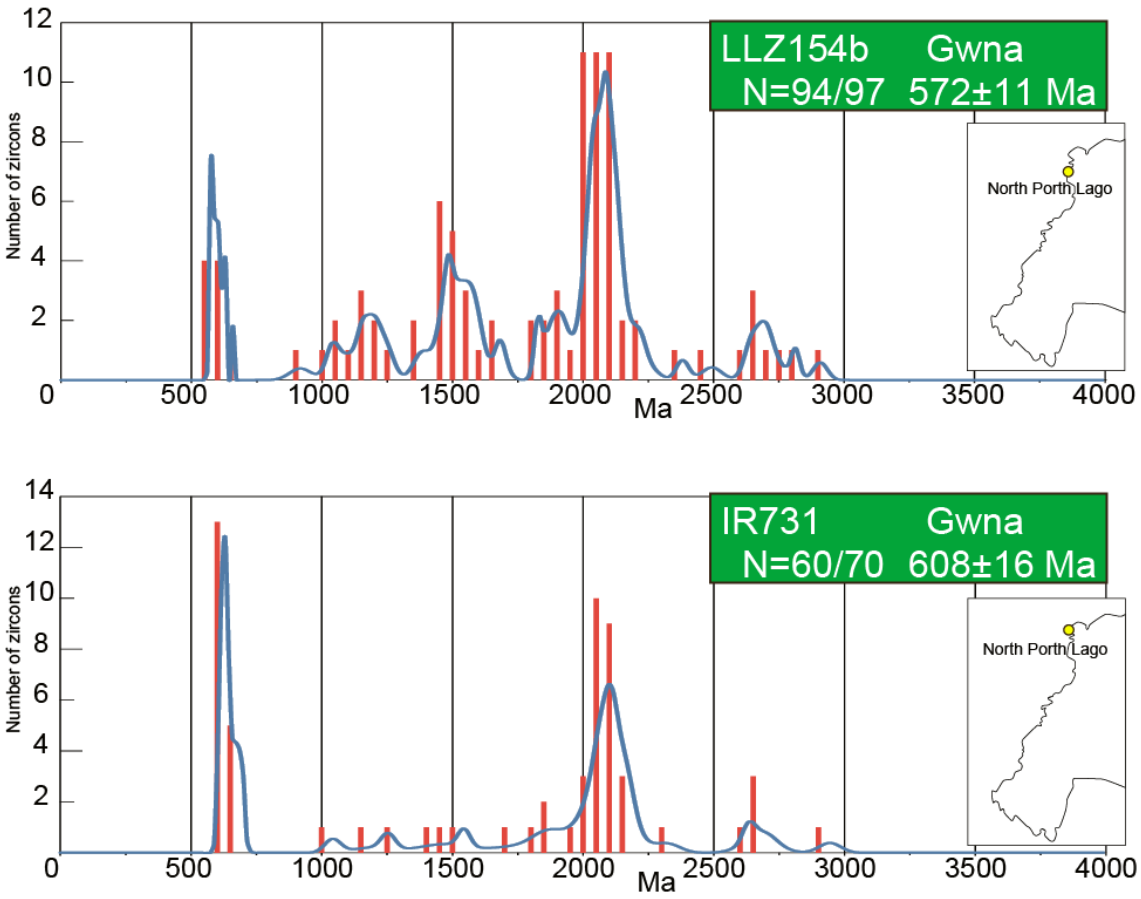

Fig. 2-23. Age distributions of detrital zircons from sandstone in Lleyn, Gwna Group.

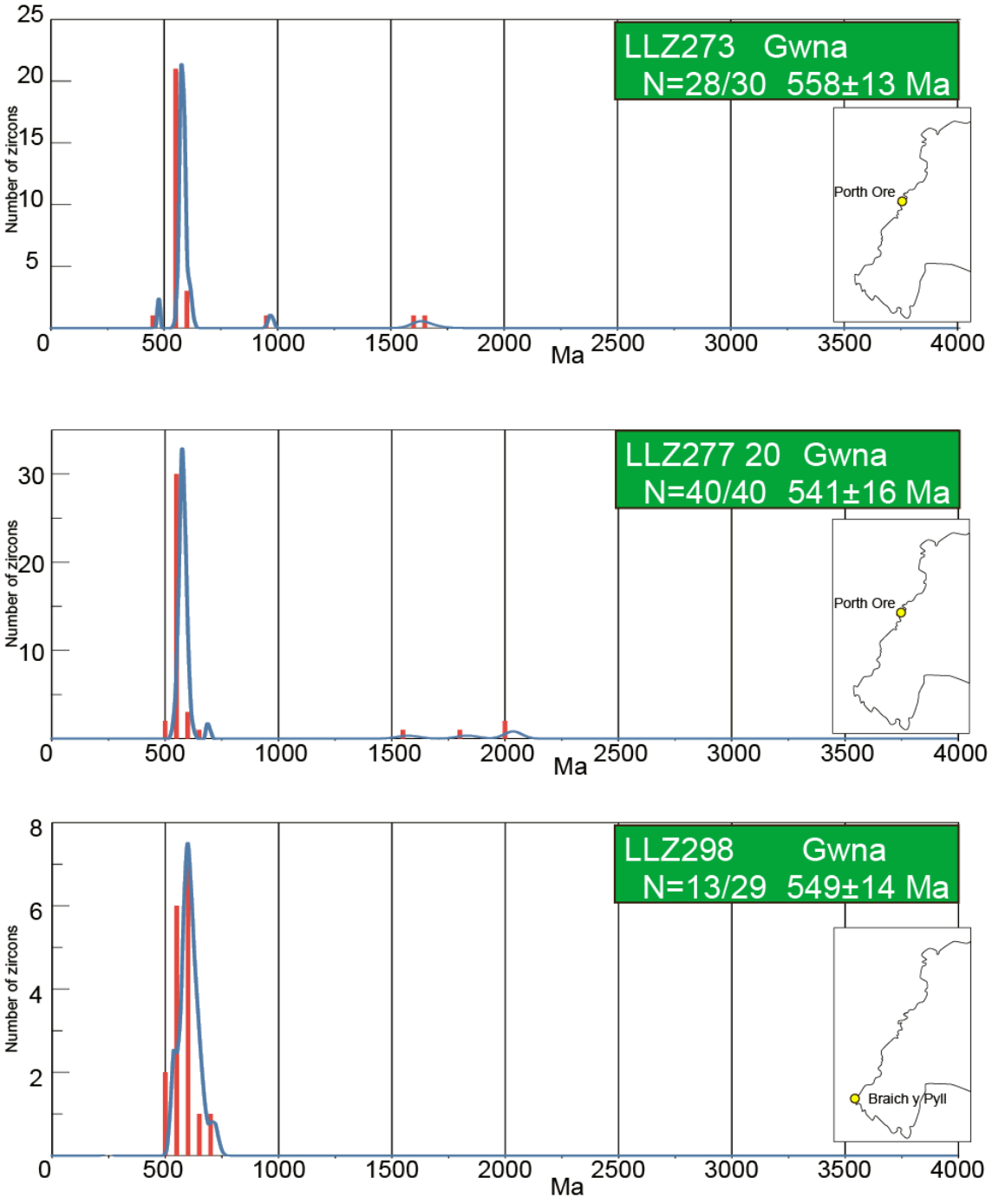

Fig. 2-24. Age distributions of detrital zircons from sandstones in Lleyn, Gwna Group. Only peak on 500-600 Ma is observed.

2-3-3. Reconstructed geological columns and depositional age

2-3-3-1. Porth Felen Southwest Coast

Porth Felen SW Coast is located in Lleyn Peninsula (Fig. 2-4). In this area, geological survey was conducted and the detailed geological map was made (Fig. 2-5). In addition, stratigraphic columns are reconstructed from five sections (Fig. 2-25). The following paragraphs mention the details of each section in Porth Felen SW Coast.

In the bottom of section 1, ca. 30 m thick basalts with quartz vein have pillow structure. The 3-7 cm thin red clay layers overlying the basalts show silica-rich layers, including 1 mm shale. The fault on the red claystone is found. The layers on fault consist of ca. 7 m massive dolostone, ca. 1m red claystone, ca. 4 m massive dolostone and red claystone, in ascending order. The upper red claystones are intercalated with shale more frequently than lower red claystones. In addition, there are ca. 4 m thick pillow lava with inter-pillow chert and dolostone. The pillow basalts in this area have similar character to that in Braich y Pwll. Moreover, 2 m red claystones overlie the pillow basalts. The overlying sequence is 3 m dolostone, 2 m red claystone and green tuff layer, in ascending order. Alternated dolostone and red claystone is found on sharp boundary of green tuff. At the top of this area, there is a tuff layer. The red claystones in this area are silica-poor and the laminations are poorly preserved in contrast with Braich y Pwll.

Section 2 has thick turbidite layer. At the bottom, 10 m thick red claystones are present. The red claystones include few chert layers, unlike red claystones in section 1. The ca. 50 m turbidite overlies the red claystones. Most of the pellets in the turbidites show 1-10 cm in size. In addition, a tuff layer in the turbidite is found.

At the bottom of section 3, ca. 10 m basalts with quartz vein have pillow structure, in the same manner as the bottom basalt in section 1. Thin (ca. 1m) red claystone overlies the basalt. Turbidite with ca. 15 m overlies the red claystone. The turbidite

layer has large sandstone boulders (50 cm-1 m) and green chert pebbles. The tuff layer has some cm thickness and is sampled to analyze absolute age. The depositional age of the tuff shows 630 ± 8 Ma by U-Pb dating of zircons.

Section 4 consists of basalt and red claystone, in ascending order. At the bottom, the basalt has ca. 10 m thickness. The ca. 5 m thick red claystone includes chert layers.

In the section 5, ca. 30 m thick basalts with pillow structure are present at the bottom. Red claystone overlies the basalt, similar to the other sections. A massive dolostone (ca. 5 m thick) overlies the red claystone. The uppermost 30 cm of the dolostone show alternation of dolostone (3-8 cm) and shale. The layers on the massive dolostone layer consist of ca. 7 m thick black mudstone, ca. 1 m thick red bedded chert and thick turbidite, in ascending order. The black mudstone can be divided into 3 parts; from the bottom to the top, (1) alternating dolomitic carbonate with black mudstone, over mm to cm scale (>50 cm), (2) black mudstone with mm or less layering (< 3 m), (3) pyrite-enriched rather massive with less developed layering occurs (ca. 3 m). Cm-scale sandstone layers are intercalated at the top of the black mudstone and at the top of the turbidite, and were sampled to analyze U-Pb ages. The youngest ages of zircons from these two sandstone layers are 637 ± 13 Ma and 610 ± 10 Ma, respectively.

The OPS in Porth Felen SW Coast mainly consists of pillow basalt, red bedded chert or claystone, dolostone, black mudstone and turbidite. The black mudstone is rare in Lleyn peninsula, only exposed in section 5 and Mynydd Carreg. The youngest age of 637 ± 13 Ma suggests that the black mudstone was likely deposited during the Marinoan Snowball Earth. Moreover, turbidite overlaying black mudstone have 610 ± 10 Ma from sandstone in same section, and depositional age of 630 ± 8 Ma from tuff in section 3. These results are consistent with the stratigraphic relation between the black mudstone

and the turbidite. On the other hand, the age of turbidite means the approximate time of accretion of the OPS. The OPS in Porth Felen SW Coast was accreted around 630 – 610 Ma.

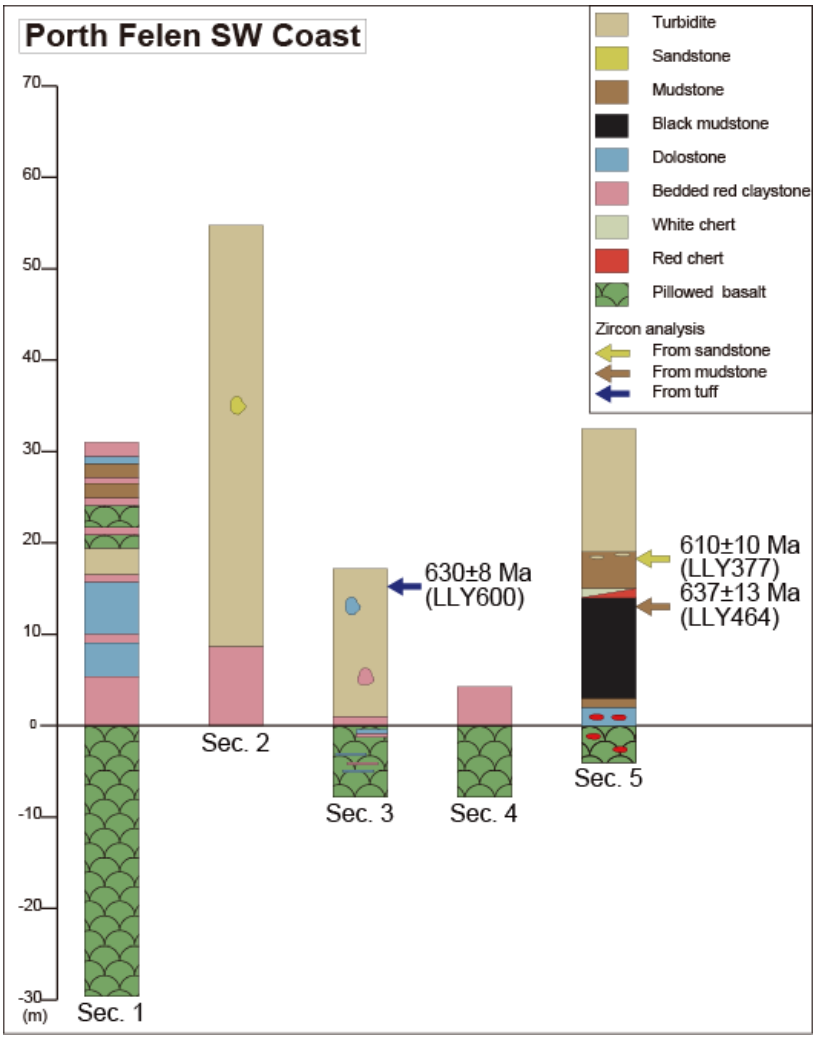

Fig. 2-25. Stratigraphic columns in Porth Felen SW Coast. The location of each section is pointed in Fig. 2-5. Allows show sample horizon for the U-Pb age analysis.

2-3-3-2. Braich y Pwll (Lighthouse and its western cost)

Braich y Pwll is located in western end of Lleyn Peninsula (Fig. 2-5). In this area, detailed geological map is made based on the field survey (Fig. 2-8). In addition,

geological columns are reconstructed for four sections in the northern area (Fig. 2-26). The following paragraphs mention detailed geological characteristics in each section.

In section 6, Fig. 2-26 is the detailed sketch of OPS that is composed mainly of alternating red claystone and grey shale, spanning 2.6 m thick. Red claystones from the bottom to 60cm above are silicified and show pale red color in contrast with the red color of the overlying claystones. The rhythmical alteration is composed of 3-5mm thick red claystone and grey shale less than 1mm. Red claystone from 60cm to 170cm above the base, is muddy than the lower unit, each layer of alternating red claystone and grey shale is 1-5mm thick. Grey shale in the stratigraphic range from 150cm~170cm increases the thickness up to 5mm. From 170cm to 260cm horizon, the red claystone is silicified, and the thickness of red claystone and grey shale ranges 3-5mm and <1mm, respectively. Two thick layers of grey shale is observed in the horizon of 220cm~260cm.

Fig. 2-26 shows the 3.2m thick OPS of Section 7. A sharp layer-parallel fault is present between the two sections. Section 7 is composed of alternating red claystone and pale pink chert, and locally silicified to some extent. The bottom 0-100cm is composed of dominantly red claystone, and the photo shows the representative alternating red claystone. The thickness of red claystone ranges 5cm in the stratigraphic level 0cm~10cm, and 2-3cm from 10cm to 100cm level. Selective deformation is observed at 30cm~40cm stratigraphic levels and recrystallized at 80cm~90cm levels. In the range of 100cm~190cm, red claystone is alternated with thin pink layer of chert. Thickness of red claystone ranges 2.0-3.0cm at level 100cm~150cm, 0.5-1.0cm at 150cm~190cm level. Pale pink chert appears at three horizons, first at 100-110cm, 110-120cm, and 140-160sm, showing the increase of the thickness at upper stratigraphic

horizons. Local recrystallization is observed at 180cm horizon. The stratum at 190 cm ~ 320 cm is alternating thin pink bedded chert. Pale pink chert is 3cm-6cm thick. The pink cherts from the lower 3 horizons are silicified and compact, whereas in the upper 190cm~320cm pink cherts include carbonated parts. At 310cm horizon, cherts are relatively deformed. Zircon dating was practiced to date separated zircons from shale (LLZ 300) and shale (LLZ298). As a result, the youngest ages of the shales are obtained as 589± 14 Ma and 541 ± 26 Ma, respectively.

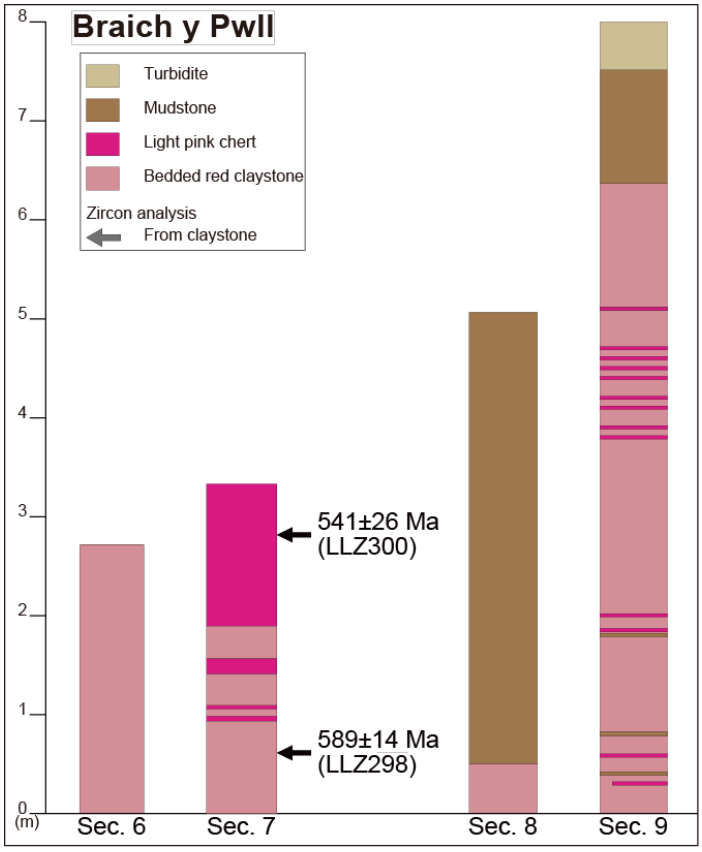

Fig. 2-26. Stratigraphic columns in Braich y Pwll. Each section is pointed in Fig. 2-8. Allows show sampling horizon to analyze U-Pb age.

In section 8, it looks apparently monotonous strata, but the three-dimensional observation indicates the presence of recumbent folding with NE-SW axis that is

parallel to the layer-parallel fault with same NE-SW strike. The OPS was carefully reconstructed. There is a NE-SW trend layer-parallel fault at the bottom of the OPS. The stratigraphical bottom is the alternating red claystones with thin cherts. The lithology changes to the alternating red mudstones and coursing-upward, and to the sandstone. At horizon 0cm~50cm, alternating red mudstone with 1cm~5cm thick is present. At 50cm~200cm horizon, alternating red claystone with sandstone ascends more coarse-grained upward (Fig. 2-11(c)). At horizons 200cm~500cm, sandstone dominates with quartz and mafic minerals and looks pale-green and massive.

Fig.2-26 displays the 8m thick OPS of Section 9. The OPS in Section 9 shows coarsening-upward trend similar to the lower red claystone in Section 8. The lowermost 0m~3m is the alternating red claystone with intercalated grey chert and silicified mudstone. Quartz vein is common at the interval of 2m~3m horizons. Grey chert and silicified mudstone are 1cm~2cm thick. At stratigraphic horizons of 3m~5m is dominated by the grey chert and silicified mudstone, both of which are 1cm~2cm thick. At the stratigraphic level, 5m~8m, pale red mudstone is present, and gradually coarse-grained to sandstone. Grey chert and silicified mudstone were not confirmed and different from the strata at the base lower than 5m horizon. The OPS in Braich y Pwll is mainly composed of red bedded claystone and chert, and mudstone. Basalt does not occur in this area. Well preserved bedded red chert or claystone are present. The youngest age is 541 ± 26 Ma of detrital zircon from shale in upper part of section 7. This age constrains the accretionary age. So, the OPS in Braich y Pwll is accreted around 540 Ma.

2-3-3-3. Mynydd Carreg (Red chert Quarry): Intermediate between Middle and South

Fig.2-27 displays the 6m thick OPS in Section 10 in the Mynydd Carreg. The OPS is composed of black mudstone, mudstone and red chert. The lowermost 0-1.2 m is the alternation of 2-5 cm thick black mudstone and 1-2 cm thick mudstone (Fig. 2-11(d)). 2 m thick grey mudstones, overlying the basalts, are highly weathered and deformed. At the stratigraphic level, 3m, acidic tuff is present between gray mudstone, corrected to analyze U-Pb age. The depositional age of the acidic tuff shows 635 ± 16 Ma by U-Pb analysis of zircons, shown as right above the Marinoan black shale horizon. Stratigraphical top is red chert with 2.5 m thickness. The red chert does not show bedding structure.

The OPS in this section has common lithological features and depositional age with the section 5 at the Windley Point in Porth Felen SW Coast. The section 5 also observed black mudstone and has same U-Pb age (635 ± 16Ma) from upper part of the black mudstone. Moreover, this area has well-exposed basalt, dolostone, black mudstone, white chert and turbidite. Thus, it is suggested that the section 5 and 10 are the same sequence.

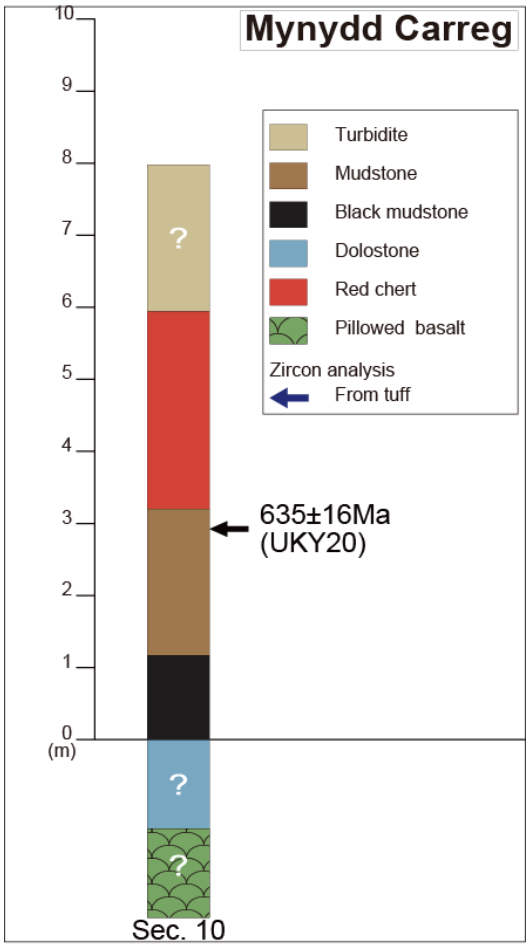

Fig. 2-27. Stratigraphic column in North Porth Lago and South Porth Lago. Each section is pointed in Fig. 2-18 and 20. Allows show sampling horizon to analyze U-Pb age.

2-3-3-4. Porthorion

We reconstruct 3 stratigraphic columns in Porthorion (Fig. 2-28). Studied section 11 is located in the south of Porthorion (Fig. 2-12 and 14). At the bottom of section 11, ca. 2 m basalts shows pillow structure. Bedded red claystone overlying the basalts has ca. 2 m thickness, including shale layers. Bedded green claystone asymptotically overlies the red claystone. It indicates that the green claystone is changed from red claystone by alteration, because the structure of the green claystone shows same structure in the red claystone.

The red bedded claystone has 16 m thickness at the bottom of section 12. The

bedded red claystone includes chert and shale layers, unlike red clay layer in section 11. The mudstone at 4 m from the bottom in the red claystone is sampled to analyze U-Pb age. The youngest age of the mudstone is 558 ± 13 Ma by U-Pb analysis of detrital zircon. In addition, sandstone layer is found on the red claystone layer.

Section 13 consists of bedded red claystone layers in the middle part of Porthorion. The layers show alternation of chert and red claystone, likely the red bedded claystone in section 12. In addition, a mudstone layer at 2 m from the bottom in the red claystone is sampled to analyze U-Pb age. The youngest age of the claystone is 541 ± 16 Ma by U-Pb of zircon.

In this region, the OPS is mainly composed of basalt, thick beded redclaystone and sandstone. The youngest age of the claystone is about 560-540 Ma, similar age in Braich y Pwll. In addition, both this area and Braich y Pwll exposed large size olistolith. As a result, it indicates that the OPS in both areas were deposited and accreted around the same time.

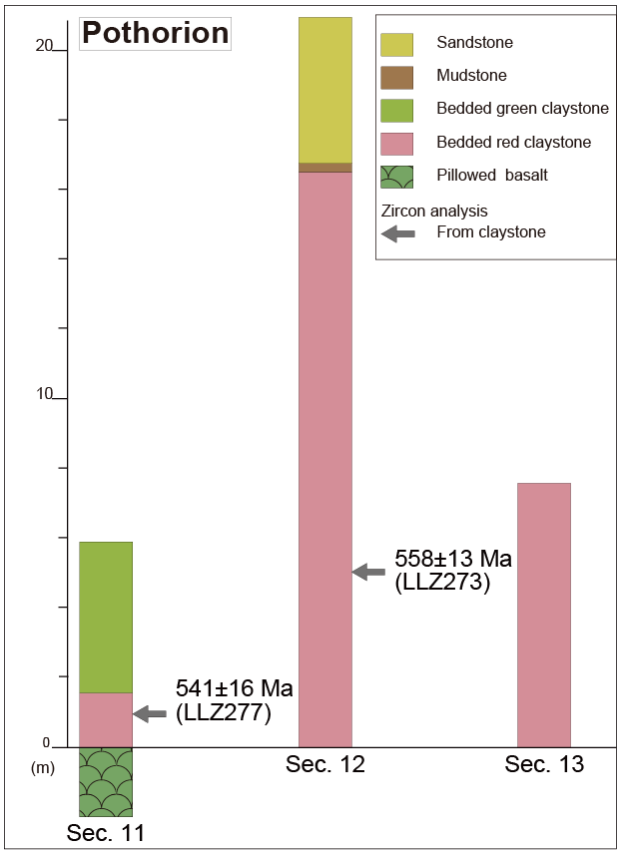

Fig. 2-28. Stratigraphic column in Porthorion. Each section is pointed in Fig. 2-12 and 14. Allows show sampling horizon to analyze U-Pb age.

2-3-3-5. Porth Oer

In the Porth Oer area, four geological columns of reconstructed oceanic plate stratigraphy are made (Fig. 2-29). Basalt, red claystone, dolostone and turbidite are exposed in this area. At the bottom of section 14, basalts have pillow structure. Bedded red claystone on the basalts is ca. 7 m thick, including chert and shale layers. This red claystone shows remarkable alteration. The layers on the red claystone consist of massive dolostone (ca. 3 m) and turbidite.

Section 15 consists of basalt and dolostone. The basalt and dolostone layer have same structure as section 14.

The thick basalt has 13 m thickness at the bottom of section 16. The basalt shows

pillow structure. The sequence overlying the basalt consists of bedded red claystone (1 m) and dolostone (3 m), in ascending order. The red bedded claystone includes chert and shale layers. In addition, the dolostone shows massive to like the structure in section 14.

In section 17, basalt and red bedded claystone are present at the bottom, in ascending order. The basalt shows pillow structure, similar to the other sections in Porth Oer. Moreover, a tuff layer with 4 cm is found in the red bedded claystone. The tuff at ca. 3 m from the bottom in the red claystone is sampled to analyze U-Pb age. The depositional age of the tuff is 619 ± 7 Ma.

In this region, the OPS mainly comsists of basalt, red beded claystone, dolostone and turbidite. The depositional age of the tuff is 619 ± 7Ma at the bottom in the red claystone. And, this area does not contain black mudstone like the outcrop in Porth Felen SW Coast. So, this area was likely accreted after Porth Felen SW Coast and Mynydd Carreg. On the other hand, the lithological characteristic in this area is also different from the Braich y Pwll and the Porthorion. The arrival time of oceanic lithosphere to trench in Braich y Pwll and Porthorion accreted about 560-540 Ma, obviously younger than the depositional age in Porth Oer. Thus, the accretionary age in Porth Oer is older than the Braich y Pwll and Porthorion.

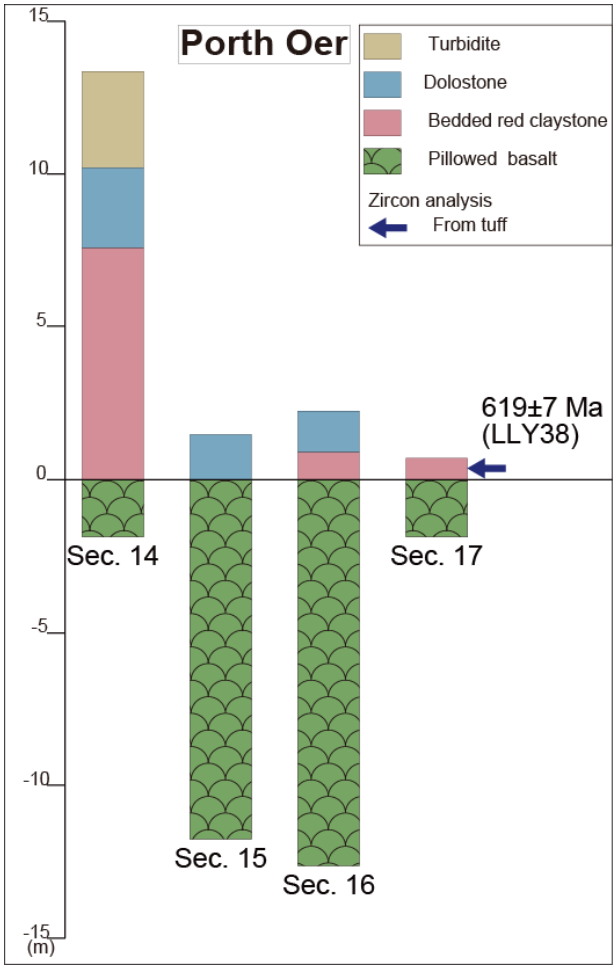

Fig. 2-29. Stratigraphic column in Porth Oer. The sections are pointed in Fig. 2-16. Allows show sampling horizon to analyze U-Pb age.

2-3-3-6. Porth Lago

In the South Porth Lago area, three stratigraphic columns are made (Fig. 2-30). The area mainly consists of basalts. The sections 18-20 have ca. 110 m, ca. 190 m and ca. 90 m thickness, respectively. The basalts show pillow structure, similar to the bottom part of the sequence in the Porth Oer area. This area does not have any age constraint.

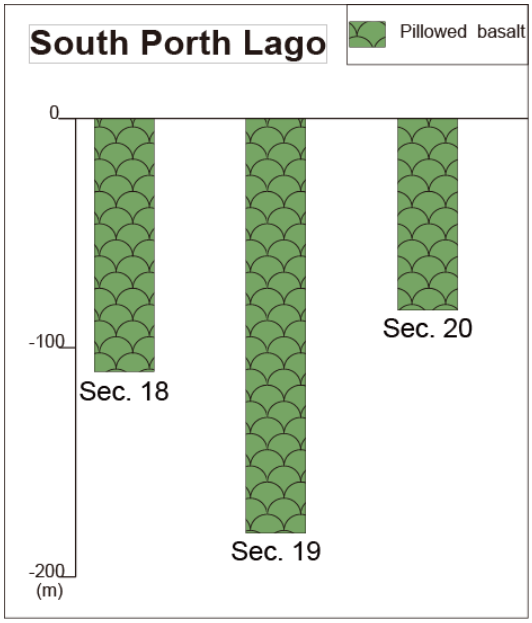

Fig. 2-30. Stratigraphic column in South Porth Lago. Each sections are pointed in Fig. 2-18. Allows show sampling horizon to analyze U-Pb age.

In North Porth Lago area, four geological columns of reconstructed oceanic plate stratigraphy are made (Fig. 2-31). Unlike the South Porth Lago area, thick turbidites are present in this area. At the bottom of section 21, basalts have pillow structure. Remarkable transform can be observed in this basalt layer. Bedded red claystone overlying the basalts has ca. 10 m thickness, including shale layers. The bedded shale-rich red claystone is characteristically observed in this North Porth Lago area. The layers on the red claystone consist of turbidite. The mudstone at 20 m from the bottom in the turbidite is sampled to analyze U-Pb age. The youngest age of the mudstone is 572 ± 11 Ma by U-Pb zircon dating.

Section 22 consists of turbidite and red claystone. At the bottom, turbidite layer has ca. 30 m thick alternation of mudstone (5 mm - 2 cm) and sandstone (1-5 m). Moreover, the turbidite has siliceous-rich layers. Bedded red claystone with intercalated chert and shale layers overlies the turbidite. At the top of this area, turbidite is observed

and has same structure in the lower turbidite.

In section 23, turbidite is observed just like section 22. The turbidite has alternation of mudstone (5 mm - 2 cm) and sandstone (1-5 m), except for thick sandstone (ca. 10 m) at 140 m from the bottom. In addition, the mudstone at the top of the turbidite (ca. 150 m) layer is sampled to analyze U-Pb age. The youngest age of the mudstone is 608 ± 16 Ma by U-Pb zircon dating. Therefore, the arrival time of oceanic lithosphere to the trench is 572-608Ma for North Porth Lago.

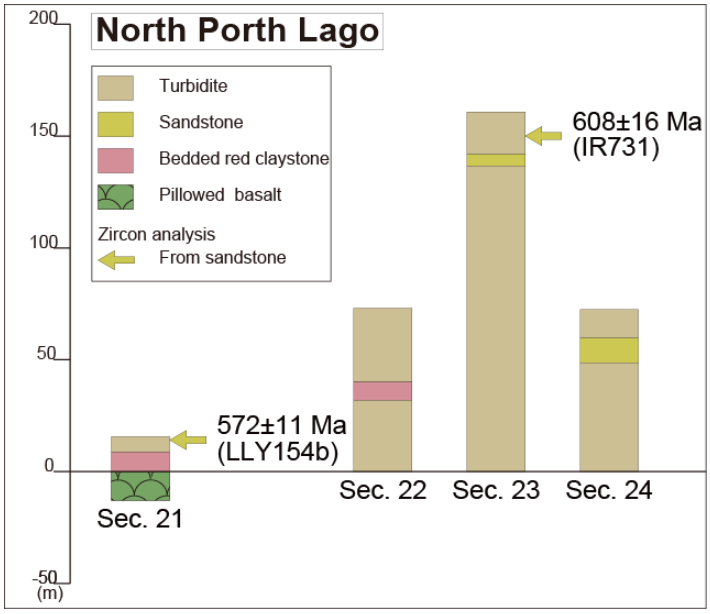

Fig. 2-31. Stratigraphic column in North Porth Lago. Each section is pointed in Fig. 2-20. Allows show sampling horizon to analyze U-Pb age.

In section 24, turbidite is observed just like section 23. The turbidite has alternation of mudstone (5 mm - 2 cm) and sandstone (1-5 m), except for thick sandstone (ca. 15 m) at 140 m from the bottom. The sandstone shows siliceous-rich.

2-3-3-7. Penrhyn Nefyn Peninsula

A unit of blueschist facies metamorphic rocks (which include glaucophane-phengite schists - Gibbons, 1981) crops out on the Penrhyn Nefyn Peninsula on the northern coast of Lleyn peninsula (Kawai et al., 2007). The protoliths of the blueschist facies metamorphic rocks on Penrhyn Nefyn Peninsula are basic greenschist (basalt), chert, carbonate and mafic mudstone (phengite schist).

In Penrhyn Nefyn Peninsula area, geological column of reconstructed oceanic plate stratigraphy are figured in Fig. 2-32. At the bottom of section 25, basalts have pillow structure. The pillow basalts are flattened and deformed extensively and contain high-pressure minerals such as barroisite, crossite, lawsonite, phengite, as well as actinolite, epidote, chlorite, albite, sphene, carbonate and quartz. Yet, the thin chilled margins, the vesicles cemented by carbonate and quartz, and the pale-green, less competent glassy matrix are clearly distinguishable from the dark green cores of the pillows. Red chert layers on the basalts have ca. 10 m thickness, including many lenses up to 2 m-long. The chert layer record a 2 m-thick bed of red chert, central lenses of chert and limestone, to upper lenses of quartzite in ascending order. The layers on the red chert consist of mudstone and sandstone. The mudstone shows ca. 20 m. The thick sandstone shows ca. 40 m. The sandstone at 60 m from the bottom is sampled to analyze U-Pb age. The youngest age of the mudstone is 628 ± 29 Ma by U-Pb zircon dating (Fig. 2-32). This is the oldest known age of turbidites in the Anglesey-Lleyn area.

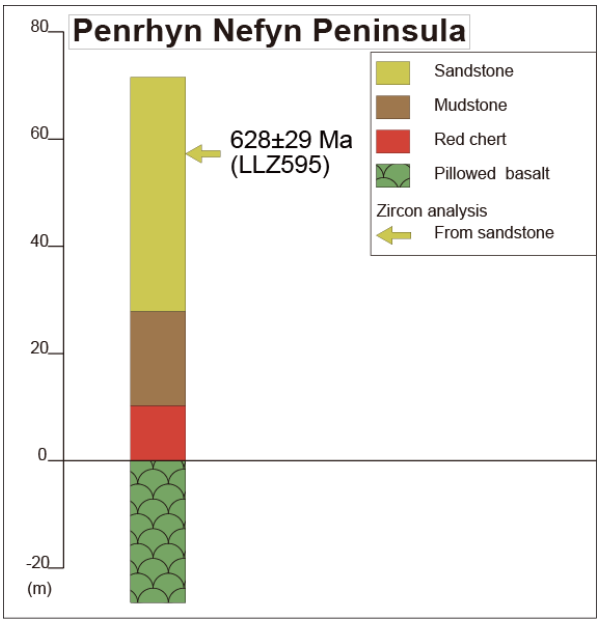

Fig. 2-32. Stratigraphic column in Penrhyn Nefyn Peninsula. Allows show sampling horizon to analyze U-Pb age.

2-4. Discussion

2-4-1. Type of ACs and formed age of the Gwna Group in Lleyn

The chaotic unit in Lleyn Peninsula shows oceanic plate stratigraphy, MORB, chert, claystone, carbonate and turbidite by detailed geological survey. Porth Felen SW Coast area consists of pillow basalt, dolostone, red claystone, turbidite and chert (Fig. 2-5). Especially in Windley Point in the Porth Felen SW Coast area, there was black mudstone (Fig. 2-7). In Braich y Pwll, Porthorion and Porth Oer areas, there are the lithofacies of OPS to like in Porth Felen SW Coast area (Fig. 2-26, 28 and 29). In Mynydd Carreg area, there is large red chert, mudstone and black mudstone, and dolostone and basalt are found by detailed geological survey (Fig. 2-10). In addition, South Porth Lago consists most of pillow basalts (Fig. 2-18), while not only turbidite but also basalt and dolostone are found in North Porth Lago by detailed geological mapping (Fig. 2-20). This observed results suggest these areas consist of accretionary

complex.

Moreover, two-type structures in these areas were found. These are the typical accretionary complex (AC), tectonically mixed with oceanic materials of MORB, OIB, bedded cherts and/or red claystone, with trench turbidites. Some of them are derived from two-step mixing (duplex-type). The one (duplex-type) is tectonic mixing at shallow depth by underplating of duplex-type ACs, and the other (olistostrome-type) is recycled ACs which had once underplated and been pushed up tectonically upward, then gravitationally collapsed. The collapsed ACs were redeposited at trench to be incorporated again into accretionary wedge. This type of ACs is apparently remarkably different in appearance (olistostrome), but the entity is two-fold mixing at trench. In these two-types of ACs, the critical characteristics are, common occurrence of layer-parallel faults, mixed lithology of oceanic materials with continental arkosic sandstone/mudstone, variation of ages of their formation with a systematic order called Ocean Plate Stratigraphy (OPS).

In Windley Point in Porth Felen SW Coast (Fig. 2-7), typically a series of duplex-type deformation is observed, because all of depositional layers are cut by faults. In Porth Felen SW Coast and Porth Oer areas, remarkable duplex structures are found to like the Windley Point (Fig. 2-5, 7, 16 and 17). Therefore, Porth Felen SW Coast and Porth Oer areas belong to duplex-type. In addition, Mynydd Carreg shows common lithofacies with Porth Felen SW Coast (Fig. 2-25 and 27). Although there is no duplex structure, Mynydd Carreg belongs to duplex-type to like in SW Coast. In North Porth Lago and Braich y Pwll areas, there are no duplex structure, but layer-parallel thrusts (Fig. 2-8 and 20). It suggests that the structure is caused by tectonic mixing at shallow depth by underplating of duplex-type accretion. The structure of layer-parallel thrusts

belongs to duplex-type. Therefore, the structures of duplex-type are observed in Porth Felen SW Coast, Porth Oer, Mynydd Carreg, North Porth Lago and Braich y Pwll areas. On the other hand, olistostrome-type indicates recycled ACs which had once by underplated and pushed up tectonically upward, then gravitationally collapsed to deposit at trench, to be incorporated again into accretionary wedge. A typical olistostrome-type mélange suggests olistostrome-type. In this detailed geological survey, olistostrome-type mélange is found in Braich y Pwll area (Fig. 2-8 and 9). Therefore, the structures of olistostrome-type are observed in Braich y Pwll area. It is need to classify the two-type structures to identify continental formation in these areas.

On the other hand, in eight samples of Lleyn (LLZ595 50, LLY154b, IR731, LLY377, LLY464, LLZ273, LLZ277 20 and LLZ298), age of zircons from sandstone is analyzed. The nine samples consist of Gwna Group. The youngest ages of LLZ595 50, LLY154b, IR731, LLY377, LLY464, LLZ273, LLZ277 20 and LLZ298 are 628 ± 29, 572 ± 11, 608 ± 16, 610 ± 10, 637 ± 13, 558 ± 13, 541 ± 16 and 549 ± 14 Ma (Fig.2-22, 23, 24). Therefore, the youngest ages in the results show three distinct ages, (1) ca. 630, (2) ca. 610, (3) ca. 550 Ma. The youngest age suggest later deposition. The Gwna Group in Lleyn was deposited during ca. 630- 540 Ma.

In Porth Felen SW Coast area, tuff (LLY600) and sandstone (LLY377 and LLY464) is sampled and show 630 ± 8 Ma, 637 ± 13 Ma and 610 ± 10 Ma, respectively. It is suggested that the Gwna Group in the Porth Felen SW Coast area depositted in 640-610 Ma, early Ediacaran. A sample in Mynydd Carreg (UKY20) shows 635 ± 16Ma and deposited in ca. 630 Ma (early Ediacaran) to like in Porth Felen SW Coast. On the other hand, a sample in Porth Oer (LLY38) has 619 ± 7 Ma. It is suggested that the samples in Porth Oer deposited in ca. ca. 610 Ma after Porth Felen SW Coast and

Mynydd Carreg areas. In North Porth Lago, turbidite samples (LLY154b and IR731) show 572 ± 11 Ma and 608 ± 16 Ma and deposited in 610-570 Ma (early Ediacaran) to like in Porth Oer. In addition, Braich y Pwll area has shale samples (LLZ300 and LLZ298) with 589± 14 Ma and 541 ± 26 Ma. The samples in Braich y Pwll area deposited in ca. 540 Ma.

OPS for each individual ACs has been established by zircon chronology, and classified them into three-types, Type 1 is 630Ma ACs (Early Ediacaran), Type 2 is 560Ma (Early Ediacaran) and the Type 3 is 540Ma (Middle Ediacaran). In Type 1, Porth Felen SW Coast and Mynydd Carreg areas show structure of duplex-type. In addition, a structure of duplex-type is observed in Porth Oer and North Porth Lago in Type 2. However, in Type 3, Braich y Pwll area has not only duplex-type structure but also olistostrome-type. Therefore, it indicates that the olistostrome-type was caused after duplex structure of duplex-type.

2-4-2. Demonstration of ACs and the type

Although the first demonstration of the presence of accretionary complex in the Anglesey Island was by Maruyama et al. (2010) at Llanddwyn island, while the regional distribution of ACs in Wales is described in this paper. Not only by the establishment of OPS, but also the exact dating of formation of ACs were demonstrated. Moreover, the sedimentation rate of bedded chert/claystone was estimated. The result showed one order of magnitude slower than that in the Phanerozoic.

The demonstration of ACs is based on following common occurrences; (1) layer-parallel thrust, particularly (2) duplex-type reverse faults indicating sense of subduction of oceanic materials, thereafter (3) chronology for each unit, establishment

of (4) OPS, and (5) the mechanism how to make ACs to emplace the oceanic materials into hanging wall unit.

Barber and Max (1979) have speculated the origin of mélange in the Gwna Group, Mona Complex, as same in California (Hamilton, 1969; Hsu, 1971). However, the California mélange is sedimentary origin, including high-pressure and low-T eclogite, high-grade garnet-bearing blueschists with much older age ca. 150-160Ma within low-T lawsonite-jadeite to lawsonite-albite schists with ca. 100-80Ma (Maruyama et al., 1985; 1986; Terabayashi and Maruyama et al., 1998). The Gwna group, Mona Complex, in Wales is different from California mélange, and similar to those in Japan (Shimanto and Inuyama type, Isozaki, 1997).

2-4-3. Travel history of accreted oceanic materials

The Gwna Group has long been a puzzling rock unit with chaotic mode of occurrence. The author applied a concept of the accretionary complex, and then constrained formational ages of each outcrop. For example, the Gwna group ranges from 637Ma to 541Ma, which gives a chaotic arrangement of rocks. However, if we reconstruct the OPS for each outcrop, and date the particular stratigraphic horizon, then a reasonable interpretation is obtained and shown in a three travel history diagrams (Fig. 2-33). The each detailed steps are mentioned in following.

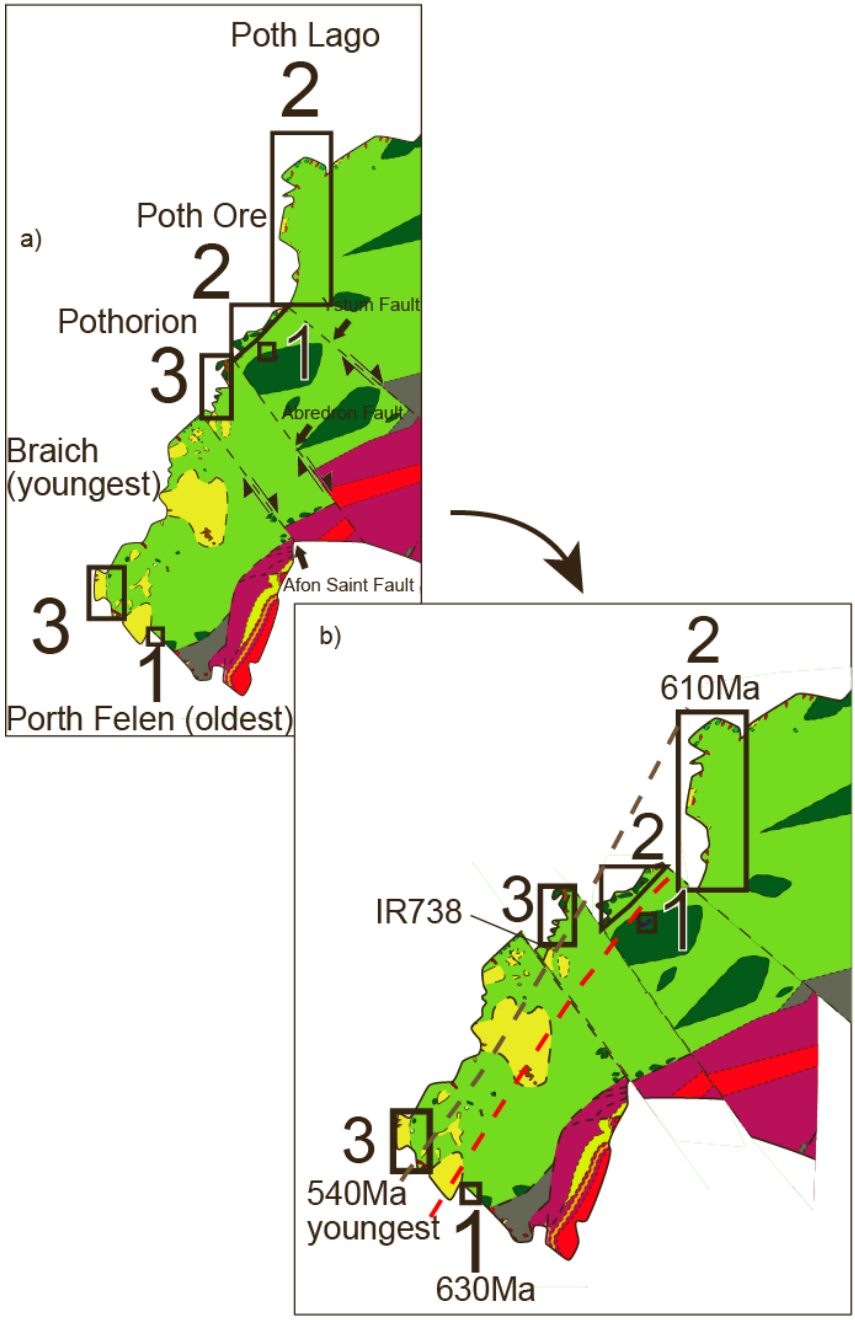

Fig. 2-33. Reconstruction of the Gwna Group before the NS-trending strike slip fault, from the present-day (above) to the before (below). Note the number 1, 2 and 3 are the Types of ACs.

2-4-3-1. Travel history of Type 1 Gwna ACs in 630-610 Ma

Type 1 ACs of Gwna Group is shown in their travel history shown in Fig. 2-34. The Type 1 is found in Penrhyn Nefyn Peninsula, Porth Felen SW Coast and Mynydd Carreg areas and has 630-600 Ma. Section 3 in Porth Felen SW Coast and section 25 in Penrhyn Nefyn Peninsula have ca. 630 Ma in turbidite. General speaking, turbidite deposited at continent margin. Therefore, it indicates that the two sections pointed at West Africa continent margin. On the other hand, the top of mudstone layers in section 5 in Windley Point of Porth Felen SW Coast and section 10 in Mynydd Carreg show ca. 630 Ma. The two sections pointed at the mid-oceanic ridge in ca. 630, because mudstone indicates deep-sea sediment (Fig. 2-34 a). Moreover, the mudstone layer overlies turbidite in the Porth Felen SW Coast and Mynydd Carreg. The bottom of the turbidite in Porth Felen SW Coast had ca. 610 Ma by U-Pb age. Therefore, Mynydd Carreg and Windley Point moved to trench near the continent by ca. 610 Ma (Fig. 2-34 b). This figure 2-34 illustrates them at ca. 610Ma along the travel from the mid-oceanic ridge to the trench.

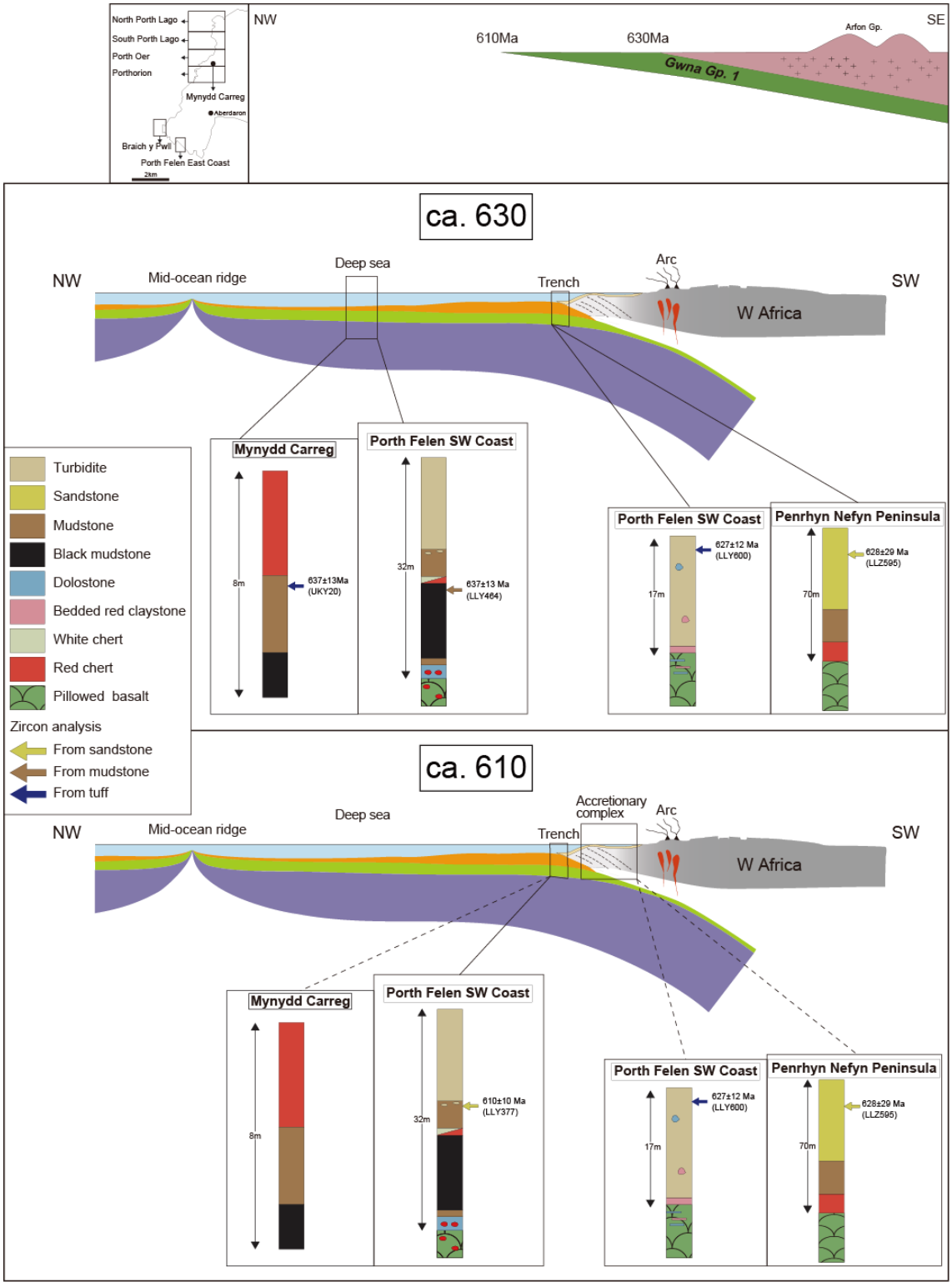

Fig. 2-34. Reconstruction at ca. 630 Ma (upper (a)) and ca. 6100 (lower (b)) Ma for the travel history of ACs for Type 1 of the Gwna Group.

2-4-3-2. Travel history of Type 2 Gwna Group in 610-570 Ma

Type 2 ACs range in formation age from 608Ma to much younger than this age, although the data are not yet available due to the absence of suitable examples in the field. Three ACs are arranged from North Porth Lago IR731 at right above the trench already accreted, while the next is North Porth Lago LLY154b. Section 23 in North Porth Lago has ca. 600 Ma at the top of turbidite layer. Generally speaking, turbidite deposits at the continental margin. There is the section 23 at the West Africa continental margin in ca. 600 Ma. On the other hand, section 17 in Porth Oer shows red claystone with ca. 610 Ma. It is suggested that the section deposited near the mid-ocean ridge in ca. 600 Ma, because claystone deposits in deep-sea sediments. In addition, the same lithofaces and structure with the section 17 are observed in the section 21 in North Porth Lago. Therefore, the section 21 in North Porth Lago might deposit near the mid-ocean ridge to like in Porth Oer (Fig. 2-35 a). Moreover, the top of the section 21 has turbidite layer with ca. 570 Ma. At ca. 570 Ma in the end of Type 2, the section 17 and 21 moved to trench at West Africa, because turbidite deposit at the continental margin (Fig. 2-35 b). The ACs of Gwna Group 2 is formed in Type 2.

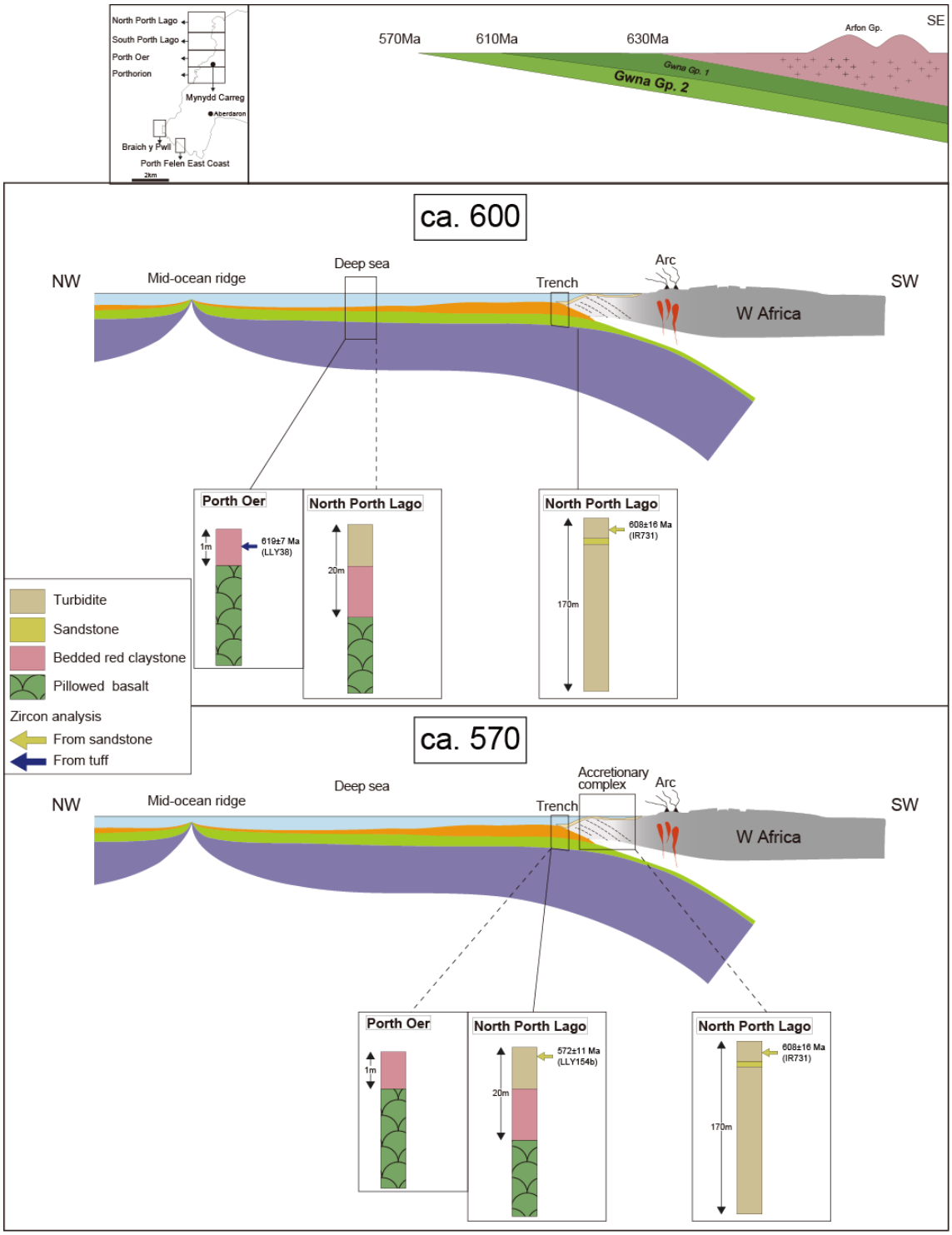

Fig. 2-35. Reconstruction at ca. 600 Ma (upper (a)) and ca. 570 (lower (b)) Ma for the travel history of ACs for Type 2 of the Gwna Group.

2-4-3-3. Travel history of Type 3 Gwna Group in ca. 540 Ma

Type 3 Gwna ACs are shown in Fig. 2-36 to delineate the travel history of ACs by observing OPSs in two Braich y Pwll and Porthorion areas. LLZ300 is the oldest AC that was attached to the hanging wall at 541Ma, when LLZ598 was on the ocean floor as well as LLZ273 and LLZ277. These are the youngest ACs in the Lleyn Peninsula, and different in mode of occurrence from similar age ACs of the Gwna ACs in Anglesey Island. The oceanic materials in the Porthorion and Braich y Pwll are recycled at hanging wall of overriding continental margin. This figure 2-36 shows the cross section of ocean-lithosphere to SW African continental margin at 540Ma (onset of Cambrian age). In ca. 590 Ma, early Type 3, the section 7 in Braich y Pwll OPSs deposited in open ocean, because there is red claystone with ca. 590 Ma at the bottom of the section 7 in Braich y Pwll OPSs. A claystone shows deep-sea sediment. In addition, the red claystone overlies light pink chert with ca. 540 and the chert might deposit at deep-sea sediment. In Porthorion, section 11 and 12 have red claystone with ca. 540 Ma to like the red claystone with ca. 590 in the section 7. Therefore, section 7 deposits at deep-sea sediment in ca. 590 Ma and moved to the West Africa continent in ca. 540 Ma, where as the ACs of Porthorion has not yet arrived at trench. And section 11 and 12 deposited in ca. 540 Ma near the point where the red claystone layer in the section 7 deposited. The Gwna Group 3 of Type 3 in these areas deposited at deep-sea sediment in ca. 590-540 Ma and appended to the continent after formed blue schist (Fig. 2-36).

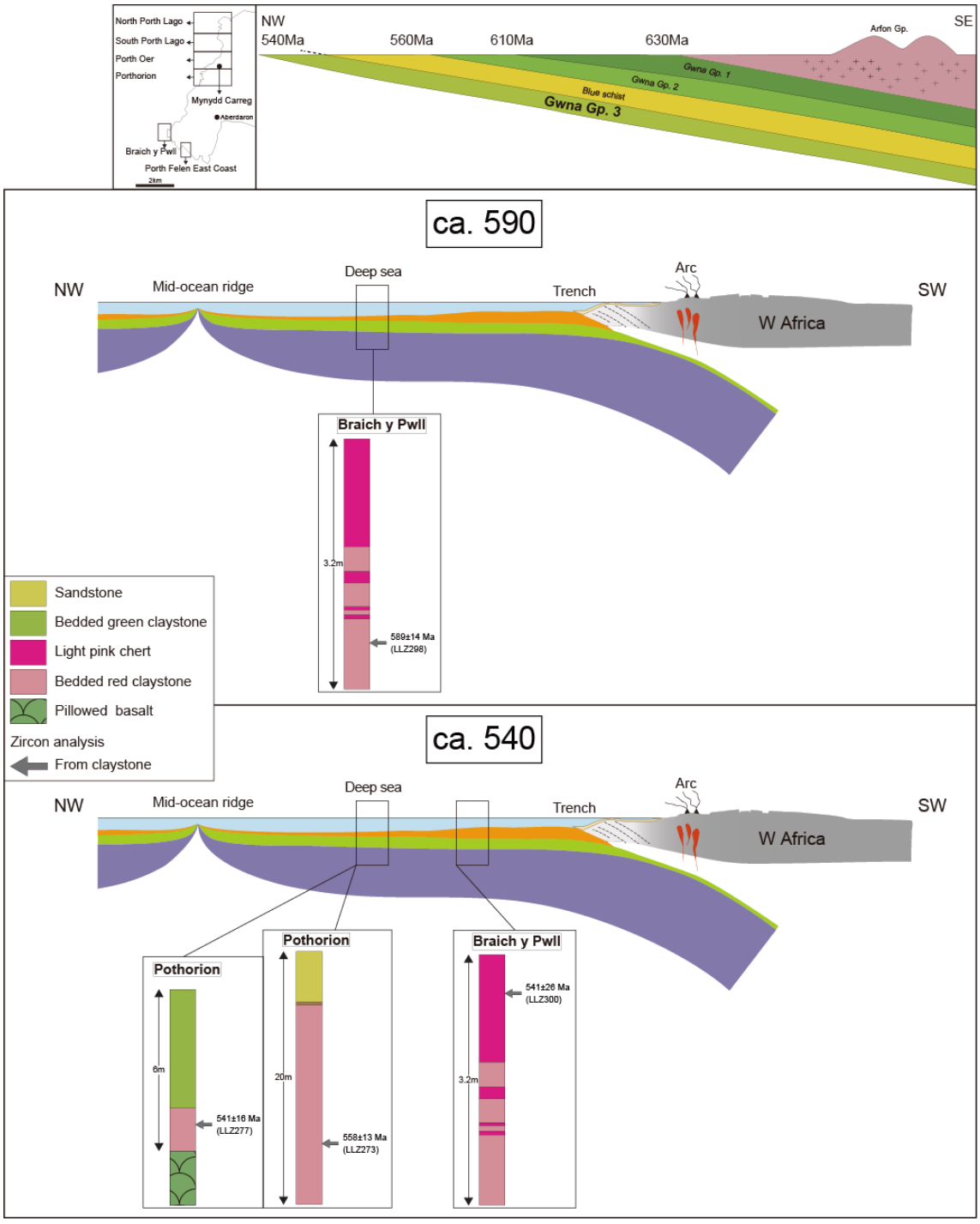

Fig. 2-36. Reconstruction at ca. 590 Ma (upper (a)) and ca. 540 (lower (b)) Ma for the travel history of ACs for Type 3 of the Gwna Group.

2-4-4. Geotectonic implications in England-Wales; role of Pacific-type orogeny

Pacific-type orogeny is composed of four elements, (1) accretionary complex, (2) high-P/T regional metamorphic belt, (3) forearc basin and (4) TTG belt from trench to inner side of continent or island arc. Topographic development of outer non-volcanic arc between volcanic front and trench is due to the tectonic exhumation of high-P/T schist belt in the arc-trench gap. The exhumation of high-P/T schist belt is the reverse movement against subducting slab, hence unusual tectonic movement and uncommon at even subduction zone. It occurs empirically at once a 100 m.y. during the past 500m.y. in Japan and California (Maruyama et al., 1996). The trigger to exhume tectonically the deep-seated high-P/T schists to the surface, is ridge subduction. The buoyant ridge subduction changes the subduction angle gradually by approaching mid-oceanic ridge to jack-up the recrystallized subduction zone complex from mantle depth to the mid-crustal level as a tectonic slice into the low-P rocks, and the final jack-up by underplating the younger ACs underneath by the final ridge subduction. The domal uplift is accompanied by associating high-angle secondary normal faults.

These scenarios are commonly observed around the circum-Pacific orogenic belts in the Phanerozoic, and also here in England-Wales. Three times of Pacific-type orogeny were confirmed here-in and equivalent TTG formation in England.

2-5. Conclusion

The chaotic unit called the Gwna Group in Lleyn Peninsula shows two two-step mixing: 1) Duplex-type structure: the typical accretionary complex (AC) by tectonic mixing at shallow depth by underplating of duplex-type accretion, 2) Olistostrome-type structure: tectonically mixed with oceanic materials of MORB, OIB, bedded cherts and/or red claystone, with trench turbidites underplated and pushed up tectonically

upward, then gravitationally collapsed to deposit at trench, to be incorporated again into accretionary wedge. This type of ACs is apparently remarkably different in appearance (olistostrome), but the entity is two-fold mixing at trench. In these two-types of ACs, the critical characteristics are, common occurrence of layer-parallel faults, mixed lithology of oceanic materials with continental arkosic sandstone/mudstone, variation of ages of their formation with a systematic order called Ocean Plate Stratigraphy (OPS).

OPS for each individual ACs has been established by zircon chronology and classified them into three-types: Type 1 (ca. 630-610 Ma), Type 2 (ca. 600-570Ma) and Type 3 (ca. 540Ma). Braich y Pwll area with the olistostrome-type structure shows Type 3, while another areas with duplex-type have Type 1 or Type 2 by zircon chronology. Therefore, the olistostrome-type was caused after duplex structure of duplex-type.

In addition, a reasonable interpretation to the Gwna Group in Lleyn Peninsula from 637 Ma to 541 Ma is shown in a three travel history diagrams. Type 1) Gwna Group 1 deposited from continental margin to mid-ocean ridge in ca. 630 Ma and appended to West Africa continent in ca. 610 Ma. Type 2) Gwna Group 2 deposited from continental margin to mid-ocean ridge in ca. 610 Ma and appended to West Africa continent in ca. 570 Ma. Type 3) Gwna Group 3 deposited at deep-sea sediment in ca. 590-540 Ma and appended to the continent after formed blue schist.

The large-scale structure of these three ACs and tectonically interlayered ca.560Ma BS belt clearly indicates the (1) nearly subhorizontal thrusts with downward younger polarity, (2) BS belt is tectonically inserted between Type 2 and 3 with NW-ward vergency, and (3) Late-stage (presumably Late Cambrian or Ordovician) vertical faulting modified the subhorizontal tectonic juxtaposition. The large-scale NS-trending displacement caused the apparent juxtaposition of ACs, ranging over 110

m.y. (630-520Ma).

References

Barber, A.J., Max, M.D., 1979. A new look at the Mona Complex, Anglesey, North Wales. Journal of the Geological Society 136, 407-432.

Cowan, D. S., Page, B. M. 1975. Recycled Franciscan material in Franciscan melange west of Paso Robles, California. Geological Society of America Bulletin, 86, 1089-1095.

Dewey, J., F., Bird, J.M. 1970. Mountain belts and new global tectonics. Journal of Geophysical Research, 75, 2625-2647.

Dewey, J., F., 1969. Evolution of the Appalachian/Caledonian Orogen. Nature, 222, 124-129.

Dewey, J.F., 1982, Plate tectonics and the evolution of British Isles. Journal of Geological Society of London, 139, 317-414

Eggins, S. M., Rudnick, R. L., McDonough, W. F. 1998. The composition of peridotites and their minerals: a laser-ablation ICP–MS study. Earth and Planetary Science Letters, 154, 53-71.

Gibbons, W. 1981. Glaucophanitic amphibole in a Monian shear zone on the mainland of North Wales. Journal of the Geological Society, London, 138, 139-143.

Gibbons, W. 1983. The Monian 'Penmynydd Zone of Metamorphism' in Llŷn, North Wales. Geological Journal, 18, 21-41.

Gibbons, W., Gyopari, M. 1986. A greenschist protolith for blueschists on Anglesey, U.K. In: Evans, B.W. and Brown, E.H. (Eds.) Blueschists and Eclogites, Geological Society of America, Memoir, 164, 217-228.

Gibbons, W. 1987. Menai Strait fault system: an early Caledonian terrane boundary in North Wales. Geology, 15, 744-747.

Gibbons, W., McCarroll, D. 1993. The Geology of Country around Aberdaron, including Bardsey Island. Memoir British Geological Survey, Sheet 133 (England and Wales).

Gibbons, W., Tietzsch, T., D., Horack, J. and Murphy, F. C. 1994. Precambrian rocks in Anglesey, southwest Llˆyn and southeast Ireland. In A Revised Correlation of Precambrian Rocks in the British Isles: Special Report 25 (edsW. Gibbons & A. L. Harris), pp.75–84. London: Geological Society.

Greenly, E. 1919. The Geology of Anglesey, Memoir Geological Survey of Great Britain, (2 vols.), HMSO, London, 980 pp.

Greenly, E. 1923. Further researches on the succession and metamorphism in the Mona Complex of Anglesey. Quarterly Journal of the Geological Society, 79, 334-351.

Günther, D., Heinrich, C. A. 1999. Enhanced sensitivity in laser ablation-ICP mass spectrometry using helium-argon mixtures as aerosol carrier. Journal of Analytical Atomic Spectrometry, 14,

1363-1368.

Hamilton, W. 1969. Mesozoic California and the underflow of Pacific mantle. Geological Society of America Bulletin, 80, 2409-2430.

Hirata, T., Iizuka, T., Orihashi, Y. 2005. Reduction of mercury background on ICP-mass spectrometry for in situ U–Pb age determinations of zircon samples. Journal of Analytical Atomic Spectrometry, 20, 696-701.

Hsü, K. J. 1971. Franciscan melanges as a model for eugeosynclinal sedimentation and underthrusting tectonics. Journal of Geophysical Research, 76, 1162-1170.

Iizuka, T., Hirata, T. 2005. Improvements of precision and accuracy in in situ Hf isotope microanalysis of zircon using the laser ablation-MC-ICPMS technique. Chemical Geology, 220(1), 121-137.

Iizuka, T., Hirata, T., Komiya, T., Rino, S., Katayama, I., Motoki, A., Maruyama, S. 2005. U-Pb and Lu-Hf isotope systematics of zircons from the Mississippi River sand: Implications for reworking and growth of continental crust. Geology, 33, 485-488.

Iizuka, T., Komiya, T., Ueno, Y., Katayama, I., Uehara, Y., Maruyama, S., Dunkley, D. J. 2007. Geology and zircon geochronology of the Acasta Gneiss Complex, northwestern Canada: new constraints on its tectonothermal history. Precambrian Research, 153, 179-208.

Isozaki, Y. 1996. Anatomy and genesis of a aubduction-related orogen: A new view of geotectonic subdivision and evolution of the Japanese Islands. The Island Arc, 5, 289-320

Isozaki, Y. 1997. Jurassic accretion tectonics of Japan. Island Arc, 6, 25-51.

Jackson, S. E., Pearson, N. J., Griffin, W. L., Belousova, E. A. 2004. The application of laser ablation-inductively coupled plasma-mass spectrometry to in situ U–Pb zircon geochronology. Chemical Geology, 211, 47-69.

Jaffey, A. H., Flynn, K. F., Glendenin, L. E., Bentley, W. T., & Essling, A. M. 1971. Precision Measurement of Half-Lives and Specific Activities of^{235} U and^{238} U. Physical Review C, 4, 1889.

Kawai, T.,Windley, B.F., Terabayashi, M., Yamamoto, H., Maruyama, S., Isozaki, Y., 2006. Mineral isograds and zones of the Anglesey blueschist belt, UK: implications for the metamorphic development of a subduction–accretion complex. J. Metamorph. Geol. 24, 591–602.

Kawai, T., Windley, B. F., Terabayashi, M., Yamamoto, H., Maruyama, S., Omori, S., Shibuya, T., Sawaki, Y., Isozaki, Y., 2007. Geotectonic framework of the Blueschist Unit on Anglesey–Lleyn, UK, and its role in the development of a Neoproterozoic accretionary orogeny. Precambrian Research, 153, 11-28.

Kawai, T., Windley, B.F., Terabayashi, M., Yamamoto, H., Maruyama, S., Isozaki, Y. 2007. Geotectonic framework of the blueschist unit on Anglesey-Lleyn, UK, and its role in the development of a Neoproterozoic accretionary orogeny. Precambrian Research, 153, 11-28.

Leggett, J. K., McKerrow, W.S., Casey, D. M. 1982. The anatomy of a Lower Palaeozoic accretionary forearc: The Southern Uplands of Scotland. In: Leggett, J.K. (Eds.) Trench-Forearc Geology. Geological Society, London, Special Publications, 10, 494-520.

Leggett, J.K., McKerrow, W.S., Eales, M.H. 1979. The Southern Uplands of Scotland: a Lower Palaeozoic accretionary prism. Journal of the Geological Society, London, 136, 755-770.

McIlroy, D., Horák, J. 2006. Neoproterozoic: the late Precambrian terranes that formed Eastern Avalonia. The Geology of England and Wales, 9-23.

Maltman, A.J. 1977. Serpentinites and related rocks of Anglesey. Geological Journal, 12, 113-128.

Maltman, A.J. 1979. Tectonic emplacement of ophiolitic rocks in the Precambrian Mona Complex of Anglesey, North Wales. Nature, 277, 327.

Matsuda, T., Isozaki, Y. 1991. Well‐documented travel history of Mesozoic pelagic chert in Japan: From remote ocean to subduction zone. Tectonics, 10, 475-499.

Maruyama, S., Liou, J. G., Sasakura, Y. 1985. Low-temperature recrystallization of Franciscan greywackes from Pacheco Pass, California. Mineralogical Magazine, 49, 345-355.

Maruyama, S., Kawai, T., Windley, B., F., 2010. Ocean plate stratigraphy and its imbrication in an accretionary orogen: the Mona Complex, Anglesey Lleyn, Wales, UK. Geological Society, London, Special Publications. 338, 55-75.

Phillips, E. 1991. The lithostratigraphy, sedimentology and tectonic setting of the Monian Supergroup, western Anglesey, North Wales. Journal of the Geological Society, London 148, 1079–90.

Roberts, B. 1979. The Geology of Snowdonia and Llÿn: an Outline and Field Guide. Adam Hilger, Bristol, 183 pp.

Shackleton, R. M. 1954. The structure and succession of Anglesey and the Lleyn Peninsula. Advancement of Science, 11, 106-8.

Shackleton, R.M., 1969. The Precambrian of North Wales, In: Woods, A. (Ed.), The Precambrian and Lower Palaeozoic Rocks of Wales. University of Wales Press, Cardiff, pp. 1-18.

Shackleton, R.M. 1975. Precambrian rocks of Wales. In: Harris, A.L. (ed.) A Correlation of Precambrian Rocks in the British Isles. Geological Society, London, Special Publications, 6, 76-82.

Stacey, J. T., & Kramers, 1. 1975. Approximation of terrestrial lead isotope evolution by a two-stage model. Earth and Planetary Science Letters, 26, 207-221.

Terabayashi, M., Maruyama, S. 1998. Large pressure gap between the Coastal and Central Franciscan belts, northern and central California. Tectonophysics, 285, 87-101.

Thorpe, R.S. 1972. Possible subduction zone origin for two Precambrian calc-alkaline plutonic complexes from southern Britain. Geological Society of America Bulletin, 83, 3663-3668.

Tunheng, A., Hirata, T. 2004. Development of signal smoothing device for precise elemental

analysis using laser ablation-ICP-mass spectrometry. Journal of Analytical Atomic Spectrometry, 19, 932-934.

Wiedenbeck, M., Alle, P., Corfu, F., Griffin, W.L., Meier, M., Ober, F., et al., 1995. Three natural zircon standards for U–Th–Pb, Lu–Hf, trace element and REE analyses. Geosand. Newsl. 19, 1 – 23.

Wiedenbeck, M., Hanchar, J.M., Peck, W.H., Sylvester, P., Valley, J., Whitehouse, M., Kronz, A., Morishita, Y., Nasdala, L., 2004. Further characterisation of the 91500 zircon crystal. Geostandards and Geoanalytical Research 28, 9–39.

Wood, D.S. 1974. Ophiolites, mélanges, blueschists, and ignimbrites: early Caledonian 21 subduction in Wales? In: Dott, R.H. and Shaver, R.H. (Eds.) Modern and Ancient Geosynclinal Sedimentation. Society of Economic Paleontologists and Mineralogists, Special Publication, 19, 334-344.

Table2-1

LA-ICP-MC U-Pb isotope analysical data for zircons from tuff samples in Lleyn Peninsula

Grain	$^{204}Pb/^{206}Pb$	U (ppm)	Th (ppm)	$^{207}Pb/^{235}U$	2σ	$^{206}Pb/^{238}U$	2σ	$^{207}Pb/^{206}Pb$	2σ	Age (Ma)						Concordance
										$^{207}Pb/^{235}U$	2σ	$^{206}Pb/^{238}U$	2σ	$^{207}Pb/^{206}Pb$	2σ	
LLY38-1	0.0003	113	109	0.831	± 0.042	0.0988	± 0.0018	0.0610	± 0.0014	614	± 23	608	± 11	638	± 104	99
LLY38-2	0.0000	110	105	0.795	± 0.042	0.0964	± 0.0018	0.0598	± 0.0015	594	± 24	593	± 11	596	± 112	100
LLY38-3	0.0002	202	184	0.824	± 0.039	0.0972	± 0.0010	0.0615	± 0.0014	610	± 22	598	± 6	657	± 102	98
LLY38-4	0.0001	252	184	0.808	± 0.038	0.0973	± 0.0017	0.0603	± 0.0013	601	± 22	598	± 10	613	± 98	100
LLY38-5	0.0000	117	94	0.824	± 0.043	0.0977	± 0.0018	0.0612	± 0.0015	610	± 24	601	± 11	646	± 109	98
LLY38-6	0.0000	210	179	0.812	± 0.037	0.0986	± 0.0017	0.0597	± 0.0012	603	± 21	606	± 10	592	± 93	101
LLY38-7	0.0000	140	105	0.846	± 0.043	0.0991	± 0.0018	0.0619	± 0.0015	622	± 24	609	± 11	670	± 104	98
LLY38-8	0.0000	77	39	0.819	± 0.047	0.0993	± 0.0020	0.0599	± 0.0016	608	± 26	610	± 12	599	± 120	100
LLY38-9	0.0000	161	161	0.811	± 0.040	0.0995	± 0.0011	0.0591	± 0.0014	603	± 22	612	± 6	571	± 107	101
LLY38-10	0.0000	120	85	0.827	± 0.046	0.0998	± 0.0022	0.0601	± 0.0015	612	± 26	613	± 13	608	± 113	100
LLY38-11	0.0000	81	119	0.851	± 0.046	0.0998	± 0.0019	0.0618	± 0.0016	625	± 25	613	± 11	669	± 112	98
LLY38-12	0.0000	43	20	0.830	± 0.054	0.1004	± 0.0020	0.0599	± 0.0018	614	± 30	617	± 12	602	± 139	101
LLY38-13	0.0000	315	364	0.827	± 0.037	0.1007	± 0.0009	0.0595	± 0.0013	612	± 21	619	± 5	587	± 99	101
LLY38-14	0.0000	163	146	0.858	± 0.041	0.1014	± 0.0011	0.0614	± 0.0014	629	± 23	622	± 6	652	± 105	99
LLY38-15	0.0000	403	238	0.869	± 0.038	0.1014	± 0.0009	0.0622	± 0.0013	635	± 21	623	± 5	680	± 95	98
LLY38-16	0.0006	101	75	0.870	± 0.046	0.1016	± 0.0019	0.0621	± 0.0015	635	± 25	624	± 11	677	± 110	98
LLY38-17	0.0000	105	79	0.844	± 0.047	0.1019	± 0.0023	0.0601	± 0.0015	621	± 26	625	± 13	608	± 116	101
LLY38-18	0.0000	363	275	0.852	± 0.038	0.1023	± 0.0009	0.0604	± 0.0013	626	± 21	628	± 5	618	± 97	100
LLY38-19	0.0000	99	91	0.866	± 0.045	0.1042	± 0.0017	0.0603	± 0.0015	633	± 25	639	± 10	614	± 110	101
LLY38-20	0.0000	75	59	0.896	± 0.049	0.1044	± 0.0018	0.0623	± 0.0016	650	± 27	640	± 11	683	± 115	99
LLY38-21	0.0003	96	67	0.885	± 0.050	0.1047	± 0.0024	0.0613	± 0.0016	643	± 27	642	± 14	649	± 116	100
LLY38-22	0.0000	134	92	0.870	± 0.047	0.1052	± 0.0023	0.0600	± 0.0015	636	± 26	645	± 14	604	± 110	101
LLY38-23	0.0000	182	120	0.896	± 0.043	0.1060	± 0.0019	0.0613	± 0.0014	650	± 24	650	± 11	649	± 100	100
LLY600-1	0.0005	69	69	0.808	± 0.051	0.0989	± 0.0024	0.0593	± 0.0017	601	± 29	608	± 14	577	± 131	101
LLY600-2	0.0000	163	148	0.832	± 0.045	0.0990	± 0.0022	0.0610	± 0.0015	615	± 25	609	± 13	638	± 109	99
LLY600-3	0.0000	119	86	0.846	± 0.086	0.0992	± 0.0023	0.0619	± 0.0031	623	± 48	610	± 14	670	± 227	98
LLY600-4	0.0006	141	183	0.849	± 0.050	0.1007	± 0.0028	0.0611	± 0.0016	624	± 28	619	± 16	643	± 117	99
LLY600-5	0.0000	114	127	0.842	± 0.048	0.1016	± 0.0023	0.0601	± 0.0016	620	± 27	624	± 14	608	± 116	101
LLY600-6	0.0000	127	121	0.847	± 0.046	0.1019	± 0.0016	0.0602	± 0.0016	623	± 25	626	± 10	612	± 115	100
LLY600-7	0.0000	93	105	0.838	± 0.089	0.1022	± 0.0025	0.0594	± 0.0031	618	± 50	628	± 15	582	± 240	102
LLY600-8	0.0000	205	399	0.861	± 0.046	0.1023	± 0.0020	0.0610	± 0.0015	631	± 25	628	± 12	641	± 110	100
LLY600-9	0.0000	165	250	0.840	± 0.043	0.1024	± 0.0015	0.0595	± 0.0015	619	± 24	629	± 9	584	± 110	102
LLY600-10	0.0000	122	160	0.878	± 0.047	0.1026	± 0.0017	0.0621	± 0.0016	640	± 26	630	± 10	677	± 114	98
LLY600-11	0.0000	145	122	0.892	± 0.049	0.1036	± 0.0021	0.0625	± 0.0016	647	± 27	635	± 12	690	± 114	98
LLY600-12	0.0005	216	425	0.876	± 0.083	0.1051	± 0.0022	0.0605	± 0.0028	639	± 46	644	± 13	621	± 214	101
LLY600-13	0.0000	168	149	0.926	± 0.048	0.1063	± 0.0016	0.0632	± 0.0015	666	± 25	651	± 10	716	± 108	98
LLY600-14	0.0000	176	178	0.934	± 0.090	0.1087	± 0.0023	0.0623	± 0.0029	670	± 48	665	± 13	684	± 214	99
UKY20-1	0.0000	246	260	0.859	± 0.059	0.1006	± 0.0022	0.0619	± 0.0020	630	± 33	618	± 13	671	± 147	98
UKY20-2	0.0000	176	282	0.833	± 0.058	0.1018	± 0.0025	0.0593	± 0.0019	615	± 33	625	± 15	580	± 148	102
UKY20-3	0.0000	335	797	0.886	± 0.060	0.1033	± 0.0023	0.0622	± 0.0020	644	± 33	634	± 13	683	± 144	98
UKY20-4	0.0000	461	303	0.883	± 0.059	0.1050	± 0.0023	0.0610	± 0.0019	643	± 32	644	± 13	639	± 143	100
UKY20-5	0.0000	444	777	0.898	± 0.060	0.1065	± 0.0023	0.0612	± 0.0019	651	± 33	653	± 13	645	± 143	100
UKY20-6	0.0000	633	1120	0.918	± 0.061	0.1076	± 0.0023	0.0618	± 0.0019	661	± 33	659	± 13	668	± 141	100
UKY20-7	0.0000	330	661	0.871	± 0.058	0.0996	± 0.0024	0.0634	± 0.0020	636	± 32	612	± 14	721	± 137	96

Note: all errors are quoted at 2 s level

Concordance = [206Pb/238U age / 206Pb/238U age]×100

Table2-2
LA-ICP-MC U-Pb isotope analysical data for zircons from sandstone samples in Lleyn peninsula

Grain	$^{204}Pb/^{206}Pb$	U (ppm)	Th (ppm)	$^{207}Pb/^{235}U$	2σ	$^{206}Pb/^{238}U$	2σ	$^{207}Pb/^{206}Pb$	2σ	Age (Ma)						Concordance
										$^{207}Pb/^{235}U$	2σ	$^{206}Pb/^{238}U$	2σ	$^{207}Pb/^{206}Pb$	2σ	
IR731-1	0.0000	166	68	7.83	± 0.61	0.416	± 0.021	0.1847	± 0.0049	2698	± 71	2702	± 112	2695	± 91	100
IR731-2	0.0000	314	148	7.47	± 0.57	0.411	± 0.021	0.1307	± 0.0035	2104	± 68	2101	± 91	2108	± 98	100
IR731-3	0.0000	181	71	7.24	± 0.56	0.400	± 0.007	0.1224	± 0.0031	1996	± 48	2000	± 32	1992	± 92	100
IR731-4	0.0000	254	239	7.09	± 0.55	0.403	± 0.020	0.1124	± 0.0030	1843	± 65	1847	± 81	1839	± 101	100
IR731-5	0.0000	104	45	7.17	± 0.56	0.400	± 0.007	0.1248	± 0.0031	2019	± 48	2012	± 32	2026	± 91	100
IR731-6	0.0000	118	26	13.06	± 1.01	0.526	± 0.022	0.0740	± 0.0011	1036	± 34	1033	± 40	1042	± 61	100
IR731-7	0.0000	963	1445	6.56	± 0.50	0.380	± 0.008	0.1262	± 0.0048	2056	± 72	2066	± 39	2046	± 141	100
IR731-8	0.0000	677	368	7.41	± 0.57	0.404	± 0.009	0.1316	± 0.0017	2132	± 31	2145	± 43	2120	± 45	101
IR731-9	0.0000	298	81	0.80	± 0.06	0.099	± 0.005	0.1319	± 0.0036	2111	± 69	2097	± 92	2124	± 100	99
IR731-10	0.0000	792	265	0.93	± 0.05	0.110	± 0.003	0.0958	± 0.0012	1533	± 27	1525	± 31	1544	± 47	99
IR731-11	0.0000	139	80	6.96	± 0.37	0.394	± 0.008	0.0800	± 0.0030	1211	± 57	1218	± 24	1198	± 158	101
IR731-12	0.0001	518	220	6.30	± 0.33	0.366	± 0.009	0.1054	± 0.0047	1737	± 80	1750	± 40	1722	± 172	101
IR731-13	0.0000	148	248	17.65	± 0.94	0.595	± 0.025	0.0616	± 0.0010	651	± 26	648	± 26	660	± 73	100
IR731-14	0.0000	216	118	0.87	± 0.05	0.106	± 0.002	0.1844	± 0.0070	2671	± 77	2642	± 46	2692	± 131	99
IR731-15	0.0001	771	381	3.89	± 0.21	0.267	± 0.007	0.0935	± 0.0042	1515	± 76	1527	± 36	1499	± 178	101
IR731-16	0.0003	164	216	6.53	± 0.35	0.368	± 0.009	0.1278	± 0.0016	2047	± 31	2025	± 41	2068	± 45	99
IR731-17	0.0007	358	115	0.80	± 0.04	0.099	± 0.003	0.1252	± 0.0045	2054	± 70	2075	± 47	2032	± 133	101
IR731-18	0.0002	247	118	6.14	± 0.33	0.364	± 0.010	0.1332	± 0.0048	2162	± 71	2185	± 49	2140	± 132	101
IR731-19	0.0005	168	35	3.29	± 0.18	0.267	± 0.006	0.1301	± 0.0017	2122	± 32	2145	± 43	2099	± 46	101
IR731-20	0.0000	327	156	6.53	± 0.22	0.364	± 0.015	0.1265	± 0.0018	2073	± 46	2095	± 76	2050	± 51	101
IR731-21	0.0000	272	80	2.33	± 0.08	0.205	± 0.004	0.2150	± 0.0054	2971	± 52	3010	± 45	2944	± 83	101
IR731-22	0.0000	1096	649	0.98	± 0.03	0.114	± 0.003	0.1275	± 0.0049	2088	± 74	2112	± 41	2064	± 143	101
IR731-23	0.0000	1038	1371	3.52	± 0.12	0.267	± 0.007	0.1314	± 0.0048	2142	± 71	2168	± 50	2117	± 133	101
IR731-24	0.0001	183	90	0.87	± 0.04	0.103	± 0.005	0.1285	± 0.0035	2052	± 67	2027	± 88	2077	± 98	99
IR731-25	0.0000	236	114	7.16	± 0.25	0.395	± 0.010	0.1303	± 0.0021	2076	± 37	2049	± 45	2103	± 57	99
IR731-26	0.0000	148	115	7.08	± 0.25	0.395	± 0.009	0.0600	± 0.0023	614	± 38	617	± 13	602	± 179	101
IR731-27	0.0000	237	515	6.51	± 0.22	0.369	± 0.016	0.1366	± 0.0019	2157	± 46	2128	± 77	2185	± 50	99
IR731-28	0.0002	193	119	7.16	± 0.25	0.385	± 0.008	0.1265	± 0.0048	2023	± 71	1996	± 36	2050	± 140	99
IR731-29	0.0009	36	18	6.72	± 0.27	0.374	± 0.009	0.0621	± 0.0008	692	± 18	697	± 15	678	± 56	101
IR731-30	0.0001	330	122	6.70	± 0.34	0.384	± 0.010	0.1800	± 0.0065	2684	± 76	2726	± 60	2653	± 125	102
IR731-31	0.0000	346	303	7.37	± 0.37	0.391	± 0.011	0.1364	± 0.0049	2211	± 72	2243	± 51	2182	± 132	101
IR731-32	0.0000	270	118	0.85	± 0.05	0.103	± 0.002	0.1348	± 0.0017	2131	± 31	2100	± 42	2161	± 45	99
IR731-33	0.0000	311	111	0.90	± 0.05	0.106	± 0.003	0.1275	± 0.0057	2094	± 85	2123	± 48	2064	± 165	101
IR731-34	0.0000	738	478	11.48	± 0.58	0.468	± 0.009	0.1288	± 0.0032	2051	± 48	2020	± 33	2081	± 91	99
IR731-35	0.0001	1077	4620	6.43	± 0.32	0.362	± 0.009	0.0905	± 0.0040	1463	± 74	1481	± 35	1437	± 179	101
IR731-36	0.0000	160	105	0.88	± 0.05	0.100	± 0.005	0.1157	± 0.0031	1922	± 66	1951	± 85	1892	± 100	101
IR731-37	0.0000	472	490	1.77	± 0.09	0.174	± 0.003	0.1282	± 0.0032	2106	± 49	2139	± 35	2074	± 92	102
IR731-38	0.0000	58	24	6.80	± 0.36	0.372	± 0.010	0.1300	± 0.0047	2132	± 72	2168	± 50	2098	± 134	102
IR731-39	0.0000	173	57	0.82	± 0.05	0.100	± 0.004	0.0602	± 0.0010	626	± 26	631	± 26	609	± 76	101
IR731-40	0.0000	108	35	6.58	± 0.52	0.378	± 0.009	0.0823	± 0.0011	1222	± 26	1204	± 26	1253	± 54	99
IR731-41	0.0000	354	145	6.33	± 0.50	0.363	± 0.007	0.0613	± 0.0015	669	± 27	675	± 12	649	± 112	101
IR731-42	0.0000	391	366	12.88	± 1.01	0.507	± 0.012	0.0615	± 0.0011	636	± 20	630	± 15	657	± 75	99
IR731-43	0.0000	316	142	0.85	± 0.07	0.104	± 0.004	0.1288	± 0.0018	2037	± 45	1992	± 72	2082	± 50	98
IR731-44	0.0000	49	34	6.82	± 0.55	0.388	± 0.010	0.1132	± 0.0050	1893	± 83	1931	± 44	1851	± 171	102
IR731-45	0.0000	193	72	0.88	± 0.07	0.108	± 0.003	0.0595	± 0.0027	607	± 45	612	± 16	586	± 212	101
IR731-46	0.0000	364	829	2.29	± 0.18	0.208	± 0.006	0.1319	± 0.0048	2169	± 71	2218	± 50	2123	± 132	102
IR731-47	0.0005	347	99	0.90	± 0.07	0.103	± 0.004	0.1328	± 0.0021	2086	± 49	2037	± 75	2135	± 58	98
IR731-48	0.0000	230	63	0.83	± 0.07	0.101	± 0.002	0.1302	± 0.0016	2050	± 30	1999	± 40	2101	± 44	98
IR731-49	0.0000	349	120	0.83	± 0.07	0.103	± 0.005	0.0599	± 0.0017	625	± 36	632	± 30	601	± 127	101
IR731-50	0.0000	287	185	3.22	± 0.30	0.258	± 0.007	0.1278	± 0.0057	2121	± 86	2176	± 48	2067	± 165	103
IR731-51	0.0000	607	246	0.83	± 0.08	0.102	± 0.003	0.1277	± 0.0046	2123	± 71	2182	± 50	2066	± 133	103
IR731-52	0.0000	158	63	0.82	± 0.08	0.100	± 0.002	0.0592	± 0.0016	599	± 26	606	± 11	573	± 118	101
IR731-53	0.0002	190	102	3.45	± 0.32	0.267	± 0.014	0.0637	± 0.0018	700	± 39	690	± 33	732	± 125	99
IR731-54	0.0000	19	52	6.74	± 0.65	0.401	± 0.017	0.0593	± 0.0011	606	± 26	613	± 25	580	± 85	101
IR731-55	0.0000	159	82	7.07	± 0.65	0.402	± 0.017	0.1779	± 0.0025	2563	± 48	2475	± 87	2633	± 47	97
IR731-56	0.0003	96	38	5.45	± 0.51	0.349	± 0.010	0.0590	± 0.0022	599	± 37	608	± 16	567	± 172	101
IR731-57	0.0000	147	77	6.86	± 0.63	0.390	± 0.010	0.0608	± 0.0027	671	± 47	684	± 17	631	± 205	102
IR731-58	0.0000	499	162	0.94	± 0.09	0.112	± 0.002	0.0892	± 0.0023	1479	± 43	1528	± 26	1409	± 101	103
IR731-59	0.0000	441	225	4.53	± 0.42	0.312	± 0.016	0.1481	± 0.0040	2228	± 69	2125	± 92	2324	± 95	95
IR731-60	0.0000	110	38	6.94	± 0.51	0.385	± 0.008	0.0594	± 0.0023	624	± 38	635	± 13	583	± 178	102
LLY154b -1	0.0000	49	53	7.41	± 0.34	0.394	± 0.007	0.1366	± 0.0029	2163	± 42	2140	± 34	2184	± 76	99
LLY154b -2	0.0000	51	86	6.81	± 0.32	0.377	± 0.007	0.1308	± 0.0028	2087	± 42	2064	± 33	2109	± 77	99
LLY154b -3	0.0000	103	100	6.65	± 0.30	0.375	± 0.007	0.1285	± 0.0027	2066	± 41	2055	± 32	2077	± 75	99
LLY154b -4	0.0000	36	51	6.86	± 0.33	0.385	± 0.007	0.1293	± 0.0028	2094	± 43	2099	± 34	2089	± 79	100
LLY154b -5	0.0000	106	138	6.96	± 0.18	0.398	± 0.003	0.1270	± 0.0015	2107	± 23	2158	± 15	2057	± 43	102
LLY154b -6	0.0000	33	29	6.77	± 0.20	0.390	± 0.004	0.1260	± 0.0018	2082	± 27	2122	± 19	2042	± 50	102
LLY154b -7	0.0000	149	194	0.84	± 0.03	0.102	± 0.001	0.0595	± 0.0009	617	± 15	625	± 6	586	± 68	101
LLY154b -8	0.0000	195	329	0.87	± 0.03	0.107	± 0.001	0.0588	± 0.0009	633	± 14	654	± 6	561	± 64	103
LLY154b -9	0.0000	89	116	7.17	± 0.19	0.397	± 0.003	0.1308	± 0.0016	2132	± 23	2157	± 16	2109	± 44	101
LLY154b -10	0.0000	53	44	6.80	± 0.19	0.384	± 0.004	0.1285	± 0.0017	2086	± 25	2094	± 17	2078	± 47	100
LLY154b -11	0.0000	105	161	6.64	± 0.17	0.386	± 0.003	0.1248	± 0.0015	2065	± 23	2104	± 15	2026	± 44	102
LLY154b -12	0.0002	125	139	0.78	± 0.03	0.098	± 0.001	0.0578	± 0.0012	585	± 19	601	± 6	523	± 94	103
LLY154b -13	0.0000	75	122	7.16	± 0.26	0.405	± 0.003	0.1283	± 0.0023	2131	± 33	2190	± 16	2075	± 64	103
LLY154b -14	0.0001	127	91	3.51	± 0.13	0.274	± 0.002	0.0931	± 0.0017	1530	± 30	1560	± 12	1490	± 70	102
LLY154b -15	0.0000	335	362	0.78	± 0.03	0.094	± 0.001	0.0603	± 0.0011	585	± 17	577	± 5	615	± 82	99
LLY154b -16	0.0000	109	142	6.93	± 0.25	0.391	± 0.003	0.1285	± 0.0023	2102	± 33	2127	± 15	2078	± 64	101
LLY154b -17	0.0000	84	50	6.46	± 0.24	0.380	± 0.003	0.1235	± 0.0022	2041	± 33	2075	± 15	2007	± 65	102
LLY154b -18	0.0000	60	24	6.35	± 0.30	0.372	± 0.005	0.1238	± 0.0028	2026	± 42	2039	± 24	2012	± 82	101
LLY154b -19	0.0002	96	80	0.86	± 0.05	0.102	± 0.002	0.0609	± 0.0015	628	± 25	626	± 9	636	± 112	100
LLY154b -20	0.0000	30	15	13.08	± 0.62	0.525	± 0.008	0.1807	± 0.0041	2685	± 46	2720	± 32	2659	± 77	101
LLY154b -21	0.0000	117	158	6.95	± 0.32	0.389	± 0.005	0.1294	± 0.0029	2105	± 42	2120	± 24	2090	± 80	101
LLY154b -22	0.0000	108	125	3.60	± 0.17	0.279	± 0.004	0.0938	± 0.0021	1551	± 38	1585	± 19	1504	± 87	102
LLY154b -23	0.0000	141	162	6.45	± 0.18	0.373	± 0.007	0.1254	± 0.0013	2039	± 25	2044	± 34	2034	± 37	100
LLY154b -24	0.0000	149	306	5.20	± 0.15	0.337	± 0.006	0.1119	± 0.0012	1853	± 25	1873	± 31	1831	± 39	101
LLY154b -25	0.0000	27	20	3.30	± 0.13	0.260	± 0.006	0.0921	± 0.0015	1482	± 30	1491	± 28	1469	± 62	101
LLY154b -26	0.0001	62	93	2.48	± 0.08	0.219	± 0.004	0.0823	± 0.0011	1267	± 25	1274	± 23	1254	± 54	101
LLY154b -27	0.0000	123	196	6.99	± 0.20	0.395	± 0.008	0.1284	± 0.0013	2110	± 26	2145	± 35	2076	± 37	102
LLY154b -28	0.0000	76	71	0.79	± 0.03	0.093	± 0.002	0.0616	± 0.0010	590	± 18	572	± 11	659	± 72	97
LLY154b -29	0.0000	40	49	0.81	± 0.04	0.094	± 0.002	0.0626	± 0.0013	604	± 22	581	± 13	693	± 95	96
LLY154b -30	0.0000	48	38	3.83	± 0.11	0.287	± 0.006	0.0967	± 0.0011	1600	± 24	1629	± 29	1562	± 41	102

Note: all errors are quoted at 2 s level
Concordance = [206Pb/238U age/ 206Pb/238U age]×100

Table2-2
LA-ICP-MC U-Pb isotope analysical data for zircons from sandstone samples in Lleyn peninsula

Grain	$^{204}Pb/^{206}Pb$	U (ppm)	Th (ppm)	$^{207}Pb/^{235}U$	2σ	$^{206}Pb/^{238}U$	2σ	$^{207}Pb/^{206}Pb$	2σ	Age (Ma)						Concordance
										$^{207}Pb/^{235}U$	2σ	$^{206}Pb/^{238}U$	2σ	$^{207}Pb/^{206}Pb$	2σ	
LLY154b -31	0.0000	45	18	3.76	± 0.11	0.278	± 0.006	0.0978	± 0.0011	1583	± 24	1583	± 28	1583	± 43	100
LLY154b -32	0.0000	228	837	5.24	± 0.12	0.340	± 0.006	0.1117	± 0.0008	1859	± 20	1888	± 31	1827	± 26	102
LLY154b -33	0.0000	101	219	1.79	± 0.05	0.175	± 0.003	0.0739	± 0.0008	1041	± 19	1042	± 19	1039	± 44	100
LLY154b -34	0.0000	224	244	3.43	± 0.08	0.268	± 0.005	0.0928	± 0.0007	1510	± 19	1529	± 26	1483	± 29	101
LLY154b -35	0.0000	112	285	2.12	± 0.06	0.196	± 0.004	0.0782	± 0.0008	1154	± 19	1154	± 21	1153	± 40	100
LLY154b -36	0.0000	23	67	5.76	± 0.22	0.346	± 0.007	0.1207	± 0.0020	1941	± 34	1917	± 34	1967	± 60	99
LLY154b -37	0.0000	57	187	5.64	± 0.19	0.347	± 0.007	0.1180	± 0.0017	1922	± 30	1919	± 32	1926	± 52	100
LLY154b -38	0.0000	286	333	3.83	± 0.12	0.280	± 0.005	0.0994	± 0.0013	1600	± 26	1590	± 26	1613	± 49	99
LLY154b -39	0.0000	291	711	2.34	± 0.08	0.212	± 0.004	0.0799	± 0.0011	1224	± 23	1241	± 21	1194	± 54	101
LLY154b -40	0.0000	64	76	6.78	± 0.23	0.389	± 0.007	0.1264	± 0.0018	2083	± 30	2117	± 34	2049	± 50	102
LLY154b -41	0.0000	155	206	5.39	± 0.19	0.337	± 0.007	0.1158	± 0.0016	1883	± 31	1874	± 34	1892	± 52	100
LLY154b -42	0.0000	104	122	6.56	± 0.23	0.378	± 0.008	0.1259	± 0.0018	2054	± 32	2067	± 37	2041	± 52	101
LLY154b -43	0.0000	153	254	9.74	± 0.34	0.462	± 0.010	0.1531	± 0.0021	2411	± 32	2447	± 42	2381	± 48	101
LLY154b -44	0.0000	58	44	12.71	± 0.45	0.516	± 0.011	0.1788	± 0.0026	2659	± 34	2681	± 46	2641	± 48	101
LLY154b -45	0.0000	198	546	3.55	± 0.13	0.270	± 0.006	0.0955	± 0.0014	1539	± 28	1540	± 28	1537	± 55	100
LLY154b -46	0.0000	95	62	3.50	± 0.13	0.267	± 0.006	0.0949	± 0.0014	1527	± 29	1527	± 29	1527	± 58	100
LLY154b -47	0.0000	229	657	2.28	± 0.08	0.206	± 0.004	0.0803	± 0.0012	1205	± 25	1207	± 23	1203	± 58	100
LLY154b -48	0.0000	128	286	5.70	± 0.20	0.353	± 0.003	0.1173	± 0.0020	1931	± 31	1947	± 16	1915	± 62	101
LLY154b -49	0.0000	143	271	1.94	± 0.07	0.184	± 0.002	0.0761	± 0.0013	1094	± 25	1091	± 10	1098	± 73	100
LLY154b -50	0.0000	131	240	1.87	± 0.07	0.182	± 0.002	0.0744	± 0.0013	1069	± 25	1078	± 10	1052	± 74	101
LLY154b -51	0.0000	86	149	2.10	± 0.08	0.195	± 0.002	0.0778	± 0.0014	1147	± 27	1150	± 11	1143	± 75	100
LLY154b -52	0.0000	42	63	7.58	± 0.28	0.401	± 0.004	0.1370	± 0.0024	2183	± 34	2176	± 21	2190	± 63	100
LLY154b -53	0.0000	99	190	3.03	± 0.11	0.249	± 0.003	0.0883	± 0.0016	1416	± 28	1434	± 13	1390	± 69	101
LLY154b -54	0.0000	25	14	3.47	± 0.15	0.270	± 0.004	0.0933	± 0.0019	1521	± 35	1542	± 19	1493	± 81	101
LLY154b -55	0.0000	129	214	17.12	± 0.59	0.590	± 0.006	0.2104	± 0.0035	2942	± 33	2990	± 23	2909	± 54	102
LLY154b -56	0.0000	119	176	2.41	± 0.09	0.215	± 0.002	0.0813	± 0.0014	1247	± 27	1257	± 12	1230	± 71	101
LLY154b -57	0.0003	20	11	3.51	± 0.16	0.267	± 0.004	0.0951	± 0.0021	1528	± 37	1527	± 20	1530	± 84	100
LLY154b -58	0.0001	77	92	7.04	± 0.24	0.390	± 0.005	0.1311	± 0.0021	2117	± 31	2121	± 21	2113	± 58	100
LLY154b -59	0.0000	80	135	3.16	± 0.12	0.261	± 0.003	0.0879	± 0.0015	1448	± 28	1495	± 16	1379	± 67	103
LLY154b -60	0.0000	81	124	7.29	± 0.25	0.400	± 0.005	0.1323	± 0.0021	2147	± 31	2167	± 22	2129	± 58	101
LLY154b -61	0.0001	52	31	13.45	± 0.46	0.525	± 0.006	0.1859	± 0.0030	2712	± 33	2719	± 27	2706	± 54	100
LLY154b -62	0.0000	58	50	13.84	± 0.47	0.544	± 0.006	0.1846	± 0.0030	2739	± 33	2799	± 27	2695	± 54	102
LLY154b -63	0.0000	79	48	3.38	± 0.12	0.264	± 0.003	0.0931	± 0.0016	1501	± 29	1508	± 16	1490	± 66	100
LLY377-1	0.0000	175	570	5.53	± 0.42	0.347	± 0.007	0.1158	± 0.0042	1906	± 67	1918	± 32	1892	± 137	101
LLY377-2	0.0007	47	16	3.14	± 0.27	0.258	± 0.006	0.0881	± 0.0036	1442	± 68	1481	± 32	1385	± 167	103
LLY377-3	0.0001	234	218	4.32	± 0.32	0.287	± 0.005	0.1090	± 0.0039	1697	± 64	1627	± 27	1783	± 138	96
LLY377-4	0.0000	197	669	1.66	± 0.13	0.170	± 0.003	0.0708	± 0.0027	994	± 51	1012	± 19	952	± 164	102
LLY377-5	0.0000	165	347	2.22	± 0.17	0.196	± 0.004	0.0819	± 0.0031	1186	± 56	1155	± 21	1244	± 156	97
LLY377-6	0.0000	139	573	5.00	± 0.35	0.324	± 0.006	0.1120	± 0.0038	1819	± 61	1809	± 28	1832	± 129	99
LLY377-7	0.0000	675	6107	0.82	± 0.06	0.099	± 0.002	0.0600	± 0.0021	608	± 33	610	± 10	603	± 156	100
LLY377-8	0.0000	175	209	3.49	± 0.25	0.269	± 0.005	0.0940	± 0.0032	1525	± 57	1537	± 24	1508	± 135	101
LLY377-9	0.0000	172	579	5.13	± 0.36	0.327	± 0.006	0.1137	± 0.0038	1841	± 61	1824	± 27	1860	± 127	99
LLY377-10	0.0000	71	25	7.13	± 0.51	0.386	± 0.007	0.1341	± 0.0046	2128	± 66	2103	± 34	2152	± 126	99
LLY377-11	0.0001	395	1149	5.16	± 0.35	0.324	± 0.005	0.1154	± 0.0038	1845	± 60	1809	± 25	1886	± 124	98
LLY377-12	0.0000	299	544	5.22	± 0.36	0.328	± 0.005	0.1156	± 0.0038	1856	± 60	1826	± 26	1889	± 125	98
LLY377-13	0.0002	121	176	13.36	± 0.92	0.515	± 0.009	0.1880	± 0.0062	2705	± 67	2679	± 38	2725	± 114	99
LLY377-14	0.0000	460	5286	2.06	± 0.20	0.188	± 0.005	0.0795	± 0.0037	1136	± 70	1111	± 29	1184	± 199	98
LLY377-15	0.0000	682	3451	2.02	± 0.20	0.186	± 0.005	0.0788	± 0.0037	1122	± 69	1099	± 28	1166	± 198	98
LLY377-16	0.0000	303	1469	3.13	± 0.31	0.249	± 0.007	0.0913	± 0.0043	1441	± 79	1432	± 36	1453	± 191	99
LLY464-1	0.0004	258	485	5.14	± 0.38	0.297	± 0.005	0.1257	± 0.0045	1843	± 65	1674	± 26	2038	± 132	91
LLY464-2	0.0001	301	382	2.60	± 0.19	0.216	± 0.004	0.0872	± 0.0032	1302	± 56	1263	± 20	1365	± 146	97
LLY464-3	0.0004	568	665	1.69	± 0.12	0.162	± 0.003	0.0755	± 0.0027	1005	± 48	970	± 15	1081	± 152	97
LLY464-4	0.0000	95	301	6.38	± 0.48	0.369	± 0.007	0.1252	± 0.0046	2029	± 69	2027	± 33	2031	± 135	100
LLY464-5	0.0000	129	192	0.92	± 0.08	0.104	± 0.002	0.0644	± 0.0027	664	± 43	637	± 13	756	± 186	96
LLY464-6	0.0000	220	469	2.27	± 0.24	0.214	± 0.004	0.0770	± 0.0040	1202	± 78	1248	± 19	1121	± 224	104
LLY464-7	0.0003	303	1147	5.06	± 0.53	0.318	± 0.005	0.1154	± 0.0059	1830	± 93	1781	± 25	1885	± 198	97
LLY464-8	0.0006	252	235	4.69	± 0.49	0.294	± 0.005	0.1159	± 0.0060	1766	± 92	1660	± 24	1893	± 199	94
LLY464-9	0.0002	621	2193	1.47	± 0.15	0.144	± 0.002	0.0739	± 0.0038	919	± 65	870	± 13	1039	± 225	95
LLZ273-1	0.0000	385	129	0.79	± 0.04	0.095	± 0.002	0.0605	± 0.0013	591	± 21	583	± 11	620	± 93	99
LLZ273-2	0.0000	471	724	3.16	± 0.13	0.229	± 0.004	0.1000	± 0.0019	1447	± 33	1330	± 22	1624	± 72	92
LLZ273-3	0.0000	485	221	0.77	± 0.03	0.096	± 0.002	0.0586	± 0.0012	581	± 20	588	± 11	553	± 92	101
LLZ273-4	0.0000	418	166	0.75	± 0.03	0.093	± 0.002	0.0585	± 0.0012	568	± 20	573	± 10	549	± 93	101
LLZ273-5	0.0000	602	186	0.74	± 0.03	0.093	± 0.002	0.0581	± 0.0012	565	± 19	573	± 10	533	± 91	101
LLZ273-6	0.0000	947	338	0.81	± 0.03	0.098	± 0.002	0.0593	± 0.0012	600	± 20	605	± 11	580	± 87	101
LLZ273-7	0.0000	263	173	0.77	± 0.04	0.094	± 0.002	0.0594	± 0.0013	581	± 21	581	± 11	581	± 98	100
LLZ273-8	0.0000	391	209	0.77	± 0.04	0.094	± 0.002	0.0595	± 0.0012	578	± 20	577	± 11	585	± 93	100
LLZ273-9	0.0000	949	320	0.79	± 0.05	0.095	± 0.002	0.0604	± 0.0016	594	± 26	587	± 14	618	± 117	99
LLZ273-10	0.0000	111	68	0.80	± 0.05	0.093	± 0.003	0.0621	± 0.0019	597	± 31	576	± 15	678	± 139	96
LLZ273-11	0.0000	294	131	0.77	± 0.05	0.093	± 0.002	0.0597	± 0.0017	579	± 27	576	± 14	593	± 125	99
LLZ273-12	0.0002	206	110	0.76	± 0.05	0.093	± 0.002	0.0594	± 0.0017	573	± 28	571	± 14	581	± 130	100
LLZ273-13	0.0000	849	10759	1.61	± 0.09	0.162	± 0.004	0.0719	± 0.0019	974	± 36	970	± 22	984	± 109	100
LLZ273-14	0.0002	176	78	0.81	± 0.05	0.095	± 0.002	0.0615	± 0.0018	603	± 29	588	± 15	658	± 130	98
LLZ273-15	0.0000	196	80	4.11	± 0.24	0.292	± 0.007	0.1020	± 0.0027	1655	± 48	1651	± 36	1661	± 100	100
LLZ273-16	0.0000	670	168	0.76	± 0.04	0.090	± 0.002	0.0612	± 0.0016	576	± 26	558	± 13	646	± 118	97
LLZ273-17	0.0000	1439	552	0.80	± 0.05	0.095	± 0.002	0.0606	± 0.0016	595	± 26	588	± 14	623	± 116	99
LLZ273-18	0.0000	188	129	0.88	± 0.05	0.100	± 0.003	0.0633	± 0.0018	639	± 30	617	± 15	718	± 126	97
LLZ273-19	0.0000	614	396	0.75	± 0.08	0.093	± 0.003	0.0582	± 0.0028	565	± 46	573	± 21	535	± 228	101
LLZ273-20	0.0000	132	95	0.76	± 0.08	0.095	± 0.004	0.0582	± 0.0029	576	± 49	587	± 22	535	± 239	102
LLZ273-21	0.0000	573	211	0.74	± 0.08	0.093	± 0.004	0.0575	± 0.0028	563	± 46	576	± 21	509	± 229	102
LLZ273-22	0.0008	142	53	0.73	± 0.08	0.092	± 0.004	0.0579	± 0.0029	557	± 48	565	± 21	526	± 239	101
LLZ273-23	0.0005	237	107	0.79	± 0.08	0.100	± 0.004	0.0573	± 0.0028	592	± 49	616	± 22	501	± 234	104
LLZ273-24	0.0003	447	165	0.76	± 0.08	0.095	± 0.004	0.0583	± 0.0028	574	± 47	583	± 21	540	± 229	102
LLZ273-25	0.0000	468	271	0.75	± 0.08	0.095	± 0.004	0.0574	± 0.0028	568	± 47	584	± 21	506	± 230	103
LLZ273-26	0.0011	199	74	0.76	± 0.08	0.096	± 0.004	0.0575	± 0.0029	575	± 48	591	± 22	512	± 235	103
LLZ273-27	0.0003	273	124	0.74	± 0.08	0.094	± 0.004	0.0572	± 0.0028	562	± 47	578	± 21	499	± 233	103
LLZ277-1	0.0000	78	38	0.72	± 0.05	0.088	± 0.003	0.0594	± 0.0017	549	± 29	541	± 16	581	± 133	99
LLZ277-2	0.0000	136	122	6.32	± 0.32	0.366	± 0.010	0.1252	± 0.0027	2021	± 46	2012	± 49	2031	± 77	100

Note: all errors are quoted at 2 s level
Concordance = [206Pb/238U age/ 206Pb/238U age]×100

Table2-2
LA-ICP-MC U-Pb isotope analysical data for zircons from sandstone samples in Lleyn peninsula

Grain	$^{204}Pb/^{206}Pb$	U (ppm)	Th (ppm)	$^{207}Pb/^{235}U$	2σ	$^{206}Pb/^{238}U$	2σ	$^{207}Pb/^{206}Pb$	2σ	Age (Ma)						Concordance
										$^{207}Pb/^{235}U$	2σ	$^{206}Pb/^{238}U$	2σ	$^{207}Pb/^{206}Pb$	2σ	
LLZ277-3	0.0000	122	70	0.75	± 0.05	0.093	± 0.003	0.0587	± 0.0015	571	± 27	574	± 16	557	± 119	101
LLZ277-4	0.0000	645	184	0.71	± 0.04	0.088	± 0.002	0.0585	± 0.0013	546	± 22	546	± 15	548	± 98	100
LLZ277-5	0.0000	325	153	0.77	± 0.04	0.095	± 0.003	0.0585	± 0.0013	578	± 24	586	± 16	547	± 103	101
LLZ277-6	0.0000	232	75	0.74	± 0.04	0.090	± 0.003	0.0595	± 0.0014	563	± 24	558	± 15	585	± 106	99
LLZ277-7	0.0000	259	202	0.76	± 0.04	0.095	± 0.003	0.0579	± 0.0014	571	± 24	582	± 16	527	± 106	102
LLZ277-8	0.0000	409	223	0.76	± 0.04	0.094	± 0.003	0.0588	± 0.0013	577	± 23	581	± 16	561	± 100	101
LLZ277-9	0.0000	416	5958	6.59	± 0.33	0.380	± 0.011	0.1258	± 0.0026	2058	± 45	2076	± 49	2040	± 75	101
LLZ277-10	0.0000	373	183	0.74	± 0.04	0.092	± 0.003	0.0583	± 0.0013	564	± 23	570	± 15	539	± 102	101
LLZ277-11	0.0005	251	162	0.78	± 0.04	0.094	± 0.002	0.0600	± 0.0015	585	± 23	581	± 10	602	± 109	99
LLZ277-12	0.0000	86	58	0.75	± 0.05	0.093	± 0.002	0.0586	± 0.0017	571	± 28	575	± 12	554	± 135	101
LLZ277-13	0.0005	424	282	0.77	± 0.04	0.094	± 0.002	0.0593	± 0.0014	581	± 22	582	± 10	578	± 104	100
LLZ277-14	0.0000	256	225	0.80	± 0.04	0.094	± 0.002	0.0616	± 0.0015	594	± 24	577	± 10	661	± 108	97
LLZ277-15	0.0000	313	194	0.77	± 0.04	0.096	± 0.002	0.0578	± 0.0014	577	± 23	592	± 10	520	± 108	103
LLZ277-16	0.0003	820	283	0.78	± 0.04	0.097	± 0.002	0.0585	± 0.0013	588	± 22	598	± 10	550	± 101	102
LLZ277-17	0.0000	369	194	0.77	± 0.04	0.092	± 0.002	0.0606	± 0.0014	578	± 22	567	± 9	623	± 105	98
LLZ277-18	0.0000	465	356	0.79	± 0.04	0.096	± 0.002	0.0600	± 0.0014	592	± 22	589	± 10	603	± 103	100
LLZ277-19	0.0009	314	318	0.81	± 0.04	0.097	± 0.002	0.0605	± 0.0014	601	± 23	596	± 10	621	± 106	99
LLZ277-20	0.0000	227	168	0.75	± 0.04	0.093	± 0.002	0.0579	± 0.0014	566	± 23	576	± 10	525	± 113	102
LLZ277-21	0.0000	380	436	3.61	± 0.19	0.269	± 0.005	0.0973	± 0.0024	1552	± 43	1537	± 24	1573	± 97	99
LLZ277-22	0.0000	345	352	0.78	± 0.04	0.095	± 0.002	0.0595	± 0.0016	587	± 25	587	± 10	587	± 119	100
LLZ277-23	0.0000	798	448	0.77	± 0.04	0.094	± 0.002	0.0592	± 0.0015	577	± 24	579	± 10	573	± 115	100
LLZ277-24	0.0000	79	46	0.79	± 0.05	0.099	± 0.002	0.0583	± 0.0018	592	± 30	606	± 13	540	± 145	102
LLZ277-25	0.0000	150	72	0.75	± 0.05	0.093	± 0.002	0.0590	± 0.0017	570	± 27	570	± 11	566	± 130	100
LLZ277-26	0.0000	518	272	0.97	± 0.05	0.113	± 0.002	0.0623	± 0.0016	690	± 28	691	± 12	686	± 113	100
LLZ277-27	0.0000	875	548	0.75	± 0.04	0.095	± 0.002	0.0578	± 0.0015	571	± 24	583	± 10	521	± 115	102
LLZ277-28	0.0000	521	257	0.74	± 0.04	0.093	± 0.002	0.0574	± 0.0015	560	± 24	573	± 10	509	± 118	102
LLZ277-29	0.0000	528	216	0.73	± 0.04	0.091	± 0.002	0.0583	± 0.0015	558	± 24	562	± 10	540	± 117	101
LLZ277-30	0.0001	275	269	5.01	± 0.27	0.324	± 0.006	0.1121	± 0.0028	1821	± 46	1809	± 28	1834	± 93	99
LLZ277-31	0.0000	494	352	0.76	± 0.03	0.092	± 0.002	0.0598	± 0.0011	572	± 20	566	± 15	597	± 80	99
LLZ277-32	0.0000	936	454	0.80	± 0.03	0.097	± 0.003	0.0601	± 0.0010	597	± 20	595	± 15	608	± 75	100
LLZ277-33	0.0000	157	53	0.78	± 0.04	0.092	± 0.003	0.0616	± 0.0013	587	± 23	568	± 15	660	± 96	97
LLZ277-34	0.0000	1082	393	0.76	± 0.03	0.092	± 0.002	0.0601	± 0.0010	575	± 19	567	± 15	608	± 75	99
LLZ277-35	0.0000	183	61	0.82	± 0.04	0.101	± 0.003	0.0587	± 0.0012	606	± 23	619	± 17	557	± 94	102
LLZ277-36	0.0000	433	323	0.79	± 0.04	0.098	± 0.003	0.0588	± 0.0011	593	± 21	602	± 16	561	± 82	101
LLZ277-37	0.0000	466	389	0.78	± 0.04	0.096	± 0.003	0.0586	± 0.0011	583	± 20	591	± 15	553	± 81	101
LLZ277-38	0.0000	73	38	0.75	± 0.05	0.091	± 0.003	0.0595	± 0.0016	567	± 27	561	± 16	587	± 123	99
LLZ277-39	0.0000	107	52	0.69	± 0.04	0.090	± 0.003	0.0558	± 0.0014	536	± 24	558	± 16	444	± 114	104
LLZ277-40	0.0000	85	38	0.76	± 0.05	0.092	± 0.003	0.0600	± 0.0015	576	± 27	569	± 16	602	± 116	99
LLZ298-1	0.0003	97	236	0.90	± 0.11	0.109	± 0.006	0.0599	± 0.0034	650	± 61	665	± 33	599	± 264	102
LLZ298-2	0.0006	162	382	0.66	± 0.08	0.087	± 0.004	0.0557	± 0.0031	518	± 51	536	± 26	439	± 267	103
LLZ298-3	0.0000	60	96	0.89	± 0.12	0.098	± 0.005	0.0656	± 0.0039	645	± 64	604	± 31	793	± 272	94
LLZ298-4	0.0000	89	202	0.84	± 0.11	0.095	± 0.005	0.0640	± 0.0037	619	± 60	585	± 29	742	± 262	95
LLZ298-5	0.0000	119	183	0.77	± 0.09	0.088	± 0.005	0.0638	± 0.0036	580	± 56	541	± 27	734	± 257	93
LLZ298-6	0.0000	204	1210	0.25	± 0.03	0.039	± 0.002	0.0467	± 0.0029	230	± 28	249	± 14	32	± 328	109
LLZ298-7	0.0000	358	641	0.86	± 0.11	0.103	± 0.006	0.0606	± 0.0033	633	± 59	635	± 33	626	± 254	100
LLZ298-8	0.0000	50	87	0.80	± 0.11	0.092	± 0.005	0.0630	± 0.0041	596	± 66	567	± 32	708	± 303	95
LLZ298-9	0.0000	108	135	0.86	± 0.11	0.096	± 0.005	0.0648	± 0.0038	630	± 63	592	± 32	766	± 267	94
LLZ298-10	0.0012	61	142	1.00	± 0.13	0.106	± 0.006	0.0686	± 0.0042	703	± 71	647	± 36	887	± 275	92
LLZ298-11	0.0000	111	266	0.88	± 0.07	0.098	± 0.005	0.0646	± 0.0023	639	± 41	605	± 27	761	± 157	95
LLZ298-12	0.0000	262	1130	0.83	± 0.06	0.100	± 0.004	0.0602	± 0.0018	612	± 35	612	± 26	612	± 136	100
LLZ298-13	0.0000	92	128	0.74	± 0.07	0.096	± 0.004	0.0563	± 0.0022	564	± 40	589	± 26	464	± 182	104
LLZ595-1	0.0000	250	68	4.03	± 0.30	0.294	± 0.011	0.0995	± 0.0031	1641	± 62	1661	± 57	1616	± 122	101
LLZ595-2	0.0000	203	120	3.39	± 0.25	0.257	± 0.010	0.0956	± 0.0030	1503	± 60	1477	± 52	1539	± 124	98
LLZ595-3	0.0000	178	62	3.26	± 0.24	0.251	± 0.010	0.0941	± 0.0030	1471	± 60	1444	± 51	1510	± 125	98
LLZ595-4	0.0000	448	1938	2.03	± 0.15	0.192	± 0.007	0.0766	± 0.0024	1126	± 52	1134	± 41	1111	± 132	101
LLZ595-5	0.0000	881	3723	4.05	± 0.30	0.289	± 0.011	0.1016	± 0.0032	1645	± 62	1638	± 56	1654	± 120	100
LLZ595-6	0.0000	65	48	3.45	± 0.27	0.269	± 0.011	0.0929	± 0.0031	1515	± 63	1536	± 55	1487	± 131	101
LLZ595-7	0.0000	296	151	4.11	± 0.30	0.293	± 0.011	0.1017	± 0.0032	1657	± 62	1658	± 57	1656	± 121	100
LLZ595-8	0.0000	344	197	3.78	± 0.28	0.273	± 0.011	0.1006	± 0.0032	1589	± 61	1555	± 54	1634	± 122	98
LLZ595-9	0.0000	698	433	2.55	± 0.19	0.220	± 0.009	0.0842	± 0.0026	1288	± 55	1282	± 45	1298	± 127	100
LLZ595-10	0.0000	302	87	4.00	± 0.30	0.284	± 0.011	0.1023	± 0.0032	1635	± 62	1611	± 56	1667	± 121	98
LLZ595-11	0.0000	404	800	3.47	± 0.24	0.261	± 0.010	0.0964	± 0.0027	1521	± 55	1497	± 52	1555	± 109	98
LLZ595-12	0.0000	747	316	3.19	± 0.22	0.242	± 0.009	0.0956	± 0.0027	1455	± 54	1398	± 49	1540	± 109	96
LLZ595-13	0.0000	410	96	4.03	± 0.27	0.297	± 0.012	0.0984	± 0.0028	1639	± 57	1674	± 58	1595	± 108	102
LLZ595-14	0.0000	200	61	4.14	± 0.28	0.301	± 0.012	0.0996	± 0.0028	1662	± 58	1697	± 59	1617	± 109	102
LLZ595-15	0.0000	229	219	2.12	± 0.15	0.196	± 0.008	0.0783	± 0.0022	1156	± 49	1156	± 42	1155	± 118	100
LLZ595-16	0.0000	140	60	2.80	± 0.20	0.242	± 0.010	0.0840	± 0.0024	1356	± 54	1397	± 50	1293	± 117	103
LLZ595-17	0.0000	161	106	3.51	± 0.24	0.279	± 0.011	0.0912	± 0.0026	1528	± 56	1586	± 55	1450	± 113	104
LLZ595-18	0.0000	226	249	2.57	± 0.18	0.229	± 0.009	0.0815	± 0.0023	1293	± 52	1329	± 47	1234	± 116	103
LLZ595-19	0.0000	296	444	2.13	± 0.15	0.183	± 0.007	0.0845	± 0.0024	1157	± 49	1081	± 39	1303	± 115	93
LLZ595-20	0.0003	298	244	5.00	± 0.34	0.324	± 0.013	0.1118	± 0.0031	1819	± 59	1811	± 62	1829	± 105	100
LLZ595-21	0.0000	178	79	2.24	± 0.15	0.201	± 0.010	0.0808	± 0.0019	1193	± 49	1181	± 52	1216	± 97	99
LLZ595-22	0.0000	191	131	2.38	± 0.16	0.220	± 0.010	0.0787	± 0.0019	1238	± 49	1280	± 56	1166	± 97	103
LLZ595-23	0.0000	487	367	2.31	± 0.15	0.208	± 0.010	0.0804	± 0.0018	1214	± 48	1218	± 53	1207	± 92	100
LLZ595-24	0.0000	193	157	2.81	± 0.19	0.225	± 0.011	0.0907	± 0.0021	1357	± 51	1306	± 57	1440	± 92	96
LLZ595-25	0.0000	284	446	1.89	± 0.13	0.174	± 0.008	0.0789	± 0.0019	1078	± 45	1033	± 46	1169	± 96	96
LLZ595-26	0.0000	307	899	1.84	± 0.12	0.176	± 0.008	0.0756	± 0.0018	1058	± 45	1046	± 46	1084	± 97	99
LLZ595-27	0.0000	158	108	0.82	± 0.06	0.102	± 0.005	0.0579	± 0.0016	606	± 34	628	± 29	525	± 125	104
LLZ595-28	0.0000	241	80	13.84	± 0.90	0.528	± 0.025	0.1901	± 0.0042	2739	± 63	2733	± 106	2743	± 75	100
LLZ595-29	0.0000	356	1727	1.27	± 0.09	0.132	± 0.006	0.0698	± 0.0017	833	± 39	800	± 36	923	± 101	96
LLZ595-30	0.0000	360	446	2.51	± 0.11	0.210	± 0.006	0.0866	± 0.0014	1275	± 32	1230	± 33	1352	± 64	96
LLZ595-31	0.0000	277	199	3.49	± 0.15	0.269	± 0.008	0.0939	± 0.0015	1524	± 35	1538	± 41	1505	± 62	101
LLZ595-32	0.0000	273	247	3.05	± 0.13	0.246	± 0.007	0.0899	± 0.0015	1420	± 34	1417	± 38	1424	± 64	100
LLZ595-33	0.0000	69	28	3.33	± 0.17	0.255	± 0.008	0.0946	± 0.0019	1488	± 41	1466	± 42	1520	± 79	98
LLZ595-34	0.0000	240	73	3.97	± 0.17	0.282	± 0.008	0.1021	± 0.0017	1628	± 36	1602	± 42	1663	± 61	98
LLZ595-35	0.0000	431	303	16.38	± 0.68	0.576	± 0.017	0.2061	± 0.0031	2899	± 41	2934	± 69	2875	± 49	101
LLZ595-36	0.0000	232	86	2.99	± 0.13	0.230	± 0.007	0.0944	± 0.0016	1406	± 35	1334	± 36	1517	± 65	95
LLZ595-37	0.0000	332	269	3.54	± 0.15	0.268	± 0.008	0.0959	± 0.0015	1535	± 35	1528	± 40	1545	± 61	100
LLZ595-38	0.0000	468	381	2.37	± 0.10	0.209	± 0.006	0.0823	± 0.0013	1234	± 31	1223	± 33	1252	± 64	99

Note: all errors are quoted at 2 s level
Concordance = [206Pb/238U age/ 206Pb/238U age]×100

Table2-2
LA-ICP-MC U-Pb isotope analysical data for zircons from sandstone samples in Lleyn peninsula

Grain	$^{204}Pb/^{206}Pb$	U (ppm)	Th (ppm)	$^{207}Pb/^{235}U$	2σ	$^{206}Pb/^{238}U$	2σ	$^{207}Pb/^{206}Pb$	2σ	Age (Ma)						Concordance
										$^{207}Pb/^{235}U$	2σ	$^{206}Pb/^{238}U$	2σ	$^{207}Pb/^{206}Pb$	2σ	
LLZ595-39	0.0000	342	127	5.40	± 0.23	0.342	± 0.010	0.1145	± 0.0018	1885	± 37	1896	± 48	1873	± 57	101
LLZ595-40	0.0012	136	108	2.22	± 0.15	0.205	± 0.007	0.0785	± 0.0023	1189	± 48	1205	± 35	1160	± 123	101
LLZ595-41	0.0000	521	573	3.47	± 0.22	0.275	± 0.008	0.0915	± 0.0025	1521	± 50	1567	± 43	1458	± 107	103
LLZ595-42	0.0000	32	41	3.96	± 0.30	0.271	± 0.010	0.1060	± 0.0036	1627	± 64	1547	± 50	1731	± 130	95
LLZ595-43	0.0000	790	1992	3.60	± 0.22	0.267	± 0.008	0.0978	± 0.0026	1549	± 50	1525	± 41	1582	± 105	98
LLZ595-44	0.0000	295	159	4.18	± 0.26	0.286	± 0.009	0.1062	± 0.0029	1670	± 53	1620	± 44	1735	± 104	97
LLZ595-45	0.0000	384	190	4.03	± 0.25	0.292	± 0.009	0.1001	± 0.0027	1640	± 52	1651	± 45	1626	± 105	101
LLZ595-46	0.0006	172	89	3.48	± 0.23	0.267	± 0.008	0.0945	± 0.0027	1523	± 52	1526	± 43	1518	± 111	100
LLZ595-47	0.0000	73	71	1.87	± 0.14	0.176	± 0.006	0.0768	± 0.0025	1069	± 50	1046	± 33	1117	± 138	98
LLZ595-48	0.0000	204	115	3.71	± 0.24	0.278	± 0.009	0.0968	± 0.0027	1573	± 53	1581	± 44	1563	± 109	100
LLZ595-49	0.0000	213	112	4.19	± 0.27	0.299	± 0.009	0.1019	± 0.0028	1673	± 54	1684	± 46	1659	± 107	101
LLZ595-50	0.0000	353	387	4.36	± 0.20	0.302	± 0.011	0.1047	± 0.0014	1705	± 39	1702	± 56	1709	± 49	100
LLZ595-51	0.0000	173	146	4.52	± 0.22	0.305	± 0.012	0.1073	± 0.0016	1734	± 41	1718	± 57	1754	± 55	99
LLZ595-52	0.0000	481	231	3.77	± 0.17	0.272	± 0.010	0.1002	± 0.0013	1585	± 37	1553	± 52	1628	± 49	98
LLZ595-53	0.0000	361	511	3.86	± 0.18	0.282	± 0.011	0.0994	± 0.0013	1606	± 38	1601	± 53	1612	± 51	100
LLZ595-54	0.0000	378	349	3.06	± 0.14	0.253	± 0.009	0.0878	± 0.0012	1422	± 36	1452	± 49	1377	± 53	102
LLZ595-55	0.0016	131	91	3.54	± 0.18	0.275	± 0.011	0.0932	± 0.0015	1536	± 41	1568	± 54	1492	± 63	102
LLZ595-56	0.0000	74	28	1.63	± 0.11	0.162	± 0.007	0.0730	± 0.0018	982	± 41	968	± 37	1015	± 105	99
LLZ595-57	0.0000	194	138	4.20	± 0.20	0.298	± 0.011	0.1022	± 0.0015	1673	± 40	1680	± 56	1665	± 55	100
LLZ595-58	0.0000	145	98	1.96	± 0.10	0.184	± 0.007	0.0772	± 0.0014	1101	± 37	1088	± 39	1126	± 76	99
LLZ595-59	0.0000	105	45	1.97	± 0.11	0.184	± 0.007	0.0774	± 0.0016	1105	± 39	1091	± 40	1132	± 84	99

Note: all errors are quoted at 2 s level

Concordance = [206Pb/238U age/ 206Pb/238U age]×100

Chapter 3 Geology of Anglesey Island

Abstract

A new stratigraphic framework of geology of Anglesey Island is first proposed in this paper to add the understanding of comparative blueschist belts in Pacific-type accretionary orogens such as Japan and California. The Anglesey Island is dominantly composed of accretionary complex (ACs) by geological survey and its metamorphosed portions along the deep Benioff plane at subduction zone. Analysis of U-Pb ages shows that the Gwna Group of the Mona Complex by Greenly (1919) is the typical ACs formed at three different stages; first at 630-610Ma (Type 1), second at 600-570Ma (Type 2), and third at latest Ediacaran to the Cambrian age (ca. 540Ma, Type 3).

The Central Shear Zone is ACs which suffered the subduction zone metamorphism. The separated zircons from this meta-ACs were measured to be 555Ma as the youngest age, suggesting the origin derived from ACs as same as the Gwna Group Type 3. The New Harbour Group is the youngest among the all ACs in Anglesey, ranging from 539Ma, 520Ma to 510Ma northwards as a depositional age. The New Harbour Group is the structurally lowest ACs, and could be metamorphosed to have penetrative fabrics at deeper subduction zone (depth <15km, T<300℃). Above the metamorphosed New Harbour schist, the ophiolite unit occurs, suggesting the presence of fore-arc ophiolite. The structural bottom is the South Stack Group composed of nearly pure quartzite. Their detrital zircon ages range from 3000 Ma to 515Ma that is remarkably different from those of the Gwna trench turbidites. Origin of the South Stack micro-continent could be deposited in an eastern margin of Laurentia, not a margin of West Africa or Amazonia. The tectonically overlying topmost units are

separated by the Carmel Head thrust. The exposure of Neoproterozoic platform carbonate olistostrome and muddy matrix including Ordovician fossils, indicate Ordovician subduction of TTG crust. The Gwna ACs, Arfon Group, Coedana complex dome-up to yield huge submarine landslides to form olistostrome. Cutting the thrust system, the final bimodal volcanism and associated caldera were formed at 437Ma (Silurian) together with hydrothermal-origin massive sulfide deposit at Parys Mountains. The final gravitational collapse under the extension stress regime occurred during the Carboniferous time, and thick carbonates covered the tectonically depressed region.

Keywords: ACs, BS-EA metamorphism, Pacific-type orogeny, olistostrome, continent subduction

3-1 Introduction

Geology of the Anglesey Island has long been investigated after the monumental work by Greenly (1919) who mapped and documented the geology of Anglesey putting the South Stack Group at the stratigraphic top. Since then, several works have been completed; Wood (1974) put blueschist into the framework of an accretionary orogen containing mélanges and ophiolitic relicts and made them comparative with rocks in California. Shackleton (1969, 1975) reevaluated the stratigraphy of Anglesey with way-up criteria which reversed Greenly's stratigraphy putting the South Stack Group at the bottom but regarded the Groups above to be in normal stratigraphic order. Barber and Max (1979) reassessed the tectonic stratigraphy, particularly proposing that the less deformed South Stack Group was thrust beneath the more highly deformed new Harbour Group. Gibbons (1983) pointed out that the evidence in Anglesey for

palaeo-subduction including the blueschists was insufficient, and Gibbons (1989) interpreted the tectonic belts in Anglesey in terms of suspect terrains. Gibbons and Mann (1983) first reported lawsonite in mafic blueschists, and Horak and Gibbons (1986) reclassified the blueschist amphiboles as crossites and barroisites. Gibbons and Gyopari (1986) proposed an anticlockwise P-T trajectory for the blueschists formed as a result of the subduction of oceanic crust, also Gibbons and Horak (1990) explained the contiguous fault-bounded metamorphic belts as suspect terranes on the margin of Avalonia. However, these previous studies have never interpreted the Anglesey blueschists in the light of a modern understanding of comparative blueschist belts in Pacific-type accretionary orogens such as Japan and California. Here I firstly indicate the role in geotectonic development on the subducting continental margin.

3-2 Geologic outline

Anglesey is a flat island without any steep relief. The characteristic geography might have made their structural relationships easier to analyze, the available detailed geologic maps, particularly of Greenly (1919), demonstrate the common presence of low-angle thrust, suggesting that the fundamental large-scale structure is subhorizontal, similar to that in many accretionary orogens worldwide (Maruyama,1997). Kawai et al., (2007) analyzed that the overall structure of the island is, from structural top to bottom, (1) Coedana granite-gneiss complex, (2) Gwna Group, (3) Blueschist and related metamorphic rocks, (4) Olistostrome-type ACs, (5) New Harbour Group, and (6) South Stack Group, which are all juxtaposed in a subhorizontal thrust-nappe pile. The sedimentary cover rocks were formed in extensional tectonic environments throughout the Ordovician, Silurian, Devonian, and Carboniferous times.

The top cover sequence is normal sedimentary cover deposited on shallow marine continental platform after the Carboniferous shown in grey color (Fig. 3-1). They are deposited tectonically depressed domains under the extension regime. Presumably it is a precursor episode of mid-Atlantic opening during the Jurassic time.

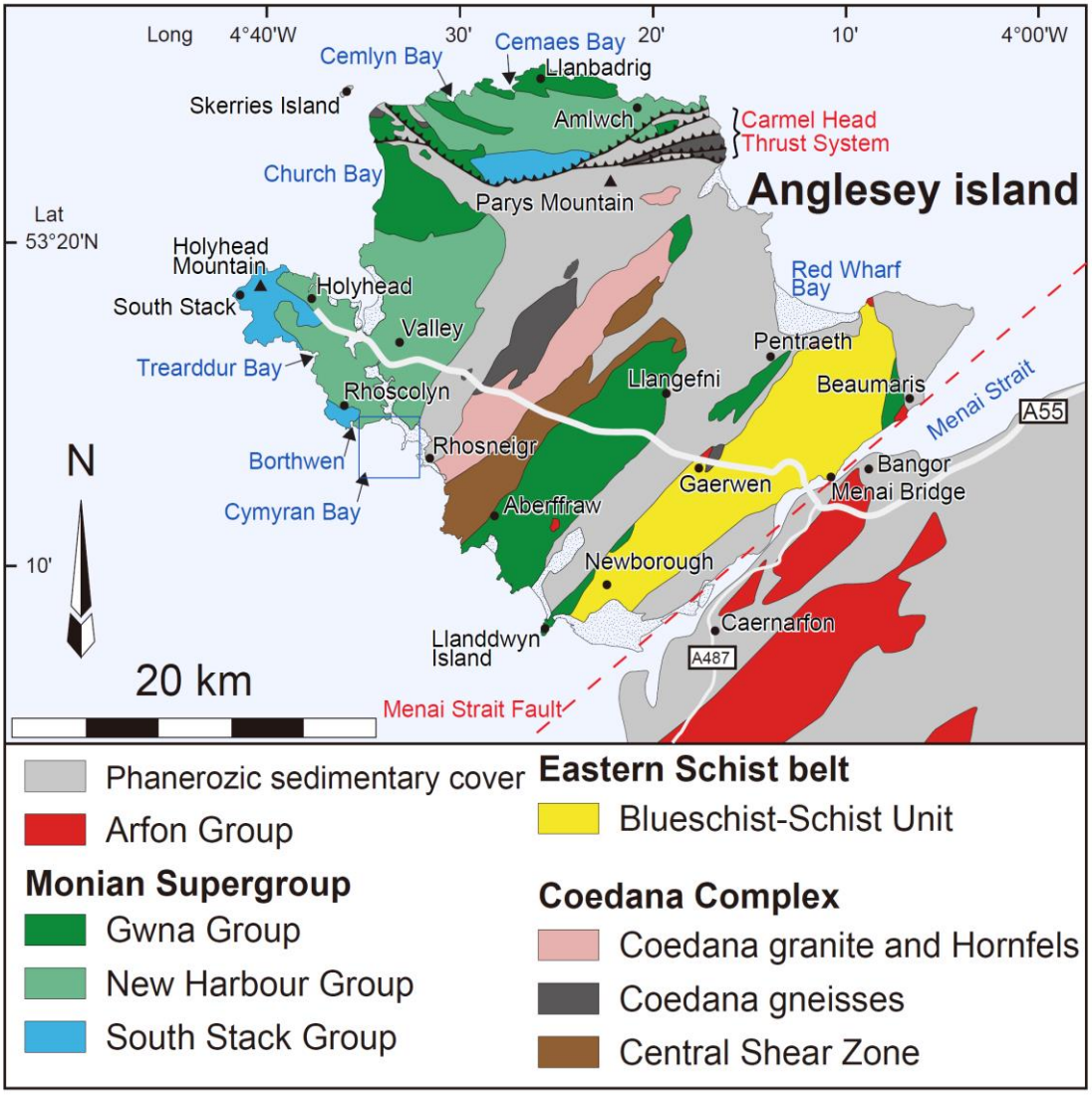

Fig. 3-1. Geological sketch map of Anglesey Island (modified from Greenly, 1919 and Shackleton, 1969).

3-2-1 BS-EA regional metamorphic belt

Henslow (1822) first mapped the belt of “chloritic schists”, and thus defined the tectonic framework in which the blueschists occur. Blake (1888) discovered the glaucophane. Although the recognition of Blueschists in England-Wales was earlier than in Japan and California, the significance of Na-amphibole in BS has not been justified until Miyashiro (1965), and followed up by Californian geologists, W. G. Ernst (1971).

The Menai Blueschist belt (proposed herein) has been regarded to be sheared mylonite at low-pressure, and Gibbons (1989) recently recognized as one of the allochtonous terranes transported along the strike-slip fault. Kawai et al. (2006) mapped the area, and divided the region by two mineral isograds. Moreover, the metamorphic facies has been determined by thermodynamic calculation based on their mineral analysis. The result indicated the zone should be redefined to be BS-EA facies regional metamorphic belt equivalent to the circum-Pacific high-P/T regional metamorphic belt.

3-2-2 Gwna Group structurally below the BS-EA unit; Llanddwyn Island as a type locality

The Gwna Group, that is exposed in about six areas widely on Anglesey (Fig. 3-1), contains many lenses up to few kilometers long of greenschist metabasalt with cherts and a few limestones in a matrix of chloritic greenschist to phyllite. On the northern coast near Cemaes Bay, one Gwna Group belt consists of a mélange made up of lenses largely of orthoquartzite and limestone (up to a kilometer long) in a matrix of chloritic schist (Wood, 1974). On LLanddwyn Island, well-preserved basaltic pillow lavas are interbedded or intercalated with limestone, jaspery phyllite (mudstone) and

bedded red jasper (chert) (Greenly, 1919).

3-2-4 Central Shear Zone, renamed as the Central regional metamorphic belt

The Central Shear Zone (CSZ) has been regarded to be a shear zone developed along the strike-slip zone same as the previous interpretation of BS belt. However, as same as the BS belt, it must be renamed to be a regional metamorphic belt, because the mineral assemblages indicate the regional change of metamorphic grade from GS to EA facies showing high-P/T geothermal gradient to suggest a subduction zone environment, and because the strongly penetrative fabrics are recorded.

On the other hand, what puzzled our mapping was the presence of klippes of Coedana Granite-Gneiss Complex (see its distribution in Fig. 3-2). The details will be shown later in this Chapter.

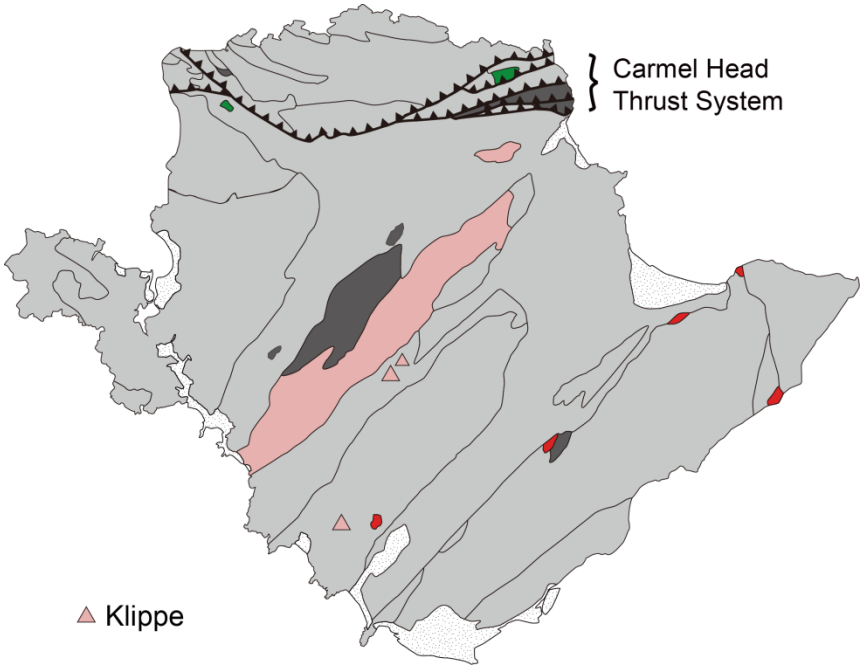

Fig. 3-2 Geological map of klippe of Coedana gneiss and associated rocks (hornfels) and Arfon Group.

3-2-4 Coedana Granite-Gneiss Complex (CGGC) and associated rocks (hornfels) and overlying unit of CGGC with unconformity; the Ordovician to Early Silurian units

In the center of the island, quartzo-feldspathic gneisses (up to sillimanite-kyanite grade) have a metamorphic U-Pb zircon aged 666±7Ma (Strachan et al., 2007), and a post-tectonic granite (Coedana granite) that has a U-Pb zircon aged 613±4Ma within the gneisses (Tucker and Pharaoh, 1991). These high-grade metamorphic rocks and associated granite, acidic supra-crustal rocks occur as a major coherent unit 3 x 20 km size, 0.5 x 1km or much smaller units having sporadic distribution on Anglesey Island (Fig. 3-1,2). They occur as klippes above the basement rocks separating nearly horizontal thrust plane. These high-grade metamorphic rocks are locally overlain conformably by the Siluro-Ordovician sedimentary rocks.

3-2-5 New Harbour Group schist belt

The New Harbour Group is dominantly composed of mafic schists with subordinate amounts of pelitic and psammitic schists. The rocks have been subjected to the deformation with strongly penetrated folding with micro-crenulation folds under ductile shear. The general dipping is horizontal to gently decline to the north or south. Close to the bottom boundary against the South Stack Group, the deformation fabric comes to yield clear reverse faults.

3-2-6 New Harbour Ophiolite belt

In the western belt contains many lenses of serpentinite and gabbro up to 2 km long (Maltman, 1977) commonly regarded as an ophiolitic remnant (Wood, 1974;

Thorpe, 1978; Maltman, 1979). Meta-basalts from the Gwna Group have MORB chemical patterns, whereas meta-basalts and meta-andesites from the New Harbour Group have supra-subduction zone arc affinities (Thorpe, 1993).

3-2-7 South Stack Group

On Holy Island, the South Stack Group mostly consists of quartzitic psammites inter-bedded with chloritic mafic pelites. The South Stack Group composed of A-type protoliths formed along the passive margin. Dominated by quartzite sandstone, extensively weathered hence no feldspars and mono-mineralic sandstone was formed. The youngest detrital zircons of the South Stack Group have U/Pb SIMS age of 501±10Ma (Collins and Buchan, 2004); this was the youngest in Anglesey to accrete to the toe of the accretionary wedge orogen (Kawai et al., 2007)

3-2-8 Parys Mountain hydrothermal ore at 430Ma

Parys Mountain is located 3km south of Amlwch in northeastern Anglesey, Wales. It forms an east-northeast trending ridge 2.5km long and 150m above sea level. Copper has been worked at Parys Mountain since the Roman Age. The major record of production was provided during 115 years between 1768 and 1883. For the substantial apart if this time was Europe's major producer.

Parys Mountain is located near the Carmel Head Thrust which carried the basement rocks of Coedana gneiss and related rocks together with the Gwna Group, Mona Complex, together with Ordovician platform sediments, over ca.200km from the Snowdonian TTG belt to the northern end of the Anglesey Island.

Carmel Head Thrust forms a zone with a few km wide, along which Parys

Mountain is located (Fig. 3-3). Thrusting occurred before or after the Ordovician, because the overthrust sedimentary rocks include Ordovician fossils of graptolite.

The NNW-SSE cross section of EW-trending Parys Mountain is shown in Fig. 3-3. The apparently symmetric of sedimentary rocks with an axis of inclined isoclinal folding suggests the presence of tight folding after the sedimentation on the platform shelf of continent. The youngest sedimentary rocks sitting on the stratigraphic top is Silurian age, whereas the stratigraphic bottom is thick Devonian formation with Precambrian basement rocks of the schistose Gwna Group. Ryodacite volcaniclastic rocks are interlayered. Along cracks and numerous veins, a series of economic ores are formed. Geologic age of the felsic magma dominated thermal event must have been between the Ordovician to Silurian. Radiometric dating has been performed to be 436 Ma ± 4Ma, or 2Ma for dacite magmatism (Barrett et al., 2001) which is consistent with the fossil constraints. The Ordovician-Silurian boundary is 444Ma, and the Silurian ends at 416Ma. Minor basalts occur in associated with dominant ryodacite lavaflows and puropclastics and dikes. Bimodal magmatism could be a key to discuss the tectonic settings.

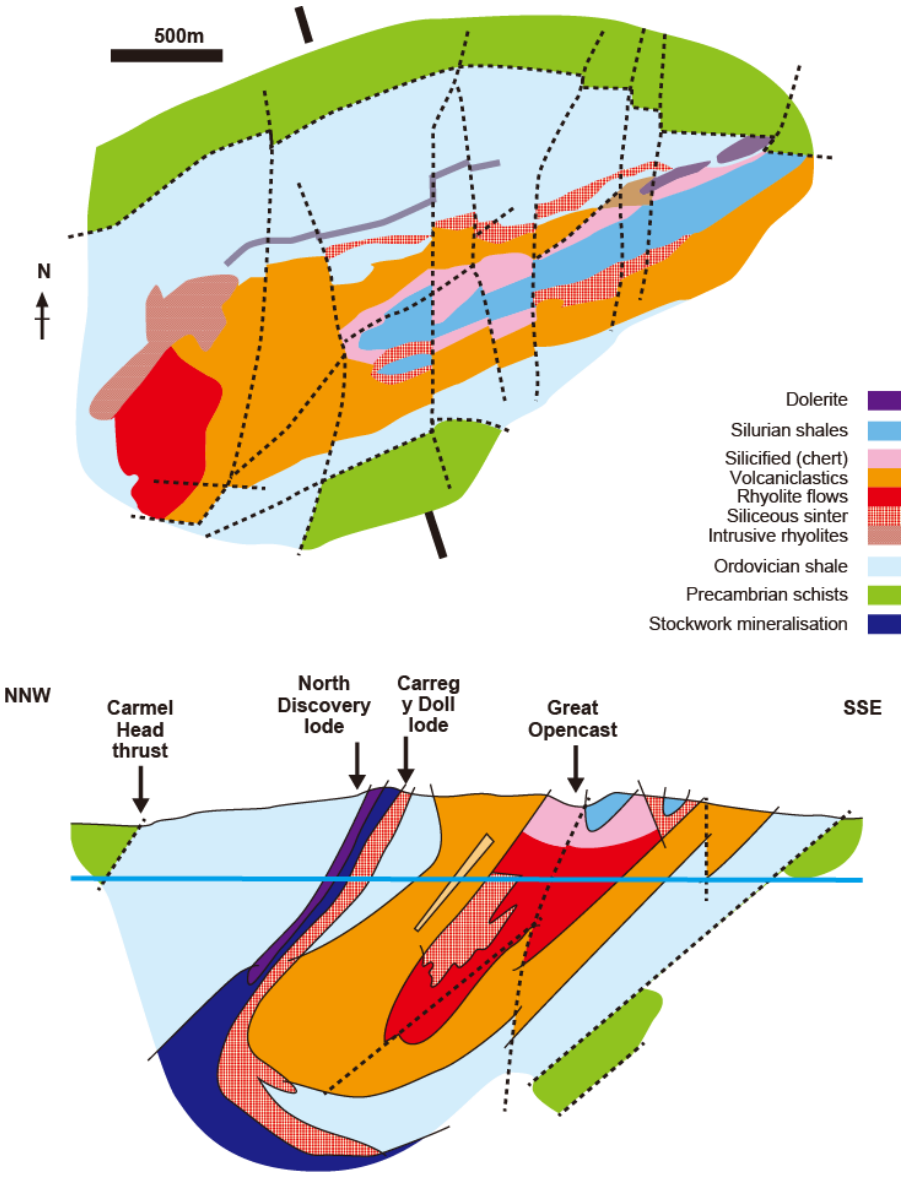

Fig. 3-3 Geologic map of Paris Mountain modified after Pointon and Ixer, (1980) (Top). Below figure show the NNW-SSE cross section. An overturned synform was inferred, however, recent extensive drilling does not support the idea.

3-3 Zircon chronology

3-3-1 Method

We separated zircons from the tuffs and sandstones. The zircons were extracted using a mineral separation system at the Tokyo Institute of Technology. *In situ* zircon U-Pb dating was carried out using a Nu AtttoM single-collector ICP-MS (Nu

instruments, Wrexham, UK) coupled to a NWR-193 laser-ablation system (ESI, Portland, US), that utilizes a 193 nm ArF excimer laser, at Department of Geology and Mineralogy, Kyoto University. The detail of zircon separation and U-Pb dating were described in Chapter 2.

3-3-2 Result

The results of U-Pb dating of detrital zircons from sandstones and tuff by LA-ICP-MS are listed in Table 1. Most zircons from the sandstones are rounded and show oscillatory zoning under CL images. Some zircons contain an inherited core. However, no systematic differences of the CL images and shapes of zircons were detected in each age population.

The A674, ANG66 samples consist of the Gwna Group in southern Anglesey. The results of zircons from two samples were plotted on a Concordia curve within 2σ error show 60 and 58 grains, respectively. Moreover, the youngest ages of A674 and ANG66 are 884 ± 52 Ma (Fig. 3-28).and 545 ± 32 Ma (Fig. 3-17). The LLZ519 sample consists of the Gwna Group at Llanddywn. The results of zircons from the samples plotted on a Concordia curve within 2σ error show 64 grains and the youngest ages are 535 ± 14 Ma (Fig. 3-16). On the other hand, the LLZ422 sample consists of Blueschist Unit. The results of zircons from the samples plotted on a Concordia curve within 2σ error show 45 grains and the youngest ages are 543 ± 20 Ma (Fig. 3-9). The results of zircons from UKY2 in Gwna Anglesey east plotted on a Concordia curve within 2σ error show 88 grains and the youngest age is 566 ± 15 Ma (Fig. 3-9).

The ANN2, ANN14, ANG26 samples consist of Central Shear Zone. The results of zircons from the samples plotted on a Concordia curve within 2σ error show 75, 60

and 28 grains, respectively. The number of disconcordance in ANG26 shows more than 10 % of all analysis of zircons, indicating a possibility of Pb loss. Moreover, the youngest ages of ANN2, ANN14 and ANG26 are 1034 ± 61, 591 ± 15 and 555 ± 9 Ma (ANN2:Fig.3-28; ANN14, ANG26:Fig.3-18). The youngest ages of ANN14 and ANG26 show similar age, white ANN2 shows older age.

The IR708 consists of Gwna Anglesey north. The results of zircons from the sample plotted on a Concordia curve within 2σ error show 68 grain s, respectively. Moreover, the youngest ages is 565 ± 9 Ma (Fig. 3-29). The results of zircons from ANG146 in New Harbour Group in Anglesey North plotted on a Concordia curve within 2σ error show 51 grains and the youngest age is 510 ± 14 Ma (Fig. 3-29). Moreover, the LLZ994 60 and AMW28 samples consist of South Stack Group in Holy Island. The results of zircons from the samples plotted on a Concordia curve within 2σ error show 47 and 59 grains, respectively. The youngest ages of LLZ994 and AMW28 are 543 ± 9 and 515 ± 16 Ma (Fig.3-27). The AMW31 and UKY-5 consist of New Harbour Group. The results of zircons from the sample plotted on a Concordia curve within 2σ error show 40 and 31 grains, respectively. Moreover, the youngest ages are 520 ± 31 and 539 ± 14 Ma (Fig.3-24).

3-4 Description of each unit

3-4-1 Menai BS-EA facies regional metamorphic belt

Menai Blueschist is the Blueschist Unit which exposes on the Anglesey Island. The metamorphic grade of Menai Blueschist has been sub-divided into three mineral zones; I, II, and III on the basis of crosstie and barroisite isograds after Kawai et al., (2006). The appearance of crosstie defines the beginning of Zone II. Zone I has a

chlorite-epidote mineral assemblage. But, the basaltic lavas of the Gwna Group to the east have only chlorite, which we ascribe to thermal hydration metamorphism on the ocean floor; i.e., they were not metamorphosed by the regional metamorphism that affected Zones I, II, and III. These chloritic basaltic lavas correspond to similar unmetamorphosed Gwna Group basaltic lavas in SW Lleyn.

The spatial distribution of the mineral zones, passing from east to west, indicates a structurally-downwards, westward increase of P and T from Zones I to II towards a central structural horizon (Zone III), and then a corresponding decrease farther westwards from III to I (Fig. 3-8) (Kawai et al., 2006).

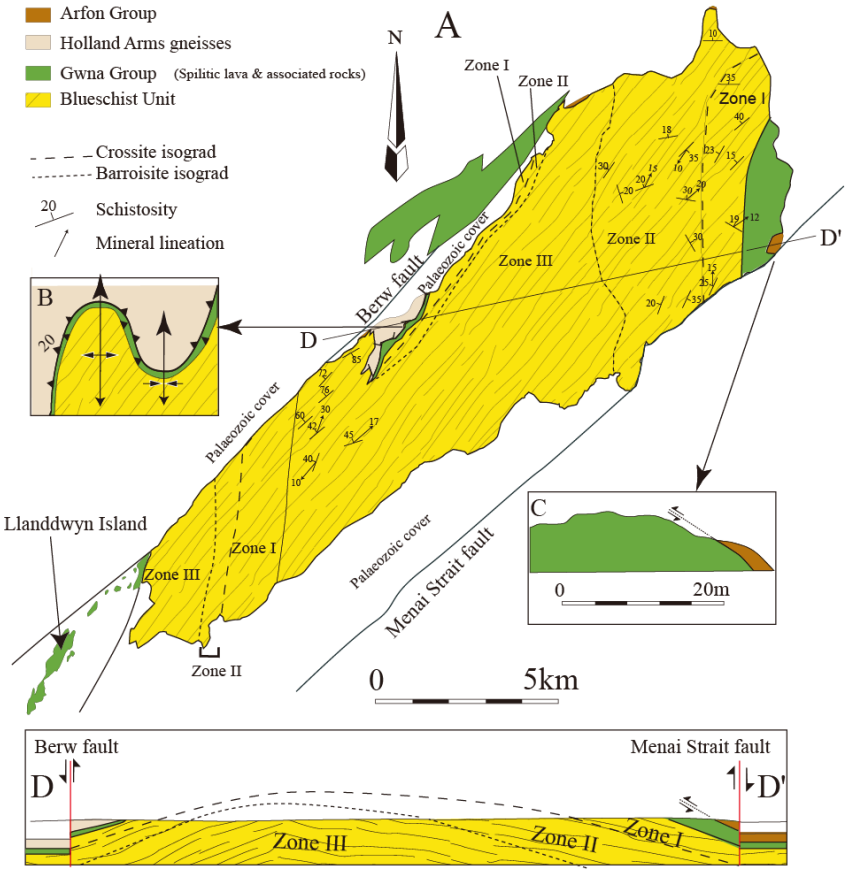

Fig. 3-8. A:Metamorphic zonal map of the Blueschist Unit in Anglesey (Kawai et al., 2006). B: Sketch of the boundary between Holland Arms gneisses, Gwna Group and Blueschist Unit. C: Sketch of the boundary between the Arfon Group and Gwna Group. D: Cross-section of the Blueschist Unit from D to D'. (Kawai, 2009)

The Blueschis Unit (5km x 25km) in Zone III contains lenses of well-preserved glaucophane-nearing metabasic rocks up to 5km long, as shown on the geological map of Anglesey (British Geological urvey, 1980), the wall-rocks of which mostly consist of chloritic and micaceous schists without glaucophane. Many meta-basic lenses consist of hornblende schist, some of which in less retrogressed areas contain glaucophane. Mineral lineation defined by well-developed Na-amphibole on foliation surfaces and crenulation fold axes trend NNE-SSW (Fig. 3-8A). Zone II (3km x 11 km) on the eastern side of Zone III also contain lenses up to 1.5km long of glaucophane-nearing metabasic rocks.

(1) Zircon ages of host metagreywackes from BS-EA unit

Formation age of Menai Blueschist Unit was analyzed by Dallmeyer and Gibbons (1987) which indicated that this unit was metamorphosed around 560Ma. I analyzed the age of zircon contained in this blueschist unit to induce the formation age of original sedimentary rocks. The result is given in Fig. 3-9, it shows the age distribution of detrital zircon is range from 600 Ma to 540 Ma. The youngest age means the maximum depositional age of original sedimentary rocks, is 543 ± 20 Ma. The age of original sedimentary rock must be older than the metamorphosed age, therefore this result seems to be inconsistent with the geotectonic evolutional model; however, considering error bar (±20Ma) of zircon chronological analysis, 543 ±20 Ma of zircon age is thought to fall in acceptable range.

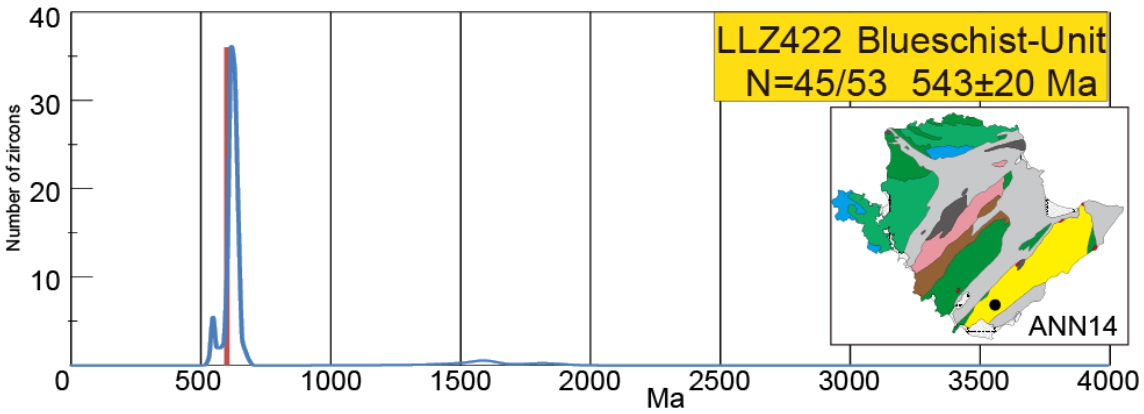

Fig. 3-9 Detrital zircon ages distribution from Blueschist Unit. N= number of plot / number of analysis. The sampling point is shown in right side.

(2) Zoning of mineral distribution

Menai Blueschist is divided into 3 zones depend on mineral assemblages; Zone I, II, and III. Zone I is epidote-chlorite facies, Zone II is crosstie-epidote facies, and Zone III is barroisite-epidote facies (Figs.3-10, 3-11, 3-12) (Kawai, 2009). Zone I metabasites contain the common mineral assemblage calcite-chlorite-epidote, in addition to excess phases; albite, quartz, titanite, phengitic mica, and presumably H_2O-rich fluid. Carbonate is calcite, and aragonite has not been identified. Zone II mafic schists yield the mineral assemblage epidote-chlorite-crossite with the excess phases; albite, quartz, titanite, phengitic mica, and presumably H_2O-rich fluid. Zone III metabasites contain epidote, chlorite and the Na-Ca amphibole of barroisite, crosstie, actinolite and winchite: the zone is defined by the appearance of barroisite that consumes epidote, crosstie and minor chlorite. $^{40}Ar/^{39}Ar$ white-mica ages of 580-590Ma (actinolite-rich concentrates) suggest that the actinolite is possibly the relic of ocean-floor metamorphism (Dallmeyer and Gibbons, 1987). Therefore, we do not use the actinolite for mineral zonation. This is the Penmynydd metamorphic zone of the Anglesey map of British Geological survey (1980). In Fig. 1-4 (Fig. 3-11) structural-metamorphic map of

the northern part of Menai Blueschist, the structural data compiled from Greenly (1919) on map of British Geological Survey (1980). Gibbons and Gyopar (1986), the data of Treagus (2007), and measurements derived by Kawai (2009), together with the metamorphic isograds. Fig. 3-11 shows that the axial trace of the fold extends along the eastern side of Zone III from the horizontal hinge al Llanfair PG village to about 546-760m from where it follows the Zone II/III boundary northwards. On the western side of the axial trance the rocks mostly dip to the west, whereas on the eastern side they mostly dip to the east; i.e. and antiform. Measurements in the axial zone indicate the fold plunges shallowly to the north. Note that metamorphic Zone III gets narrower to the north, where the structural antiform apparently get tighter, and where there are some vertical dips in the north of Zone II, taken from British Geological Survey (1980); from our experience these represent the steep limbs of local minor folds.

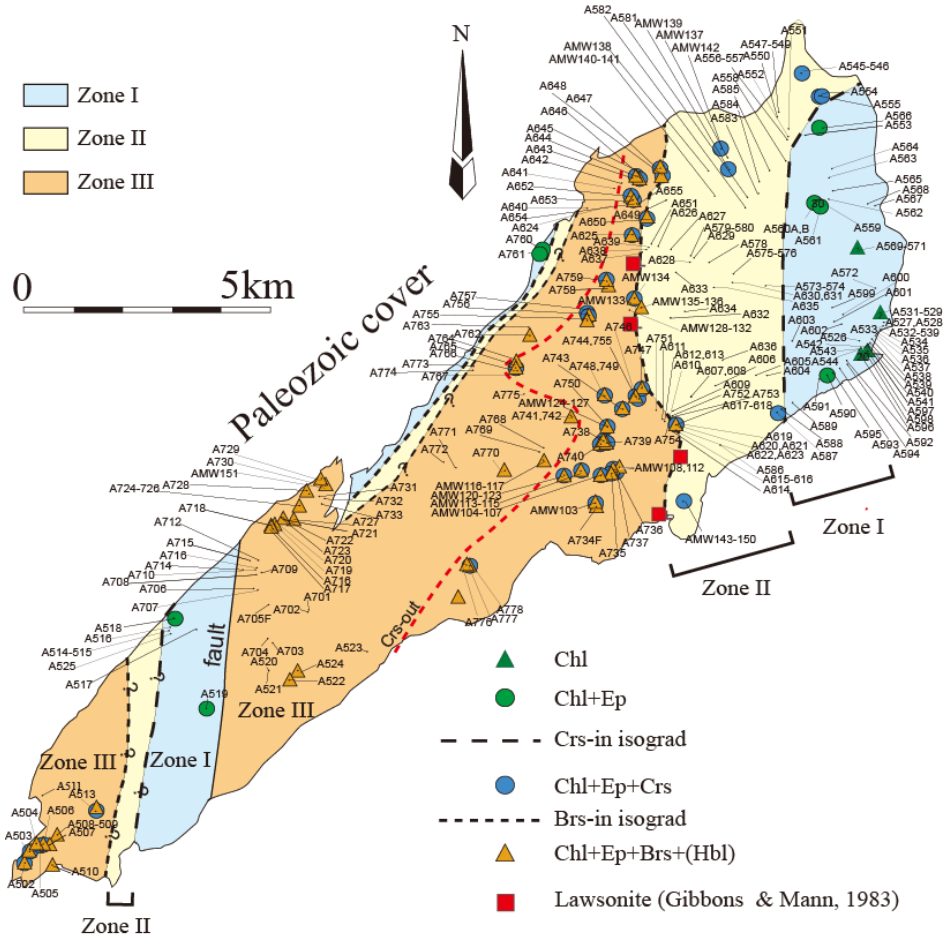

Fig. 3-10 Sample localities and distribution of mineral assemblages in metabasites in three metamorphic Zones. (Kawai, 2006)

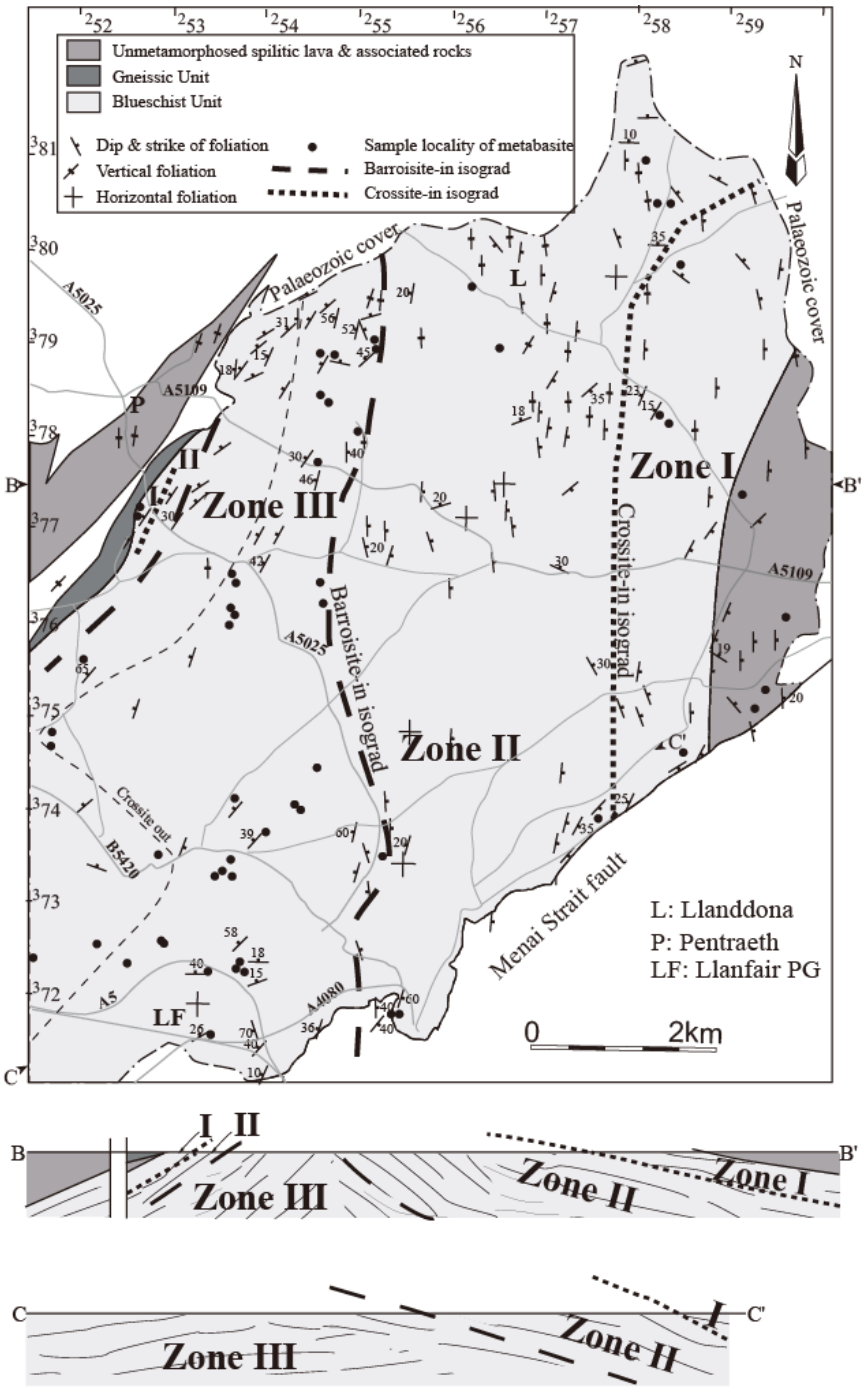

Fig. 3-11 Structural and metamorphic zonal map and cross-section of the northern, main part of Blueschist Unit in Anglesey. Dip and strike data are compiled from British Geological Survey (1980), Gibbons and Gyopari(1986), Treagus (2007) and Kawai (2009). This grey lines indicate roads. The solid black lines indicate faults. The dash-dot lines indicate faulted or unconformable junction against Paleozoic sedimentary cover. Marginal numbers refer to the national Grid of the Ordnance Survey of Great Britain. Simplified cross-sections B-B' and C-C' show the antiformal structure of the Blueschist Unit. Structural relationships between the Blueschist Unit and bordering rocks are

from Kawai et al., (2007). (Kawai,2009)

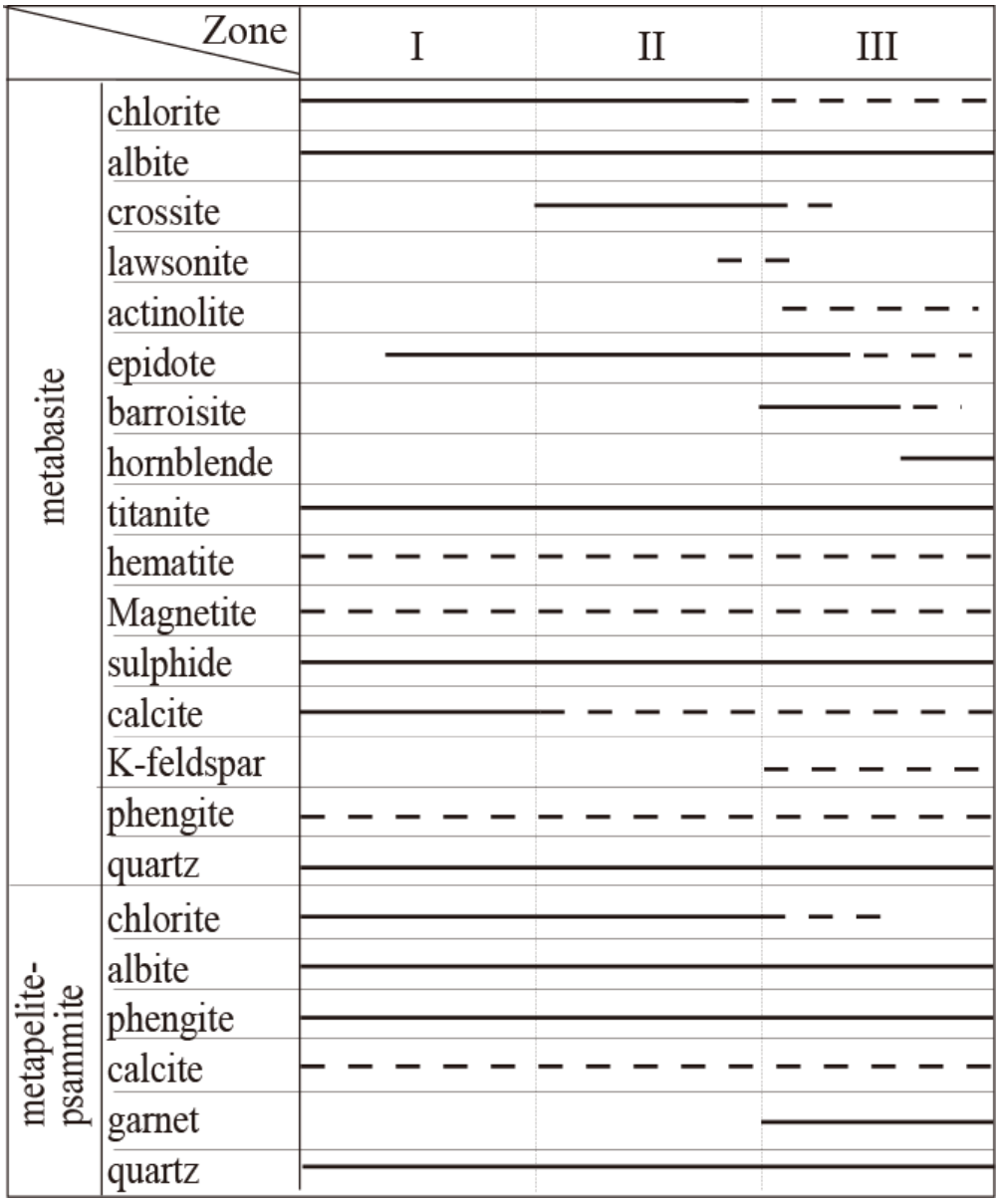

Fig. 3-12 The stable occurrence of minerals in metabasites and metapelite-psammites in the three zones. Solid line means major constituent, and dashed line means minor constituent. (Kawai et al., 2006)

(3) P-T conditions of each metamorphic zone in Menai Blueschist

P-T condition of metamorphic belt provides significant information where this metamorphism has occurred. According to mineral zones, mineral assemblages and

mineral compositions derived from Kawai (2009), it is indicated that a subduction zone geotherm that ranged from 15km (300℃) to 35km (500℃), following a high-pressure intermediate metamorphic facies series similar to that of the Cretaceous Sambagawa belt, Japan (Miyashiro, 1965, 1994). The P-T –time path and metamorphic facies series shows an anticlockwise evolution that is consistent with the calculated geothermal gradient along a Benioff zone (e.g. Peacook, 2001). Recent well-documented analyses of the P-T trajectory and metamorphic facies series of comparable blueschist belts support an anticlockwise, rather than a classic clockwise path (Ota et al., 2004). On the other hand, the Kokchetav diamond-coesite-bearing rocks in Kazakhstan have a similar anticlockwise P-T path (Omori et al., 2004). The Menai Blueschist is a small piece of an accretionary orogen. Both the Sambagawa and Franciscan blueschist which may be regarded as representative world-standard of high-pressure rocks in accretionary orogens, occur as thin (<1km), flat-lying tectonic slices cut on the top and bottom by normal and reverse faults respectively. The shallow sub-horizontal strucuture, size and thickness of the Menai Blueschist and the range of metamorphic grade from sub-greenschist through blueschist to epidote-amphibolite facies, all demonstrate that this is a typical blueschist belt. Horak et al.(1996) pointed out that a calc-alkaline magmatic arc crops out in the Snowdonia Mountains to the east of the blueschist belt, which they envisaged was created by the eastward subduction of the Anglesey rocks. Accordingly, the subduction zone should have been located between the arc and the blueschists near the present-day Menai trait fault. It is interesting to note in passing that the section across Anglesey is very similar to the Cenozoic trench-arc section across Japan with the Ryukyu arc on the west side of the fault of the Median Tectonic Line (Maruyama et al., 1997). The tectonic belts and metamorphic zones on Anglesey have a

symmetrical arrangement. The map of British Geology Survey (1980) shows that the central high-pressure 'Penmynydd metamorphic zone' with blueschist and mica schists (Zone III) is bordered on both sides by Gwna Group that contain lower grade grenschists, spilitic lavas and albite diabases (Zone I). The western half of the eastern Gwna shows evidence of blueschist metamorphism (Zone II). Such an arrangement of metamorphic belts and zones with the highest pressure and deepest rocks in the centre and flanked by lower grade rocks on either side suggests an antiformal structure. The tectonic model of the Pacific-type accretionary orogen is consistent with the fact that the last rocks to be under-plated in the west were passive margin sediments (mostly quartzite) of the South Stack Group that contain zircons with the youngest age of 501±10Ma (Collins and Buchan, 2004).

(4) Characteristic occurrence of Menai Blueschist

Menai Blueschist in the Anglesey Island was formed at consuming plate boundary during the Neoproterozoic time, based on mineral isograds to define three mineral zones and facies ranging from GS/BS transition through BS facies to EA facies with sandwiched thermal structure, which is the most characteristic feature of this geological unit, and concluded SE-ward subduction of oceanic lithosphere under England (Kawai et al., 2006). The previous researchers have long considered it to be formed during the strike-slip movement of simply along shear zone.

As one of the typical examples of ACs for the small area of the Llanddwyn Island off southern Anglesey Island, Maruyama et al. (2010) led a conclusion of duplex-type accretion of the Cambrian oceanic crust on the hanging wall of England. Moreover, the dropstones in trench turbidites have also been reported in the Llanddwyn Island (Kawai

et al., 2008).

3-4-2 Gwna Group observed on the Llanddwyn Island

Llanddwyn Island (300 x 700m) is off the southwest coast of Anglesey (Fig. 3-13). It is a fault-bound tectonic slice between the Menai Blueschist unit to the east and a coherent Carboniferous carbonate cover to the west, both sides being marked by high-angle faults.

It is dominantly composed of Gwna Group pillow basalts and subordinate pillow breccias or hydaoclastites, mafic mudstone, limestones, bedded cherts and in places turbiditic sediments that have a general strike to 030-045°and a vertical to overturned dip of 70-80°W. Two close parallel NS-trending, late strike-slip faults with a left-lateral sense of movement divide the island into eastern and western units. A 30m thick brecciated clayey shear zone is developed between these faults.

Kawai (2008) made a detailed geological map of 5 x 4 m^2 area in western Llanddwyn Island to illustrate the imbricated OPS which consists of repeated basalt, red chert and mudstone and sandstone. Many faults are sub-conformable with bedding planes within the cherts and mudtstones. In some places, such as on the limbs of isoclines, thrusts can be seen to be parallel to bedding, but elsewhere some thrusts can be any observed by the presence of finely sheared material on the bedding places. Three isoclinal folds in bedded cherts are seen. Similar isocline folds in bedded cherts are common in OPS sections of the Shimanto Group in Japan.

A large-scale text-book like duplex is well preserved on Llanddwyn Island (Fig. 3-14). The eastern unit is subdivided by several bedding-parallel link thrusts (F1) into 6 separate horses separated by two roof- and floor-thrusts (F2). The eastern and western

units are separated by two F3 close and parallel strile-slip faults. The western unit has 17 horses separated by two major roof- and floor-thrusts (F2) (Fig. 3-14).In spite of extensive tectonic modification by layer-parallel shortening, the stratigraphic top of each horse can be easily determined by the primary shapes of un-deformed pillows. It indicates that all the units face upwards to the southeast. In each horse, the stratigraphic bottom is a MORB-like, pillow lava or massive basaltic sheet flow. Pillows are 30-60cm in diameter and are cemented by a glassy matrix. Each pillow is well identified by its chilled margin that is a few mm to 1 cm thick. In places pillows mutually connect to form an elongate tube or channel. Under the microscope the pillow lava is fine-grained and intersertal ophitic with swallow-tail augites and plagioclase laths. The matrix consists of red jasper or limestone.

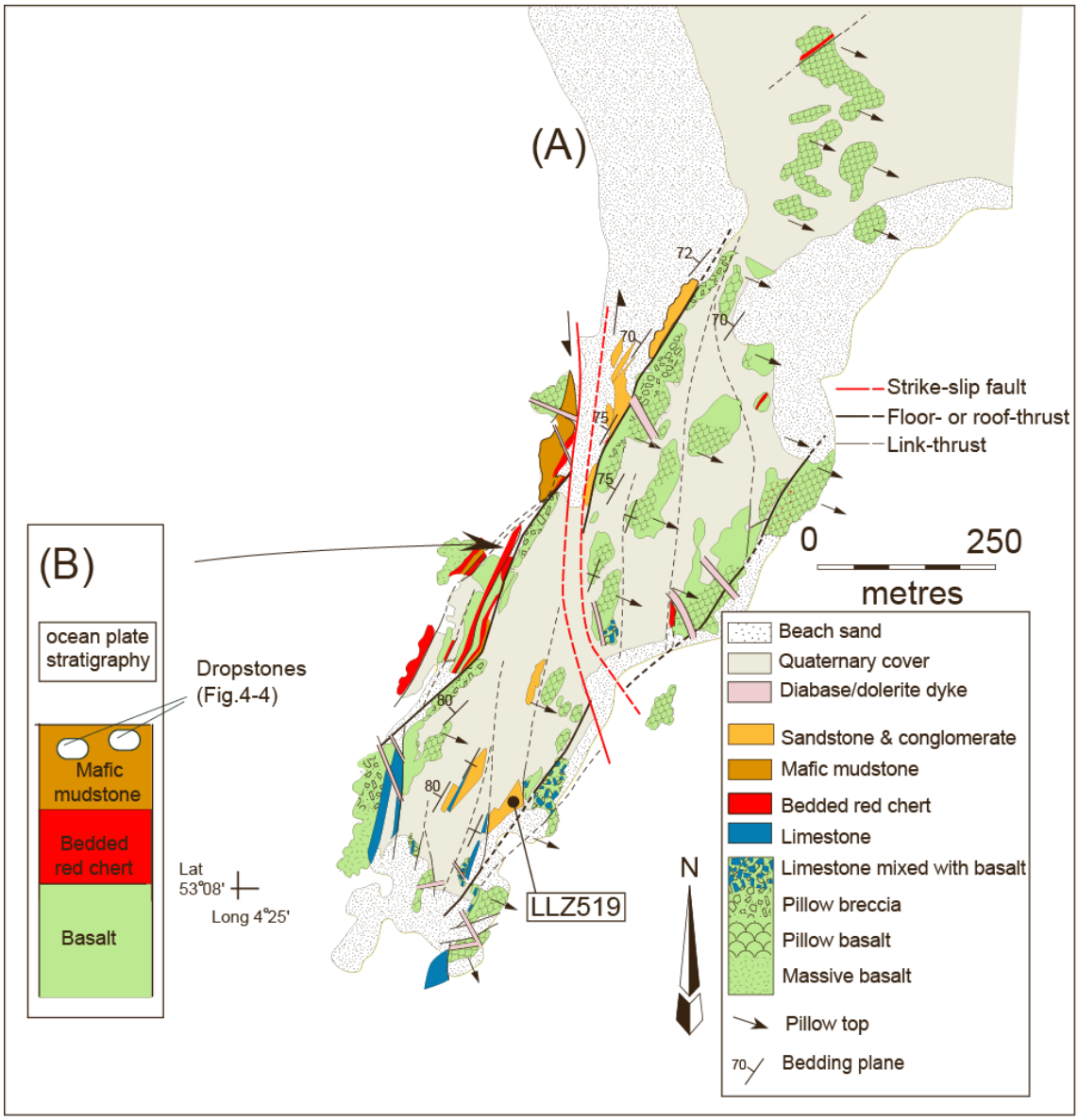

Fig. 3-13. A: Geologocal map of Llanddwyn Island showing the distribution of main lithologies, and the principal structural relations. B: The ocean plate stratigraphy of western Llanddwyn Island showing the location of dropstones in the upper mafic mudstone (Maruyama et al., 2010). LLZ519 is the location where rock sample was collected for zircon chronology analysis.

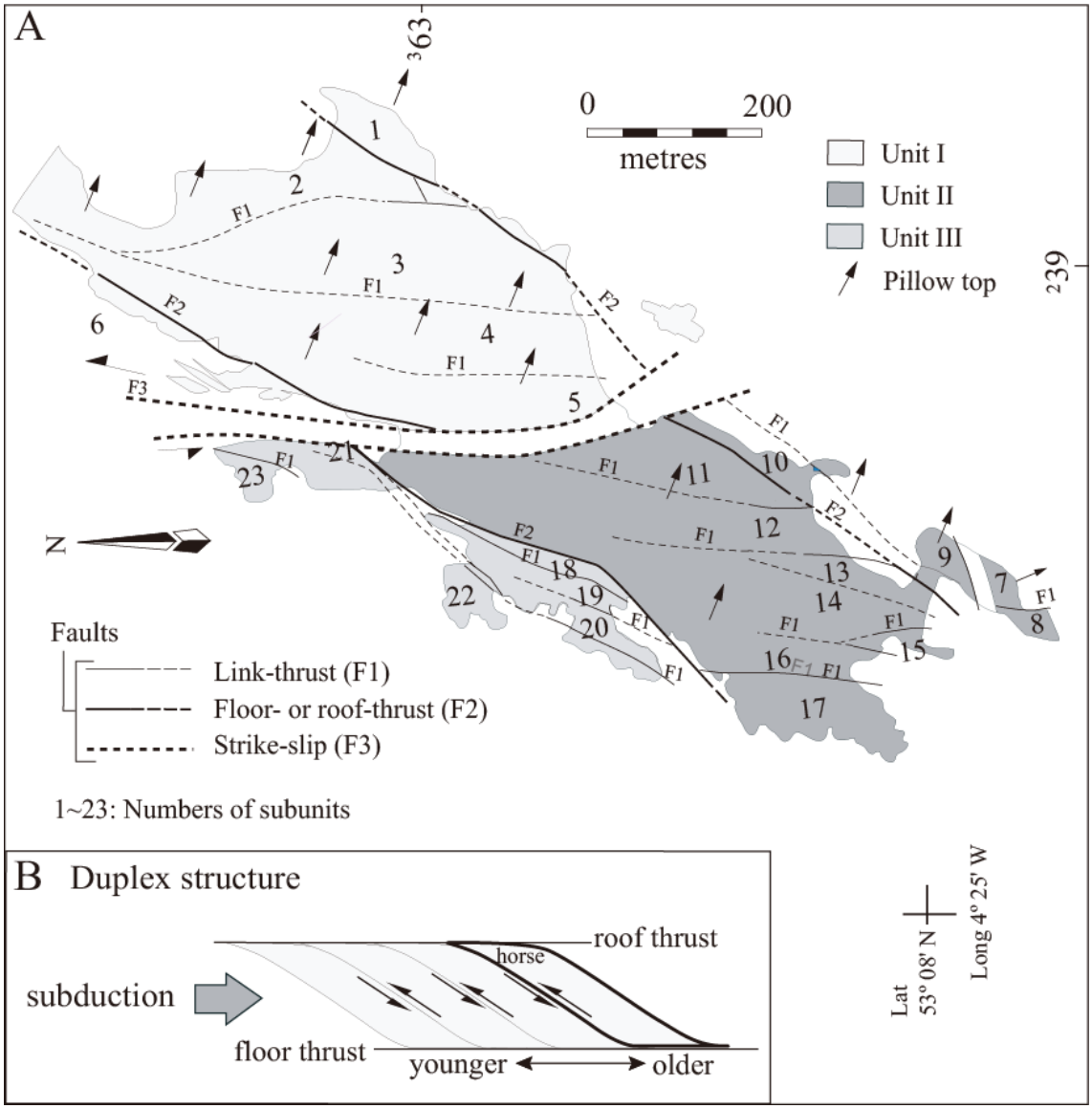

Fig. 3-14 Map showing the distribution of duplex horses on Llanddwyn Island. (Maruyama et al., 2010)

In unit I, the horses (Fig. 3-15) are numbered from 1 to 6. In general, this unit is composed of 100m thick (maximum) MORB-like pillow lava with red chert in the inter-pillow and overlying 20m thick chlorite-rich sandstone.

In unit II the horse, numbered from 7 to 17, in general comprise 100m thick.

MORB-like pillow lava flows, overlain by 40m thick pillow breccias (up to 20 m thick), which matrix is mafic mudstone contain several lenses of limestone, in turn succeeded by 40m thick pelagic carbonates, overlain by a ca. 50m thick sandstone. A special situation exists in eastern Llanddwyn where unit II basalts with inter-pillows of red chert are succeeded by basalts with inter-pillows of limestone, overlain by 2m of grey limestone, and 5m of pink manganiferous rhodochrosite limestone, which we interpret as pelagic limestone deposited at or near a thick, high-standing ridge.

I collected sandstone sample from horse 12 to determine accretion age for U-Pb zircon dating. As a result, it was showed that the youngest age is 535 ±14 Ma, the Early Cambrian (Fig. 3-16). So, unit II arrived at trench around Early Cambrian.

In unit III the horses, numbered from 18 to 23, are characterized by a 2m thick red bedded chert capped by 18m thick hemi-pelagic mafic mudstone and 20cm sandstone.

In general, the sedimentological changes reflect the gradual change in environment from eruption of vesicle-absent lavas in the deep ocean at or near a ridge, through deposition of pelagic chert or limestone in an ocean remote from a continent, via hemi-pelagic mudstone either approaching or on the lip of a trench, to a deep trench flooded by an arkosic-quartzitic sandstone to conglomerate in the form of a cap turbidite. This is OPS (Matsuda and Isozaki, 1991) that contains a record of the travel history from the birth of an oceanic plate to its demise at a trench.

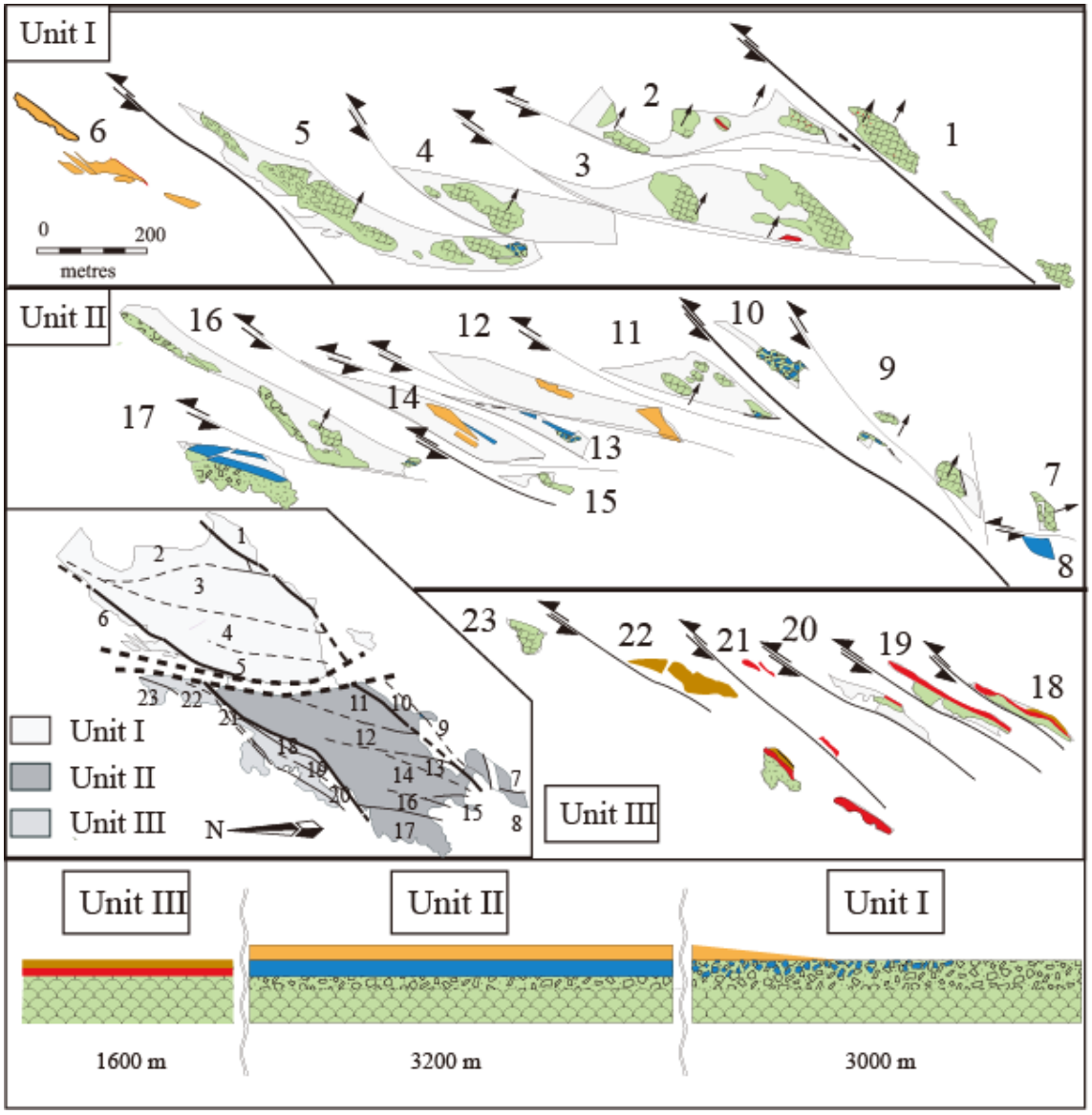

Fig. 3-15 Strong lateral shoretening for the geotectopnic development of Llanddwyn island by plate tectonics (Maruyama et al.. 2010).

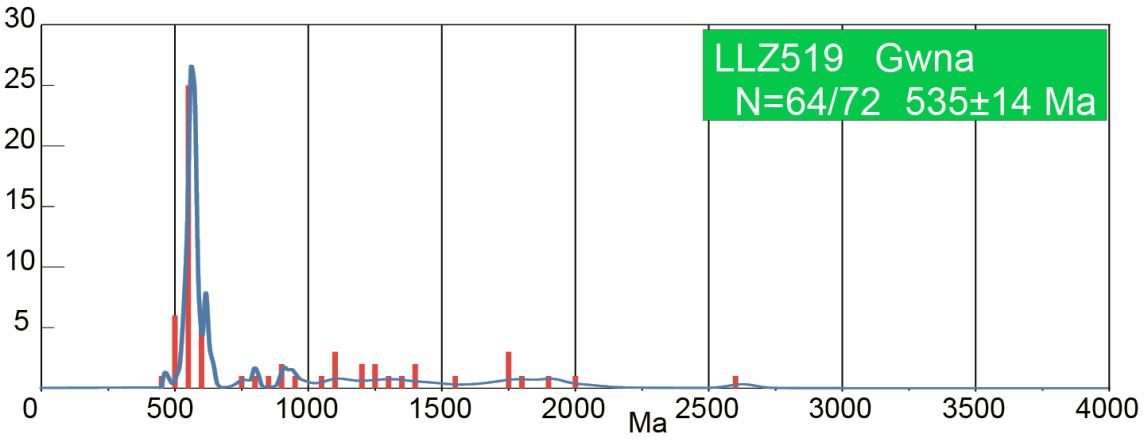

Fig. 3-16 Detrital zircon ages distribution from Llanddwyn Island.. N= number of plot / number of analysis. The sampling point is shown in right side

3-4-3 Gwna Group observed on central Anglesey

The central Gwna Group is about 5 km northern side of the Llanddwyn Island (Fig. 3-1). It is a fault-bound tectonic slice between the Central Shear Zone to the west and a coherent Carboniferous carbonate cover to the east. It is dominantly composed of greenstone, greenschist, mafic mudstone, limestones, and in places turbiditic sediments.

I collected sandstone sample, ANG66, from coast side to determine accretional age for U-Pb zircon dating. As a result, it was showed that the youngest age is 545±32 Ma, end of the Ediacaran (Fig. 3-17). On the other hand, the age distribution of zircons is similar to the result of Llanddywn (Fig. 3-16). So, the Gwna Group in this area and the Llanddywn are the same.

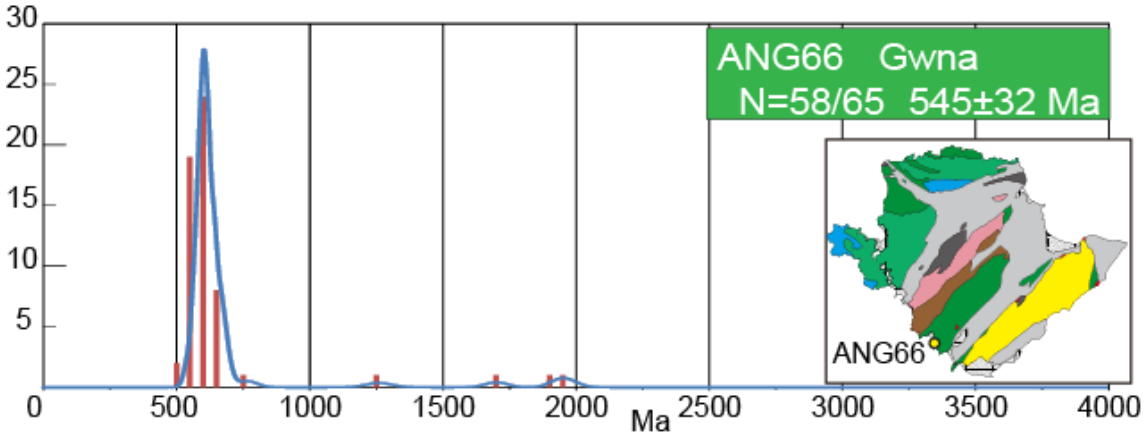

Fig.3-17 Detrital zircon ages distribution from southern coast.. N= number of plot / number of analysis. The sampling point is shown in right side

3-4-4 Central Shear Zone (renamed as the Central regional metamorphic belt)

The Central Shear Zone (CSZ = Central regional metamorphic belt) runs NE-SW direction in the central Anglesey Island, which is a thin (>1km) tectonic unit separated on the top and bottom by feebly metamorphosed ACs, the Gwna Group and/or late-stage accidental tectonic juxtaposition of klippe of Snowdonian TTG and associated metamorphic rocks.

CSZ is regionally metamorphosed units with strongly penetrative fabrics at high-P/T conditions, ranging PA, GS to EA facies conditions. This strongly suggests that the protoliths of CSZ Gwna Group were brought to deep subduction zone.

(1) Protoliths of CSZ

The CSZ is not a simple fault zone but is of schist belt with strongly penetrative fabrics. Protoliths of rock type are oceanic materials such as greenstones and cherts with clastic rocks such as sandstones and mudstones, hence similar to the ACs of the Gwna

Group. However, different from the Gwna Group, the field occurrence looks like coherent unit because of highly penetrative fabrics and extensive flattening of rock units. The protolith ages are also different. Two samples ANG26 and ANN2 are psammitic schists selected for age dating (Fig. 3-18). As a result, both samples are similar in age frequency with a sharp peak at around 700-550Ma. The youngest age is 555±9Ma, indicating the formation of ACs at trench was end Ediacaran, and similar age of the Gwna Group in Anglesey(Fig. 3-16, 17).

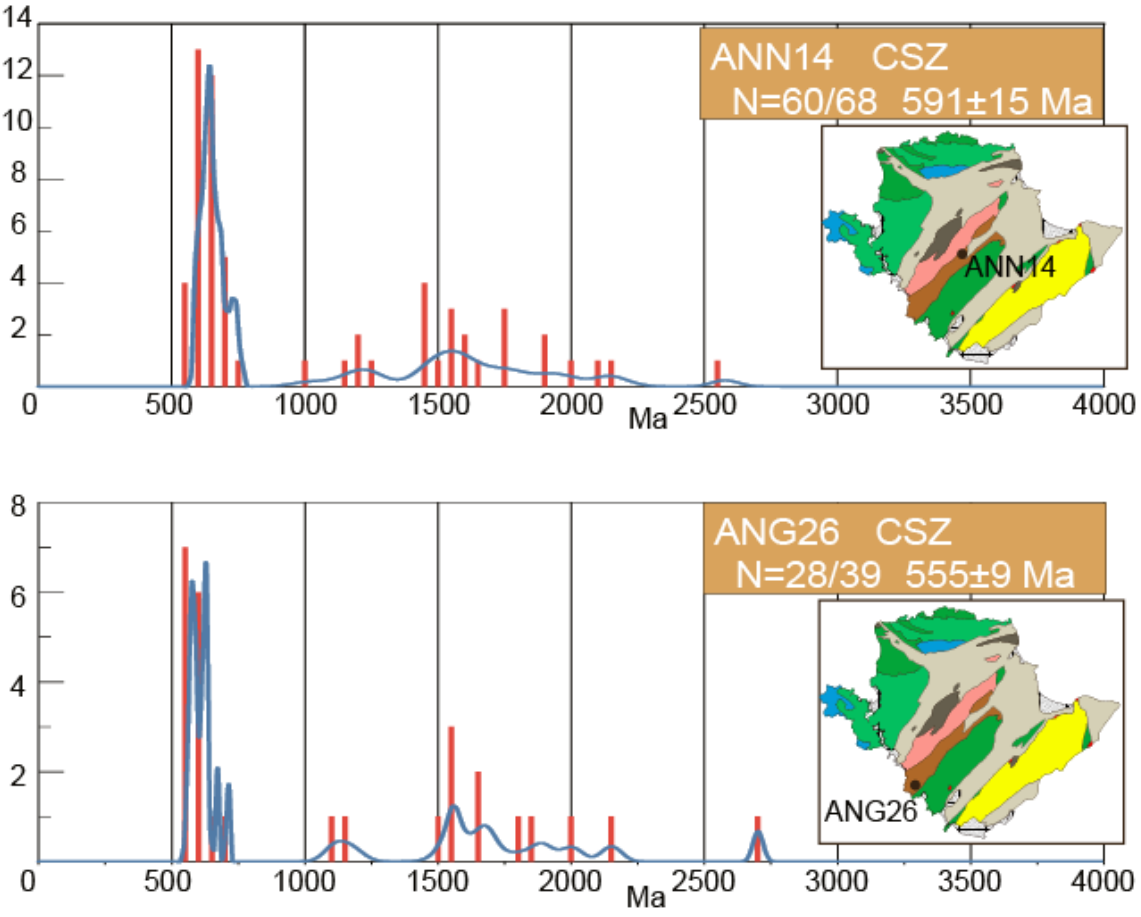

Fig. 3-18 Age distribution of detrital zircon from psammitic schists of CSZ, ANN2 and ANG66. Note the predominant occurrence of zircons with 700-550Ma with subordinate amounts of Proterozoic ages.

(2) Progressive metamorphism of CSZ in the Cambrian age

The mineral assemblages of metabasites and pelitic/psammitic schists were examined under microscope in addition to the metamorphic textures (Fig, 3-19). Field exposures are poor on land, but excellent along the western coast of the central Anglesey Island. The characteristic minerals in metabasites are Ca-amphibole (actinolite and hornblende), Ca-Na plagioclase (albite and hornblende), Ca-Al silicates (epidote) and other minors such as quartz, sphene, hematite, magnetite, sulphide, carbonates, and phengitic mica (Fig, 3-20). Those are listed up and the two zones were recognized; Zones I and II (Fig. 3-19). The former belongs to so-called greenschit (GS) facies, whereas the latter to epidote amphibolite (EM) facies. Further, Zone I could be subdivides into the two, pumpellyite-actinolite facies, and/or prehnite-pumpellyite facies. If the detailed mineral assemblages are clarified for the Ca-Na plagioclase, and their composition, in relation to Ca-Na amphiboles, the higher-grade portion can be also subdivided (e.g., Liou and Maruyama, 2006).

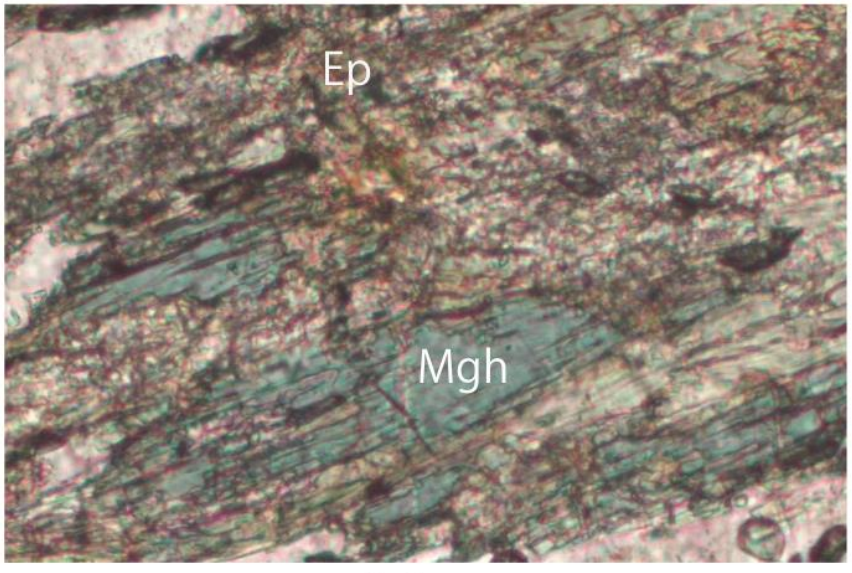

Fig. 3-19 Metamorphic texture and major rock-forming minerals. two Ca-amphbioles (actinolite + magnesohornblende) coexist in fine-grained matrix of Qz, Sph, Chl, Ep, carbonate, and phengitic mica.

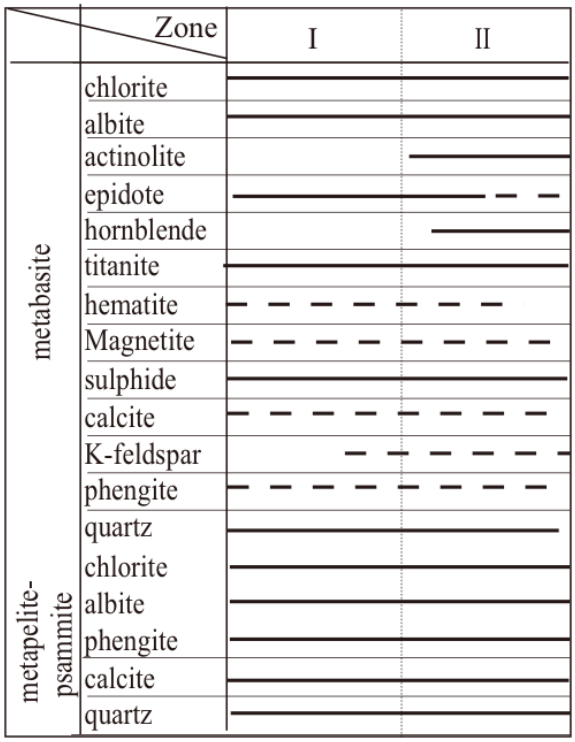

Fig. 3-20 The stable occurrence of minerals in metabasites and metapelite- psammites in the two zones. Solid line means major constituent, and dashed line means minor constituent.

(3) Regional isograds of the Central Shear Zone

More than 50 samples were collected systematically and mineral assemblages were carefully examined. For the metabasites which are sensitive to P-T changes, are plotted on the map to delineate the metamorphic isograds (Fig. 3-21). As shown in Fig. 3-21, the higher grade assemblage of Ca-amphibole-bearing rocks appear only to the south, whereas the northern region belongs to GS facies. The southern zone (II) corresponds to albite-epidote amphibolite facies. The zone boundary between I and II is exposed along the coast, indicating Zone I is underthrust to the southern Zone II, and the deformation fabrics along the boundary indicate top-to-south movement.

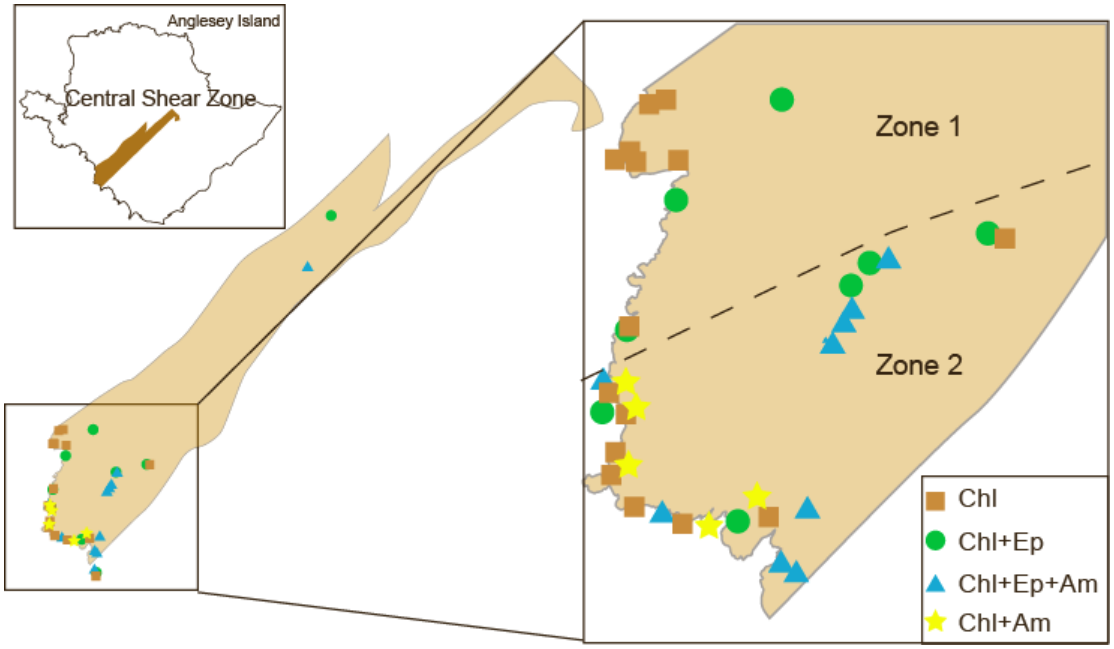

Fig. 3-21 Regional distribution of metamorphic minerals of Central Shear Zone. Appearance of Ca-amphibole, hornblende is restricted to the south as shown by the broken line. The metamorphic reaction of Ep + Chl + Ab = Ca-amphibole (Act + Hb) + Water (fluid) is suggested. Also, the immiscibility gap between the two phases is also suggested. The southern area is hence higher-P and –T areas compared to the north.

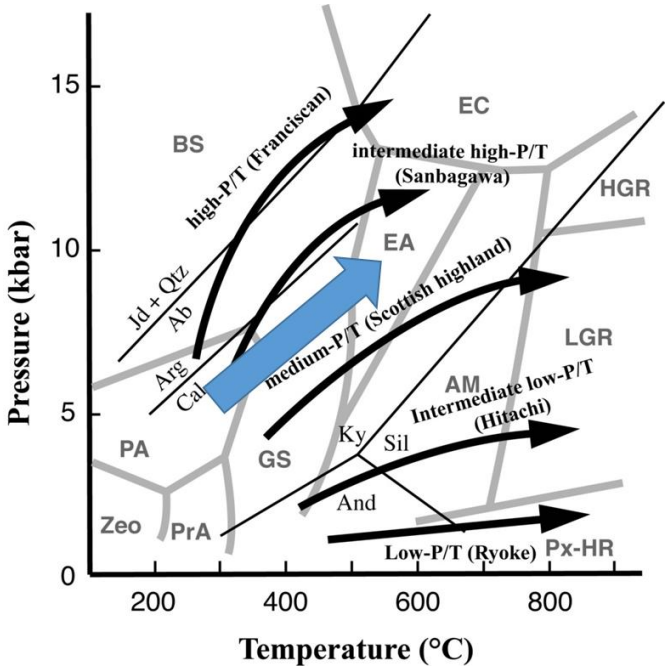

Fig. 3-22 P-T estimate of Central Shear Zone (regional metamorphic belt).

(4) Metamorphic reactions

GS, PA, EA facies have been identified by mineral assemblages, also strongly penetrative fabrics are common. Metamorphic reaction between Zones I and II corresponds to the facies boundary between GS and EA (Fig. 3-22). If GS facies is subdivide into the two, PA and GS, and also EA into albite epidote amphibolite faces and low-pressure EA (oligoclase-coexisting with actinolite), the detailed P-T gradient can be delineated. The facies series suggests the metamorphic thermal gradient low-T high-P type, and the subduction zone metamorphism. The Central Shear Zone belongs to the high-pressure intermediate type according to Miyashiro (1965, 1979)'s definition.

(5) Internal P-T structure

The internal thermobaric structure has not yet analyzed at this moment. Sampling has been completed, but not yet all have not been thin sectioned. The representative samples have been mineralogically analyzed to delineate the P-T conditions.

	Zone 2					
Sample No.	A697				A698	
Mineral	Ep	Chl	Act	Pl	Ep	Act
SiO_2	38.81	28.14	54.53	68.43	38.55	54.07
TiO_2	0.06	0.00	0.06	0.01	0.19	0.11
Al_2O_3	24.97	18.81	3.16	19.23	25.05	1.41
Cr_2O_3	0.00	0.00	0.04	0.00	0.00	0.01
Fe_2O_3	10.39	0.00	0.37		9.50	0.21
FeO	0.00	18.71	10.01	0.07	0.00	12.34
MnO	0.16	0.33	0.26	0.00	0.19	0.25
MgO	0.01	19.46	16.36	0.01	0.04	15.51
CaO	22.39	0.13	11.79	0.08	22.68	11.87
Na_2O	0.00	0.01	0.60	11.66	0.03	0.29
K_2O	0.06	0.02	0.07	0.04	0.02	0.05
Total	95.81	85.61	99.34	99.53	95.30	98.18
Oxygens	12.50	14	23	8	12.5	23
Si	3.098	2.886	7.770	3.002	3.091	7.884
Ti	0.003	0.003	0.006	0	0.012	0.012
Al	2.349	2.406	0.530	0.994	2.367	0.243
Cr	0	0	0.005	0	0	0.001
Fe^{3+}	0.562	0	0.040		0.516	0.023
Fe^{2+}	0	1.692	1.193	0.003	0	1.505
Mn	0.011	0.031	0.031	0	0.013	0.031
Mg	0.001	2.868	3.475	0.001	0	3.371
Ca	1.92	0.012	1.799	0.004	1.948	1.854
Na	0	0	0.165	0.992	0.005	0.083
K	0.006	0.002	0.012	0.002	0.002	0.009

Table 3-2 Representative mineral analysis of CSZ metabasites.

3-4-5 New Harbour Schist belt

The New Harbour Group is dominantly composed of mafic schists with subordinate amounts of pelitic and psammitic schists. The rocks have been subjected to the deformation with strongly penetrated folding with micro-crenulation folds under ductile shear. The metamorphic grade of New Harbour schists ranges from PA facies through GS facies to albite epidote-amphibolite facies, although the details have not yet shown in a regional scale. About 100 samples have been collected systemically in 2013 summer expedition. The details will be petrologically analyzed. Several representative outcrops and deformation are shown in Fig. 3-23.

The boundary between the New Harbour Ophiolite and presumably underlying New Harbour schist belt has been examined in the field in 2013, but the direct observation was not possible. Yet when mapped the both units in the field, the boundary seems to be nearly flat and the structural top seems to be the New Harbour ophiolite belt, suggesting the nearly subhorizontal tectonic exhumation of the schist belt from SE to NW, above the new Harbour fore-arc ophiolite unit.

AMW31 collected from the New Harbour and shows zircons ranging from ca. 500 to 1000 Ma with a largest peak of ca. 600 Ma. The youngest age of AMW31 has 520 ± 31 Ma (Fig. 3-24). On the other hand, UKY5-2 in the New Harbour shows zircons ranging from ca. 500 to 600 Ma. The largest peak of zircons in the sample has ca. 550 Ma and there are same minor peaks (Fig. 3-24). The youngest age of UKY5-2 is 539 ± 14 Ma to coincide with AMW31.

Fig. 3-23 The mode of occurrence of New Harbour schists with strongly penetrative fabrics, along the western coast near

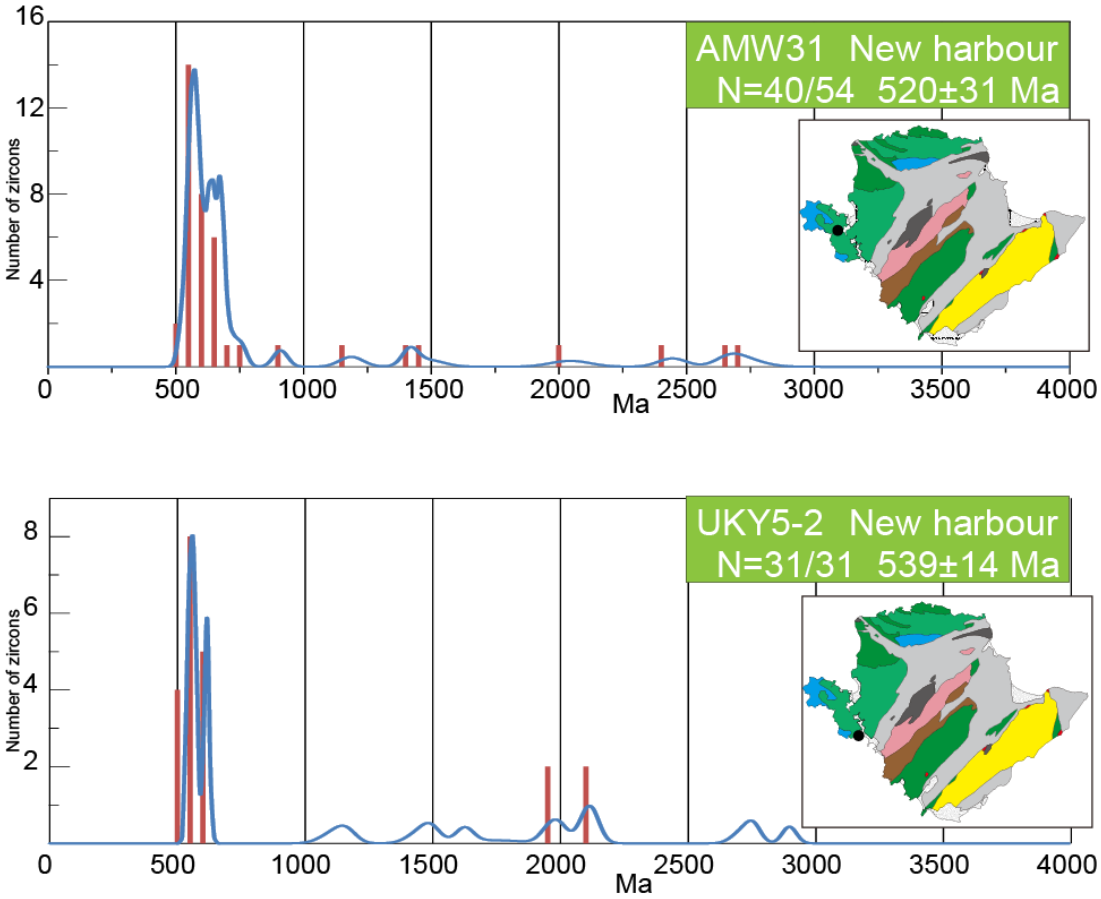

Fig. 3-24 Age distribution of detrital zircon from psammitic schists of New Harbour group, AMW31 and UKY5-2. Note the predominant occurrence of zircons with 700-520Ma with subordinate amounts of Proterozoic ages. The youngest zircons range 520-530Ma, presumably derived from volcanic front in Early Cambrian.

3-4-6 New Harbour Ophiolite belt

The New Harbour Schist Unit occurs as a thin <2km unit, overlain by the New Harbour Ophiolite on the top and underlain by the South Stack Group. The presence of fore-arc ophiolite is suggested, although the ophiolite never preserved the original paleostratigraphy, and the strongly serpentinized peridotite, gabbro, rodingite, and minor dikes are reported, but effusive rocks such as pillow basalts and deep-sea chert are absent. Presence of rodingite suggests the strong metasomatism and common in the hydrothermally altered rocks under the extremely low-XCO_2 partial pressure during the

formation (Fig. 3-2). Rodingite is common on the modern ocean-floor, too.

Fig. 3-25 Strongly serpentinized periodotite mass with several tectonically blocked gabbros metasomatically altered to rodingites

Possible presence of fore-arc ophiolite suggests the presence of small ocean basins such as fore-arc basin of Weber Deep in Indonesia where 6000m deep basin with 200km wide are present between volcanic front and no-volcanic second arc. The fore-arc of Timor-Tanimber in Indonesia is the region where the world-youngest BSE belt is being exposed (Kaneko et al., 2007). For the exhumation of New Harbour Schist Unit seems to be closely similar to that of Indonesian region.

3-4-7 Church Bay Tuff (465Ma): 436Ma acidic tuff Unit (Skerrie island equivalents)

To the northernmost tip of Anglesey Island, the highly altered rock unit is regarded as a part of South Stack Group. However, this unit has been suspected to be Skerrie island tuff or Church Bay Tuff. The author collected these samples and separated zircons from Tuff layer as ANG212. The result is reproduced in Fig. 3-26. The result shows 436.9±4.2Ma, Silurian age, which is close to the Paris Mountain bimodal volcanism.

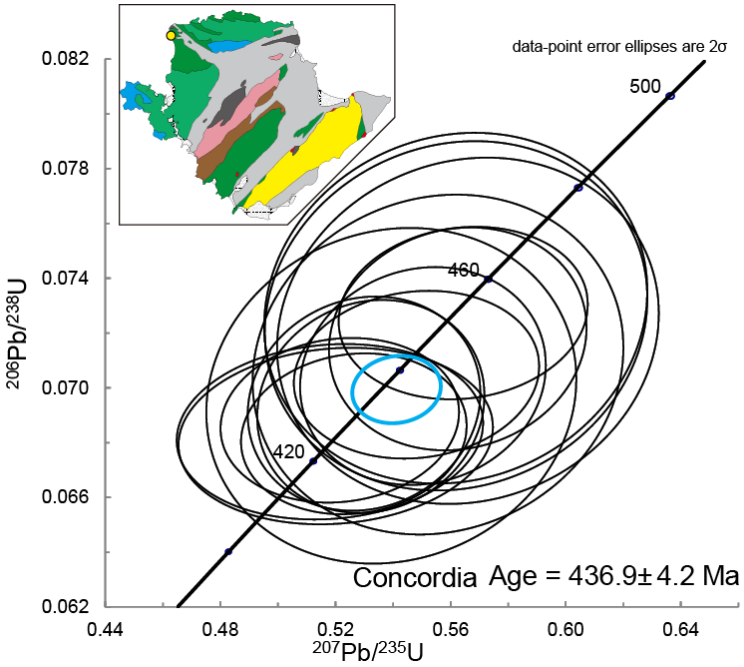

Fig. 3-26 Concordia diagram of zircons from Church Bay Tuff in northernmost Anglesey.

3-4-8 South Stack group

Collins and Buchan (2004) have analyzed the age population from sandstones of South Stack Group. They have shown a strong peak at 500-650Ma and 1600-2700Ma with rather continuous age population spanning in-between (Fig. 3-27). I also collected sandstone samples of South Stack Group and analyzed. The result has shown similar

age distributions for Collins and Buchan (2004). The age pattern of zircon from the South Stack is quite different from those of Neoproterozoic trench turbidite such as the Gwna and New Harbour Group.

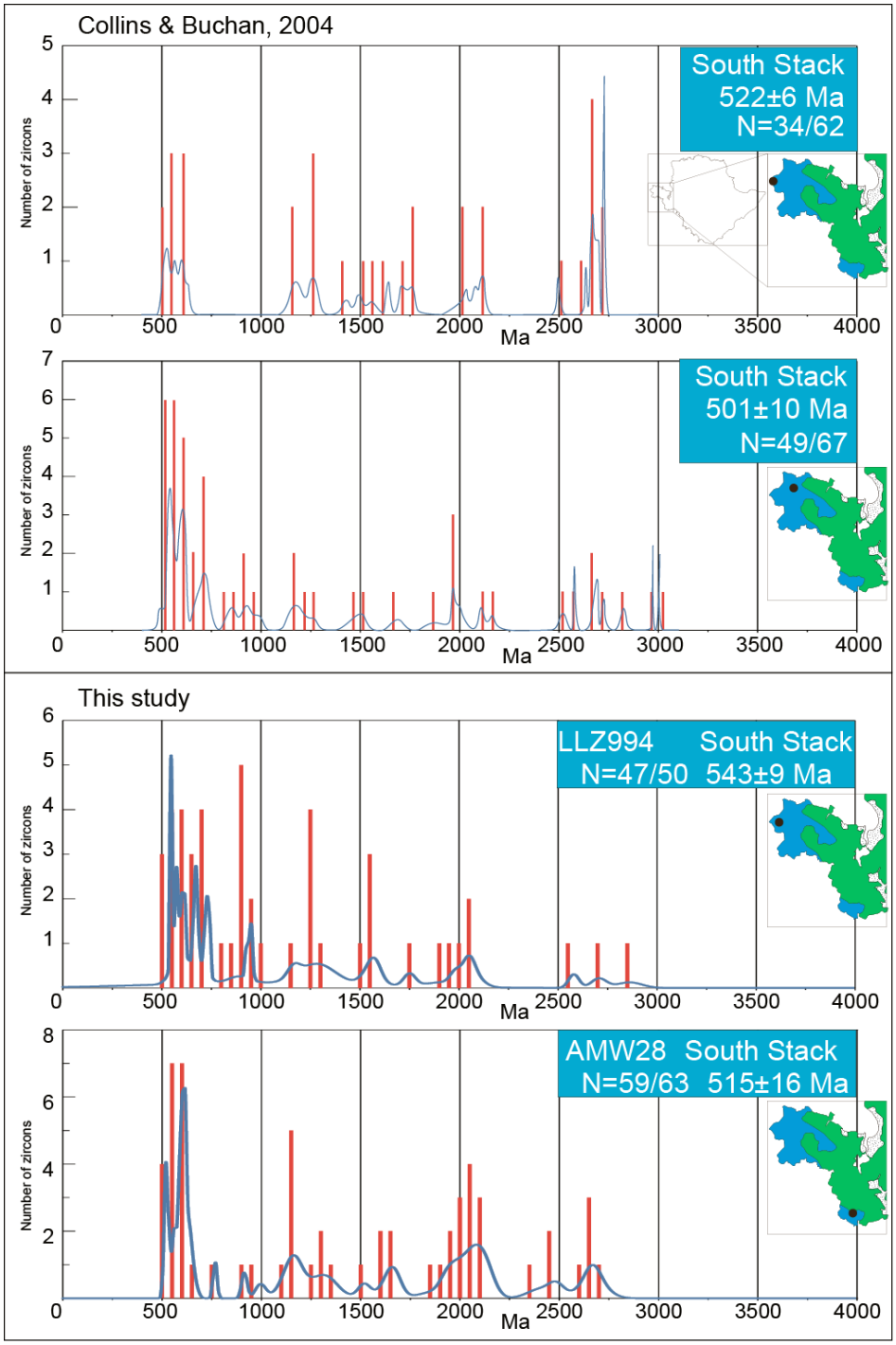

Fig. 3-27 Age distribution of detrital zircon from sandstone of South Stack Group. LL994 and AMW28 are the results of this study. Upper part is reported by Collins and Buchan (2004).

3-4-9 Klippe associated with post-Devonian overthrust

There are numbers of klippes right above the basement rocks of the Anglesey Island (Fig. 3-2). They are the Arfon Group (Neoproterozoic volcano-plutonic sequence with sandstone, conglomerate and mudstone), the Coedana gneiss and granite complex (Neoproterozoic), and Proterozoic shallow marine carbonate and associated rocks. The Gwna Group itself is also included.

More than 10 klippes have been already described in references since the extremely detailed map by Greenly (1919). Through the mappings by our group since 2006, we have also accumulated samples, and three new localities were discovered. For example, ANN2 resting right above Central Shear Zone, contains zircons ranging from 1034Ma to 2259Ma with a peak of 1400-1200 Ma, with minor peat at 2800Ma (Fig. 3-28). A674 which was collected in the region of the Gwna Group on the hill of Anglesey Island, ca. 5 km north of Llanddywn island (Fig. 3-28) yielded a similar age population pattern and quite different from those of Gwna group (Fig. 3-30). The youngest age is 884Ma with a peak of 1200Ma with subordinate continuous age range as old as 2250Ma with minor about 2850Ma. The age pattern of ANN2 is quite similar to the high-grade gneiss at Malvern (Strachan et al., 2007) (See Fig. 3-28). The similarity of age pattern between the klippes and Arfon group and Malvern suggests the origin of klippes.

IR738 was collected in the region of the Gwna Group on the hill of Porthorion, contains zircons ranging from *ca.* 1150Ma to 3500Ma with a peak of 2000-2200 Ma and 2500-3000 Ma, with minor peat at 1700 Ma and 3500 Ma. This characteristic is different of A674 and ANN. So, the provenance of IR738 may be related to the West African craton.

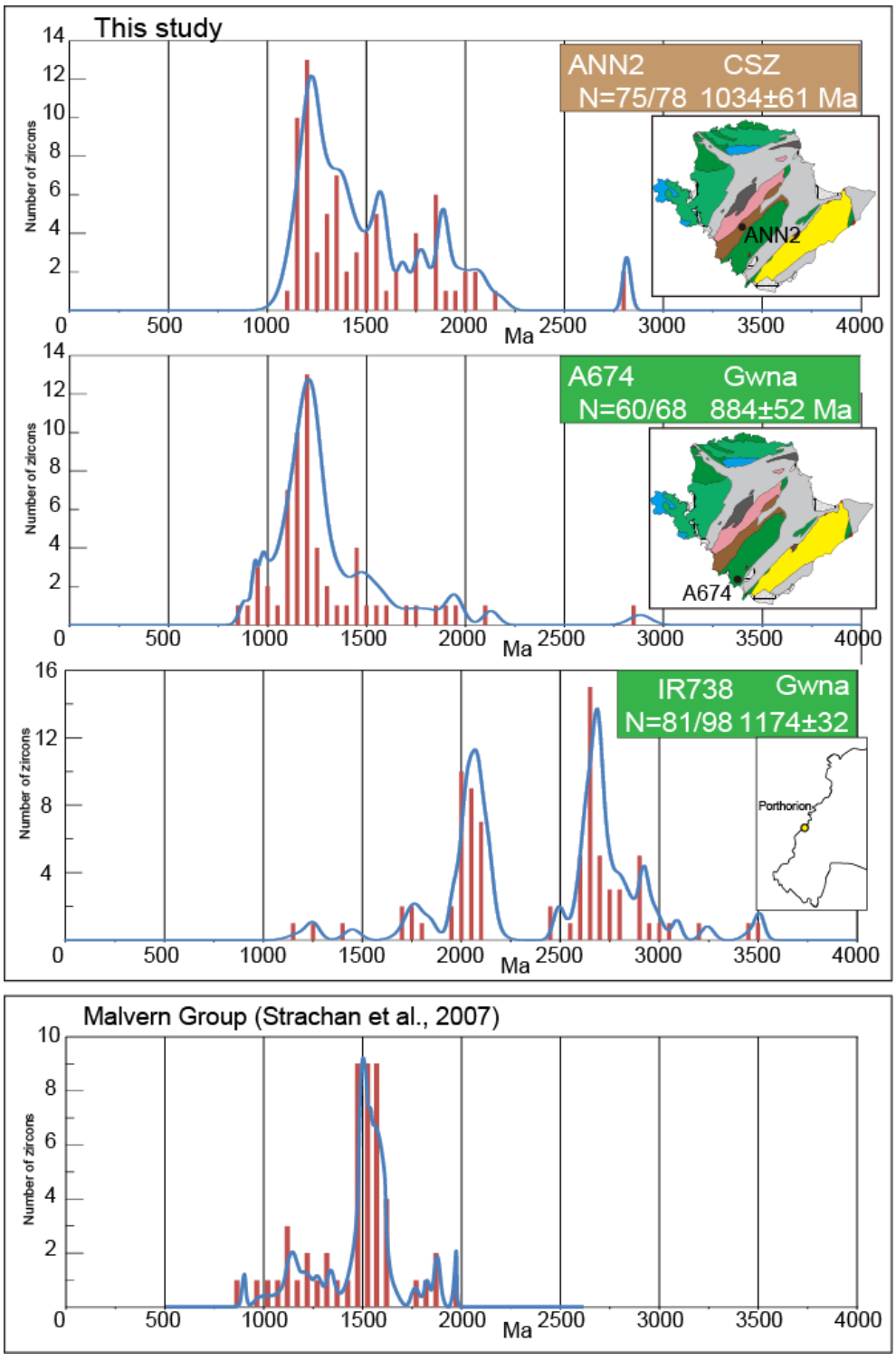

Fig. 3-28 Zircon age population diagram of high-grade gneiss ANN2; a klippe rests on Central Shear Zone. Also A674 could be a sample of Arfon group sitting as klippe right above the Gwna group. The bottom diagram is from Malvern Group, far south of Anglesey island, and intermediate between London and Wales (See a sketch map in Chapter 1) (Strachan et al., 2007).

The northernmost unit separated from the Carmel Head Thrust is composed of miscellaneous rock units and confusion is present. Platform-type carbonates with stromatolite structure formed in Neoproterozoic time ca. 800-700Ma, together with coarse-grained clastics conglomerate, sandstone and minor mudstone must be dated to differentiate from matrix mudstone with graptolite fossils form in Devonian time (Neuman and Bate, 1978), presumably huge-scale landslide.

IR708 collected from the Gwna Group in the Cmlyn Bay and shows zircons ranging from ca. 550 to 1700 Ma with a largest peak of ca. 600 Ma. In addition, there are some minor peaks in this sample, ca. 1100- 1200 Ma and ca. 1400-1700 Ma. The youngest age of IR708 has 565 ± 9 Ma to coincide with Type 2 (Fig. 3-29). On the other hand, ANG146 from the New Harbour in Anglesey North shows zircons ranging from from ca. 500 to 2300 Ma, varying in long term. The largest peak of zircons in the sample has ca. 500-600 Ma and there are same minor peaks (Fig. 3-29). The youngest age of ANG146 is 510 ± 14 Ma, similarly youngest age and age distribution of detrital zircon from UKY5-2 and AMW31 in the New Harbour Group.

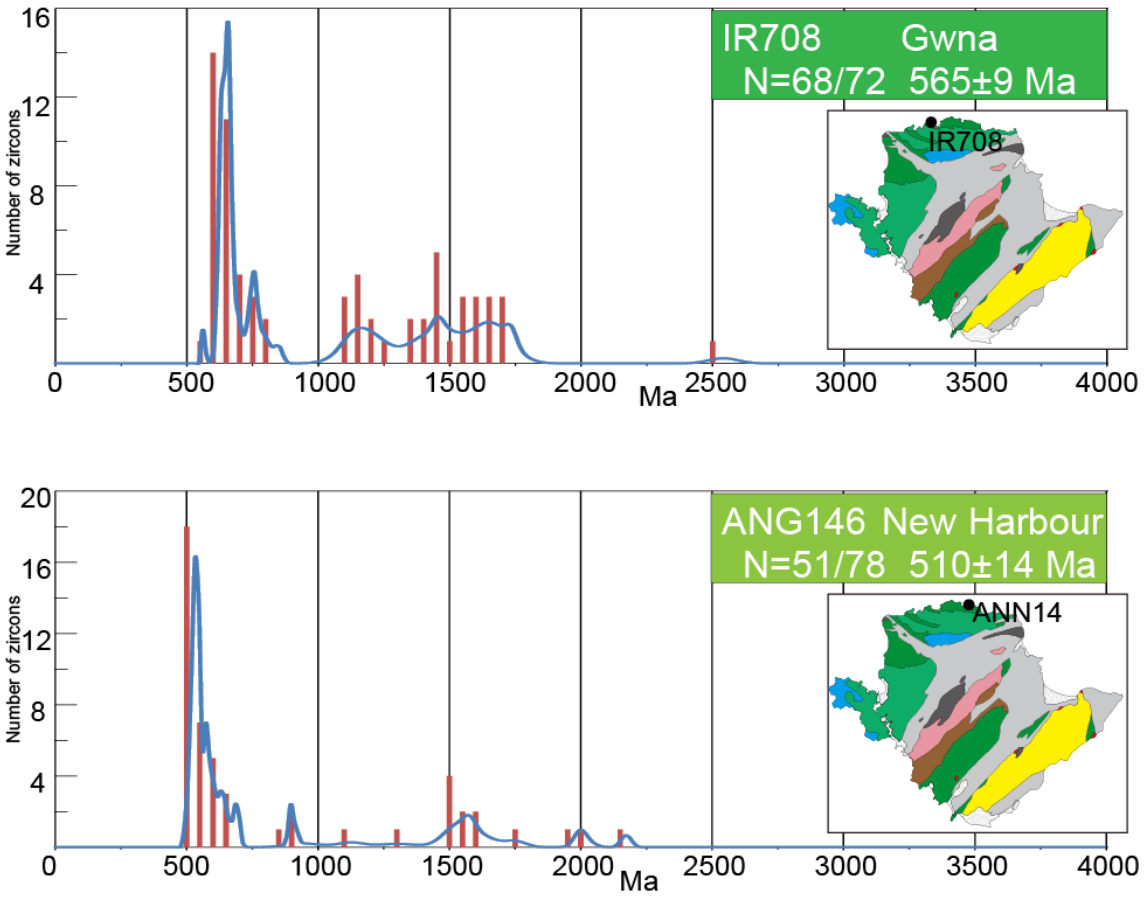

Fig. 3-29 Age distribution of detrital zircon from sandstone from northern coastline, ANN2 and ANG66.

3-4-10 Mid-Paleozoic graven sediments

Along the high-angle normal faults, a series of shallow marine platform sediments were accumulated since mid-Paleozoic age. These sedimentary rocks cover ca. 40% of the Anglesey Island (Fig. 3-1). A series of extensional events locally associated with extensive volcanism in the whole British Isles may be a precursor event of opening of Mid-Atlantic Ocean. It began to open since ca. 200Ma, but its precursor could be back to Carboniferous. The detailed descriptions of sedimentary cover are reported by Greenly (1919) and Shackleton, (1969).

3-5 Discussion

3-5-1 Geochronological relation of the Gwna, New Harbour and South Stack Group

The Monian Supergroup consists of the Gwna, New Harbour and South Stack Group. The South Stack Group is structural bottom in the Monian Supergroup, overlain by the New Harbour and the Gwna group, in ascending order. Previous studies reported that the South Stack Group is the oldest sequence (e.g. Carney, 2000; Collins & Buchan, 2004); however, Kawai et al, (2007) indicated the South Stack Group is the youngest than other groups, because Monian Supergroup represents accretionaly complex at a subduction zone. To judge this problem, it is important to reveal formation ages of each group. But, the chronological constraints of each group have been limited. The South Stack Group is reported no older than 501 ± 10 Ma by detrital zircon (early Cambrian) (Collins and Buchan, 2004). Horack and Evans (2011) showed that some of limestone melange in the Gwna Group is of Early Neoproterozoic age.

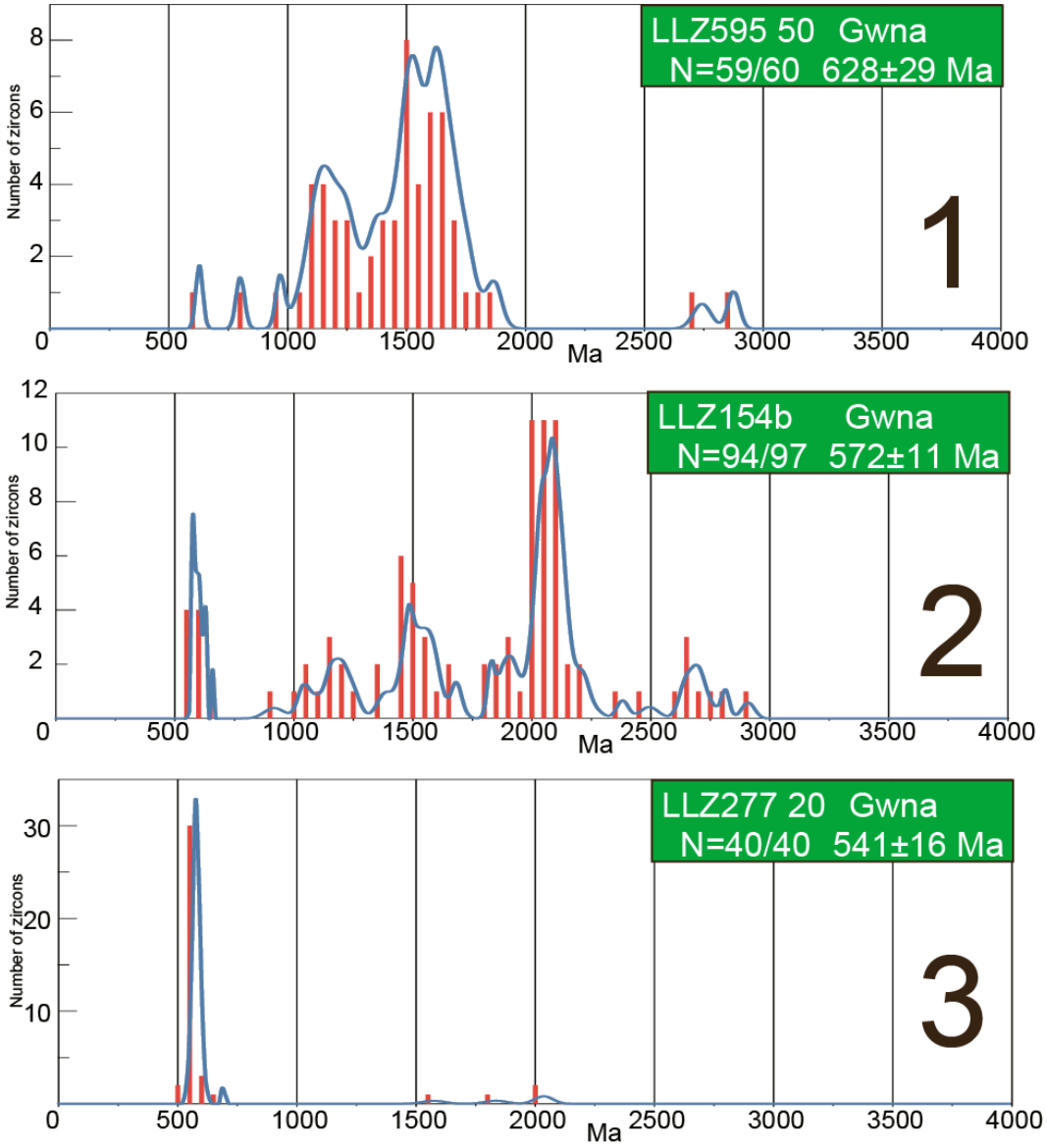

Fig. 3-30 Typical age distributions of zircons from the Gwna Group in the Lleyn peninsula. 1, 2and 3 in figure represent the Type 1, Type 2 and Type 3 of Gwna.

In chapter 2, this study already reported that the Gwna group in Lleyn peninsula is accretionaly complex, and classified it into three-types; Type 1 is 630-610Ma ACs (early Ediacaran), Type 2 is 600-570Ma (early Ediacaran) and Type 3 is about 540Ma (middle Ediacaran). Youngest ages of the Gwna Group in Anglesey are 535 ± 14 Ma from Llanddwyn and 545 ± 32 Ma from western coast. Both ages are similar with Type

3. In the New Harbour Group, AMW31 and UKY-5 are 520 ± 31 Ma and 539 ± 14 Ma, slightly younger than the Type 3 of the Gwna Group. This work first reported the age of the New Harbour Group, about 540-520 Ma. The South Stack Group is reported 501 ± 10 Ma and 522 ± 6 Ma by detrital zircon, as a youngest age (Collins and Buchan, 2004). Results of this study in the South Stack Group, 515 ± 16 Ma (LLZ994) and 543 ± 9 Ma (AMW28). Consequently, it is suggested that the structural bottom is the youngest, the South Stack Group. Those results supported Monian Supergroup represents accretionaly complex at a subduction zone. But, the South Stack Group is not accretionaly complex because it is composed of A-type protoliths formed along the passive margin. This fact suggests that the South Stack Group represents collision to the toe of the West African craton.

3-5-2 Provenance area for ACs during the Neoproterozoic to Paleozoic

The zircon age distribution of trench turbidites of ACs from the Gwna group in the Lleyn peninsula is reproduced in Fig. 3-30. According to the age difference, the provenance site seems to be changed clearly. Age cluster is subdivided into three; 630-610Ma (Type 1), 600-570Ma (Type 2) and 540Ma (Type 3) (chapter. 2). Zircons of Type 1 dominate the range from 3000 to 1000Ma, whereas Type 2 associates similar range. The Type 3 is remarkably different from those two. Trench sandstones are rare including much older zircons than 750Ma, and predominates ca. 700-550Ma (Fig. 3-30). In the Anglesey, about 70 % of zircons from the Gwna and New Harbour Group are younger than 800 Ma (Fig. 3-24). This trend is the same feature with the Type 3 in Lleyn peninsula (Fig. 3-30). So, the Type 3 includes of the Gwna Group in Anglesey.

Zircons of Menai Blueschist Unit have ages younger than 700Ma (Fig. 3-9), similar distribution of the Type 3 of the Gwna Group and New Harbour Group. Moreover, the age distribution of CSZ is also corresponding to Type 3. So, the age distribution of Type 1 and 2 only dominate the range from 3000 to 1000Ma. This difference may reflect the volcano-plutonic sequence that may have formed a topographic high, huge barrier to stop the river transportations from backside to England, or separation of Avalonia from West African craton.

On the other hand, the age distribution of detrital zircon from sandstone in the South Stack Group has different feature from those of the Neoproterozoic trench turbidite, contains range from 3000-500Ma with a peak of 700–500 Ma including about 30-50 % of total zircons, with minor peak around 2800, 2000 and 1200 Ma. This difference reflects the hinterland; the former could be derived from parts of Laurentia, whereas the latter is from West Africa craton.

3-5-3 New Harbour Schist Belt

The New Harbour Schist Unit has not been treated as a schist belt, but has been described to be sheared, same as the Central Shear Zone. Sense of shear is parallel to the bedding plane in general, and its vergency faces NW. Strongly penetrative fabrics and micro-foldings and their lineation all indicate the subduction zone metamorphism of originally ACs formed at trench. Metamorphic thermal gradient shows high-pressure intermediate ranging from pumpellyite-actinolite facies, through greenschist facies to epidote-amphibolite facies that is similar to the Cretaceous Sambagawa metamorphism (Miyashiro, 2002).

If this interpretation is correct, the driving force of exhumation of NHS belt could

reflect the subduction of mid-oceanic ridge (Maruyama et al., 1996). During the tectonic growth of Anglesey Island, three times of mid-oceanic ridge must have subducted under the England-Wales arc called Avalonia.

3-5-4 Three regional metamorphic belts in the Anglesey Island

Kawai et al., (2006) showed the Menai blueschist Unit is equivalent to the circum-Pacific high-P/T regional metamorphic belt. The Menai BS-EA schist belt was metamorphosed around 560Ma (Dallmeyer and Gibbons, 1987). On the other hand, the Central Shear Zone is also high-P/T regional metamorphic belt by mineral assemblage and the P-T gradient. The New Harbour schists could be metamorphosed to have penetrative fabrics at deeper subduction zone. The metamorphic grade of the New Harbour schists ranges from PA facies through GS facies to albite epidote-amphibolite facies. This study interpreted the New Harbour schist is a regional metamorphic belt.

Therefore, the Anglesey Island have preserved occurrences of three times regional metamorphic belts. Three regional metamorphic belts are all belong to Pacific-type because of protoliths are ACs origin, whereas South Stack group belongs to A-type (collision type).

The Menai BS-EA schist belt is derived from the Gwna Group Type 3. Moreover, the protoliths of Central Shear Zone are also ACs. The New Harbour schist belt is also derived from ACs. The timing of regional metamorphism is also estimated by the youngest zircon age and constrained by the timing of formation of structurally underlying ACs. Therefore, the timing of metamorphism of the Central Shear Zone is constrained by the youngest age of the New Harbour Group, about 530Ma. The metamorphosed age of New Harbour schist belt is constrained about 520-510 Ma

presumably.

3-5-5 A summary of geochronology for the Wales-Anglesey Island

Fig. 3-31 shows the summary of OPS from Lleyn and Anglesey Island. Left column indicates the stages of AC formation of the Gwna Group at 630-610Ma (Type 1), 600-570Ma (Type 2) and at 540Ma (Type 3) in Lleyn peninsula. The ACs of the Gwna Group in the Anglesey Island belongs to the Type 3. Moreover, The Menai BS belt is a metamorphosed part of the Type 3 presumably. The Central Shear Zone could be derived from the Type 3. The New Harbour Group seems to be slightly younger ACs in origin and metamorphosed regionally at deep subduction zone.

The normal sequence of sedimentary unit of South Stack Group were accumulated at 540-500Ma. The buoyant subduction of South Stack Continent may be around 500-470Ma presumably. The overthrusting event occurred in the Ordovician time, and related to the underthrusting South Stack micro-continent to jack-up the overriding TTG belt, to transfer those rocks along the gravity slide, over 100km from the Snowdonian Mt to the northern end of Anglesey Island.

After the passive collision between Laurantia (Scotland-Ireland) and Avalonia, hotspot-like bimodal volcanism occurred to associate huge calderas sporadically. Lake district and two or three regions at Paris Mountain, Church Bay, and Skellies islands all belong to this category.

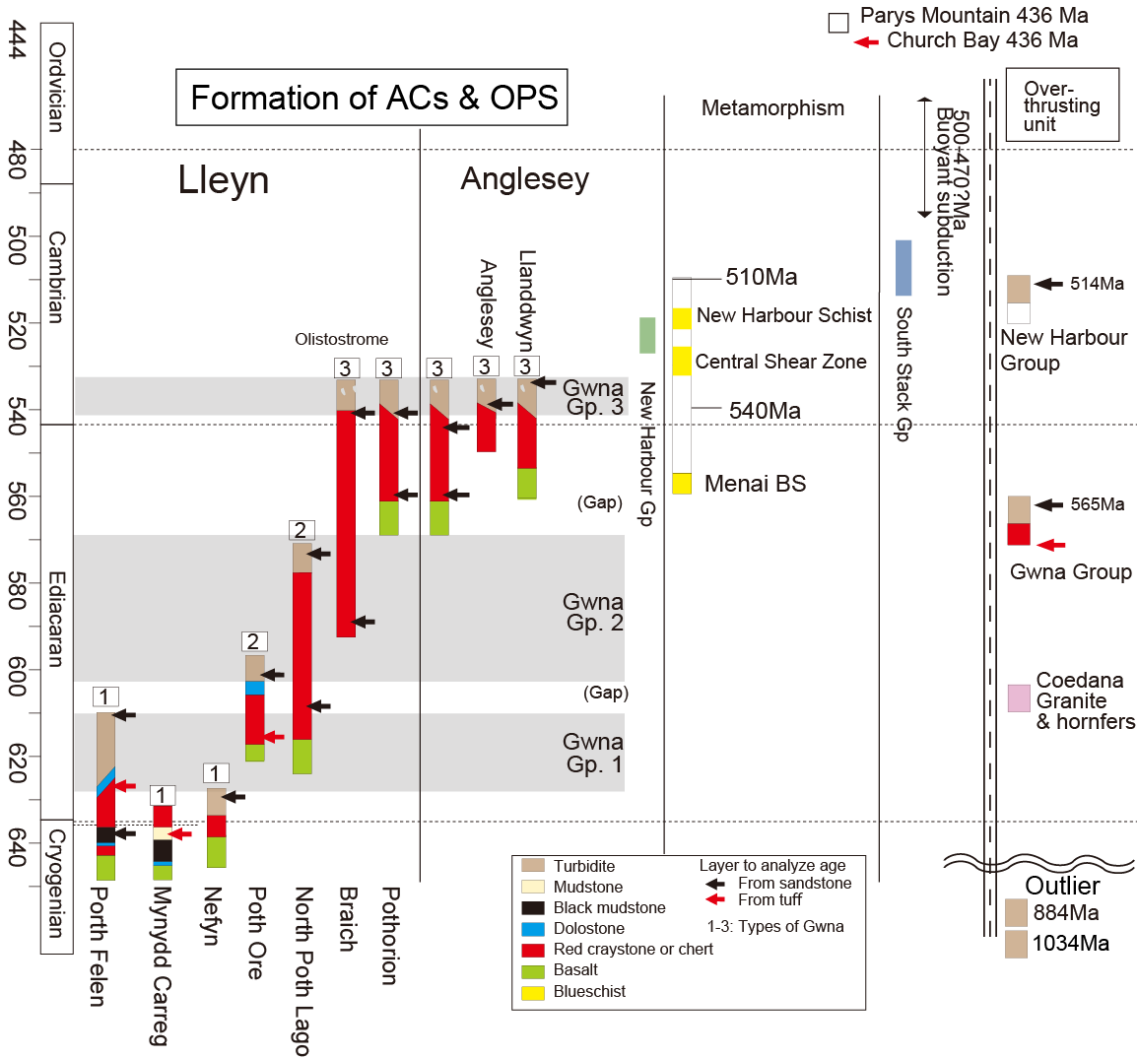

Fig. 3-31 A summary of event sequence in the Wales-Anglesey Island. Lleyn Peninsula (Left), Anglesey island (middle), and Overthrusting event (right). Left shows Ocean Plate Stratigraphy and three times of formation of ACs and absence of ACs. Middle shows the events of sedimentary formation and ACs for New Harbour G, and normal sequence of South Stack Group. In addition, Parys Mountain bimodal volcanism and ore formation, and Church Bay tuff is also shown. Regional metamorphism is also summarized, the Menai BS, Central Shear Zone, and New Harbour regional metamorphism are shown. Right column shows the overthrusting event at Devonian, and rock units delivered to the north including Gwna group Type 2, Coedana Granite-gneiss complex, supracrustal rocks such as Arfon group.

3-5-6 Structural relationship between all units in Anglesey Island

The Anglesey Island is composed of three tectono-stratigraphic units; the most predominant unit is ACs and its metamorphosed counterparts (three regional metamorphic belts and one collision-type). The normal sequence deposited on the grabens formed since mid-Paleozoic covering about 40% of the Anglesey Island, and the overthrust units during the collision-orogeny by the South Stack Group.

These structural and stratigraphic relationships are summarized as below. By introducing the concept of ACs, the debate of the stratigraphic relationship on Anglesey Island is solved. The downward growth of ACs, and episodic intrusion of regional metamorphic belts, and associated normal faulting with dome-up structures are the major structures (Fig. 3-32).

In addition, the Ordovician huge-scale landslide could explain the origin of chaotic units of olistostrome and a series of kilppes right above the basement rocks. This event could be cause by the collision orogeny by buoyant subduction of South Stack continents down to the volcanic front in those days.

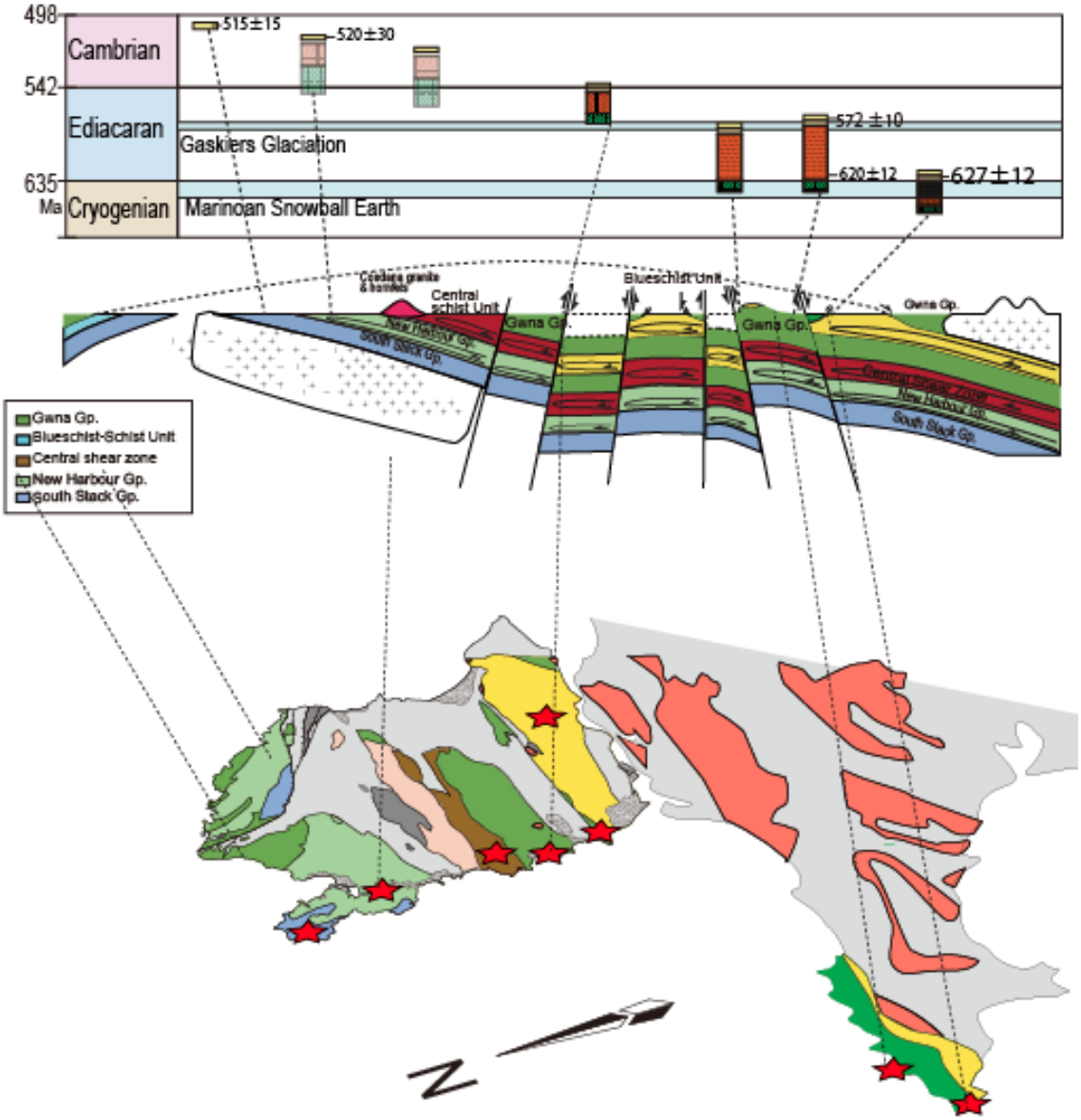

Fig. 3-32 NS cross section of Anglesey-Llyen regions, NW part of England. Note the downward growth of ACs through time, and episodic intrusion of regional metamorphic belts in shallow depth ACs. The final buoyant subduction of South Stack continent caused the apparent overthrusting of TTG rocks over 100km northward.

3-6 Conclusion

The Anglesey Island is composed of accretionary complex (ACs), regional metamorphic belts and mid-Paleozoic covering sediment. The Gwna Group in the Lleyn peninsula and Anglesey Island is the typical ACs formed to the downward at three different stages; at 630-610Ma (Type 1), 600-570Ma (Type 2), and around (Type 3).

The Central Shear Zone and New Harbour Group are ACs which suffered the subduction zone metamorphism. The age of metamorphosed is constrained by the timing of formation of structurally underlying ACs. The metamorphosed age of the Central Shear Zone and New Harbour Group are constrained around 530 Ma and 520-510 Ma. Above the metamorphosed New Harbour Group, the ophiolite unit occurs, suggesting the presence of fore-arc ophiolite.

The structural bottom is the South Stack Group composed of nearly pure quartzite. Their detrital zircon ages range from 3000 Ma to 515Ma that is remarkably different from those of the Gwna trench turbidites. Therefore, the origin of the South Stack micro-continent could be an eastern margin of Laurentia, not a margin of West Africa or Amazonia.

The buoyant subduction of South Stack Continent may be around 500-470Ma presumably. The overthrusting event occurred in the Ordovician time, and related to the underthrusting South Stack micro-continent. This micro-continent elevates the overriding TTG belt and already accreted ACs. After that, these rocks transfer over 100km from the Snowdonian Mt to the northern end of Anglesey Island because of a gravitational collapse.

Cutting the thrust system, the final bimodal volcanism and associated caldera were formed at 437Ma (Silurian) together with hydrothermal-origin massive sulfide

deposit at Parys Mountains. The final gravitational collapse under the extension stress regime occurred during the Carboniferous time, and thick carbonates covered the tectonically depressed region.

References

Barrett, T. J., MacLean, W. H., Tennant, S. C. 2001. Volcanic sequence and alteration at the Parys Mountain volcanic-hosted massive sulfide deposit, Wales, United Kingdom: applications of immobile element lithogeochemistry. Economic Geology, 96, 1279-1305

Barber, A.J., Max, M.D., 1979. A new look at the Mona Complex, Anglesey, North Wales. Journal of the Geological Society 136, 407-432.

Blake, J.F. 1888. The occurrence of glaucophane-bearing rocks in Anglesey. Geological Magazine, 5, 125-127.

Carney, J. N., 2000. Precambrian rocks of England and Wales (Vol. 20). Joint Nature Conservation Committee.

Collins, A.S., Buchan, C., 2004. Provenance and age constraints of the South Stack Group, Anglesey, UK: U-PbSIMS detrital zircon data. Journal of the Geological Society 161, 743-746.

Dallmeyer, R.D., Gibbons, W., 1987. The age of blueschist metamorphism in Anglesey, north Wales – evidence from Ar 40/ Ar 39 mineral dates of the Penmynydd schists. Journal of Journal of the Geological Society 144, 843-852.

Ernst, W. G. 1971. Metamorphic zonations on presumably subducted lithospheric plates from Japan, California and the Alps. Contributions to Mineralogy and Petrology, 34, 43-59.

Gibbons, W. 1983. The Monian 'Penmynydd Zone of Metamorphism' in Llÿn, North Wales. Geological Journal, 18, 21-41.

Gibbons, W., Mann, A., 1983. Pre-Mesozoic Iawsonite in Anglesey, northern Wales: Preservation of ancient blueschists. Geology, 11, 3-6.

Gibbons, W., Gyopari, M., 1986. A greenschist protolith for blueschists on Anglesey, U.K., In: Evans, B.W., Brown, E.H. (Eds.), Blueschists and Eclogites. Geological Society of America, pp. 217-228.

Gibbons, W. 1989. Suspect terrane definition in Anglesey, North Wales. Geological Society of America, Special Papers, 230, 59-65.

Gibbons, W., Horak, J., 1990. Contrasting metamorphic terranes in northwest Wales, In: D'Lemos, R.S., Strachan, R.A., Topley, C.G. (Eds.), The Cadomian Orogeny. Geological Society London, pp. 315-327.

Greenly, G., 1919. The Geology of Anglesey. HMSO.

Henslow, J.S. 1822. Geological description of Anglesea, Transactions of the Cambridge Philiosophical

Society, 1, 359-452.

Horak, J. M., & Evans, J. A. 2011. Early Neoproterozoic limestones from the Gwna Group, Anglesey. Geological Magazine, 148, 78-88.

Kaneko, Y., Maruyama, S., Kadarusman, A., Ota, T., Ishikawa, M., Tsujimori, T., Ishikawa, A., Okamoto, K., 2007. On-going orogeny in the outer-arc of the Timor-Tanimbar region, eastern Indonesia. Gondwana Res. 11, 218-233.

Kawai, T., Windley, B. F., Terabayashi, M., Yamamoto, H., Maruyama, S., Isozaki, Y. 2006. Mineral isograds and metamorphic zones of the Anglesey blueschist belt, UK: implications for the metamorphic development of a Neoproterozoic subduction–accretion complex. Journal of Metamorphic Geology, 24, 591-602.

Kawai, T., Windley, B.F., Terabayashi, M., Yamamoto, H., Maruyama, S., Isozaki, Y., 2007. Metamorphic zones in the Anglesey blueschist belt and implications for the development of a Neoproterozoic subduction-accretion complex: Reply. Journal of Metamorphic Geology 25, 509-510.

Kawai, T., Windley, B.F., Terabayashi, M., Yamamoto, H., Maruyama, S., Omori, S., Shibuya, T., Sawaki, Y., Isozaki, Y., 2007. Geotectonic framework of the Blueschist Unit on Anglesey-Lleyn, UK, and its role in the development of a Neoproterozoic accretionary orogen. Precambrian Research 153, 11-28.

Kawai, T., Windley, B. F., Terabayashi, M., Yamamoto, H., Isozaki, Y., Maruyama, S. 2008. Neoproterozoic glaciation in the mid-oceanic realm: An example from hemi-pelagic mudstones on Llanddwyn Island, Anglesey, UK. Gondwana Research, 14(1), 105-114.

Kawai, T., 2009. New orogenic division of British Iles: addition of two Pacific-type orogens, and orogenic structure of Scottish Caledonian collision-type orogen revisited. PhD thesis, Department of earth and planetary sciences, Tokyo institute of technology.

Maltman, A.J. 1977. Serpentinites and related rocks of Anglesey. Geological Journal, 12, 113-128.

Maruyama, S., Liou, J.G., Terabayashi, M., 1996. Blueschists and Eclogites of the World and their Exhumation. International Geology Review 38, 485-594.

Maruyama, S., 1997. Pacific-type orogeny revisited: Miyashiro-type orogeny proposed. Island Arc 6, 91-120.

Maruyama, S., Kawai, T.,Windley, B. F., 2010. Ocean plate stratigraphy and its imbrication in an accretionary orogen: the Mona Complex, Anglesey–Lleyn, Wales, UK. Geological Society, London, Special Publications, 338, 55-75.

Matsuda, T., Isozaki, Y. 1991. Well‐documented travel history of Mesozoic pelagic chert in Japan: From remote ocean to subduction zone. Tectonics, 10, 475-499.

Miyashiro, A. 1965. Metamorphic rocks and metamorphic belts. Tokyo, Iwanami-shoten.

Miyashiro, A., 1979. Metamorphism and Metamorphic Belts. Allen and Unwin, London, 492

Miyashiro, A. 1994. *Metamorphic petrology*. CRC Press.

Neuman, R. B., Bates, D. E. B., 1978. Reassessment of Arenig and Llanvirn age (Early Ordovician)

brachiopods from Anglesey, north-west Wales. Palaeontology, 21, 571-613.

Oliver, G.J.H. 2001. Reconstruction of the Grampian episode in Scotland: its place in the Caledonian orogeny. Tectonophysics, 332, 23-49.

Omori, S., Masago, H. 2004. Application of thermodynamic forward-modeling to estimate of a Metamorphic P-T path, Journal of Geography, 113, 647-663.

Ota, T., Terabayashi, M., Katayama, I. 2004. Thermobaric structure and metamorphic evolution of the Iratsu eclogite body in the Sanbagawa belt, central Shikoku, Japan. Lithos, 73, 95-126.

Pointon, C.R. Ixer, R.A., 1980, Parys Mountain mineral deposit, Anglesey, Wales: Geology, and ore mineralogy. Transactions of the Institution of Mining and metallurgy (Section B: Applied Earth Scuience), 89, 143-155.

Shackleton, R.M., 1969. The Precambrian of North Wales, In: Woods, A. (Ed.), The Precambrian and Lower Palaeozoic Rocks of Wales. University of Wales Press, Cardiff, pp. 1-18.

Shackleton, R.M., 1975. Precambrian rocks of Wales, In: Harris, A.L. (Ed.), A correlation of Precambrian Rocks in the British Isles. Geological Society, London, pp. 76-82.

Strachan, R.A., Collins, A.S., Buchan, C., Nance, R.D., Murphy, J.B., D'Lemos, R.S., 2007. Terrane analysis along a Neoproterozoic active margin of Gondwana: insights from U-Pb zircon geochronology. Journal of the Geological Society London 164, 57-60.

Treagus, J. 2007. Metamorphic zones in the Anglesey blueschist belt and implications for the development of a Neoproterozoic subduction‐accretion complex: discussion. Journal of Metamorphic Geology, 25, 507-508.

Thorpe, R. S. 1978. Tectonic emplacement of ophiolitic rocks in the Precambrian Mona Complex of Anglesey.

Thorpe, R. S. 1993. Geochemistry and eruptive environment of metavolcanic rocks from the Mona Complex of Anglesey, North Wales, UK. GEOLOGICAL MAGAZINE-LONDON-, 130, 85-85.

Tucker, R.D., Pharaoh, T.C., 1991. U-Pb zircon ages for Late Precambrian igneous rocks in southern Britain. Journal of the Geological Society, 148, 435-443..

Wood, D.S., 1974. Ophiolite, melanges, blueschists, and ignimbrites; early Caledonian subduction in Wales?, In: Dott, R.H., Shaver, R.H. (Eds.), Modern and Ancient Geocynclinal Sedimentation. Society of Economic Paleontologists and Mineralogists, London, pp. 334-344.

Wood, M., 2012. The historical development of the term 'Melange' and its relevance to the Precambrian geology of Anglesey and the Lleyn Peninsula in Wales, UK. Journal of Geography (Chigaku Zassi) 121, 168-180.

Table3-1

LA-ICP-MC U-Pb isotope analysical data for zircons from sandstone samples in Anglesey

Grain	$^{204}Pb/^{206}Pb$	U (ppm)	Th (ppm)	$^{207}Pb/^{235}U$	2σ	$^{206}Pb/^{238}U$	2σ	$^{207}Pb/^{206}Pb$	2σ	Age (Ma)						Concordance
										$^{207}Pb/^{235}U$	2σ	$^{206}Pb/^{238}U$	2σ	$^{207}Pb/^{206}Pb$	2σ	
A674-1	0.0000	166	380	1.567	± 0.128	0.1626	± 0.0063	0.0699	± 0.0025	957	± 52	971	± 35	925	± 155	101
A674-2	0.0000	100	352	3.248	± 0.263	0.2554	± 0.0099	0.0923	± 0.0033	1469	± 65	1466	± 51	1473	± 141	100
A674-3	0.0000	185	519	2.285	± 0.183	0.2081	± 0.0080	0.0797	± 0.0028	1208	± 58	1218	± 43	1189	± 145	101
A674-4	0.0000	48	56	2.278	± 0.197	0.2012	± 0.0080	0.0821	± 0.0031	1205	± 63	1182	± 43	1247	± 158	98
A674-5	0.0000	720	1975	2.267	± 0.178	0.2024	± 0.0077	0.0812	± 0.0028	1202	± 57	1188	± 41	1227	± 141	99
A674-6	0.0000	503	1199	3.759	± 0.294	0.2743	± 0.0104	0.0994	± 0.0034	1584	± 65	1563	± 53	1613	± 133	99
A674-7	0.0000	117	249	2.308	± 0.188	0.2067	± 0.0080	0.0810	± 0.0029	1215	± 59	1211	± 43	1222	± 148	100
A674-8	0.0000	355	969	1.416	± 0.113	0.1469	± 0.0092	0.0699	± 0.0017	896	± 49	884	± 52	925	± 105	99
A674-9	0.0001	223	640	2.293	± 0.183	0.2089	± 0.0131	0.0796	± 0.0020	1210	± 58	1223	± 70	1187	± 101	101
A674-10	0.0007	74	192	2.150	± 0.180	0.2028	± 0.0128	0.0769	± 0.0021	1165	± 60	1190	± 69	1119	± 114	102
A674-11	0.0000	200	587	2.247	± 0.180	0.2055	± 0.0129	0.0793	± 0.0020	1196	± 58	1205	± 69	1180	± 102	101
A674-12	0.0000	43	138	1.724	± 0.156	0.1671	± 0.0107	0.0748	± 0.0024	1018	± 60	996	± 59	1064	± 134	98
A674-13	0.0000	85	94	3.619	± 0.294	0.2753	± 0.0173	0.0954	± 0.0024	1554	± 67	1568	± 88	1535	± 100	101
A674-14	0.0000	190	671	2.442	± 0.195	0.2172	± 0.0136	0.0816	± 0.0020	1255	± 59	1267	± 72	1235	± 101	101
A674-15	0.0004	74	147	2.303	± 0.192	0.2109	± 0.0133	0.0792	± 0.0022	1213	± 61	1234	± 71	1177	± 112	102
A674-16	0.0000	93	151	2.994	± 0.271	0.2438	± 0.0194	0.0891	± 0.0019	1406	± 71	1406	± 102	1406	± 85	100
A674-17	0.0000	59	74	2.345	± 0.220	0.2111	± 0.0169	0.0806	± 0.0020	1226	± 69	1235	± 91	1211	± 100	101
A674-18	0.0000	154	256	1.786	± 0.162	0.1698	± 0.0135	0.0763	± 0.0016	1040	± 61	1011	± 75	1102	± 89	97
A674-19	0.0000	203	331	1.905	± 0.171	0.1835	± 0.0146	0.0753	± 0.0016	1083	± 61	1086	± 80	1075	± 85	100
A674-20	0.0000	120	337	1.701	± 0.156	0.1711	± 0.0136	0.0721	± 0.0016	1009	± 60	1018	± 76	988	± 95	101
A674-21	0.0000	276	702	2.287	± 0.203	0.2037	± 0.0162	0.0814	± 0.0016	1208	± 65	1195	± 87	1232	± 79	99
A674-22	0.0000	171	455	3.152	± 0.280	0.2491	± 0.0198	0.0917	± 0.0018	1445	± 71	1434	± 103	1462	± 78	99
A674-23	0.0000	62	63	5.827	± 0.525	0.3509	± 0.0280	0.1204	± 0.0025	1950	± 81	1939	± 135	1962	± 77	99
A674-24	0.0000	155	339	2.182	± 0.196	0.1974	± 0.0157	0.0802	± 0.0017	1175	± 65	1162	± 85	1201	± 85	99
A674-25	0.0000	56	105	2.197	± 0.176	0.2063	± 0.0120	0.0772	± 0.0021	1180	± 57	1209	± 65	1128	± 113	102
A674-26	0.0000	218	436	2.667	± 0.195	0.2244	± 0.0129	0.0862	± 0.0020	1319	± 56	1305	± 68	1343	± 90	99
A674-27	0.0000	132	304	2.357	± 0.176	0.2109	± 0.0121	0.0811	± 0.0019	1230	± 55	1234	± 65	1223	± 97	100
A674-28	0.0000	154	289	2.058	± 0.154	0.1918	± 0.0110	0.0778	± 0.0019	1135	± 52	1131	± 60	1143	± 98	100
A674-29	0.0000	132	218	2.190	± 0.164	0.1966	± 0.0113	0.0808	± 0.0019	1178	± 54	1157	± 61	1216	± 98	98
A674-30	0.0000	159	308	2.213	± 0.165	0.1943	± 0.0112	0.0826	± 0.0020	1185	± 53	1145	± 61	1260	± 95	97
A674-31	0.0000	138	435	3.473	± 0.256	0.2696	± 0.0155	0.0934	± 0.0022	1521	± 60	1539	± 79	1497	± 90	101
A674-32	0.0000	188	590	2.409	± 0.178	0.2194	± 0.0126	0.0796	± 0.0018	1245	± 54	1279	± 67	1188	± 94	103
A674-33	0.0000	77	171	2.404	± 0.179	0.2149	± 0.0061	0.0811	± 0.0028	1244	± 55	1255	± 32	1225	± 142	101
A674-34	0.0000	83	57	2.496	± 0.185	0.2343	± 0.0066	0.0772	± 0.0026	1271	± 55	1357	± 34	1127	± 143	107
A674-35	0.0000	75	92	5.131	± 0.368	0.3409	± 0.0095	0.1092	± 0.0036	1841	± 63	1891	± 46	1785	± 126	103
A674-36	0.0000	69	153	1.600	± 0.125	0.1560	± 0.0046	0.0744	± 0.0027	970	± 50	934	± 25	1052	± 154	96
A674-37	0.0000	219	140	4.763	± 0.332	0.3304	± 0.0089	0.1046	± 0.0034	1778	± 60	1840	± 43	1706	± 123	103
A674-38	0.0000	401	1561	3.292	± 0.229	0.2582	± 0.0069	0.0925	± 0.0030	1479	± 56	1481	± 36	1477	± 127	100
A674-39	0.0000	40	26	5.453	± 0.405	0.3470	± 0.0101	0.1140	± 0.0039	1893	± 66	1920	± 48	1864	± 129	101
A674-40	0.0000	163	351	2.452	± 0.175	0.2206	± 0.0060	0.0806	± 0.0027	1258	± 53	1285	± 32	1212	± 136	102
A674-41	0.0000	66	43	16.846	± 1.180	0.5900	± 0.0163	0.2071	± 0.0067	2926	± 69	2990	± 66	2883	± 109	102
A674-42	0.0000	102	224	2.319	± 0.172	0.2034	± 0.0117	0.0827	± 0.0019	1218	± 54	1194	± 63	1262	± 94	98
A674-43	0.0000	57	68	3.549	± 0.267	0.2633	± 0.0153	0.0978	± 0.0023	1538	± 61	1507	± 78	1582	± 92	98
A674-44	0.0003	162	383	2.347	± 0.170	0.2068	± 0.0119	0.0823	± 0.0018	1227	± 53	1212	± 64	1253	± 88	99
A674-45	0.0001	166	486	2.581	± 0.186	0.2167	± 0.0124	0.0864	± 0.0019	1295	± 54	1265	± 66	1347	± 86	98
A674-46	0.0003	81	109	6.915	± 0.495	0.3792	± 0.0218	0.1322	± 0.0028	2101	± 66	2073	± 103	2128	± 77	99
A674-47	0.0000	229	597	2.312	± 0.165	0.2037	± 0.0117	0.0823	± 0.0018	1216	± 52	1195	± 63	1253	± 86	98
A674-48	0.0000	108	295	2.380	± 0.175	0.2160	± 0.0124	0.0799	± 0.0018	1237	± 54	1261	± 66	1195	± 94	102
A674-49	0.0002	119	187	2.158	± 0.159	0.1991	± 0.0115	0.0786	± 0.0018	1168	± 52	1170	± 62	1162	± 94	100
A674-50	0.0000	227	276	5.744	± 0.403	0.3518	± 0.0201	0.1184	± 0.0024	1938	± 63	1943	± 97	1932	± 75	100
A674-51	0.0000	118	430	1.749	± 0.131	0.1717	± 0.0099	0.0739	± 0.0018	1027	± 49	1022	± 55	1038	± 99	100
A674-52	0.0000	109	88	2.192	± 0.185	0.1968	± 0.0068	0.0808	± 0.0031	1178	± 61	1158	± 37	1216	± 160	98
A674-53	0.0000	117	158	2.295	± 0.193	0.2151	± 0.0074	0.0774	± 0.0030	1211	± 61	1256	± 39	1131	± 161	104
A674-54	0.0000	171	418	2.270	± 0.188	0.2090	± 0.0071	0.0788	± 0.0030	1203	± 60	1224	± 38	1167	± 157	102
A674-55	0.0000	308	322	1.719	± 0.141	0.1718	± 0.0058	0.0726	± 0.0027	1016	± 54	1022	± 32	1002	± 160	101
A674-56	0.0003	185	1280	2.552	± 0.210	0.2130	± 0.0072	0.0869	± 0.0033	1287	± 62	1245	± 38	1358	± 152	97
A674-57	0.0000	173	459	2.195	± 0.182	0.2035	± 0.0069	0.0783	± 0.0030	1180	± 59	1194	± 37	1153	± 158	101
A674-58	0.0008	46	49	2.146	± 0.193	0.2023	± 0.0073	0.0769	± 0.0032	1164	± 64	1188	± 39	1119	± 174	102
A674-59	0.0000	115	305	2.312	± 0.194	0.2093	± 0.0072	0.0801	± 0.0031	1216	± 61	1225	± 38	1199	± 159	101
A674-60	0.0000	123	252	2.193	± 0.184	0.1939	± 0.0067	0.0820	± 0.0031	1179	± 60	1143	± 36	1246	± 158	97
AMW28-1	0.0000	158	171	12.620	± 0.866	0.5037	± 0.0270	0.1817	± 0.0039	2652	± 67	2630	± 117	2669	± 73	99
AMW28-2	0.0000	203	314	6.297	± 0.434	0.3585	± 0.0192	0.1274	± 0.0028	2018	± 62	1975	± 92	2062	± 79	98
AMW28-3	0.0000	53	72	6.751	± 0.485	0.3675	± 0.0199	0.1332	± 0.0031	2079	± 66	2018	± 95	2141	± 85	97
AMW28-4	0.0000	146	247	0.753	± 0.059	0.0916	± 0.0050	0.0596	± 0.0017	570	± 35	565	± 30	589	± 126	99
AMW28-5	0.0000	71	53	0.891	± 0.076	0.0974	± 0.0054	0.0663	± 0.0021	647	± 41	599	± 32	816	± 140	93
AMW28-6	0.0000	68	159	6.447	± 0.458	0.3528	± 0.0191	0.1325	± 0.0031	2039	± 64	1948	± 92	2132	± 83	96
AMW28-7	0.0000	626	3435	9.929	± 0.676	0.4422	± 0.0236	0.1628	± 0.0034	2428	± 65	2361	± 106	2485	± 73	97
AMW28-8	0.0000	110	223	2.799	± 0.201	0.2346	± 0.0127	0.0865	± 0.0021	1355	± 55	1358	± 66	1350	± 95	100
AMW28-9	0.0000	129	155	6.352	± 0.442	0.3550	± 0.0191	0.1298	± 0.0029	2026	± 63	1959	± 91	2095	± 80	97
AMW28-10	0.0000	73	121	2.404	± 0.138	0.2067	± 0.0065	0.0844	± 0.0020	1244	± 42	1211	± 35	1301	± 96	97
AMW28-11	0.0000	96	150	0.613	± 0.043	0.0832	± 0.0027	0.0534	± 0.0017	486	± 28	515	± 16	348	± 148	106
AMW28-12	0.0000	25	13	0.636	± 0.071	0.0841	± 0.0034	0.0549	± 0.0028	500	± 45	521	± 20	407	± 249	104
AMW28-13	0.0000	110	323	1.533	± 0.088	0.1524	± 0.0048	0.0730	± 0.0018	944	± 36	914	± 27	1013	± 101	97
AMW28-14	0.0000	181	358	3.548	± 0.180	0.2536	± 0.0077	0.1015	± 0.0021	1538	± 41	1457	± 40	1652	± 77	95
AMW28-15	0.0000	521	549	0.838	± 0.043	0.0963	± 0.0029	0.0631	± 0.0013	618	± 24	593	± 17	713	± 92	96
AMW28-16	0.0000	523	1861	2.010	± 0.100	0.1878	± 0.0056	0.0776	± 0.0015	1119	± 34	1109	± 31	1137	± 81	99
AMW28-17	0.0000	137	277	2.006	± 0.108	0.1859	± 0.0057	0.0782	± 0.0017	1117	± 37	1099	± 31	1153	± 91	98
AMW28-18	0.0000	173	179	5.076	± 0.255	0.3105	± 0.0094	0.1186	± 0.0024	1832	± 43	1743	± 46	1935	± 73	95
AMW28-19	0.0000	212	365	0.819	± 0.056	0.1022	± 0.0056	0.0582	± 0.0012	608	± 32	627	± 33	535	± 92	103
AMW28-20	0.0000	54	91	4.226	± 0.287	0.3027	± 0.0168	0.1012	± 0.0020	1679	± 57	1705	± 84	1647	± 74	102
AMW28-21	0.0000	302	778	3.578	± 0.225	0.2747	± 0.0150	0.0945	± 0.0015	1545	± 51	1565	± 76	1517	± 60	101
AMW28-22	0.0000	147	330	0.808	± 0.058	0.0965	± 0.0054	0.0607	± 0.0014	601	± 33	594	± 32	630	± 101	99
AMW28-23	0.0000	196	313	0.906	± 0.062	0.1077	± 0.0059	0.0610	± 0.0012	655	± 34	659	± 35	640	± 90	101
AMW28-24	0.0000	71	56	1.612	± 0.117	0.1670	± 0.0093	0.0700	± 0.0016	975	± 47	996	± 52	928	± 98	102
AMW28-25	0.0000	213	665	2.356	± 0.151	0.2163	± 0.0119	0.0790	± 0.0013	1229	± 47	1262	± 63	1173	± 68	103
AMW28-26	0.0000	99	107	3.969	± 0.259	0.2799	± 0.0154	0.1029	± 0.0018	1628	± 54	1591	± 78	1676	± 66	98
AMW28-27	0.0000	367	1493	0.746	± 0.049	0.0943	± 0.0052	0.0573	± 0.0011	566	± 29	581	± 31	505	± 83	103
AMW28-28	0.0000	243	468	2.191	± 0.167	0.2009	± 0.0060	0.0791	± 0.0028	1178	± 55	1180	± 32	1174	± 146	100
AMW28-29	0.0000	93	69	6.245	± 0.478	0.3597	± 0.0108	0.1259	± 0.0044	2011	± 69	1981	± 52	2042	± 130	99
AMW28-30	0.0000	396	1644	9.092	± 0.678	0.4290	± 0.0126	0.1537	± 0.0053	2347	± 71	2301	± 57	2388	± 122	98
AMW28-31	0.0000	92	447	6.656	± 0.508	0.3806	± 0.0114	0.1268	± 0.0045	2067	± 70	2079	± 54	2054	± 129	101
AMW28-32	0.0000	127	286	11.815	± 0.889	0.4603	± 0.0137	0.1862	± 0.0064	2590	± 73	2441	± 61	2709	± 119	94
AMW28-33	0.0000	103	94	6.180	± 0.471	0.3580	± 0.0107	0.1252	± 0.0044	2002	± 69	1973	± 51	2032	± 130	99
AMW28-34	0.0000	41	52	0.906	± 0.091	0.0993	± 0.0035	0.0662	± 0.0031	655	± 50	610	± 21	811	± 209	93
AMW28-35	0.0000	118	244	5.160	± 0.394	0.3302	± 0.0099	0.1133	± 0.0040	1846	± 67	1839	± 48	1854	± 133	100
AMW28-36	0.0000	446	477	0.679	± 0.053	0.0841	± 0.0025	0.0585	± 0.0021	526	± 32	521	± 15	550	± 165	99
AMW28-37	0.0000	56	67	0.873	± 0.085	0.0995	± 0.0029	0.0637	± 0.0030	637	± 47	611	± 17	731	± 211	96
AMW28-38	0.0000	352	487	2.389	± 0.190	0.2176	± 0.0053	0.0796	± 0.0030	1239	± 59	1269	± 28	1187	± 157	102
AMW28-39	0.0000	24	40	0.940	± 0.110	0.1012	± 0.0036	0.0673	± 0.0037	673	± 59	622	± 21	848	± 250	92
AMW28-40	0.0000	98	176	12.543	± 0.995	0.5106	± 0.0126	0.1782	± 0.0067	2646	± 78	2659	± 54	2636	± 131	100
AMW28-41	0.0000	37	83	4.065	± 0.348	0.2976	± 0.0081	0.0991	± 0.0040	1647	± 72	1679	± 40	1607	± 160	102
AMW28-42	0.0000	120	134	1.126	± 0.097	0.1263	± 0.0033	0.0647	± 0.0026	766	± 47	767	± 19	763	± 182	100
AMW28-43	0.0000	58	105	2.527	± 0.216	0.2194	± 0.0058	0.0835	± 0.0034	1280	± 64	1279	± 31	1281	± 167	100
AMW28-44	0.0000	161	259	0.816	± 0.070	0.0998	± 0.0026	0.0593	± 0.0024	606	± 40	613	± 15	577	± 189	101
AMW28-45	0.0000	95	65	10.724	± 0.853	0.4861	± 0.0120	0.1600	± 0.0061	2500	± 77	2554	± 52	2456	± 134	102
AMW28-46	0.0000	62	80	5.931	± 0.459	0.3555	± 0.0194	0.1210	± 0.0033	1966	± 70	1961	± 93	1971	± 101	100
AMW28-47	0.0000	145	177	6.964	± 0.523	0.3855	± 0.0208	0.1310	± 0.0034	2107	± 69	2102	± 98	2112	± 95	100
AMW28-48	0.0000	162	248	13.125	± 0.978	0.5238	± 0.0283	0.1817	± 0.0047	2689	± 73	2715	± 121	2669	± 88	101
AMW28-49	0.0003	226	275	0.928	± 0.074	0.0987	± 0.0054	0.0682	± 0.0020	666	± 39	607	± 32	874	± 124	91

Note: all errors are quoted at 2 s level

Concordance = [206Pb/238U age/ 206Pb/238U age]×100

Table3-1
LA-ICP-MC U-Pb isotope analysical data for zircons from sandstone samples in Anglesey

Grain	$^{204}Pb/^{206}Pb$	U (ppm)	Th (ppm)	$^{207}Pb/^{235}U$	2σ	$^{206}Pb/^{238}U$	2σ	$^{207}Pb/^{206}Pb$	2σ	Age (Ma)						Concordance
										$^{207}Pb/^{235}U$	2σ	$^{206}Pb/^{238}U$	2σ	$^{207}Pb/^{206}Pb$	2σ	
AMW28-50	0.0000	87	90	5.853 ±	0.447	0.3485 ±	0.0189	0.1218 ±	0.0033	1954 ±	69	1927 ±	91	1983 ±	99	99
AMW28-51	0.0000	328	751	2.035 ±	0.154	0.1876 ±	0.0101	0.0787 ±	0.0021	1127 ±	53	1109 ±	55	1163 ±	109	98
AMW28-52	0.0000	720	1666	5.317 ±	0.409	0.3019 ±	0.0101	0.1277 ±	0.0044	1872 ±	68	1701 ±	50	2067 ±	127	91
AMW28-53	0.0008	47	23	2.340 ±	0.203	0.1987 ±	0.0072	0.0854 ±	0.0034	1225 ±	64	1168 ±	39	1325 ±	161	95
AMW28-54	0.0000	41	56	12.166 ±	0.969	0.4869 ±	0.0172	0.1812 ±	0.0065	2617 ±	78	2557 ±	75	2664 ±	124	98
AMW28-55	0.0000	886	769	0.720 ±	0.056	0.0899 ±	0.0030	0.0581 ±	0.0020	551 ±	34	555 ±	18	533 ±	162	101
AMW28-56	0.0006	155	149	0.860 ±	0.073	0.0972 ±	0.0034	0.0642 ±	0.0025	630 ±	40	598 ±	20	747 ±	171	95
AMW28-57	0.0000	138	70	0.871 ±	0.074	0.1049 ±	0.0037	0.0602 ±	0.0023	636 ±	41	643 ±	22	611 ±	177	101
AMW28-58	0.0002	186	158	0.666 ±	0.057	0.0857 ±	0.0030	0.0563 ±	0.0022	518 ±	35	530 ±	18	466 ±	181	102
AMW28-59	0.0000	128	180	6.177 ±	0.483	0.3630 ±	0.0124	0.1234 ±	0.0043	2001 ±	71	1996 ±	59	2006 ±	130	100
ANG26-1	0.0000	135	137	0.813 ±	0.051	0.0950 ±	0.0035	0.0620 ±	0.0016	604 ±	29	585 ±	21	675 ±	114	97
ANG26-2	0.0000	42	26	6.407 ±	0.370	0.3774 ±	0.0138	0.1231 ±	0.0028	2033 ±	52	2064 ±	65	2002 ±	82	102
ANG26-3	0.0000	116	75	0.807 ±	0.053	0.0953 ±	0.0035	0.0615 ±	0.0016	601 ±	30	587 ±	21	656 ±	119	98
ANG26-4	0.0000	120	84	3.708 ±	0.206	0.2597 ±	0.0093	0.1035 ±	0.0022	1573 ±	45	1488 ±	48	1689 ±	80	95
ANG26-5	0.0000	119	87	0.769 ±	0.050	0.0925 ±	0.0034	0.0603 ±	0.0016	579 ±	29	571 ±	20	613 ±	121	99
ANG26-6	0.0000	140	1029	3.525 ±	0.194	0.2592 ±	0.0093	0.0986 ±	0.0021	1533 ±	45	1486 ±	48	1598 ±	80	97
ANG26-7	0.0001	64	56	6.483 ±	0.363	0.3509 ±	0.0127	0.1340 ±	0.0029	2044 ±	51	1939 ±	61	2151 ±	77	95
ANG26-8	0.0000	743	1621	2.012 ±	0.107	0.1904 ±	0.0067	0.0766 ±	0.0015	1119 ±	37	1124 ±	36	1111 ±	81	100
ANG26-9	0.0000	137	229	2.049 ±	0.117	0.1878 ±	0.0068	0.0791 ±	0.0017	1132 ±	40	1109 ±	37	1175 ±	90	98
ANG26-10	0.0036	145	44	1.841 ±	0.106	0.1038 ±	0.0038	0.1286 ±	0.0029	1060 ±	39	637 ±	22	2079 ±	81	60
ANG26-11	0.0023	65	44	1.375 ±	0.078	0.0977 ±	0.0020	0.1021 ±	0.0027	878 ±	34	601 ±	12	1663 ±	101	68
ANG26-12	0.0001	68	51	0.848 ±	0.053	0.0996 ±	0.0020	0.0617 ±	0.0018	624 ±	29	612 ±	12	665 ±	131	98
ANG26-13	0.0000	531	731	3.979 ±	0.156	0.2809 ±	0.0040	0.1027 ±	0.0019	1630 ±	32	1596 ±	20	1674 ±	69	98
ANG26-14	0.0000	102	54	0.900 ±	0.049	0.1022 ±	0.0018	0.0639 ±	0.0016	652 ±	27	627 ±	11	739 ±	113	96
ANG26-15	0.0004	145	87	0.759 ±	0.040	0.0940 ±	0.0016	0.0586 ±	0.0014	573 ±	23	579 ±	10	550 ±	111	101
ANG26-16	0.0000	114	105	0.840 ±	0.045	0.0940 ±	0.0017	0.0648 ±	0.0017	619 ±	25	579 ±	10	767 ±	112	94
ANG26-17	0.0004	42	8	5.759 ±	0.267	0.3606 ±	0.0063	0.1158 ±	0.0025	1940 ±	41	1985 ±	30	1893 ±	79	102
ANG26-18	0.0037	517	341	2.308 ±	0.093	0.1208 ±	0.0018	0.1386 ±	0.0026	1215 ±	29	735 ±	10	2209 ±	66	61
ANG26-19	0.0000	315	376	3.588 ±	0.144	0.2730 ±	0.0040	0.0953 ±	0.0018	1547 ±	32	1556 ±	20	1535 ±	72	101
ANG26-20	0.0077	158	87	3.248 ±	0.140	0.1118 ±	0.0018	0.2108 ±	0.0042	1469 ±	34	683 ±	11	2911 ±	66	47
ANG26-21	0.0008	109	82	0.930 ±	0.049	0.1084 ±	0.0036	0.0622 ±	0.0013	667 ±	26	664 ±	21	680 ±	90	99
ANG26-22	0.0000	60	55	0.806 ±	0.053	0.1024 ±	0.0036	0.0571 ±	0.0016	600 ±	30	629 ±	21	494 ±	127	105
ANG26-23	0.0000	159	172	0.826 ±	0.041	0.1016 ±	0.0033	0.0590 ±	0.0011	612 ±	23	624 ±	19	566 ±	83	102
ANG26-24	0.0000	283	383	1.633 ±	0.067	0.1440 ±	0.0046	0.0822 ±	0.0011	983 ±	26	867 ±	26	1251 ±	52	88
ANG26-25	0.0000	291	476	3.521 ±	0.137	0.2644 ±	0.0083	0.0966 ±	0.0011	1532 ±	31	1512 ±	43	1559 ±	44	99
ANG26-26	0.0000	143	85	0.763 ±	0.039	0.0948 ±	0.0031	0.0584 ±	0.0012	576 ±	23	584 ±	18	545 ±	90	101
ANG26-27	0.0004	118	56	0.821 ±	0.044	0.0985 ±	0.0033	0.0605 ±	0.0013	609 ±	25	606 ±	19	620 ±	93	100
ANG26-28	0.0002	99	94	12.813 ±	0.500	0.5014 ±	0.0160	0.1853 ±	0.0021	2666 ±	37	2620 ±	69	2701 ±	38	98
ANG26-29	0.0045	209	99	1.965 ±	0.083	0.0967 ±	0.0031	0.1473 ±	0.0020	1104 ±	29	595 ±	18	2315 ±	48	54
ANG26-30	0.0035	128	74	1.541 ±	0.072	0.0976 ±	0.0032	0.1145 ±	0.0019	947 ±	29	601 ±	19	1872 ±	61	63
ANG26-31	0.0002	153	120	0.952 ±	0.074	0.1097 ±	0.0021	0.0630 ±	0.0024	679 ±	39	671 ±	12	707 ±	169	99
ANG26-32	0.0000	1238	959	9.481 ±	0.668	0.6501 ±	0.0105	0.1058 ±	0.0036	2386 ±	67	3228 ±	41	1728 ±	131	135
ANG26-33	0.0010	90	62	1.030 ±	0.084	0.1144 ±	0.0023	0.0653 ±	0.0026	719 ±	43	698 ±	13	784 ±	175	97
ANG26-34	0.0000	191	206	3.989 ±	0.287	0.2985 ±	0.0051	0.0969 ±	0.0034	1632 ±	60	1684 ±	25	1566 ±	137	103
ANG26-35	0.0001	668	667	1.037 ±	0.075	0.1164 ±	0.0019	0.0646 ±	0.0023	722 ±	38	710 ±	11	762 ±	155	98
ANG26-36	0.0182	214	150	11.758 ±	0.837	0.1986 ±	0.0034	0.4295 ±	0.0148	2585 ±	69	1168 ±	18	4016 ±	107	45
ANG26-37	0.0004	304	199	0.769 ±	0.058	0.0900 ±	0.0016	0.0620 ±	0.0023	579 ±	34	555 ±	9	674 ±	164	96
ANG26-38	0.0000	185	87	4.808 ±	0.345	0.3165 ±	0.0054	0.1102 ±	0.0038	1786 ±	62	1772 ±	26	1803 ±	132	99
ANG26-39	0.0005	109	164	0.785 ±	0.064	0.1026 ±	0.0020	0.0555 ±	0.0022	588 ±	37	630 ±	12	431 ±	188	107
ANG212-1	0.0000	233	263	0.598 ±	0.038	0.0750 ±	0.0035	0.0578 ±	0.0013	476 ±	24	466 ±	21	522 ±	99	98
ANG212-2	0.0000	317	277	0.631 ±	0.039	0.0758 ±	0.0035	0.0603 ±	0.0012	497 ±	24	471 ±	21	615 ±	90	95
ANG212-3	0.0000	317	304	0.568 ±	0.035	0.0692 ±	0.0032	0.0595 ±	0.0012	457 ±	23	431 ±	19	587 ±	93	94
ANG212-4	0.0005	434	278	0.532 ±	0.032	0.0693 ±	0.0032	0.0557 ±	0.0011	433 ±	22	432 ±	19	440 ±	91	100
ANG212-5	0.0005	194	204	0.566 ±	0.037	0.0645 ±	0.0030	0.0636 ±	0.0015	455 ±	24	403 ±	18	728 ±	102	89
ANG212-6	0.0000	316	256	0.530 ±	0.033	0.0694 ±	0.0032	0.0554 ±	0.0012	432 ±	22	433 ±	19	427 ±	97	100
ANG212-7	0.0000	224	225	0.657 ±	0.042	0.0795 ±	0.0037	0.0600 ±	0.0013	513 ±	26	493 ±	22	602 ±	97	96
ANG212-8	0.0011	95	81	0.525 ±	0.040	0.0647 ±	0.0031	0.0588 ±	0.0017	428 ±	27	404 ±	19	560 ±	134	94
ANG212-9	0.0000	261	231	0.550 ±	0.035	0.0704 ±	0.0032	0.0567 ±	0.0012	445 ±	23	439 ±	20	479 ±	99	99
ANG212-10	0.0000	207	225	0.562 ±	0.037	0.0718 ±	0.0033	0.0568 ±	0.0013	453 ±	24	447 ±	20	485 ±	104	99
ANG212-11	0.0001	461	347	0.524 ±	0.050	0.0664 ±	0.0048	0.0573 ±	0.0018	428 ±	34	414 ±	29	503 ±	145	97
ANG212-12	0.0003	141	114	0.704 ±	0.070	0.0738 ±	0.0053	0.0692 ±	0.0024	541 ±	43	459 ±	32	904 ±	148	85
ANG212-13	0.0003	276	256	0.562 ±	0.054	0.0729 ±	0.0052	0.0559 ±	0.0018	453 ±	36	454 ±	32	448 ±	151	100
ANG212-14	0.0000	296	271	0.564 ±	0.054	0.0696 ±	0.0050	0.0588 ±	0.0019	454 ±	36	434 ±	30	560 ±	147	95
ANG212-15	0.0011	465	546	0.812 ±	0.077	0.0699 ±	0.0050	0.0842 ±	0.0026	604 ±	44	436 ±	30	1298 ±	125	72
ANG212-16	0.0000	538	358	0.556 ±	0.053	0.0708 ±	0.0051	0.0569 ±	0.0018	449 ±	35	441 ±	31	487 ±	143	98
ANG212-17	0.0000	286	250	0.562 ±	0.054	0.0726 ±	0.0052	0.0561 ±	0.0018	453 ±	36	452 ±	31	457 ±	151	100
ANG212-18	0.0000	320	265	0.557 ±	0.054	0.0703 ±	0.0050	0.0574 ±	0.0018	449 ±	36	438 ±	30	508 ±	148	97
ANG212-19	0.0000	253	279	0.539 ±	0.053	0.0697 ±	0.0050	0.0561 ±	0.0018	438 ±	35	434 ±	30	457 ±	153	99
ANG212-20	0.0000	365	264	0.566 ±	0.054	0.0721 ±	0.0052	0.0570 ±	0.0018	455 ±	36	449 ±	31	490 ±	147	99
ANN2-1	0.0000	170	476	3.289 ±	0.230	0.2589 ±	0.0109	0.0921 ±	0.0026	1479 ±	56	1484 ±	56	1470 ±	110	100
ANN2-2	0.0000	49	42	6.342 ±	0.457	0.3794 ±	0.0162	0.1212 ±	0.0035	2024 ±	65	2074 ±	76	1974 ±	107	102
ANN2-3	0.0000	254	778	2.781 ±	0.193	0.2365 ±	0.0099	0.0853 ±	0.0024	1350 ±	53	1369 ±	52	1322 ±	112	101
ANN2-4	0.0000	329	902	2.269 ±	0.158	0.2095 ±	0.0087	0.0786 ±	0.0022	1203 ±	50	1226 ±	47	1161 ±	114	102
ANN2-5	0.0000	351	688	2.836 ±	0.196	0.2435 ±	0.0102	0.0845 ±	0.0023	1365 ±	53	1405 ±	53	1304 ±	111	103
ANN2-6	0.0000	95	185	3.408 ±	0.244	0.2636 ±	0.0111	0.0938 ±	0.0027	1506 ±	58	1508 ±	57	1503 ±	113	100
ANN2-7	0.0000	100	211	2.184 ±	0.159	0.2020 ±	0.0086	0.0784 ±	0.0023	1176 ±	52	1186 ±	46	1157 ±	122	101
ANN2-8	0.0000	175	221	4.290 ±	0.298	0.3065 ±	0.0128	0.1015 ±	0.0028	1691 ±	59	1724 ±	64	1652 ±	107	102
ANN2-9	0.0000	113	149	2.321 ±	0.167	0.2133 ±	0.0090	0.0789 ±	0.0023	1219 ±	53	1246 ±	48	1171 ±	120	102
ANN2-10	0.0000	242	273	3.038 ±	0.265	0.2533 ±	0.0152	0.0870 ±	0.0027	1417 ±	69	1455 ±	79	1360 ±	127	103
ANN2-11	0.0000	69	70	5.304 ±	0.471	0.3348 ±	0.0203	0.1149 ±	0.0037	1870 ±	79	1862 ±	99	1879 ±	122	100
ANN2-12	0.0000	224	400	3.149 ±	0.275	0.2521 ±	0.0152	0.0906 ±	0.0029	1445 ±	70	1449 ±	79	1438 ±	125	100
ANN2-13	0.0000	139	762	4.393 ±	0.385	0.2961 ±	0.0179	0.1076 ±	0.0034	1711 ±	75	1672 ±	89	1759 ±	121	98
ANN2-14	0.0000	243	737	4.886 ±	0.424	0.3119 ±	0.0188	0.1136 ±	0.0036	1800 ±	76	1750 ±	93	1858 ±	117	97
ANN2-15	0.0000	276	903	2.257 ±	0.197	0.2074 ±	0.0125	0.0789 ±	0.0025	1199 ±	63	1215 ±	67	1170 ±	131	101
ANN2-16	0.0000	163	387	2.330 ±	0.206	0.2115 ±	0.0128	0.0799 ±	0.0026	1221 ±	65	1237 ±	68	1194 ±	133	101
ANN2-17	0.0000	22	18	1.937 ±	0.205	0.1740 ±	0.0111	0.0807 ±	0.0034	1094 ±	74	1034 ±	61	1214 ±	177	95
ANN2-18	0.0000	176	945	2.387 ±	0.210	0.2127 ±	0.0128	0.0814 ±	0.0026	1239 ±	65	1243 ±	69	1231 ±	131	100
ANN2-19	0.0000	437	649	2.146 ±	0.117	0.1923 ±	0.0066	0.0809 ±	0.0017	1164 ±	38	1134 ±	36	1219 ±	86	97
ANN2-20	0.0000	102	450	2.818 ±	0.164	0.2316 ±	0.0081	0.0882 ±	0.0021	1360 ±	45	1343 ±	43	1388 ±	92	99
ANN2-21	0.0000	165	424	2.266 ±	0.129	0.1975 ±	0.0069	0.0832 ±	0.0019	1202 ±	41	1162 ±	37	1275 ±	91	97
ANN2-22	0.0000	49	100	2.068 ±	0.138	0.1911 ±	0.0070	0.0785 ±	0.0022	1138 ±	47	1127 ±	38	1159 ±	115	99
ANN2-23	0.0000	95	77	3.279 ±	0.190	0.2532 ±	0.0089	0.0939 ±	0.0022	1476 ±	46	1455 ±	46	1507 ±	90	99
ANN2-24	0.0000	187	562	2.615 ±	0.147	0.2172 ±	0.0075	0.0873 ±	0.0019	1305 ±	42	1267 ±	40	1368 ±	87	97
ANN2-25	0.0000	113	262	2.060 ±	0.122	0.1873 ±	0.0066	0.0798 ±	0.0019	1136 ±	41	1107 ±	36	1192 ±	97	97
ANN2-26	0.0000	107	177	2.329 ±	0.137	0.1992 ±	0.0070	0.0848 ±	0.0020	1221 ±	43	1171 ±	38	1311 ±	95	96
ANN2-27	0.0000	92	52	6.606 ±	0.368	0.3714 ±	0.0129	0.1290 ±	0.0028	2060 ±	50	2036 ±	61	2085 ±	79	99
ANN2-28	0.0000	272	878	2.246 ±	0.124	0.1991 ±	0.0069	0.0818 ±	0.0018	1196 ±	40	1171 ±	37	1241 ±	87	98
ANN2-29	0.0000	76	143	2.385 ±	0.142	0.2037 ±	0.0057	0.0849 ±	0.0022	1238 ±	44	1195 ±	30	1314 ±	106	97
ANN2-30	0.0000	45	81	2.417 ±	0.156	0.2102 ±	0.0061	0.0834 ±	0.0024	1248 ±	48	1230 ±	33	1278 ±	117	99
ANN2-31	0.0000	435	1894	3.399 ±	0.177	0.2566 ±	0.0067	0.0961 ±	0.0022	1504 ±	42	1473 ±	34	1549 ±	88	98
ANN2-32	0.0000	116	160	7.298 ±	0.389	0.3906 ±	0.0103	0.1355 ±	0.0031	2149 ±	49	2126 ±	48	2171 ±	83	99
ANN2-33	0.0000	204	321	2.715 ±	0.147	0.2253 ±	0.0059	0.0874 ±	0.0021	1333 ±	41	1310 ±	31	1369 ±	94	98
ANN2-34	0.0000	120	278	3.617 ±	0.199	0.2693 ±	0.0072	0.0974 ±	0.0023	1553 ±	45	1537 ±	37	1576 ±	93	99
ANN2-35	0.0000	140	313	2.141 ±	0.121	0.1963 ±	0.0053	0.0791 ±	0.0020	1162 ±	40	1156 ±	28	1175 ±	101	99
ANN2-36	0.0000	182	492	2.176 ±	0.120	0.1929 ±	0.0051	0.0818 ±	0.0020	1173 ±	39	1137 ±	28	1241 ±	98	97
ANN2-37	0.0000	230	264	6.578 ±	0.344	0.3729 ±	0.0097	0.1279 ±	0.0029	2056 ±	47	2043 ±	46	2070 ±	82	99
ANN2-38	0.0001	55	63	4.833 ±	0.215	0.3232 ±	0.0086	0.1085 ±	0.0019	1791 ±	38	1805 ±	42	1774 ±	67	101

Note: all errors are quoted at 2 s level
Concordance = [206Pb/238U age/ 206Pb/238U age]×100

Table3-1
LA-ICP-MC U-Pb isotope analysical data for zircons from sandstone samples in Anglesey

Grain	$^{204}Pb/^{206}Pb$	U (ppm)	Th (ppm)	$^{207}Pb/^{235}U$	2σ	$^{206}Pb/^{238}U$	2σ	$^{207}Pb/^{206}Pb$	2σ	Age (Ma)						Concordance
										$^{207}Pb/^{235}U$	2σ	$^{206}Pb/^{238}U$	2σ	$^{207}Pb/^{206}Pb$	2σ	
ANN2-39	0.0000	270	223	3.546	± 0.139	0.2632	± 0.0066	0.0977	± 0.0015	1538	± 31	1506	± 34	1581	± 57	98
ANN2-40	0.0000	199	266	4.830	± 0.189	0.3228	± 0.0081	0.1085	± 0.0016	1790	± 33	1803	± 40	1775	± 56	101
ANN2-41	0.0000	463	683	2.228	± 0.087	0.2002	± 0.0050	0.0807	± 0.0012	1190	± 28	1176	± 27	1214	± 60	99
ANN2-42	0.0000	70	123	3.429	± 0.154	0.2562	± 0.0067	0.0971	± 0.0018	1511	± 36	1470	± 35	1569	± 70	97
ANN2-43	0.0000	325	4496	2.096	± 0.083	0.1896	± 0.0048	0.0802	± 0.0012	1147	± 28	1119	± 26	1201	± 62	98
ANN2-44	0.0001	625	712	4.922	± 0.185	0.3096	± 0.0077	0.1153	± 0.0016	1806	± 32	1739	± 38	1884	± 52	96
ANN2-45	0.0000	124	363	3.413	± 0.142	0.2555	± 0.0065	0.0969	± 0.0016	1507	± 33	1467	± 34	1565	± 63	97
ANN2-46	0.0000	34	31	15.326	± 1.110	0.5584	± 0.0376	0.1991	± 0.0026	2836	± 71	2860	± 157	2819	± 44	101
ANN2-47	0.0000	101	84	5.690	± 0.408	0.3555	± 0.0238	0.1161	± 0.0015	1930	± 64	1961	± 114	1897	± 47	102
ANN2-48	0.0000	258	421	14.576	± 1.024	0.5330	± 0.0356	0.1983	± 0.0022	2788	± 69	2754	± 151	2813	± 36	99
ANN2-49	0.0000	231	475	2.401	± 0.172	0.2129	± 0.0142	0.0818	± 0.0011	1243	± 53	1244	± 76	1240	± 51	100
ANN2-50	0.0000	141	44	5.354	± 0.382	0.3382	± 0.0226	0.1148	± 0.0014	1878	± 63	1878	± 110	1877	± 45	100
ANN2-51	0.0003	72	104	3.550	± 0.262	0.2630	± 0.0177	0.0979	± 0.0015	1538	± 60	1505	± 91	1584	± 58	98
ANN2-52	0.0000	39	21	3.424	± 0.263	0.2760	± 0.0187	0.0900	± 0.0016	1510	± 62	1571	± 95	1425	± 72	104
ANN2-53	0.0000	71	153	2.898	± 0.216	0.2395	± 0.0161	0.0877	± 0.0014	1381	± 58	1384	± 84	1377	± 63	100
ANN2-54	0.0000	29	54	2.291	± 0.190	0.2060	± 0.0141	0.0806	± 0.0019	1209	± 60	1207	± 76	1213	± 95	100
ANN2-55	0.0000	238	636	3.896	± 0.277	0.2738	± 0.0183	0.1032	± 0.0012	1613	± 59	1560	± 93	1683	± 45	97
ANN2-56	0.0000	158	610	2.353	± 0.194	0.2093	± 0.0118	0.0815	± 0.0025	1228	± 61	1225	± 63	1234	± 123	100
ANN2-57	0.0000	118	161	4.622	± 0.379	0.3123	± 0.0176	0.1074	± 0.0032	1753	± 71	1752	± 87	1755	± 113	100
ANN2-58	0.0000	91	95	3.262	± 0.271	0.2505	± 0.0142	0.0945	± 0.0029	1472	± 67	1441	± 74	1517	± 119	98
ANN2-59	0.0000	135	327	3.093	± 0.255	0.2448	± 0.0138	0.0916	± 0.0027	1431	± 65	1412	± 72	1459	± 118	99
ANN2-60	0.0000	34	119	3.144	± 0.276	0.2588	± 0.0149	0.0881	± 0.0029	1443	± 70	1484	± 77	1384	± 133	103
ANN2-61	0.0001	165	371	2.391	± 0.197	0.2128	± 0.0120	0.0815	± 0.0024	1240	± 61	1244	± 64	1233	± 122	100
ANN2-62	0.0000	101	127	5.395	± 0.442	0.3369	± 0.0190	0.1162	± 0.0034	1884	± 73	1872	± 92	1898	± 111	99
ANN2-63	0.0000	243	363	6.472	± 0.523	0.3800	± 0.0214	0.1235	± 0.0036	2042	± 74	2076	± 101	2008	± 107	102
ANN2-64	0.0000	21	84	2.302	± 0.221	0.2126	± 0.0125	0.0785	± 0.0030	1213	± 70	1243	± 67	1160	± 159	102
ANN2-65	0.0000	257	548	2.709	± 0.221	0.2261	± 0.0127	0.0869	± 0.0026	1331	± 62	1314	± 67	1358	± 118	99
ANN2-66	0.0000	165	274	2.228	± 0.164	0.2044	± 0.0023	0.0791	± 0.0029	1190	± 53	1199	± 13	1174	± 151	101
ANN2-67	0.0000	191	415	3.336	± 0.243	0.2644	± 0.0029	0.0915	± 0.0033	1490	± 58	1512	± 15	1457	± 143	102
ANN2-68	0.0000	379	1100	2.245	± 0.162	0.2007	± 0.0021	0.0812	± 0.0029	1195	± 52	1179	± 11	1225	± 147	99
ANN2-69	0.0000	391	807	2.018	± 0.146	0.1882	± 0.0020	0.0778	± 0.0028	1122	± 50	1112	± 11	1141	± 149	99
ANN2-70	0.0000	129	273	3.894	± 0.285	0.2808	± 0.0032	0.1006	± 0.0036	1612	± 61	1595	± 16	1635	± 141	99
ANN2-71	0.0000	358	287	6.205	± 0.445	0.3655	± 0.0037	0.1231	± 0.0044	2005	± 65	2008	± 17	2002	± 132	100
ANN2-72	0.0000	147	95	5.846	± 0.423	0.3559	± 0.0039	0.1191	± 0.0043	1953	± 65	1963	± 19	1943	± 134	100
ANN2-73	0.0000	51	56	2.678	± 0.209	0.2264	± 0.0033	0.0858	± 0.0033	1322	± 59	1316	± 18	1333	± 156	99
ANN2-74	0.0000	68	49	2.610	± 0.200	0.2273	± 0.0031	0.0833	± 0.0031	1303	± 58	1320	± 16	1276	± 154	101
ANN2-75	0.0000	109	146	2.251	± 0.169	0.1995	± 0.0025	0.0819	± 0.0030	1197	± 54	1172	± 13	1242	± 152	98
		0	0													
ANN14-1	0.0000	218	150	1.017	± 0.076	0.1160	± 0.0030	0.0636	± 0.0022	713	± 39	707	± 18	729	± 155	99
ANN14-2	0.0000	488	287	5.807	± 0.410	0.3619	± 0.0092	0.1164	± 0.0038	1947	± 63	1991	± 44	1901	± 123	102
ANN14-3	0.0000	216	277	0.993	± 0.074	0.1062	± 0.0028	0.0678	± 0.0024	700	± 39	651	± 16	863	± 152	93
ANN14-4	0.0000	708	2570	1.785	± 0.127	0.1769	± 0.0045	0.0732	± 0.0024	1040	± 47	1050	± 25	1019	± 140	101
ANN14-5	0.0000	535	633	0.883	± 0.064	0.1021	± 0.0026	0.0627	± 0.0021	643	± 35	627	± 15	700	± 151	98
ANN14-6	0.0000	286	463	0.998	± 0.073	0.1121	± 0.0029	0.0646	± 0.0022	703	± 38	685	± 17	762	± 152	97
ANN14-7	0.0000	185	270	0.827	± 0.063	0.0960	± 0.0026	0.0625	± 0.0022	612	± 36	591	± 15	691	± 161	97
ANN14-8	0.0000	39	54	6.429	± 0.482	0.3782	± 0.0104	0.1233	± 0.0043	2036	± 68	2068	± 49	2005	± 129	102
ANN14-9	0.0000	275	1566	3.429	± 0.245	0.2572	± 0.0066	0.0967	± 0.0032	1511	± 58	1476	± 34	1561	± 130	98
ANN14-10	0.0000	266	930	0.873	± 0.075	0.1054	± 0.0026	0.0601	± 0.0025	637	± 41	646	± 15	606	± 187	101
ANN14-11	0.0000	201	269	0.886	± 0.077	0.1063	± 0.0027	0.0604	± 0.0025	644	± 42	651	± 16	618	± 189	101
ANN14-12	0.0000	618	1068	3.538	± 0.291	0.2504	± 0.0061	0.1025	± 0.0040	1536	± 67	1441	± 31	1669	± 153	94
ANN14-13	0.0000	105	207	3.081	± 0.261	0.2405	± 0.0061	0.0929	± 0.0038	1428	± 67	1389	± 32	1486	± 162	97
ANN14-14	0.0000	304	467	1.063	± 0.090	0.1250	± 0.0031	0.0617	± 0.0025	735	± 45	759	± 18	663	± 183	103
ANN14-15	0.0000	255	640	3.104	± 0.258	0.2428	± 0.0059	0.0927	± 0.0037	1434	± 66	1401	± 31	1482	± 159	98
ANN14-16	0.0000	129	106	0.983	± 0.087	0.1117	± 0.0029	0.0638	± 0.0027	695	± 45	683	± 17	736	± 190	98
ANN14-17	0.0000	106	276	1.089	± 0.097	0.1207	± 0.0032	0.0654	± 0.0028	748	± 48	735	± 18	788	± 190	98
ANN14-18	0.0000	200	284	4.363	± 0.362	0.2925	± 0.0072	0.1082	± 0.0043	1705	± 71	1654	± 36	1769	± 152	97
ANN14-19	0.0000	211	113	0.925	± 0.080	0.1099	± 0.0028	0.0610	± 0.0025	665	± 43	672	± 16	641	± 188	101
ANN14-20	0.0000	130	216	0.831	± 0.069	0.0964	± 0.0028	0.0625	± 0.0024	614	± 39	593	± 16	693	± 175	97
ANN14-21	0.0000	207	198	0.933	± 0.074	0.1078	± 0.0030	0.0628	± 0.0023	669	± 40	660	± 17	701	± 166	99
ANN14-22	0.0000	158	384	2.334	± 0.180	0.2096	± 0.0058	0.0808	± 0.0029	1223	± 56	1227	± 31	1216	± 148	100
ANN14-23	0.0000	84	126	6.770	± 0.517	0.3609	± 0.0100	0.1361	± 0.0048	2082	± 70	1986	± 48	2178	± 129	95
ANN14-24	0.0000	90	113	4.508	± 0.347	0.2984	± 0.0083	0.1096	± 0.0039	1732	± 66	1683	± 41	1793	± 137	97
ANN14-25	0.0000	866	1644	2.966	± 0.221	0.2313	± 0.0062	0.0930	± 0.0032	1399	± 58	1341	± 32	1488	± 138	96
ANN14-26	0.0000	61	52	0.838	± 0.077	0.1020	± 0.0031	0.0596	± 0.0026	618	± 43	626	± 18	591	± 199	101
ANN14-27	0.0000	241	156	0.822	± 0.065	0.0989	± 0.0027	0.0603	± 0.0022	609	± 37	608	± 16	614	± 169	100
ANN14-28	0.0000	134	369	5.527	± 0.419	0.3365	± 0.0092	0.1191	± 0.0042	1905	± 67	1870	± 44	1943	± 132	98
ANN14-29	0.0000	259	270	0.850	± 0.064	0.1007	± 0.0040	0.0612	± 0.0020	624	± 36	618	± 24	646	± 144	99
ANN14-30	0.0000	163	282	3.499	± 0.255	0.2660	± 0.0105	0.0954	± 0.0029	1527	± 59	1520	± 54	1536	± 119	100
ANN14-31	0.0000	439	1658	3.303	± 0.236	0.2612	± 0.0103	0.0917	± 0.0027	1482	± 57	1496	± 53	1461	± 118	101
ANN14-32	0.0001	267	130	0.969	± 0.072	0.1069	± 0.0043	0.0657	± 0.0021	688	± 38	655	± 25	798	± 139	95
ANN14-33	0.0002	184	131	0.959	± 0.073	0.1104	± 0.0044	0.0631	± 0.0021	683	± 39	675	± 26	710	± 145	99
ANN14-34	0.0005	142	146	0.889	± 0.070	0.1041	± 0.0042	0.0620	± 0.0021	646	± 38	638	± 25	673	± 151	99
ANN14-35	0.0001	231	538	2.150	± 0.157	0.1886	± 0.0075	0.0827	± 0.0025	1165	± 52	1114	± 41	1261	± 125	96
ANN14-36	0.0000	71	43	0.901	± 0.077	0.1069	± 0.0045	0.0611	± 0.0023	652	± 42	655	± 26	644	± 170	100
ANN14-37	0.0000	457	1102	6.630	± 0.472	0.3626	± 0.0142	0.1326	± 0.0039	2063	± 65	1995	± 68	2133	± 108	97
ANN14-38	0.0000	471	1016	10.490	± 0.745	0.4422	± 0.0174	0.1720	± 0.0051	2479	± 68	2361	± 78	2578	± 102	95
ANN14-39	0.0000	430	1005	2.271	± 0.150	0.2053	± 0.0040	0.0802	± 0.0025	1203	± 48	1204	± 21	1202	± 130	100
ANN14-40	0.0000	58	41	0.894	± 0.075	0.1042	± 0.0026	0.0622	± 0.0025	648	± 41	639	± 15	680	± 182	99
ANN14-41	0.0000	79	112	0.951	± 0.075	0.1039	± 0.0024	0.0664	± 0.0025	679	± 40	637	± 14	820	± 166	94
ANN14-42	0.0000	252	257	0.899	± 0.063	0.1043	± 0.0021	0.0626	± 0.0021	651	± 34	639	± 12	693	± 149	98
ANN14-43	0.0000	155	189	3.399	± 0.229	0.2529	± 0.0050	0.0975	± 0.0031	1504	± 54	1453	± 26	1577	± 125	97
ANN14-44	0.0000	479	569	1.068	± 0.072	0.1212	± 0.0024	0.0639	± 0.0021	738	± 36	737	± 14	740	± 142	100
ANN14-45	0.0000	48	34	4.399	± 0.312	0.2970	± 0.0065	0.1074	± 0.0036	1712	± 60	1676	± 32	1756	± 129	98
ANN14-46	0.0000	224	186	1.067	± 0.083	0.1186	± 0.0050	0.0653	± 0.0021	737	± 41	722	± 29	783	± 143	98
ANN14-47	0.0000	417	813	0.848	± 0.065	0.1015	± 0.0042	0.0606	± 0.0019	623	± 36	623	± 25	623	± 144	100
ANN14-48	0.0000	219	197	0.938	± 0.073	0.1122	± 0.0047	0.0606	± 0.0020	672	± 39	686	± 27	626	± 149	102
ANN14-49	0.0000	262	301	0.940	± 0.073	0.1064	± 0.0045	0.0640	± 0.0021	673	± 39	652	± 26	743	± 144	97
ANN14-50	0.0000	258	386	0.970	± 0.075	0.1116	± 0.0047	0.0631	± 0.0020	689	± 39	682	± 27	711	± 145	99
ANN14-51	0.0000	168	190	0.836	± 0.067	0.0998	± 0.0042	0.0608	± 0.0021	617	± 38	613	± 25	630	± 154	99
ANN14-52	0.0004	131	175	0.833	± 0.075	0.0971	± 0.0040	0.0622	± 0.0025	615	± 43	598	± 24	681	± 182	97
ANN14-53	0.0003	201	380	0.974	± 0.085	0.1183	± 0.0048	0.0597	± 0.0023	690	± 45	721	± 28	593	± 176	104
ANN14-54	0.0000	238	519	3.618	± 0.304	0.2605	± 0.0105	0.1007	± 0.0037	1553	± 69	1492	± 54	1637	± 144	96
ANN14-55	0.0000	262	409	3.772	± 0.317	0.2812	± 0.0114	0.0973	± 0.0036	1587	± 70	1598	± 57	1573	± 144	101
ANN14-56	0.0001	128	108	0.881	± 0.079	0.1024	± 0.0042	0.0624	± 0.0025	641	± 44	628	± 25	687	± 181	98
ANN14-57	0.0004	236	257	0.849	± 0.074	0.0970	± 0.0040	0.0634	± 0.0024	624	± 41	597	± 23	723	± 172	96
ANN14-58	0.0000	440	699	2.207	± 0.185	0.2019	± 0.0081	0.0793	± 0.0029	1183	± 60	1186	± 44	1179	± 153	100
ANN14-59	0.0002	102	63	0.839	± 0.077	0.1009	± 0.0042	0.0603	± 0.0025	619	± 44	620	± 25	614	± 189	100
ANN14-60	0.0000	157	189	3.853	± 0.326	0.2792	± 0.0113	0.1001	± 0.0037	1604	± 71	1587	± 57	1625	± 145	99
LLZ519-1	0.0000	86	75	0.760	± 0.078	0.0945	± 0.0065	0.0584	± 0.0022	574	± 46	582	± 39	544	± 176	101
LLZ519-2	0.0000	83	161	0.703	± 0.074	0.0834	± 0.0058	0.0611	± 0.0024	541	± 45	517	± 34	643	± 178	96
LLZ519-3	0.0000	86	231	3.038	± 0.278	0.2423	± 0.0166	0.0909	± 0.0028	1417	± 73	1399	± 87	1445	± 121	99
LLZ519-4	0.0000	207	234	1.133	± 0.104	0.1251	± 0.0085	0.0657	± 0.0020	769	± 51	760	± 49	797	± 134	99
LLZ519-5	0.0000	90	137	0.691	± 0.072	0.0874	± 0.0060	0.0573	± 0.0022	533	± 44	540	± 36	504	± 179	101
LLZ519-6	0.0000	115	234	0.678	± 0.068	0.0888	± 0.0061	0.0554	± 0.0020	526	± 42	548	± 36	428	± 172	104
LLZ519-7	0.0000	279	3938	2.638	± 0.234	0.2231	± 0.0152	0.0857	± 0.0024	1311	± 68	1298	± 81	1332	± 114	99
LLZ519-8	0.0000	163	14498	1.570	± 0.144	0.1613	± 0.0110	0.0706	± 0.0022	958	± 58	964	± 61	946	± 130	101
LLZ519-9	0.0000	149	1660	11.506	± 1.012	0.4714	± 0.0321	0.1770	± 0.0049	2565	± 86	2490	± 142	2625	± 96	97
LLZ519-10	0.0000	115	243	1.293	± 0.095	0.1326	± 0.0033	0.0707	± 0.0025	843	± 43	803	± 19	949	± 149	95
LLZ519-11	0.0000	249	521	0.759	± 0.054	0.0913	± 0.0022	0.0602	± 0.0020	573	± 32	563	± 13	613	± 153	98

Note: all errors are quoted at 2 s level
Concordance = [206Pb/238U age/ 206Pb/238U age]×100

Table3-1
LA-ICP-MC U-Pb isotope analysical data for zircons from sandstone samples in Anglesey

Grain	$^{204}Pb/^{206}Pb$	U (ppm)	Th (ppm)	$^{207}Pb/^{235}U$	2σ	$^{206}Pb/^{238}U$	2σ	$^{207}Pb/^{206}Pb$	2σ	Age (Ma)						Concordance
										$^{207}Pb/^{235}U$	2σ	$^{206}Pb/^{238}U$	2σ	$^{207}Pb/^{206}Pb$	2σ	
LLZ519-12	0.0000	56	92	1.406	± 0.115	0.1509	± 0.0040	0.0676	± 0.0026	891	± 50	906	± 22	855	± 170	102
LLZ519-13	0.0000	101	79	0.796	± 0.064	0.0986	± 0.0025	0.0585	± 0.0022	594	± 37	606	± 15	550	± 177	102
LLZ519-14	0.0000	337	4778	0.743	± 0.052	0.0925	± 0.0022	0.0583	± 0.0019	564	± 31	570	± 13	540	± 150	101
LLZ519-15	0.0000	107	100	0.885	± 0.070	0.0996	± 0.0025	0.0645	± 0.0024	644	± 38	612	± 15	757	± 166	95
LLZ519-16	0.0000	87	175	0.784	± 0.066	0.0889	± 0.0023	0.0639	± 0.0026	588	± 38	549	± 14	740	± 178	93
LLZ519-17	0.0000	116	326	0.806	± 0.064	0.0894	± 0.0023	0.0654	± 0.0024	600	± 36	552	± 13	787	± 165	92
LLZ519-18	0.0000	204	197	0.728	± 0.054	0.0909	± 0.0022	0.0581	± 0.0020	556	± 32	561	± 13	534	± 160	101
LLZ519-19	0.0000	43	54	6.461	± 0.524	0.3774	± 0.0102	0.1242	± 0.0047	2041	± 74	2064	± 48	2017	± 142	101
LLZ519-20	0.0000	92	175	0.769	± 0.071	0.0918	± 0.0026	0.0608	± 0.0027	579	± 41	566	± 15	632	± 201	98
LLZ519-21	0.0000	218	575	4.804	± 0.372	0.3123	± 0.0080	0.1116	± 0.0041	1786	± 67	1752	± 39	1825	± 139	98
LLZ519-22	0.0000	172	212	0.705	± 0.060	0.0897	± 0.0024	0.0570	± 0.0023	542	± 37	554	± 14	493	± 190	102
LLZ519-23	0.0000	51	89	2.068	± 0.181	0.1933	± 0.0054	0.0776	± 0.0032	1138	± 62	1139	± 29	1137	± 174	100
LLZ519-24	0.0000	240	365	0.780	± 0.064	0.0930	± 0.0024	0.0608	± 0.0024	585	± 37	573	± 14	634	± 178	98
LLZ519-25	0.0001	93	283	2.165	± 0.178	0.1931	± 0.0052	0.0813	± 0.0032	1170	± 59	1138	± 28	1229	± 161	97
LLZ519-26	0.0000	98	210	4.325	± 0.343	0.2913	± 0.0076	0.1077	± 0.0040	1698	± 68	1648	± 38	1761	± 144	97
LLZ519-27	0.0005	175	382	0.730	± 0.062	0.0865	± 0.0023	0.0612	± 0.0025	557	± 37	535	± 14	647	± 184	96
LLZ519-28	0.0000	63	129	0.655	± 0.095	0.0872	± 0.0026	0.0545	± 0.0039	512	± 60	539	± 15	392	± 353	105
LLZ519-29	0.0000	412	571	0.731	± 0.096	0.0897	± 0.0023	0.0590	± 0.0038	557	± 58	554	± 14	569	± 309	99
LLZ519-30	0.0000	108	189	0.723	± 0.099	0.0896	± 0.0025	0.0585	± 0.0039	552	± 60	553	± 15	547	± 325	100
LLZ519-31	0.0000	370	658	4.403	± 0.573	0.2915	± 0.0075	0.1095	± 0.0070	1713	± 114	1649	± 37	1792	± 252	96
LLZ519-32	0.0000	18	18	1.412	± 0.216	0.1562	± 0.0052	0.0656	± 0.0049	894	± 95	936	± 29	793	± 349	105
LLZ519-33	0.0000	77	106	4.707	± 0.620	0.3135	± 0.0083	0.1089	± 0.0070	1769	± 117	1758	± 41	1781	± 256	99
LLZ519-34	0.0000	190	335	0.716	± 0.096	0.0928	± 0.0025	0.0560	± 0.0037	549	± 59	572	± 15	451	± 322	104
LLZ519-35	0.0000	194	638	4.246	± 0.554	0.3155	± 0.0082	0.0976	± 0.0062	1683	± 113	1768	± 40	1579	± 261	105
LLZ519-36	0.0000	235	1394	1.932	± 0.253	0.1868	± 0.0049	0.0750	± 0.0048	1092	± 92	1104	± 26	1068	± 283	101
LLZ519-37	0.0000	90	243	3.137	± 1.577	0.2756	± 0.0134	0.0825	± 0.0207	1442	± 487	1569	± 68	1258	± 1531	109
LLZ519-38	0.0000	268	436	3.721	± 1.869	0.3071	± 0.0148	0.0879	± 0.0220	1576	± 512	1726	± 74	1380	± 1494	110
LLZ519-39	0.0004	76	139	3.111	± 1.565	0.2749	± 0.0134	0.0821	± 0.0205	1436	± 486	1566	± 68	1247	± 1535	109
LLZ519-40	0.0001	180	856	2.562	± 1.287	0.2424	± 0.0117	0.0766	± 0.0192	1290	± 455	1399	± 61	1112	± 1576	108
LLZ519-41	0.0000	242	799	1.898	± 0.954	0.2006	± 0.0097	0.0686	± 0.0172	1080	± 405	1178	± 52	887	± 1653	109
LLZ519-42	0.0000	147	388	3.818	± 1.918	0.3060	± 0.0148	0.0905	± 0.0226	1597	± 516	1721	± 74	1436	± 1479	108
LLZ519-43	0.0000	427	1839	0.585	± 0.047	0.0754	± 0.0015	0.0563	± 0.0022	468	± 30	468	± 9	464	± 182	100
LLZ519-44	0.0000	143	262	0.796	± 0.068	0.0929	± 0.0020	0.0622	± 0.0026	594	± 39	572	± 12	680	± 187	96
LLZ519-45	0.0000	67	120	0.772	± 0.074	0.0920	± 0.0022	0.0608	± 0.0028	581	± 43	567	± 13	633	± 213	98
LLZ519-46	0.0000	84	172	0.731	± 0.068	0.0917	± 0.0021	0.0578	± 0.0026	557	± 41	565	± 12	522	± 210	102
LLZ519-47	0.0000	311	320	0.747	± 0.060	0.0938	± 0.0019	0.0577	± 0.0022	566	± 35	578	± 11	520	± 181	102
LLZ519-48	0.0000	156	142	0.839	± 0.071	0.1002	± 0.0021	0.0607	± 0.0025	619	± 40	615	± 12	630	± 186	99
LLZ519-49	0.0000	360	557	0.752	± 0.060	0.0952	± 0.0019	0.0572	± 0.0022	569	± 35	586	± 11	501	± 180	103
LLZ519-50	0.0000	276	425	0.733	± 0.059	0.0906	± 0.0018	0.0586	± 0.0023	558	± 35	559	± 11	553	± 181	100
LLZ519-51	0.0000	136	253	0.750	± 0.064	0.0913	± 0.0026	0.0596	± 0.0024	569	± 38	563	± 15	590	± 184	99
LLZ519-52	0.0000	78	170	0.697	± 0.065	0.0927	± 0.0027	0.0545	± 0.0024	537	± 40	571	± 16	394	± 212	106
LLZ519-53	0.0000	160	271	0.750	± 0.063	0.0937	± 0.0026	0.0581	± 0.0023	568	± 37	577	± 15	533	± 182	102
LLZ519-54	0.0000	165	614	2.590	± 0.199	0.2234	± 0.0060	0.0841	± 0.0030	1298	± 58	1300	± 32	1295	± 147	100
LLZ519-55	0.0000	80	101	0.879	± 0.079	0.1007	± 0.0029	0.0633	± 0.0027	640	± 43	619	± 17	719	± 191	97
LLZ519-56	0.0000	185	259	0.904	± 0.073	0.1047	± 0.0029	0.0626	± 0.0024	654	± 40	642	± 17	696	± 171	98
LLZ519-57	0.0000	118	115	0.925	± 0.078	0.1020	± 0.0029	0.0658	± 0.0026	665	± 42	626	± 17	799	± 176	94
LLZ519-58	0.0000	105	140	0.817	± 0.071	0.0945	± 0.0027	0.0627	± 0.0026	606	± 40	582	± 16	698	± 185	96
LLZ519-59	0.0003	84	186	5.875	± 0.472	0.3629	± 0.0244	0.1174	± 0.0026	1958	± 72	1996	± 116	1917	± 81	102
LLZ519-60	0.0000	123	317	0.799	± 0.071	0.0925	± 0.0063	0.0627	± 0.0018	597	± 41	570	± 37	698	± 127	96
LLZ519-61	0.0000	260	506	0.799	± 0.066	0.0936	± 0.0063	0.0619	± 0.0015	596	± 38	577	± 37	671	± 108	97
LLZ519-62	0.0001	755	3429	1.943	± 0.153	0.1846	± 0.0124	0.0763	± 0.0016	1096	± 54	1092	± 68	1103	± 84	100
LLZ519-63	0.0000	506	1182	0.739	± 0.060	0.0903	± 0.0061	0.0594	± 0.0013	562	± 35	557	± 36	581	± 101	99
LLZ519-64	0.0000	71	84	0.781	± 0.075	0.0896	± 0.0061	0.0632	± 0.0021	586	± 44	553	± 36	716	± 150	94
LLZ994-1	0.0000	46	22	1.092	± 0.131	0.1180	± 0.0042	0.0671	± 0.0038	749	± 65	719	± 25	840	± 258	96
LLZ994-2	0.0000	187	25	0.773	± 0.078	0.0915	± 0.0026	0.0613	± 0.0030	582	± 46	564	± 15	649	± 223	97
LLZ994-3	0.0000	278	65	5.339	± 0.486	0.3293	± 0.0083	0.1176	± 0.0051	1875	± 81	1835	± 40	1920	± 166	98
LLZ994-4	0.0000	512	121	0.960	± 0.089	0.1100	± 0.0028	0.0632	± 0.0028	683	± 47	673	± 16	716	± 202	99
LLZ994-5	0.0007	271	113	0.953	± 0.092	0.1085	± 0.0029	0.0637	± 0.0029	679	± 49	664	± 17	732	± 209	98
LLZ994-6	0.0000	525	158	1.116	± 0.103	0.1193	± 0.0030	0.0679	± 0.0030	761	± 51	726	± 17	865	± 196	95
LLZ994-7	0.0000	84	74	2.398	± 0.236	0.2079	± 0.0059	0.0837	± 0.0039	1242	± 73	1217	± 32	1285	± 195	98
LLZ994-8	0.0000	184	85	0.996	± 0.098	0.1108	± 0.0031	0.0652	± 0.0031	702	± 51	678	± 18	781	± 213	97
LLZ994-9	0.0000	447	143	0.830	± 0.078	0.0955	± 0.0025	0.0630	± 0.0029	614	± 44	588	± 15	708	± 205	96
LLZ994-10	0.0000	234	217	2.424	± 0.225	0.2094	± 0.0054	0.0840	± 0.0037	1250	± 69	1225	± 29	1292	± 184	98
LLZ994-11	0.0000	6	5	4.017	± 4.817	0.3060	± 0.3499	0.0952	± 0.0172	1638	± 3271	1721	± 2011	1532	± 897	105
LLZ994-12	0.0000	13	3	1.500	± 1.799	0.1563	± 0.1787	0.0696	± 0.0126	931	± 1291	936	± 1082	918	± 1000	101
LLZ994-13	0.0000	23	5	1.559	± 1.870	0.1537	± 0.1758	0.0736	± 0.0132	954	± 1331	922	± 1066	1030	± 976	97
LLZ994-14	0.0000	34	5	1.320	± 1.583	0.1386	± 0.1585	0.0691	± 0.0124	855	± 1164	837	± 967	901	± 1000	98
LLZ994-15	0.0000	76	17	1.861	± 2.231	0.1834	± 0.2098	0.0736	± 0.0132	1068	± 1536	1086	± 1258	1030	± 974	102
LLZ994-16	0.0000	86	12	1.466	± 1.758	0.1527	± 0.1747	0.0696	± 0.0125	917	± 1266	916	± 1059	918	± 994	100
LLZ994-17	0.0000	22	5	1.497	± 1.795	0.1511	± 0.1727	0.0719	± 0.0129	929	± 1289	907	± 1048	983	± 985	98
LLZ994-18	0.0000	75	11	1.523	± 1.826	0.1597	± 0.1827	0.0692	± 0.0124	940	± 1306	955	± 1105	904	± 997	102
LLZ994-19	0.0000	422	148	6.509	± 0.223	0.3874	± 0.0057	0.1219	± 0.0019	2047	± 31	2111	± 26	1984	± 56	103
LLZ994-20	0.0000	396	751	4.765	± 0.165	0.3227	± 0.0047	0.1071	± 0.0017	1779	± 29	1803	± 23	1751	± 58	101
LLZ994-21	0.0000	298	500	6.880	± 0.237	0.3964	± 0.0058	0.1259	± 0.0020	2096	± 31	2152	± 27	2041	± 56	103
LLZ994-22	0.0000	188	72	6.748	± 0.237	0.3850	± 0.0058	0.1271	± 0.0020	2079	± 32	2100	± 27	2059	± 57	101
LLZ994-23	0.0000	466	191	3.872	± 0.134	0.2883	± 0.0042	0.0974	± 0.0015	1608	± 28	1633	± 21	1575	± 60	102
LLZ994-24	0.0000	220	105	0.770	± 0.033	0.0928	± 0.0015	0.0602	± 0.0012	580	± 19	572	± 9	610	± 87	99
LLZ994-25	0.0000	425	385	1.667	± 0.060	0.1592	± 0.0024	0.0760	± 0.0012	996	± 23	952	± 13	1094	± 67	96
LLZ994-26	0.0000	668	458	2.220	± 0.077	0.2045	± 0.0030	0.0787	± 0.0012	1187	± 25	1200	± 16	1165	± 64	101
LLZ994-27	0.0000	387	95	0.680	± 0.027	0.0882	± 0.0014	0.0559	± 0.0010	527	± 16	545	± 8	448	± 83	103
LLZ994-28	0.0000	423	431	12.027	± 0.408	0.5063	± 0.0074	0.1723	± 0.0026	2607	± 32	2641	± 32	2580	± 52	101
LLZ994-29	0.0000	267	173	12.529	± 1.546	0.4888	± 0.0563	0.1859	± 0.0041	2645	± 123	2565	± 248	2706	± 75	97
LLZ994-30	0.0000	337	68	1.016	± 0.127	0.1151	± 0.0133	0.0640	± 0.0015	712	± 66	702	± 77	743	± 103	99
LLZ994-31	0.0000	219	101	0.709	± 0.089	0.0896	± 0.0103	0.0574	± 0.0015	544	± 55	553	± 61	506	± 116	102
LLZ994-32	0.0000	104	88	1.697	± 0.214	0.1792	± 0.0207	0.0687	± 0.0017	1008	± 84	1063	± 114	889	± 108	105
LLZ994-33	0.0000	297	294	3.457	± 0.428	0.2605	± 0.0300	0.0962	± 0.0022	1518	± 102	1493	± 155	1553	± 87	98
LLZ994-34	0.0000	308	211	3.792	± 0.469	0.2845	± 0.0328	0.0967	± 0.0022	1591	± 105	1614	± 167	1561	± 87	101
LLZ994-35	0.0000	336	70	0.824	± 0.103	0.1002	± 0.0115	0.0596	± 0.0014	610	± 59	616	± 68	590	± 108	101
LLZ994-36	0.0000	753	9489	0.876	± 0.109	0.1038	± 0.0119	0.0612	± 0.0014	639	± 61	636	± 70	646	± 102	100
LLZ994-37	0.0000	49	40	7.331	± 0.915	0.4116	± 0.0475	0.1292	± 0.0031	2153	± 118	2222	± 221	2087	± 86	103
LLZ994-38	0.0000	530	187	0.764	± 0.060	0.1006	± 0.0018	0.0551	± 0.0021	576	± 35	618	± 11	415	± 179	107
LLZ994-39	0.0000	257	100	2.939	± 0.227	0.2479	± 0.0044	0.0860	± 0.0032	1392	± 60	1428	± 23	1337	± 153	103
LLZ994-40	0.0000	904	408	0.706	± 0.055	0.0889	± 0.0016	0.0576	± 0.0022	542	± 33	549	± 9	515	± 175	101
LLZ994-41	0.0000	640	531	0.677	± 0.053	0.0879	± 0.0016	0.0559	± 0.0021	525	± 32	543	± 9	447	± 178	103
LLZ994-42	0.0000	687	718	2.559	± 0.197	0.2245	± 0.0039	0.0827	± 0.0031	1289	± 58	1306	± 21	1262	± 154	101
LLZ994-43	0.0000	203	1664	1.493	± 0.118	0.1555	± 0.0029	0.0696	± 0.0027	927	± 49	932	± 16	917	± 166	100
LLZ994-44	0.0000	136	123	2.571	± 0.202	0.2268	± 0.0042	0.0822	± 0.0031	1293	± 59	1317	± 22	1251	± 157	102
LLZ994-45	0.0000	274	205	0.790	± 0.063	0.0982	± 0.0018	0.0584	± 0.0023	591	± 36	604	± 11	543	± 179	102
LLZ994-46	0.0000	226	66	15.617	± 1.197	0.5544	± 0.0097	0.2043	± 0.0076	2854	± 76	2843	± 40	2861	± 127	100
LLZ994-47	0.0000	126	68	1.041	± 0.085	0.1213	± 0.0024	0.0622	± 0.0025	724	± 43	738	± 14	681	± 179	102

Note: all errors are quoted at 2 s level
Concordance = [206Pb/238U age/ 206Pb/238U age]×100

Chapter 4. Geotectonic Evolution of England-Wales made by Pacific-type orogeny from Neoproterozoic to Cambrian

Abstract

British Isles have long been interpreted by evolution through twice of collision orogenies in the Early and Late Paleozoic. Here, I propose a tectonic history against the classic idea by Dewey (1969), alternatively a Pacific-type orogeny had contributed to British Isles more effectively than collision orogenies. First of all, England has grown through the Pacific-type orogeny, since 670 Ma to 500 Ma over 170 million years with three peaks of the culminations of episodic exhumation of regional metamorphic belts from mantle depth to the surface. Namely three sets of Pacific-type orogens are preserved in Wales to Anglesey Island.

The final collision of South Stack micro-continent underneath the hanging wall of Avalonia margin may had triggered to rift the margin to open the Rheic Ocean at 460-470 Ma (middle Ordovician period). Subduction of TTG crust of South Stack caused buoyant stacking under the leading edge of Gondwana margin (West Africa), and the slab-breakoff triggered the jack-up of the exhumed New Harbour Group at mid-crustal level by doming of all sandwiched units to the surface. During the collision-type subduction of South Stack micro-continent, apparent over-thrusting of deep-seated TTG and related high-grade unites under the volcanic front in Snowdonia occurred NW-ward over 100 km essentially due to the subduction of TTG materials. After the slab-breakoff, the jack-up events obliterated the overthrusting TTG crust to generate a huge scale of submarine landslide. This event has long been regarded to be

origin of mélange in this region, but this was caused by normal fault proposed here-in.

In spite of the extensive tectonic modification of orogenic belts in front of leading edge of continental lithosphere at the end of orogenic growth of England, the predominant crust-forming process of major parts of England was Pacific-type orogeny which had grown 200-300 km wide in major portion of England. The British island has been grown through 3-4 times Pacific-type orogeny and 1 collision-type orogeny. The second continents were accumulated by the subduction beneath the Iapetus Ocean, which was attributed to spread the Atlantic Ocean in the Jurassic.

Keywords; Pacific-type vs collision-type, British Isles, orogeny, crustal growth, olistostrome

4-1 Introduction

British Isles has long contributed to provide basis of geology since its birth by Lyell back to 200 years ago. Immediate after plate tectonics was introduced in 1968, Dewey (1969) and Dewey and Bird (1970) speculated a geotectonic evolution of the British Isles by plate tectonics. They proposed two times of continent collision orogeny, the first was Paleozoic continent collision by Laurentia (North America) against Baltica and the second was Late Paleozoic collision of North America against Africa (Fig. 4-1). Since then, several changes of speculation were proposed for the geotectonic history model such as Laurentia collision against intra-oceanic island arc (e.g., Oliver, 2001), and terrane accretion model was also applied by Gibbons (1989).

Accretionary complex model has been introduced first by Leggett et al. (1979, 1987) for the Southern Upland terrane, and later by Ogawa (1998). Nevertheless, this idea has not been well accepted, since neither mafic-ultramafic rocks nor cherts are

present, instead, highly disrupted turbiditic sedimentary rocks are present with graptolite fossils. Therefore, their speculative interpretation has not been well established. To discuss accretionary complex model, they must recognize the ocean plate stratigraphy (OPS), including MOR greenstone and associated bedded chert overlain by hemipelagite and turbidite. These are exposed along the western coast of Scotland near Ballantrae. Previous workers have separated radiolarians from bedded cherts to constrain the depositional age (Malets, 2004). Such work has been done later by Sawaki et al. (2010), who have reconstructed OPSs by detailed geological mapping. In addition, they suggested repetition of the OPS by using zircon U-Pb dating for the interlayered acidic tuffs within the cherts, which is a characteristic of accretionary complex.

Another memorial work was one of the oldest world classic areas of blueschist belt in Anglesey Island as well as Ballantrae complex in Scotland (Kawai et al., 2007). They have speculated that the blueschist belts were formed by simply strike-slip tectonic juxtaposition originally created by shearing at low-pressure condition. Previous workers have never considered that this high-grade metamorphic rock is index-rock of a subduction zone. Kawai et al. (2007), based on detailed sampling of rocks, defined two mineral isograds on the map, and clarified blueschist and epidote-amphibolite facies rocks. Judging from themobaric structure within the blueschist belt and the structural relationship, they have proposed sense of subduction polarity from NW to SE, and exhumed SE to NW at *ca.* 560 Ma.

In this paper, I speculate the geotectonic evolution of Anglesey-Wales and emphasize the role of Pacific-type orogeny, rather than collision-type orogeny, based on the result newly obtained by this study.

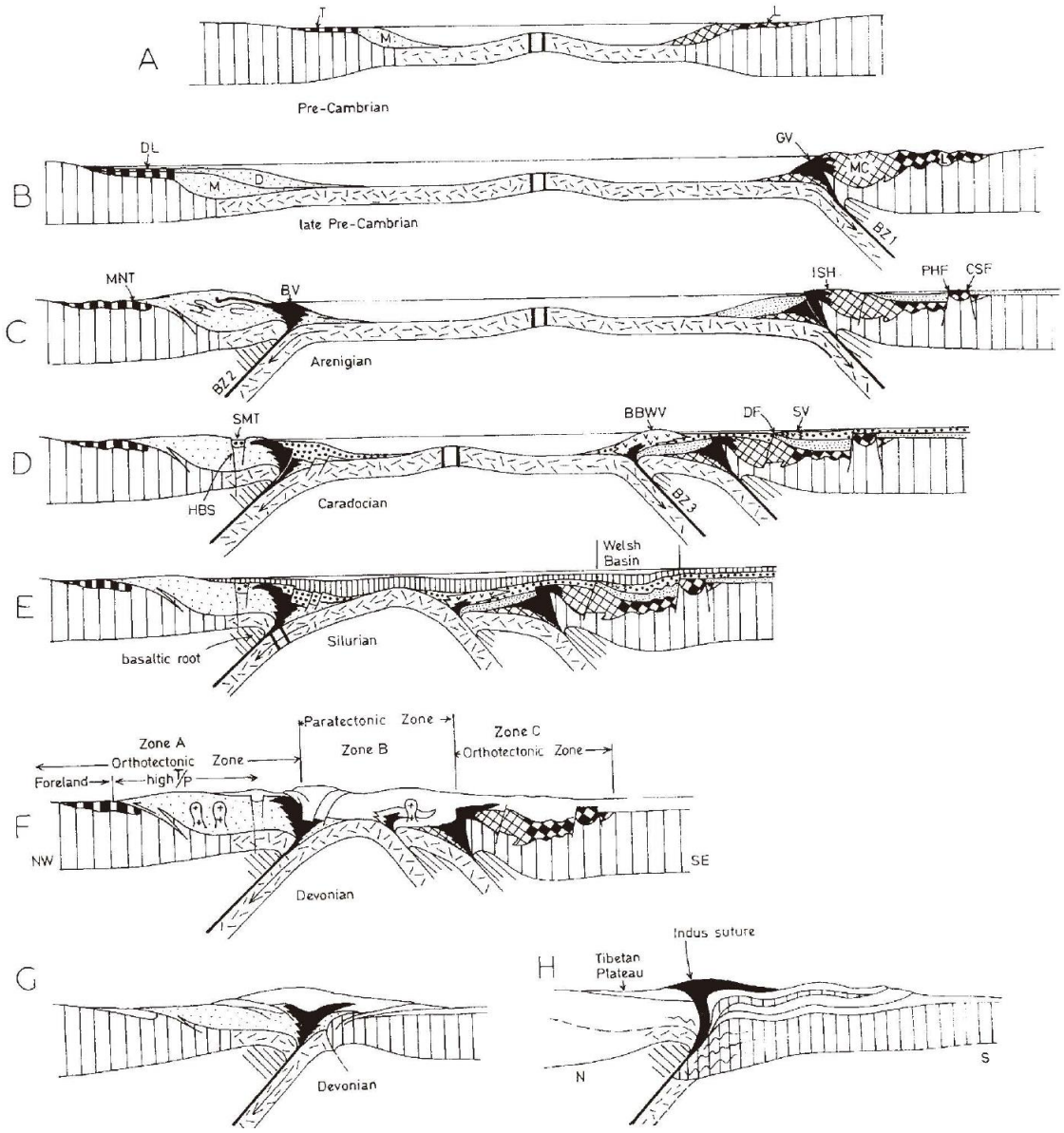

Figure 4-1. A model for geotectonic history of British Isles, proposed by Dewey (1969).

4-2 Recognition of Pacific-type orogeny in Anglesey Island to Lleyn peninsula, England-Wales

The Avalonia micro-continent was formed by the late Proterozoic to Ordovician Pacific-type accretionary orogen (Kawai et al., 2007). A 680-450 Ma calc-alkaline igneous belt extends southeastwards from the 560-550 Ma blueschist belt in Anglesey

via northern Wales to central England (Fig. 4-2; Dallmeyer and Gibbons, 1987; Tucker and Pharaoh, 1991; Noble et al., 1993; Horák et al., 1996; Compston et al., 2002). This structure suggests that the subduction polarity of oceanic lithosphere was southeastward (Kawai et al., 2007). The bottom of the blueschist belt is exposed on the southwestern Lleyn Peninsula, where an unmetamorphosed accretionary complex rests on the blueschist belt by low angle fault (see chapter 2 for details). The accretionary complex composed of repeated ocean plate stratigraphies as mentioned in chapter 2.

The members of our group proposed successive geotectonic development of this area as following (Kawai et al. 2007). (A) Formation of ocean plate stratigraphy from ridge to trench, (B) Formation of an accretionary complex in the Avalonia continental margin (Gwna Group), (C) Formation of an olistostrome-type accretionary complex, (D) Subduction of accreted material into mantle depths induced blueschist-epidote amphibolite facies metamorphism, and subsequent exhumation to an upper crustal level, (E) Doming and related extensional brittle faulting. Throughout these stages (B~E), calc-alkaline volcanic arcs were formed during 680-450 Ma.

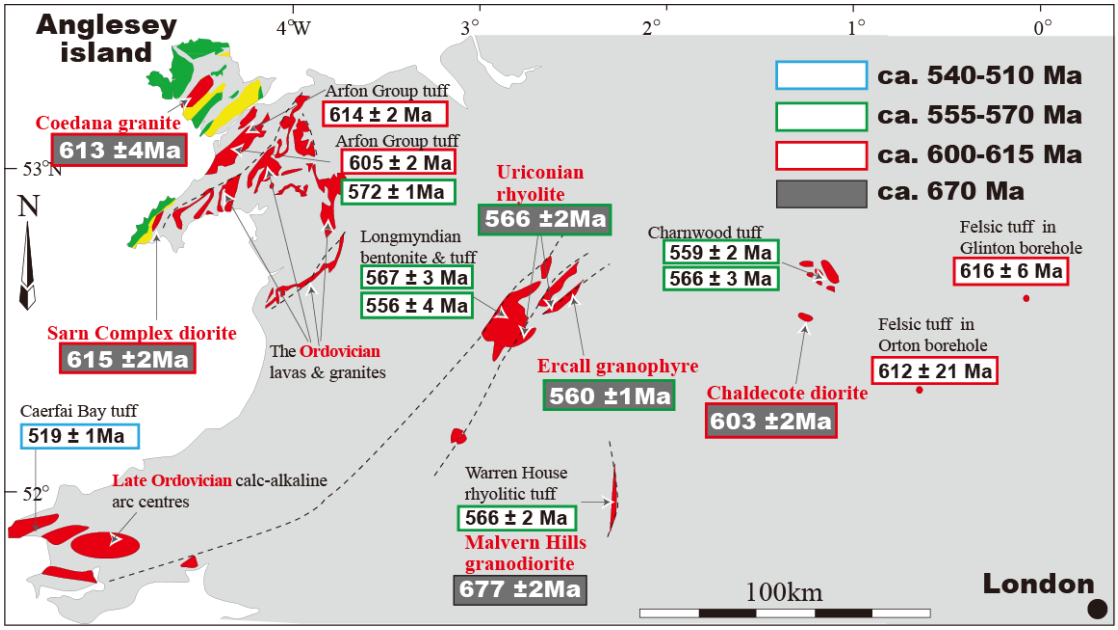

Figure 4-2. Simplified map showing the distribution of felsic igneous rocks (Dallmeyer and Gibbons, 1987; Tucker and Pharaoh, 1991; Noble et al., 1993; Horák et al., 1996; Compston et al., 2002).

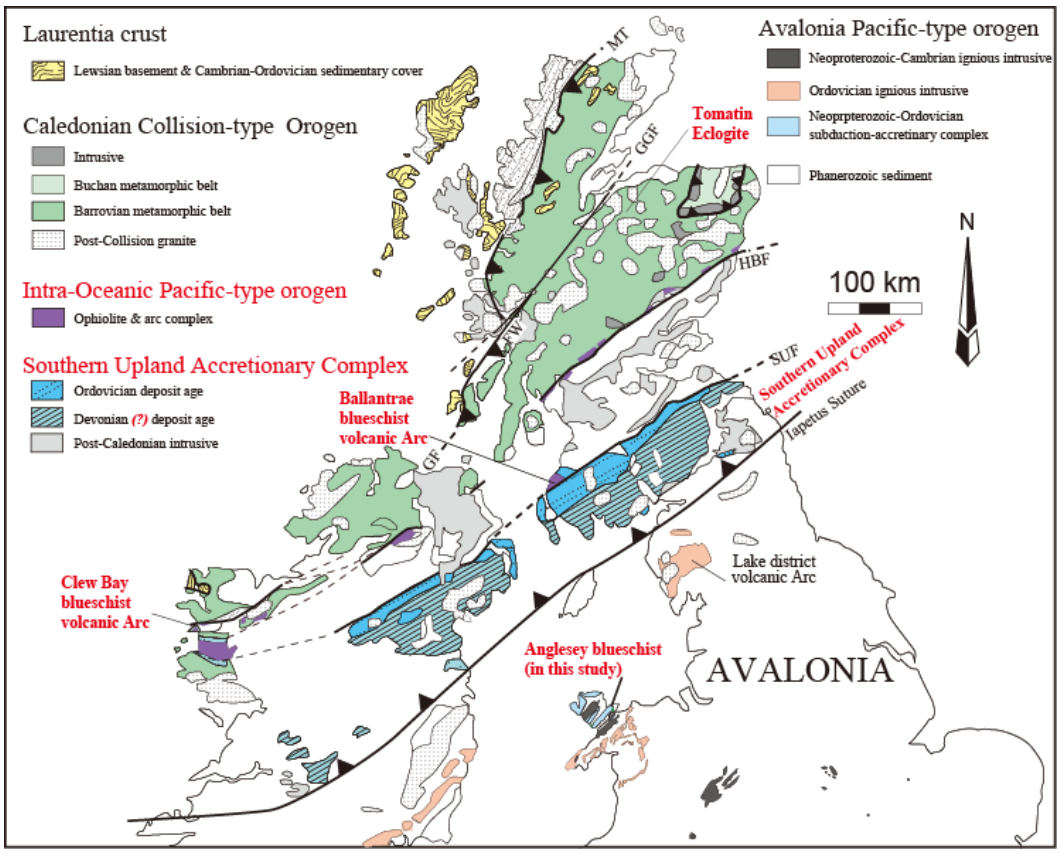

Figure 4-3. A simplified geological map of British Isles (modified after Dewey, 1969; Kawai et al., 2008)

4-3 Pacific-type Orogeny through time

4-3-1 Pacific-type orogeny in British Islands

An orogenic belt consists of 4 fundamental components: ophiolite, regional metamorphic belt, accretionary complex and fore-arc basin, respectively. To put it other way, the number of these belts indicate the number of subduction events and oceanic plates. High pressure metamorphic rocks in British Islands are exposed as eclogite in Tomatin and as blueschist in Anglesey, Ballantrae and Clew Bay (Fig. 4-3; Gray and Yardley, 1979; Kawai et al., 2007). In addition, many accretionary complexes are assigned in Anglesey (this study), Ballantrae (Sawaki et al., 2010) and Southern Upland (Leggett et al., 1979). Fragment of ophiolite also crops out in zone between Highland Boundary Fault and Southern Uplands Fault (Fig. 4-3). These remnants of orogenic belt indicate that the British Islands has been formed by several times of Pacific-type orogenies. Their metamorphic age ranges from *ca.* 900 Ma to 400 Ma.

4-3-2 Crustal growth of British Islands by Pacific-type orogeny

Contributions of a Pacific-type orogeny to a TTG batholith belt (677 Ma - 519 Ma) in England and Wales have never been considered for a long time. One of the reasons is that the TTG batholith belt is mostly covered by Phanerozoic sediments. On the other hand, the recognition of continent-continent collision orogen such as Himalaya and Alps is also remarkable. Specifically, the Alps has been centered in Europe, and the recognition of Caledonides and Hecynides were main components in Europe.

Fig. 4-2 shows distributions of felsic igneous rocks and their igneous ages in England and Wales. These rocks outcrop on 300 km × 500 km area southeast of the Anglesey island and Llyen peninsula. The ages had been reported by previous work

based on a zircon U-Pb analysis and range from 677 Ma to 519 Ma (Dallmeyer and Gibbons, 1987; Tucker and Pharaoh, 1991; Noble et al., 1993; Horák et al., 1996; Compston et al., 2002). When considering the genesis, it is suggested by previous works that these igneous belts were formed by a subduction of an oceanic plate into a mantle in the Neoproterozoic to the Cambrian (Thorpe, 1972; Thorpe et al., 1984; Kawai et al., 2007).

Calc-alkaline igneous rock outcrops in three areas in England and Wales. Firstly, the Malvern Complex mainly comprises calc-alkaline granodiorite, diorite, tonalite and granite (Thorpe et al., 1984), and has a U-Pb zircon age of 677 ± 2 Ma. Secondly, the Sarn Igneous Complex in the Lleyn Peninsula consists of calc-alkaline monzogranite, gabbro, granodiorite, diorite, and tonalite and has a $^{207}Pb/^{206}Pb$ zircon age of 615 ± 2 Ma (Gibbons and Horak, 1996; Horak et al., 1996). Thirdly, a rhyolitic tuff occurring within a calc-alkaline tholeiitic basalt-andesite-rhyolite association in the Warren House volcanic group (Thorpe et al., 1984) has a U-Pb zircon age of 566 ± 2 Ma in the Malvern Hills (Tucker and Pharaoh, 1991). These calc-alkaline igneous rock support that there had been the subduction of slabs, which corresponds to a series of events that the Iapetus ocean closed between these ages.

A polarity of the subduction was suggested to be southeastward (Kawai et al., 2007). Kawai et al. (2007) proposed that an exhumation of the blueschist belt was caused by the southwestward subduction of an oceanic plate, in a consideration of positional relationship between a TTG batholith belt and the BS belt and a gradation of the metamorphic grade in Anglesey blueschist Unit. In addition, formational ages of OPSs discussed in a chapter 2 strongly support the southeastward polarity of the subduction. The formation ages of OPSs become older southeastward or structurally

upward, which suggested that the polarity of the subduction was southeastward (see chapters 2 and 3). This is consistent with the locations and geneses of the TTG belt and blueschist belt. Therefore, the TTG belt was formed by a series of the southwestward ocean-plate subduction, accompanied by the exhumation of the blueschist belt and the accretionary orogeny.

4-3-3 Comparison to Japanese Islands

Japan Islands has been grown through 4-5 times of Pacific-type orogeny. The Ocean Drilling Program which started drilling of extant ocean floor in 1966 has now completed more than 2000 drill sites in the world's oceans. The OPS of the Pacific Ocean has been well established by this Program.

The world's largest segment of oceanic lithosphere, the Pacific plate, was born at the ridge of the East Pacific Rise, which is not yet covered by deep-sea sediments, because it is so young. In open ocean, deep-sea sedimentation proceeds very slowly by the deposition of 'marine snow' (plankton) formed near the surface of the sea by photosynthesis at a speed of a few mm per 1000 years. The measured thickness of pelagic sediment reaches 1200 m on *ca.* 60 Ma oceanic crust in the mid-Pacific, and finally it reaches 2000 m thick off the Mariana trench. The pelagic clay, which is originated from aeolian dust and organic matter, accumulates on the seafloor at a rate depending on biological activity and the production rate of the aeolian dust. The average sedimentation rate is a few m/million years.

In Japan trench-forearc accretionary wedges are commonly capped by crustal-derived clastics that are interbedded with arc-derived, mafic or even siliceous volcani-clastic sediments. On Anglesey-Lleyn, very comparable trench-fill clastic

turbiditic sediments are commonly interbedded with mafic mudstones that probably formed as mafic volcaniclastic sediments derived from nearby arc volcanoes, and were later transformed into chlorite schists during accretion.

Red bedded chert is up to 10 m thick in SW Lleyn Peninsula. This suggests that the subducted plate was as old as a few Ma, to < 10 Ma, although the thickness of bedded chert may be difficult to be assessed due to folding and layer-parallel faulting.

The OPS of the Gwna Group on Anglesey is characterized by a ridge-trench transition either with mafic mudstone as a cap sediment or with continental-derived sandstone-conglomerate as a cap turbidite that commonly contains beds of arc-derived volcaniclastic mafic sediments, suggesting that the sedimentological environment was similar to that of the present-day western Pacific.

4-4 Discussion

4-4-1 Paleogeographic Reconstruction

The early Cambrian faunal province has long been one of hot topics in paleontology right after when plate tectonics appeared, because continental dispersion and subsequent collision-amalgamation explains well those faunal and floristic provinces (Santosh et al., in press). The Cambrian trilobites in England are quite different from those of Euroamerica Group, suggesting that England was not a part of Laurentia and Baltica (Cocks and Torsvik, 2002). Based on the trilobite faunal province together with paleo-magnetic constraints, the Avalonia was a part of Western African craton, and rifted away from there sometime after the Cambrian. If so, the new ocean between Avalonia and West Africa must have been born. The Ocean was named as Rheic Ocean (Fig. 4-4). The southern side of Avalonia micro continent was created by

the Variscan orogeny. The Variscan orogen was formed by the closure of Rheic ocean (Matte, 2001).

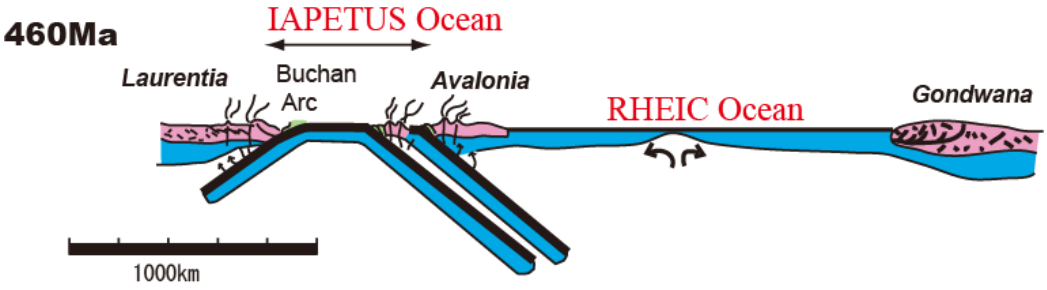

Figure 4-4. Simplified cross sections along a NW-SE profile across the British island.

The ancient position of the Avalonia micro continent is still debated by the previous workers. Palaeomagnetic data indicate that the Avalonia was in the ocean between Laurentia and Gondwana (Trench and Torsvik, 1991; Torsvik et al., 1993; Van der Voo, 1993). In the Cambrian, the Avalonia had positioned around the Gondwana supercontinent (Fig. 4-5). During the Ordovician, the Avalonia had approached to the Baltica and Laurentia, and gap between the Avalonia and Gondwana became wider (Fortey and Cocks, 2003; Nance and Linnemann, 2008). In 460 Ma, the Avalonia had occurred at -2000 km south of Laurentia and -2100 km north of Gondwana continent (Mac Niocaill and Smethrust, 1994; Cocks and Torsvik, 2002; Hamilton and Murphy, 2004). However, many problems remain about the origins of Avalonia and Rheic Ocean: (1) Which continents did connect with the Avalonia, Amazonia or Western Africa? (2) Where was the rifted margin? (3) Where was the final suture? (4) When was Avalonia rifted? (5) What was the mechanism of the Rheic ocean separation? In this section, we will access the problem No. 1 and 4 using zircon U-Pb dating and age spectrum of detrital zircons.

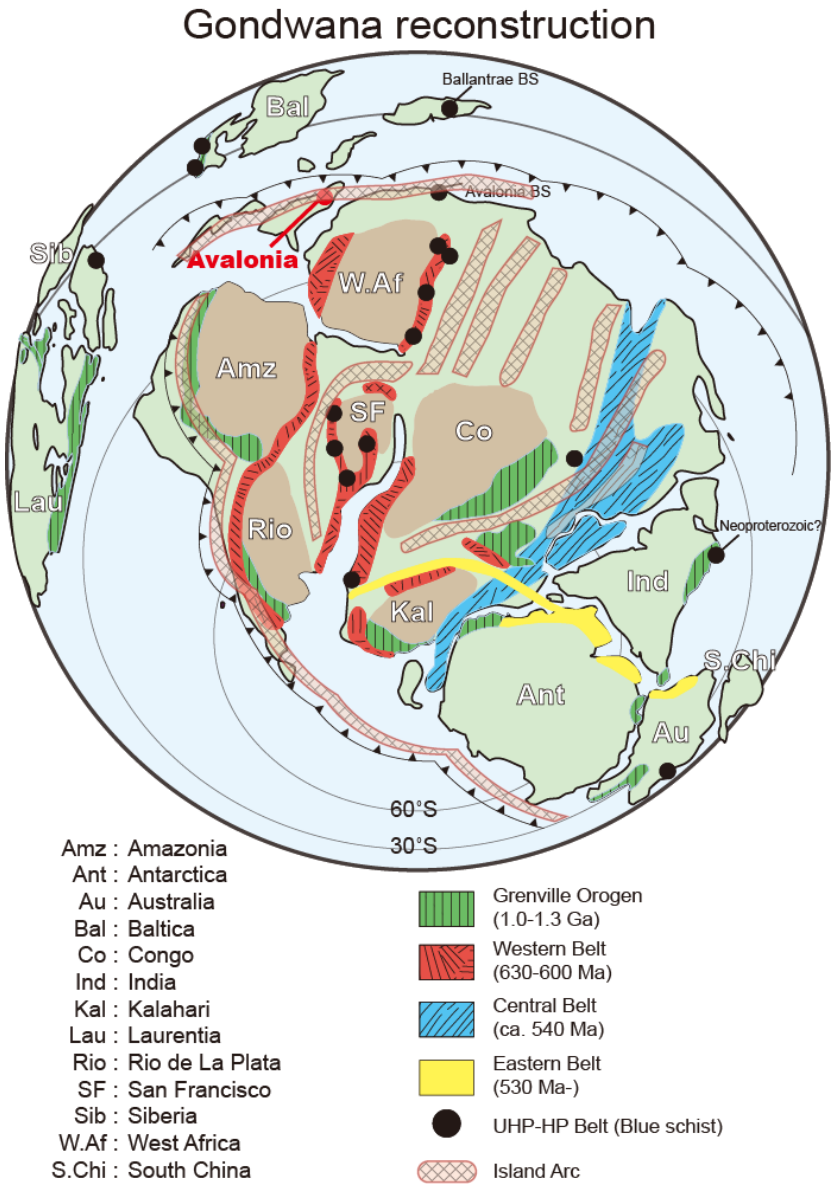

Figure 4-5. Paleogeographic reconstruction of Gondwana at 540 Ma.

An age spectrum of detrital zircon from a sandstone can provide information about ancient provenance. A comparison of the age population of zircons in sandstones with the age distribution of the basement rocks (Fig. 4-6) constrains the hinterland of the Avalonia. Both Amazonia and Western Africa consist of Neoproterozoic and

Paleoproterozoic basement rocks. The candidate of the Neoproterozoic (*ca.* 1000-1600 Ma) population is Amazonia, on the other hand the prominent peak at 1900 Ma is only originated from Western African continent. In addition, Archean zircons older than 2700 Ma are only discovered from Western African continent. Although fossil zonal distribution indicates proximity of Avalonia to the Western Africa, the age frequency distribution of detrital zircons suggest that the Avalonia had been situated between Amazonia and Western Africa continents. Similar position of the Avalonia was also suggested by the age distribution of detrital zircons in the Cadomia (Fig. 4-7; Fernández-Suárez et al., 2002).

It has been traditionally considered that the Iapetus and Rheic oceans began to open in the Ediacaran and the Ordovician, respectively. However, the youngest ages of detrital zircons and the eruption age of the tuff in this study demonstrate that the Gwna Group consists of the earliest Ediacaran sediments. This implies that the birth of Iapetus ocean goes back in the time of the Cryogenian. All collected rock samples in this study were deposited in the Iapetus ocean, not in the Rheic ocean. Therefore, we will estimate the age of birth of the Rheic ocean based on the change of provenance. Age spectra of detrital zircons in the Cambrian sediment lack zircons older than the Cryogenian. In sum, the Avalonia was separated from the Amazonia and Western Africa in the Cambrian, and then began to approach toward the Laurentia.

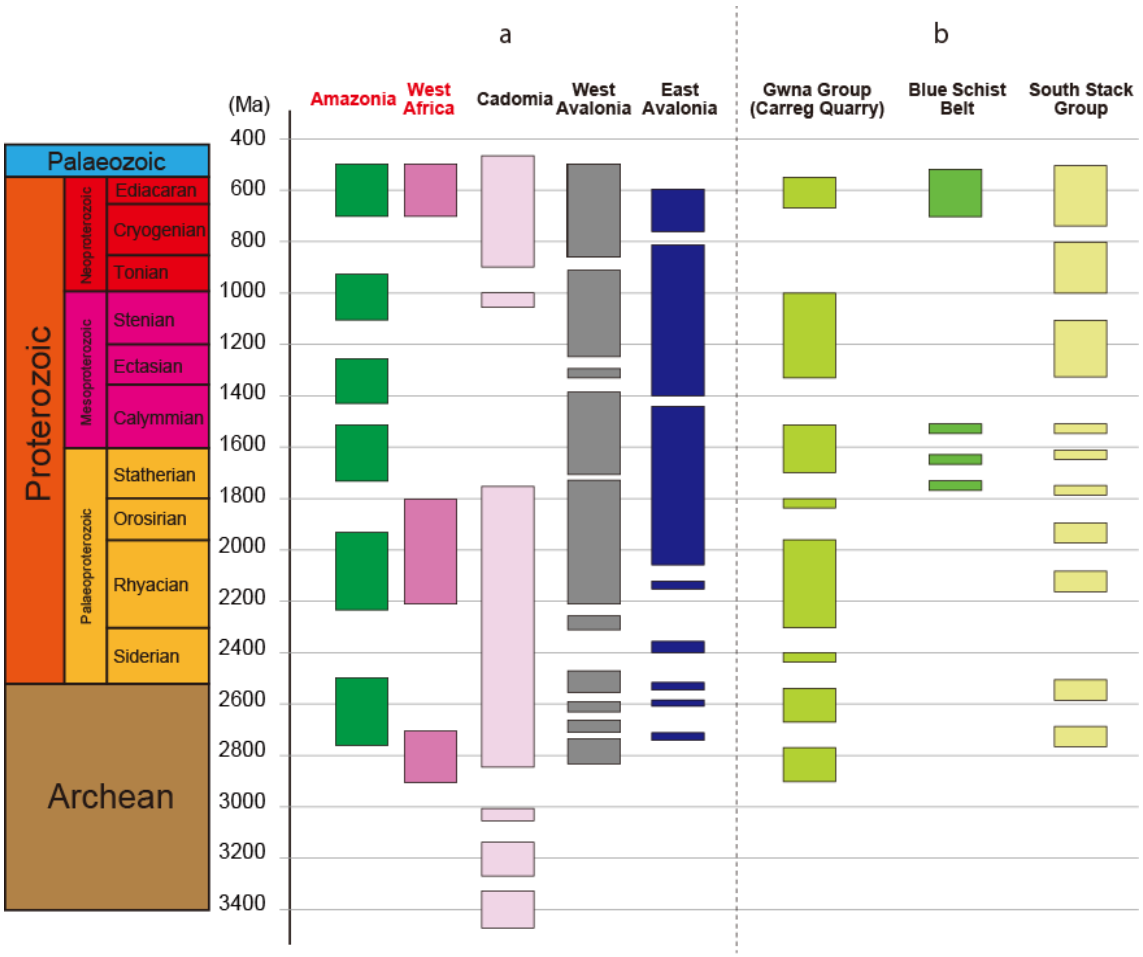

Figure 4-6. Areal distribution of the basement rocks of individual continents (modified after Collins and Buchan (2004) and Ustaomer et al. (2011)).

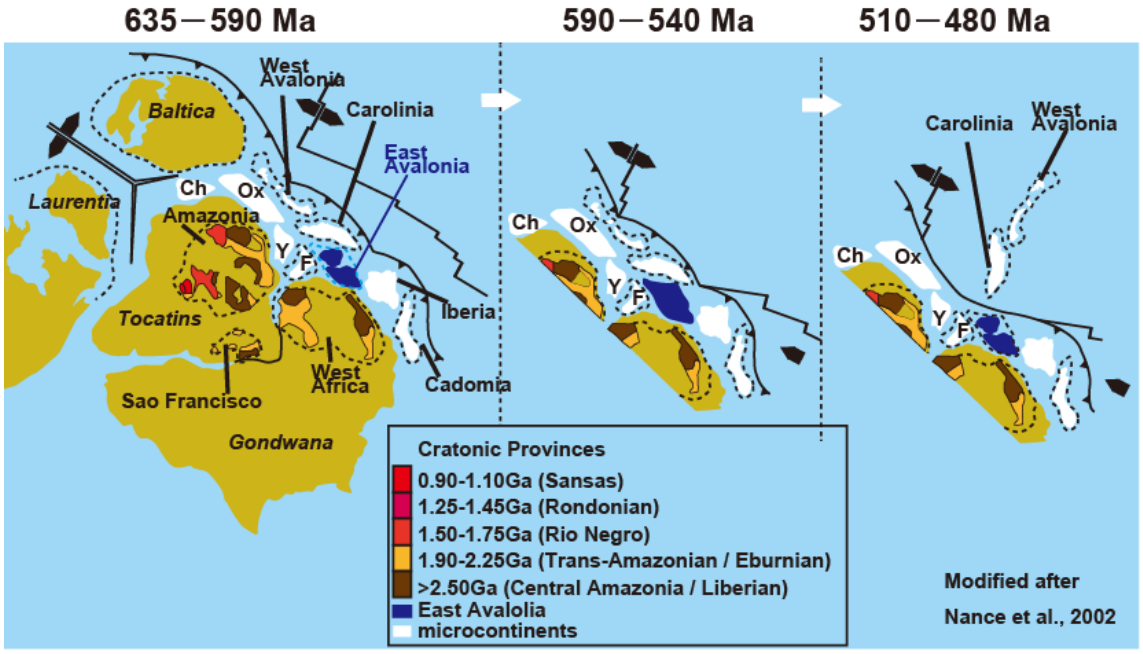

Figure 4-7. Simplified geographic map showing the ancient position of the Avalonia (modified after Nance et al., 2002).

4-4-2 When Iapetus Ocean was born?

Birth of Iapetus Ocean has long been debated without any rigid geological evidences. The originally Dewey (1972) proposed it was born in Cambrian and later modified by Van Staal et al. (1998). The discovery of the Gwna Group ACs, back to 630 Ma clearly demonstrates that Iapetus must have been already present back to Ediacaran period, 90 m.y. older than the onset of Cambrian.

Moreover the oldest CA plutonism 677 Ma has been reported on Malvern Hills which is located 200 km NE side from the assumed trench. These TTG rocks can be formed only by subduction of oceanic lithosphere. This strongly constraint the presence of ocean, i.e., back to 677 Ma. By these reasons, the author point out the Iapetus Ocean must have been present back to 677 Ma.

4-3 Birth of Rheic Ocean

Previous worker reported the Rheic Ocean opened around 480 Ma, Early Ordvician (e.g. Cock et al., 2002; Nance et al., 2004). Provenance site of sedimentary clastics, however, never support the idea of 480Ma. Instead, the onset of Cambrian age at 540 Ma is proposed in this thesis (Chapter 3). The Gwna ACs deposited at 630–570 Ma (Type 1 and 2), as typically documented, contains age-frequency peak at 570-610Ma trench turbidites 1800-2000 Ma peaks with subordinate peaks at 2600Ma, 2300Ma, 1200-1500Ma. But it suddenly changed after 545Ma, since which rare Precambrian detrital zircons were transported from West African craton (Type 3 and New Harbour Group). This strongly suggests the rifting of Avalonia from West Africa craton, by the similar process of rifting of Miocene Japan from East Asia at ca. 20-15Ma. The Rheic Ocean was separated by opening of back-arc basin, and enlarged through time.

4-5 Summary

Whole scenario: Summary of geotectonic evolution of England-Wales

The British Isles and adjacent regions are composed of four units (Fig. 4-3): (1) Late Archean to Early Proterozoic basement rocks with Neoproterozoic cover sequence, (2) metamorphosed cover sequence deposited on the Laurentian passive continental margin from the Neoproterozoic to the Cambrian which was formed by Barrovian metamorphism and late-stage intrusion of Siluro-Devonian TTG plutons, (3) accretionary complex from the Ordovician to the Silurian, calc-alkaline volcanic sequence in Lake District, and Pacific-type orogenic belts exposed at Anglesey Island to England, (4) Lizard ultramafic ophiolitic unit exposed on the western end of England to mark the Variscan suture of Rheic ocean which corresponds to the site of collision of

Gondwana against Laurentia.

Recognition of accretionary complex in the Gwna Group strongly indicates the presence of Pacific-type orogeny (see Chapters 2 and 3). Here, I try to synthesize the orogenic development of England-Wales, by picking up two major components of orogeny, accretionary complexes formation and synchronous TTG formation (Fig. 4-2).

(1) Stage I (680 Ma): Initiation of Pacific-type orogeny

The oldest felsic plutonic rock was reported in Malvern Hills (Fig. 4-2; Thorpe et al., 1984). Igneous age of granodiorite from there is 677 ± 2 Ma and these rocks show a characteristic of calc-alkaline igneous rock. These evidences suggest that the Pacific-type orogeny had already initiated by 677 Ma (Fig. 4-8).

(2) Stage II (630-610 Ma): Formation of the oldest accretionary complex, Type 1 Gwna Group.

OPSs reconstructed in the Penrhyn Nefyn Peninsula, Porth Felen, Southwestern Coast and Mynydd Carreg had already accreted to a continental margin as a part of an accretionary complex ca. 610 Ma (Fig. 4-8). These OPSs are parts of the oldest accretionary complex, Type 1 Gwna, which is now structurally uppermost and crops out on the east side of the Gwna Group. While accretionary complexes had been formed from 630 Ma to 610 Ma, the series of the ocean-plate subduction is thought to have generated the TTG belt on the back-arc side of the trench at the time. A piece of the TTG belt is recognized as Coedana granite (613 ± 4 Ma), Arfon group (614 ± 2 Ma) and Sarn complex diorite (615 ± 2 Ma) on forearc side and Glinton tuff (616 ± 6 Ma), Orton tuff (612 ± 21 Ma), Chadecote diorite (603 ± 2 Ma) on back-arc side (Gibbons and Horak, 1996; Horak et al., 1996). From these evidences, Type 1 Gwna Group and these

plutonic rocks were formed by a series of Pacific-type orogeny.

(3) Stage III (600-570 Ma): Accretion of Type 2 Gwna Group

The depositional age of the Type 2 Gwna Group is slightly younger than both that of Type 1 Gwna Group and igneous age of above plutonic rocks (see Chapter 2). Accretion of Type 2 Gwna Group without any igneous events occurred at *ca.* 570 Ma (Fig. 4-8).

(4) Stage IV (Pacific-type Orogeny 1, *ca.* 560 Ma): Exhumation of Blueschist unit

The blueschist (BS) belt extends from the Anglesey to Llyen peninsula (Fig. 4-2). This was assigned as a regional metamorphic belt and was exhumed to the surface as a result of ridge subduction (Kawai et al., 2007). The formation age of oceanic crust is estimated to be *ca.* 590-580 Ma based on an $^{40}Ar/^{39}Ar$ mineral age of actinolite, whereas the age of peak metamorphism is thought to be *ca.* 560 Ma based on an $^{40}Ar/^{39}Ar$ mineral age of glaucophane (Dallmeyer and Gibbons, 1987). Many felsic igneous rocks exist on the England-Wales area (Fig. 4-2; Tucker and Pharaoh, 1991; Noble et al., 1993; Horák et al., 1996; Compston et al., 2002); Longmyndian bentonite and tuff (567 ± 3 Ma and 556 ± 4 Ma), Uniconian rhyolite (566 ± 2 Ma), Charnwood tuff (559 ± 2 Ma and 566 ± 3 Ma), Ercall granophyres (560 ± 1 Ma), Warren House rhyolitic tuff (566 ± 2 Ma) and Arfon Group tuff (572 ± 1 Ma). These lines of evidences indicate that the fore-arc region had turned to be active by intrusion of TTG and calc-alkaline volcanic rocks. The blueschist unit was exhumed by a ridge subduction (Fig. 4-8). This is the first Pacific-type orogeny in the Anglesey-Lleyn region.

(5) Stage V (540 Ma): Formation of Type 3 Gwna accretionary complexes

At stage **V**, Type 3 Gwna group was accreted at a toe of overriding plate at *ca.* 540 Ma (Fig. 4-8). In this period, a variety of ACs such as olistostrome-type ACs was formed (see Chapter 2). The already formed older ACs were gravitationally collapsed to accumulate on the trench, and subducted again along the Benioff thrust (decollment plane) to be a hanging wall ACs. At the different site, other types of ACs which dominated clastic-wedge were also formed.

Age spectra in detrital zircons separated from ACs indicate the change of provenance sites (see Chapters 2 and 3). Sediments in the type 3 Gwna Group lack zircons derived from old cratons, which suggests that Avalonia micro-continent (England) was divided from West African craton at *ca.* 540 Ma. If so, this corresponds to the timing of birth of Rheic ocean (Fig. 4-8).

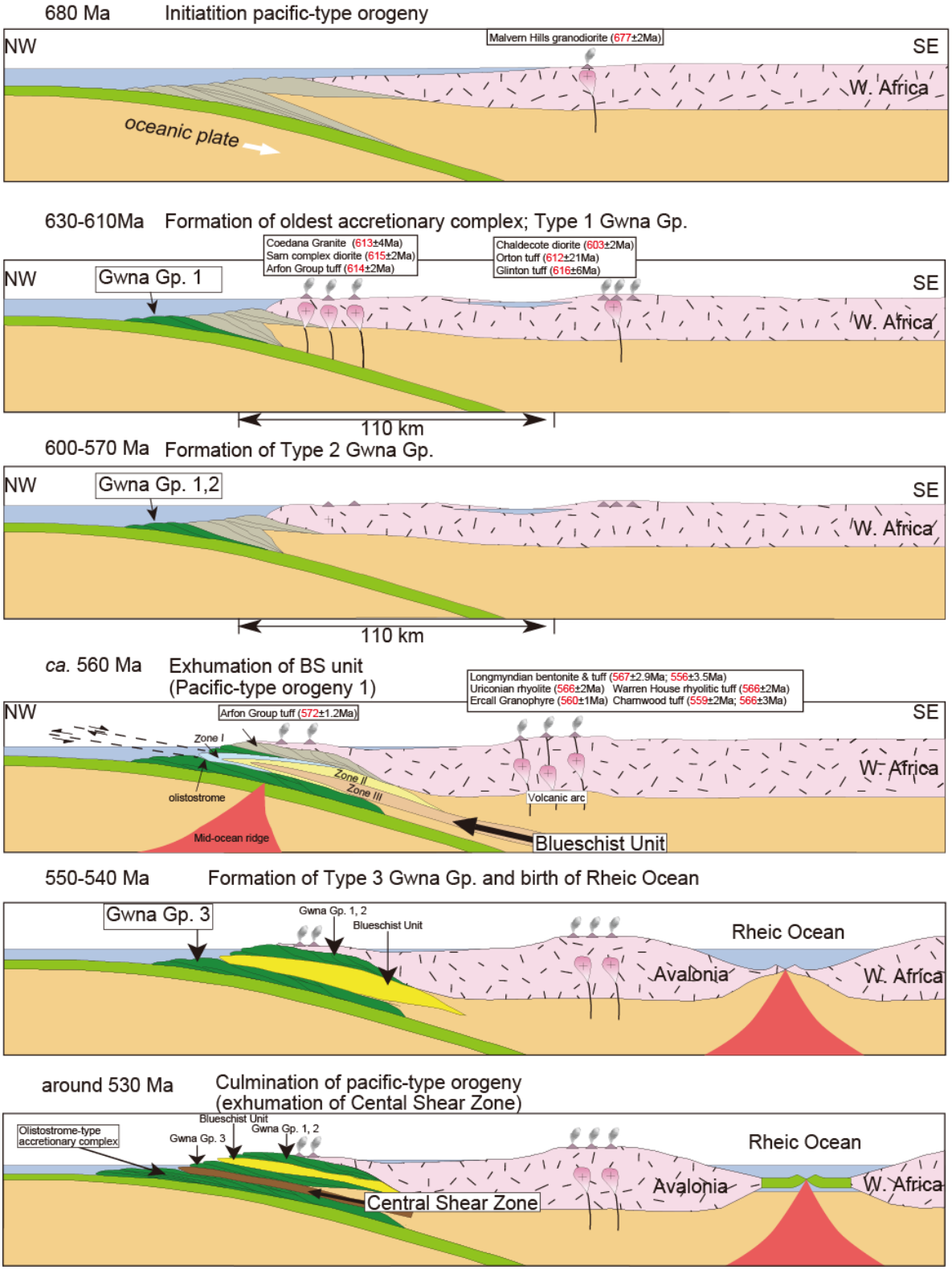

Figure 4-8. Simplified cross-sections along a NW–SE profile from Anglesey through Wales to Central England, to illustrate the geodynamic evolution of the active western margin of Avalonia during the late Neoproterozoic. See text for more details.

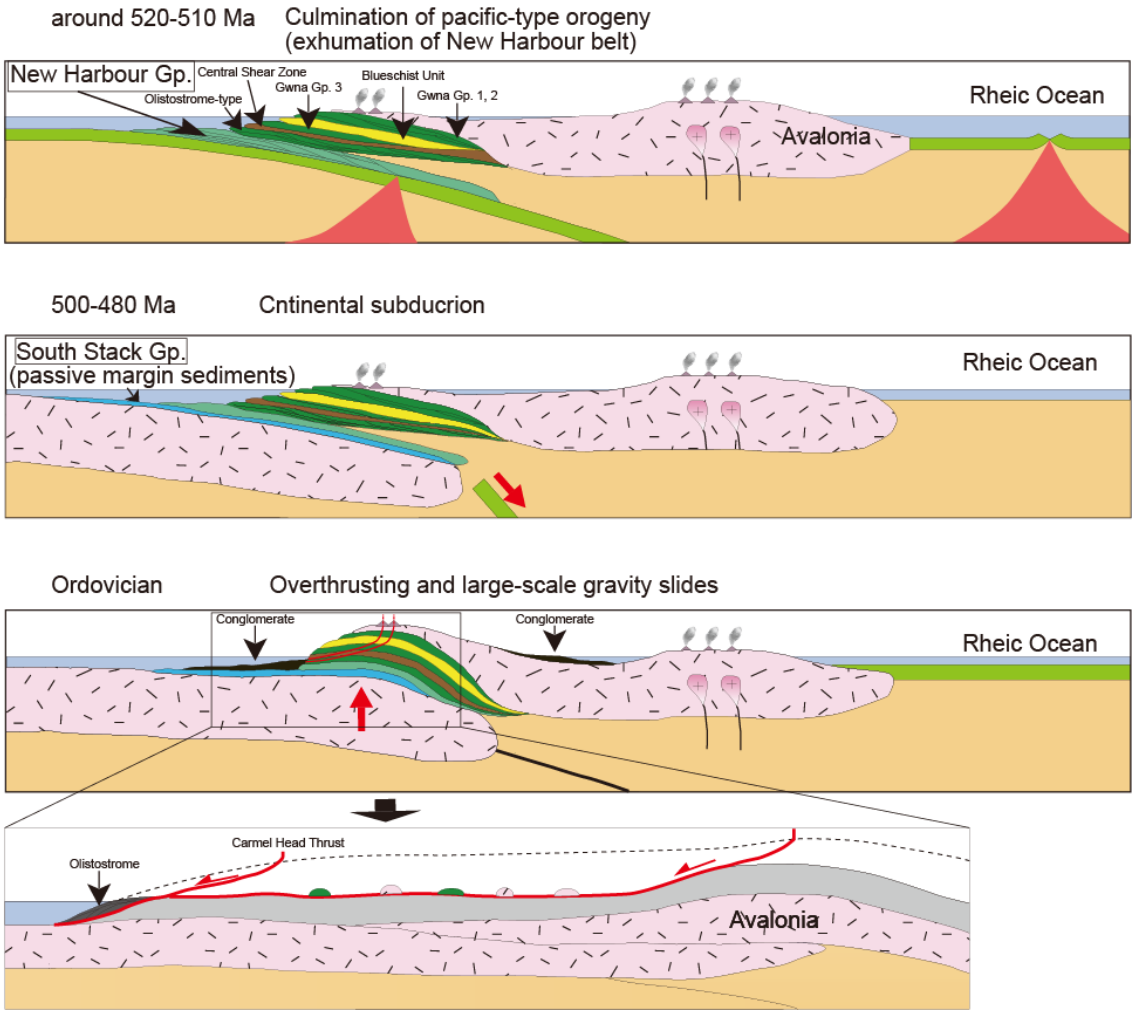

Figure 4-9. Simplified cross-sections along a NW–SE profile from Anglesey through Wales to Central England, to illustrate the geodynamic evolution of the active western margin of Avalonia from *ca.* 520–480 Ma. See text for more details.

(6) Stage VI (Pacific-type Orogeny 2, 530 Ma): Exhumation of regional metamorphic belt, now assigned as Central Shear Zone

At 530 Ma, the second Pacific-type orogeny started and the deep-subducted ACs were returned back to the surface (Fig. 4-9). If exhumation of the deep- subducted ACs is caused by change in subduction angle because of approaching mid-oceanic ridge (Maruyama et al., 1996), then the ridge subduction is necessary to exhume a accretionary complex (Fig. 4-9). Present position of two metamorphic belts seems to be

too close to assume the preceding Menai BS-EA belt exhumation at 560 Ma, and seems to be unrealistic. However, in the case of the Sanbagawa belt, Japan, the age of regional metamorphism was long believed to be early Cretaceous, but recently it was clarified that the so-called Sanbagawa belt is composed of two independent BS belt, one is the Cretaceous metamorphism at *ca.* 120-100 Ma (protolith age: 130 Ma), and the other is BS metamorphism at *ca.* 65 Ma (protolith age: *ca.* 80 Ma; Aoki et al., 2009). These two correspond to the ridge subductions by Izanagi-Kula followed by Kula-Pacific, where both of them are now closely spaced. Therefore, the case of Wales in the Neoproterozoic to early Paleozoic seems to be not abnormal.

(7) Stage VII (Pacific-type Orogeny 3, 520-510 Ma): Exhumation of regional metamorphic belt (New Harbour Schist)

This is the case of third Pacific-type orogeny, slightly after 530 Ma orogeny (Fig. 4-9). The peak metamorphic age must be close to the calc-alkaline volocanic event and is constrained by a Caefai Bay tuff (519 ± 1 Ma; Fig. 4-2) (Landing et al., 1998). This estimated age seems to be very close to metamorphism and ACs formed by second Pacific type orogeny. Although the details have not yet been clarified, short-time span could be a characteristic aspect of Iapetus Ocean. Such a short-time span looks too short as orogenic cycle. Like Western Pacific domain in the post-Miocene, Iapetus Ocean could be composed of many oceanic microplates, where numbers of plate boundaries were present. This suggests that more frequent ridge subductions may have prevailed.

Mantle convection depends on size of individual circle. If the double-layered mantle convection occurs, the size of plate must be in an order of 700 km across. Conversely, if the whole mantle convection occurs, the size of plate could be 2900 km

across and 9-10 major plates cover the whole Earth' surface. This is similar to the modern Earth. If plate motion around Japan is reconstructed, ridge subduction occurs every 100 million years for the last 200 Ma. This rate presumably indicates 5 times ridge subductions during the last 500 Ma, along the margin of South China craton. This calculation is inconsistent with short-time span of ridge subduction estimated from Anglesey-Lleyn unit. Therefore, double-layered mantle convection could be dominant below the Anglesey-Lleyn region.

The top- and bottom-boundaries of New Harbour Schist belt have not yet been identified. Moreover, the progressive nature of metamorphism has also not yet been clarified, as well as age of metamorphism. It should be noteworthy that the presence of ophiolite on the top of New Harbour Schist belt, and its chemistry suggests the origin of intra-oceanic ophiolite (Thorpe, 1973). Recognition of metamorphic belt, determination of peak metamorphic age and estimating P-T history are next keys for further understanding of the third Pacific-type orogeny.

(8) Stage VIII (Collision-type Orogeny at 520-490 Ma): South Stack Group

The final and important event was the collision-type orogeny by the subduction of buoyant micro-continent. The protoliths of South Stack Group are typical A-type (like shelf sediment; Maruyama et al., 1996), and age frequency pattern in detrital zircons is quite different from that of West African craton. Origin of the South Stack micro-continent presumably could be a part of Laurentian margin. The micro-continent had started to be subducted under the Northwestern margin of Avalonia at 500-490 Ma (Latest Cambrian; Fig. 4-9).

(9) Stage IX (Overthrusting and large-scale gravity slides): Formation of olistostrome in the Ordovician.

Subduction of buoyant micro-continent and underplating beneath the edge of Avalonia made thickness of continental crusts up to 60-70 km (twice the size of modern continental crust). This doming pushed up the Avalonian continental margin, which caused the huge-scale landslide to transport the TTG and associated high-grade gneiss together with Afron CA-volcano plutonic sequence, from Snowdonian mountain to the northern margin of Anglesey Island (lower panels in Fig. 4-9).

The duration from starting of subduction of buoyant micro-continent, through pushup the Snowdonian mountain range to landslide under the extensional stress regime could be from the Late Cambrian to the Ordovician. The toe of gravity slide could be branched to mix the Ordovician mudstone matrix. This is the olistostrome which is currently observed along the northern coast of Anglesey Island (see Chapter 3). Olistoliths changed from *ca.* 600-500 Ma TTG and associated high-grade metamorphic rocks, Gwna Group, platform carbonates with stromatolite structure, Arfon felsic volcanics. All of these also remain as klippes on the hill of Anglesey Island (see Chapter 3 for details).

(10) Stage X (Parys Mountain and Church Bay acidic volcanism

After the collision-type orogeny against the NW margin of Avalonia, Avalonia (England) was wandering in the Iapetus Ocean (Figs. 4-4and 4-5). On the other hand, a huge continent (North America) approached to Avalonia from the north. In between them, an oceanic lithosphere subducted both northward and southward as reducing the intervening ocean (Fig. 4-4). Mode of consuming plate system could be very similar to the modern Mollucca Sea plate in the south of Philippine arc. Approaching two arcs

finally collided, and the intervening ocean disappeared at some time *ca.* 450 Ma. The final annihilation of intermediate oceanic lithosphere triggered the next mantle upwelling as a spot and caused the caldera-bearing bimodal volcanism. A series of felsic volcano-plutonic sequence are seen in the Lake District in England, as well as equivalents in Ireland. Parys Mountain and Church Bay tuffs, which were formed during the closure of ocean, are all belong to these categories.

Following figures (Figs. 4-10 and 4-11) also show the tectonic history of the Anglesey and Lleyn region, including Laurentian margin and mid oceanic ridges.

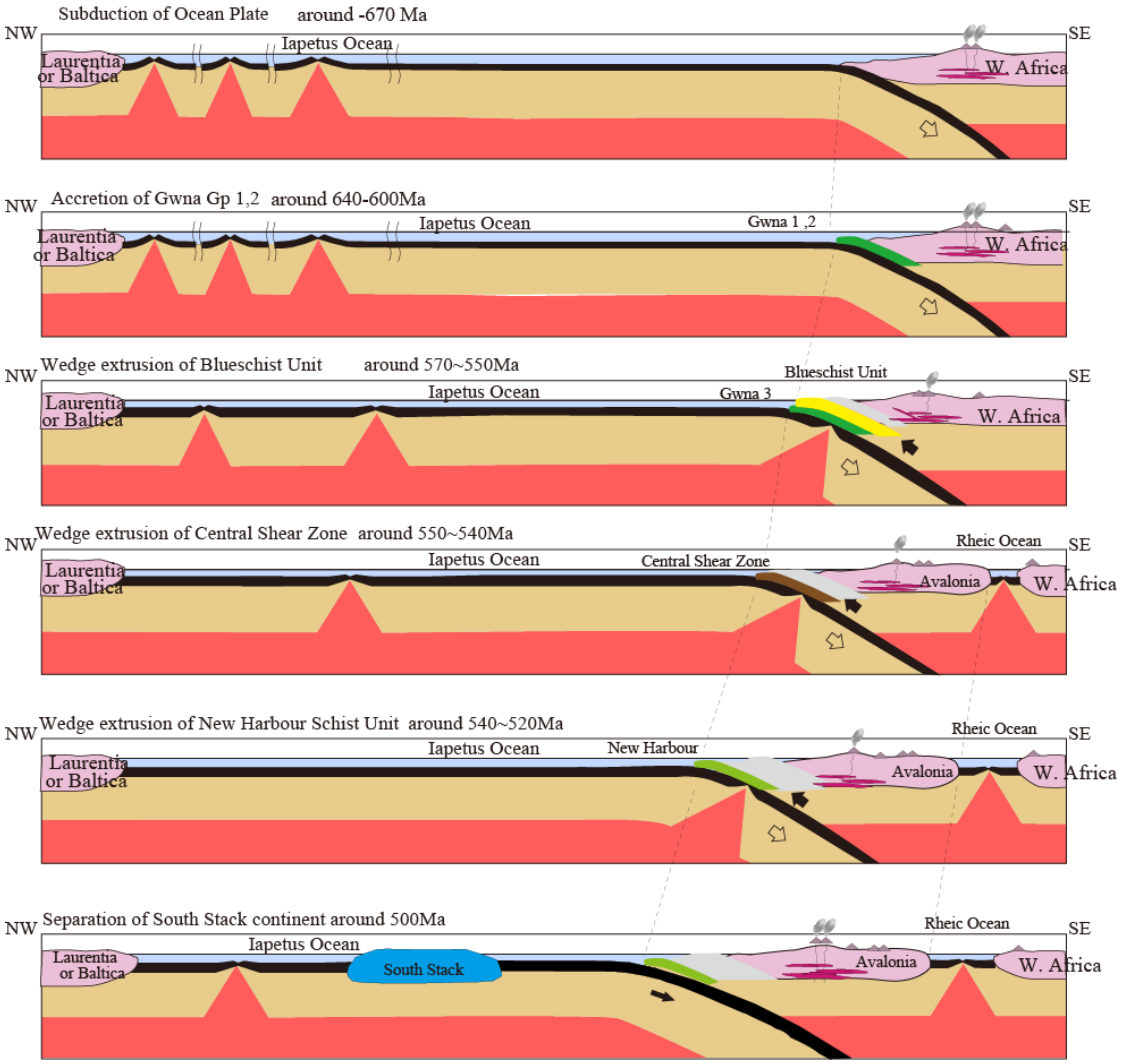

Figure 4-10. A model of geotectonic evolution of British Isles, from 677 Ma to *ca.* 480 Ma. A schematic illustration along a profile of NW-SE direction.

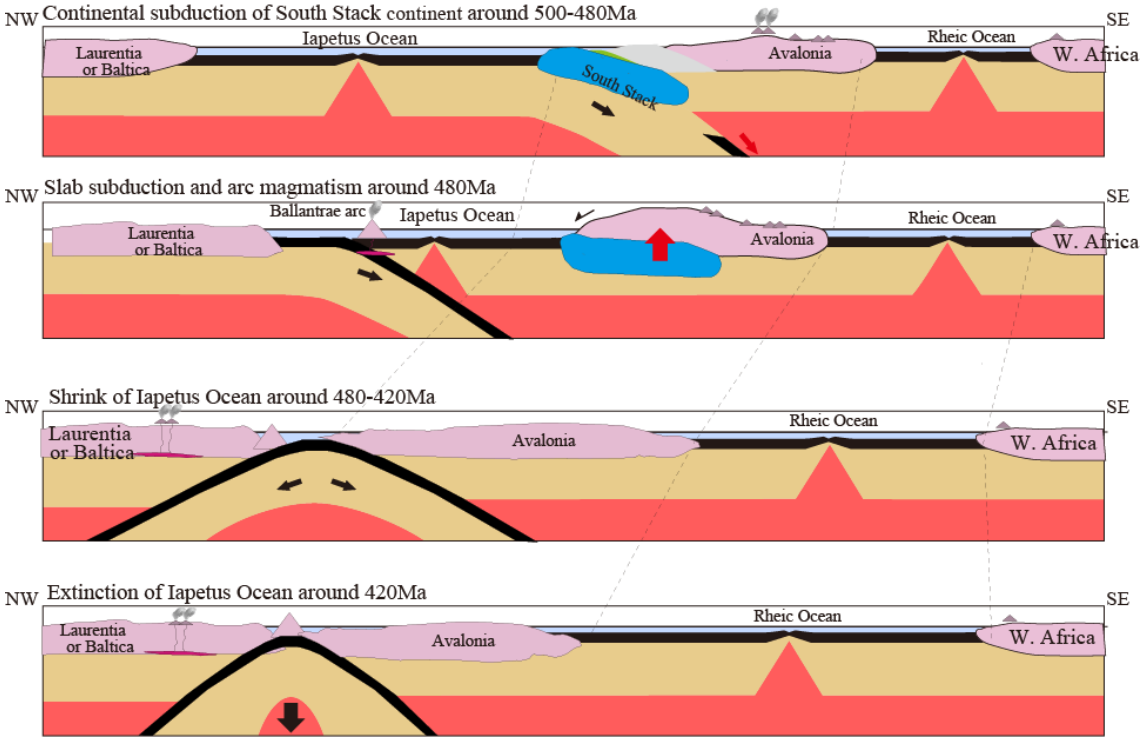

Figure 4-11. Continued form Fig. 4-4. The final consumption of Iapetus ocean at 420 Ma through the passive collision of two continents, laurntia against Avalonia. Rheic Ocean was born at 560 Ma (see above figure), and enlarged until 420 Ma.

Referecnces

Cocks, L. R. M., Torsvik, T. H., 2002. Earth geography from 500 to 400 million years ago: a faunal and palaeomagnetic review. Journal of Geological Society, London, 159, 631-644.

Collins, A. S., Buchan, C., 2004. Provenance and age constraints of the South Stack Group, Anglesey, UK: U-Pb SIMS detrital zircon data. Journal of Geological Society, London, 161, 743-746.

Compston, W., Wright, A. E., and Toghill, P., 2002. Dating the Late Precambrian volcanicity of England and Wales. Journal of the Geological Society, 159, 323-339.

Dallmeyer, R.D., Gibbons, W. 1987. The age of blueschist metamorphism on Anglesey, North Wales: evidence from 40Ar/39Ar mineral dates of the Penmynydd schists. Journal of the Geological Society, London, 144, 843-850.

Dewey, J.F. 1969. Evolution of the Appalachian/Caledonian Orogen. Nature, 222, 124-129.

Dewey, J., F., Bird, J.M. 1970. Mountain belts and new global tectonics. Journal of Geophysical Research, 75, 2625-2647.

Dewey, J.F., 1982, Plate tectonics and the evolution of British Isles. Journal of Geological Society of London, 139, 317-414.

Fernández-Suárez, J., Gutiérrez-Alonso, G., and Jeffries, T. E., 2002. The importance of

along-margin terrane transport in northern Gondwana: Insights from detrital zircon parentage in eoproterozoic rocks from Iberia and Brittany. Earth and Planetary Science Letters, 204, 75-88.

Fortey, R. A., Cocks, L. R. M., 2003. Palaeontological evidence bearing on global Ordovician-Silurian continental reconstructions. Earth Science Reviews, 61, 245-307.

Gibbons, W. 1989. Suspect terrane definition in Anglesey, North Wales. Geological Society of America, Special Papers, 230, 59-65.

Gibbons, W., Horak, J. M., 1996. The evolution of the Neoproterozoic Avalonian subduction system: Evidence from the British Isles. GSA Special Papers**,** 304, 269-280.

Gray, J. R., Yardley, B. W. D., 1979. A Caledonian blueschist from the Irish Dalradian. Nature, 278, 736-737.

Hamilton, M. A., Murphy, J. B., 2004. Tectonic significance of a Llanvirn age for the Dunn Point volcanic rocks, Avalon terrane, Nova Scotia, Canada: implications for the evolution of the Iapetus and Rheic Oceans. Tectonophysics, 379, 199-209.

Horák, J. M., Doig, R., Evans, J. A., and Gibbons, W., 1996. Avalonian magmatism and terrane linkage: new isotopic data from the Precambrian of North Wales. Journal of the Geological Society, 153, 91-99.

Isozaki, Y. and Maruyama, S., 1991. Studies on orogeny based on plate tectonics in Japan and new geotectonic subdivision of the Japanese Isands. Journal of Geo- graphy 100, 697-761 (in Japanese with English abstract).

Isozaki, 1997. Permo-Triassic Boundary Superanoxia and Stratified Superocean: Records from Lost Deep Sea. SCIENCE , 276 , 235.

Kawai, T., Windley, B.F., Terabayashi, M., Yamamoto, H., Maruyama, S., Isozaki, Y. 2007. Geotectonic framework of the blueschist unit on Anglesey-Lleyn, UK, and its role in the development of a Neoproterozoic accretionary orogeny. Precambrian Research, 153, 11-28.

Kawai, T., Windley, B.F., Shibuya, T., Omori, S., Sawaki, Y., Maruyama, S., 2008. Large P-T gap between Ballantrae blueschist/garnet pyroxenite and surrounding ophiolite, southern Scotland, UK: Diapiric exhumation of a Caledonian serpentinite melange. Lithos 104, 337-354.

Komiya, T., Maruyama, S., Masuda, T., Nohda, S., Hayashi, M., and Okamoto, K., 1999. Plate Tectonics at 3.8–3.7 Ga: Field Evidence from the Isua Accretionary Complex, Southern West Greenland. The Journal of Geology, 107, 515–554.

Landing, E., Bowring, S. A., Davidek, K. L., Westrop, S. R., Geyer, G., Heldmaier, W. 1998. Duration of the Early Cambrian: U-Pb ages of volcanic ashes from Avalon and Gondwana. Canadian Journal of Earth Sciences, 35, 329-338.

Leggett, J.K., McKerrow, W.S., Eales, M.H. 1979. The Southern Uplands of Scotland: a Lower Palaeozoic accretionary prism. Journal of the Geological Society, London, 136, 755-770.

Leggett, J. K., 1987. The Southern Uplands as an accretionary prism: the importance of analogues in

reconstructing palaeogeography. Journal of the Geological Society, 144, 737-751.

Niocaill, C. M., Smethrust, M. A., 1994. Palaeozoic palaeogeography of Laurentia and its margins: a reassessment of palaeomagnetic data. Geophysical Journal International, 116, 715-725.

Maletz, J., Stone, P., Rushton, A. W. A., 2004. Late Castlemainian (Ca 4, Arenig) graptolites from the Ballantrae Complex, SW Scotland. Scottish Journal of Geology, 40, 185-187.

Maruyama, S., Liou, G. J., Terabayashi, M., 1996. Blueschists and eclogites of the world and their exhumation. International Geology Review, 38, 485-594.

Matte, P., 2001. The Variscan collage and orogeny (480-290 Ma) and the tectonic definition of the Armorica microplate: a review. Terra Nova, 13, 122-128.

Nance, R. D., Linnemann, U., 2008. The Rheic Ocean: Origin, Evolution, and Significance. GSA today, 18, 4-12.

Noble, J. C., and Vines, R. G., 1993. Fire Studies in Mallee (Eucalyptus Spp.) Communities of Western New South Wales: Grass Fuel Dynamics and Associated Weather Patterns. The Rangeland Journal, 15, 2, 270–297.

Ogawa, Y., 1998. Tectonostratigraphy of the Glen App area, Southern Uplands, Scotland: anatomy of an Ordovician accretionary complex. Journal of the Geological Society, 155, 651-662.

Ogawa, T. and Taniguchi, H., 1989. Origin and emplacement of basaltic rocks in the accretionary complexes in SW Japan. Ofioliti, 14, 177-193.

Oliver, G.J.H. 2001. Reconstruction of the Grampian episode in Scotland: its place in the Caledonian orogeny. Tectonophysics, 332, 23-49.

Santosh, M., Maruyama, S., Sawaki, Y., Meert, J. G., in press. The Cambrian Explosion: Plume-driven birth of the second ecosystem on Earth. Gondwana Research.

Sawaki, Y., Shibuya, T., Kawai, T., Komiya, T., Omori, S., Iizuka, T., Hirata, T., Windley, B.F., Maruyama, S., 2010. Imbricated ocean-plate stratigraphy and U-Pb zircon ages from tuff beds in cherts in the Ballantrae complex, SW Scotland. Geological Society of America Bulletin 122, 454-464.

Thorpe, R. S., 1972. Ocean Floor Basalt Affinity of Precambrian Glaucophane Schist from Anglese. Nature, 240, 164-166.

Thorpe, R. S., Beckinsale, R. D., Patchett, P. J., Piper, J. D. A., Davies, G. R., Evans, J. A., 1984. Crustal growth and late Precambrian-early Palaeozoic plate tectonic evolution of England and Wales. Journal of the Geological Society, 141, 521-536.

Torvik, T. H., Trench, A. T., Svensson, I., Walderhaugh, H. J., 1993. Palaeogeographic significance of mid-Silurian palaeomagnetic results from southern Britain-major revision of the apparent polar wander path for eastern Avalonia Geophysical Journal International, 113, 651-668.

Trench, T. H., Torsvik, A., 1991. The Ordovician history of the Iapetus Ocean in Britain: new palaeomagnetic constraints. Journal of the Geological Society, 148, 423-425.

Tucker, R. D., and Pharaoh, T. C., 1991. U-Pb zircon ages for Late Precambrian igneous rocks in southern Britain. Journal of the Geological Society, 148, 435-443.

Ustaömer, P. A., Ustaömer, T., Gerdes, A., Zulauf, G., 2011. Detrital zircon ages from a Lower Ordovician quartzite of the İstanbul exotic terrane (NW Turkey): evidence for Amazonian affinity. International Journal of Earth Sciences, 100, 23-41.

Van Staal, C., R., Dewey, J., F., Mac Niocaill, C., McKerrow, W., S., 1998. The Cambrian-Silurian tectonic evolution of the northern Appalachians and British Caledonides: history of a complex, west and southwest Pacific-type segment of Iapetus. Geological Society, London, Special Publications, 143, 197-242.

Van der Voo, R., 1993. Palaeomagnetism of the Atlantic, Tethys and Iapetus Oceans. Cambridge University Press, Cambridge.

Chapter 5 Discovery of deep-sea sediments formed during the Marinoan Superanoxia

Abstract

Here I present the discovery of deep-sea sediments that record deep-sea anoxia, the "Marinoan Superanoxia", during 670-635 Ma in the accretionary complex in Llyen Peninsula, Wales, UK. The oceanic plate stratigraphy at Porth Felen, NW Llyen Peninsula, consists of mid-ocean ridge basalts (formed at 680-670 Ma), bedded dolostones, ca. 7 m-thick black mudstones, hemipelagic siliceous mudstones (deposited older than 637±13 Ma) and turbidites, in ascending order. The accreted deep-sea sediments span the Marinoan Snowball Earth from 670 Ma to 635 Ma, for ca. 35 million years. The acidic tuff layer separated from hemipelagite gives an age 627 Ma, and top bedded chert gives another constraint return to oxidized condition before the arrival to the trench. Turbidite sequence often contains dropstones suggesting glacier events may have continued after the Marinoan Snowball Earth, although it is limited to local area. Within black mudstone layer, lithological change can be observed, spanning 7 m-thick, (1) alternating dolomitic carbonate with black mudstone, over mm to cm scale over 50 cm, (2) black mudstone with mm or less layering (< 3 m), (3) FeS-enriched rather massive with less developed layering occurs ca. 3 m-thick, and (4) rhythmically alternating layers upward, and gradually turns into bedded white chert sequence.

The sedimentological change of deep-sea sediments during the travel from mid-oceanic ridge to the trench in the Iapetus Ocean suggests the environmental change

from red bedded chert through 7 m-thick black mudstone to red bedded chert again, reflecting redox change in the deep-sea environment through time; firstly oxic before 655 Ma, secondly anoxic until 635 Ma, and finally oxic after that. The center of the anoxia is characterized by FeS-enriched rather massive black mudstone with less developed layering.

Keywords: Marinoan Snowball Earth, accretionary complex, deep-sea sediments, Superanoxia, mass extinction

5-1 Introduction

Snowball Earth events are widely recognized to have occurred in the Palaeoproterozoic and Neoproterozoic. All present-day animal phyla appeared following the Marinoan Snowball Earth, which is the last recorded global glaciation. The Neoproterozoic Snowball Earth has been studied for the last 20 years as the most important event in the Earth's history. The Snowball Earth is regarded to have an important role in the birth of metazoans that happened right after the glaciation (Hoffman & Schrag, 2002). The critical constraints to believe the Snowball Earth was the combination of paleomagnetic evidence of equatorial origin of continents covered by thick glacial deposits of tillite was directly covered by cap carbonates suggesting instantaneous change of climate from Snowball to warm condition with stromatolites (Fig. 5-1). It often associate with Fe-Mn ore, suggesting the pO_2 was low during the Snowball event, and followed by free oxygen increased after the melting of Snowball.

Three models that attempt to explain the onset and termination of Snowball Earth events are: (1) episodic decrease of greenhouse gases, (2) changes of the albedo of the

Earth accompanied by the arrangement of the continents, and (3) an increase in cosmic-ray bombardment to the Earth due to Starbursts in the Milky Way Galaxy or transects of Earth through nebula (Kataoka et al., 2013). Recently, some researchers are trying to show the quantitative estimates of the cosmic-ray intensity from geological evidence (Asanuma et al., 2013).

To analyze the drastic change of surface environmental change, chemostratigraphic data base were completed in many areas such as Russia, Australia, Oman, China, Namibia and North America. One of the most reliable works has been completed using the on-land drilled cores in China (Ishikawa et al., 2008; Sawaki et al., 2008; Shu, 2008; Shu et al., 2014; Maruyama et al., 2014). Yet, the data source has been restricted only to shallow marine platform deposits, and no reports at all from the deep-sea sediments. Here I report the first discovery of pelagic deep-sea sediments found in Wales, UK.

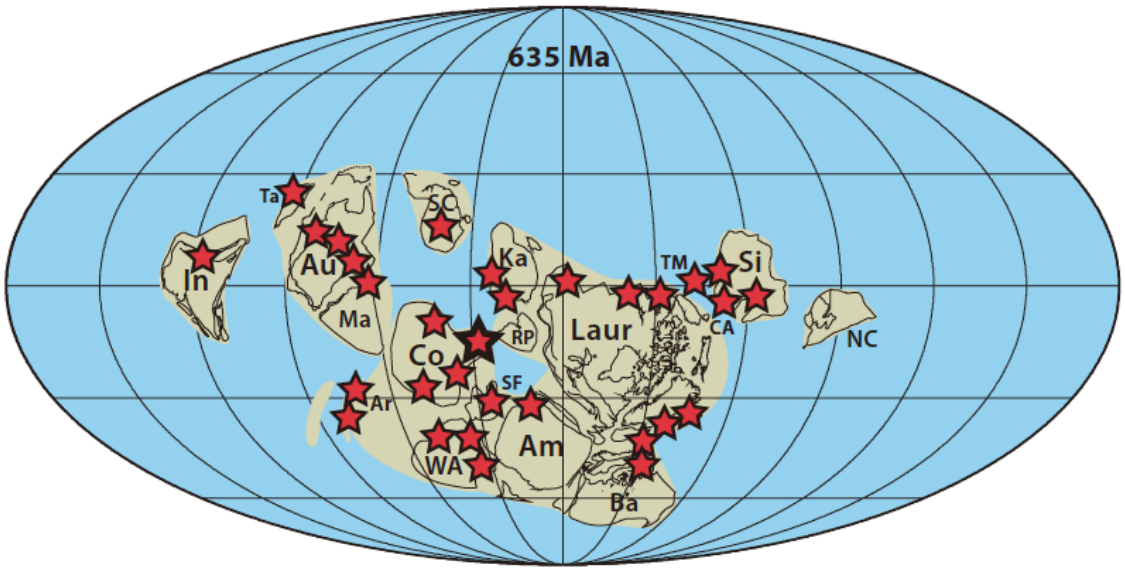

Fig. 5-1. Paleogeographic map in the Neoproterozoic (ca. 635 Ma) showing the distribution of Snowball Earth event over the world (modified from Hoffman & Li, 2009).

5-2 Geological Outline

The Gwna Group, Wales, Lleyn Peninsula, UK has not been well investigated, in spite of pioneering work by Greenly (1919). The Gwna Group is composed of greenstone with low-K tholeitic composition (Thorpe, 1972), claystone/chert sequence, greywacke sandstone which is boudinaged often with matrix-supported, and looks similar to the so-called mélange. Part of the Gwna Group has been subjected to blueschist to epidote amphibolite facies metamorphism at ca. 600 Ma (Dallmeyer & Gibbons, 1987; Kawai et al., 2007), hence suggested as the Neoproterozoic subduction zone in this area.

The Gwna Group has been reinterpreted by Barber & Max (1979) who has suggested the rock unit to have been formed at subduction zone in Neoproterozoic. Later, the concept of Avalonian terrane was proposed to suggest the site of Gwna Group could have been along the western margin of Western Africa craton before the opening of Rheic Ocean.

The Gwna Group occurs in many places sporadically from Lleyn Peninsula to the northwestern tip of Anglesey Island over 200 km across the general strike of NE-SW (Fig. 5-2, 3, 4). I demonstrated the Gwna Group is subduction zone complex based on mode of occurrence, lithology, zircon chronology, and reconstruction of ocean plate stratigraphy. I subdivided the Gwna Group into four Units, according to the formation age defined by hemipelagic claystone.

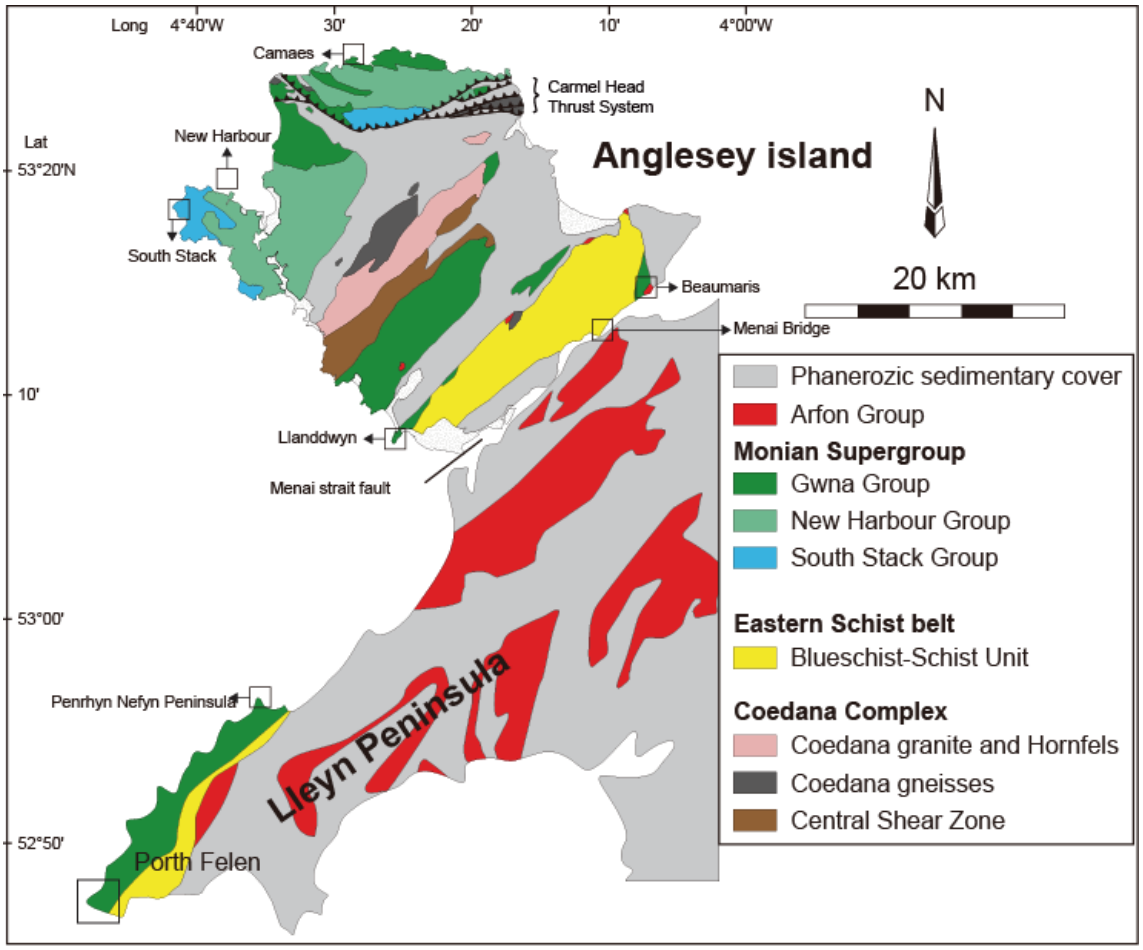

Fig. 5-2. Geologic map of Anglesey-Lleyn, Wales, UK (modified after Greenly, 1919; Kawai et al., 2007).

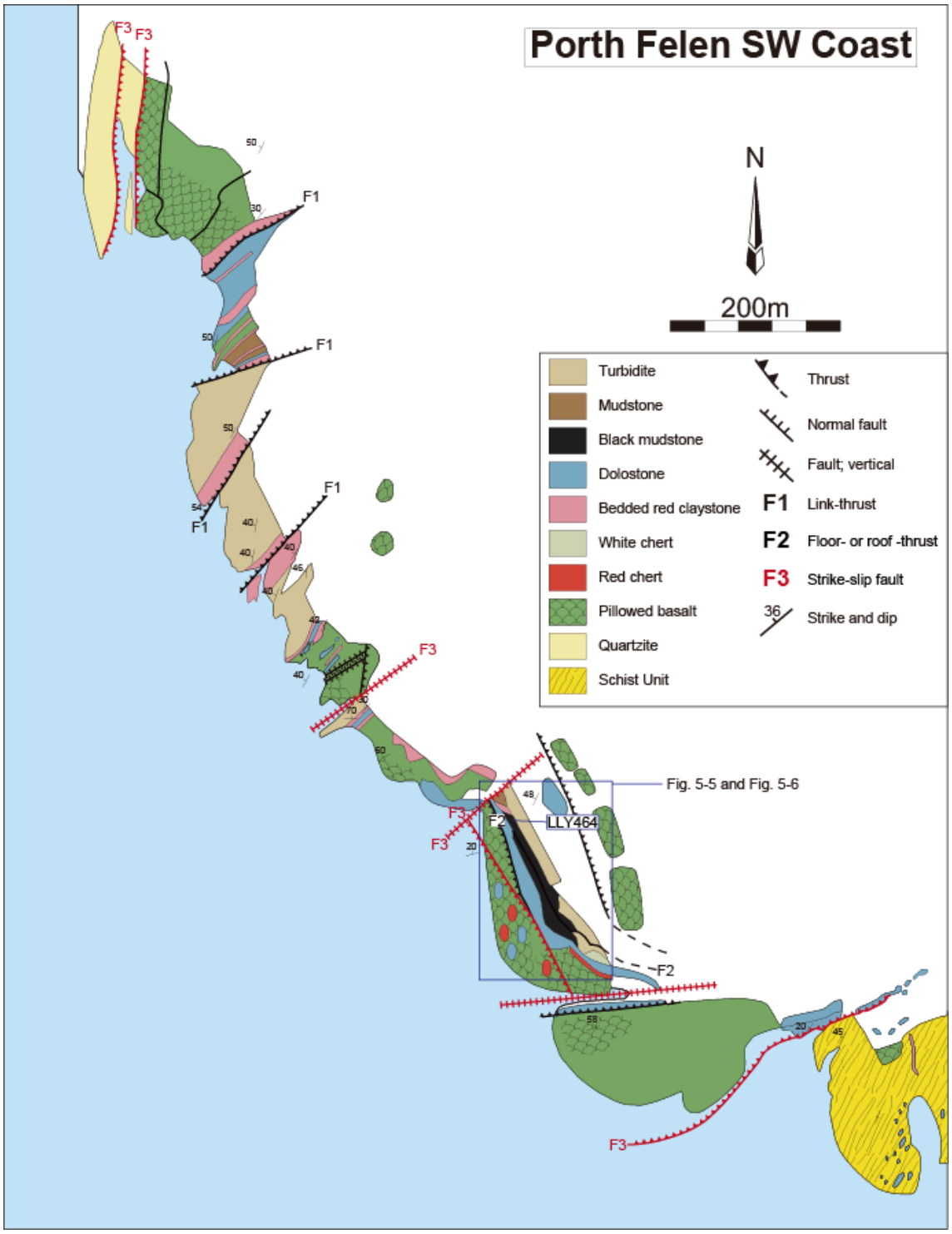

Fig. 5-3. Geologic map and tectonic cross section of the Lleyn Peninsula. (modified after Kawai et al., 2007)

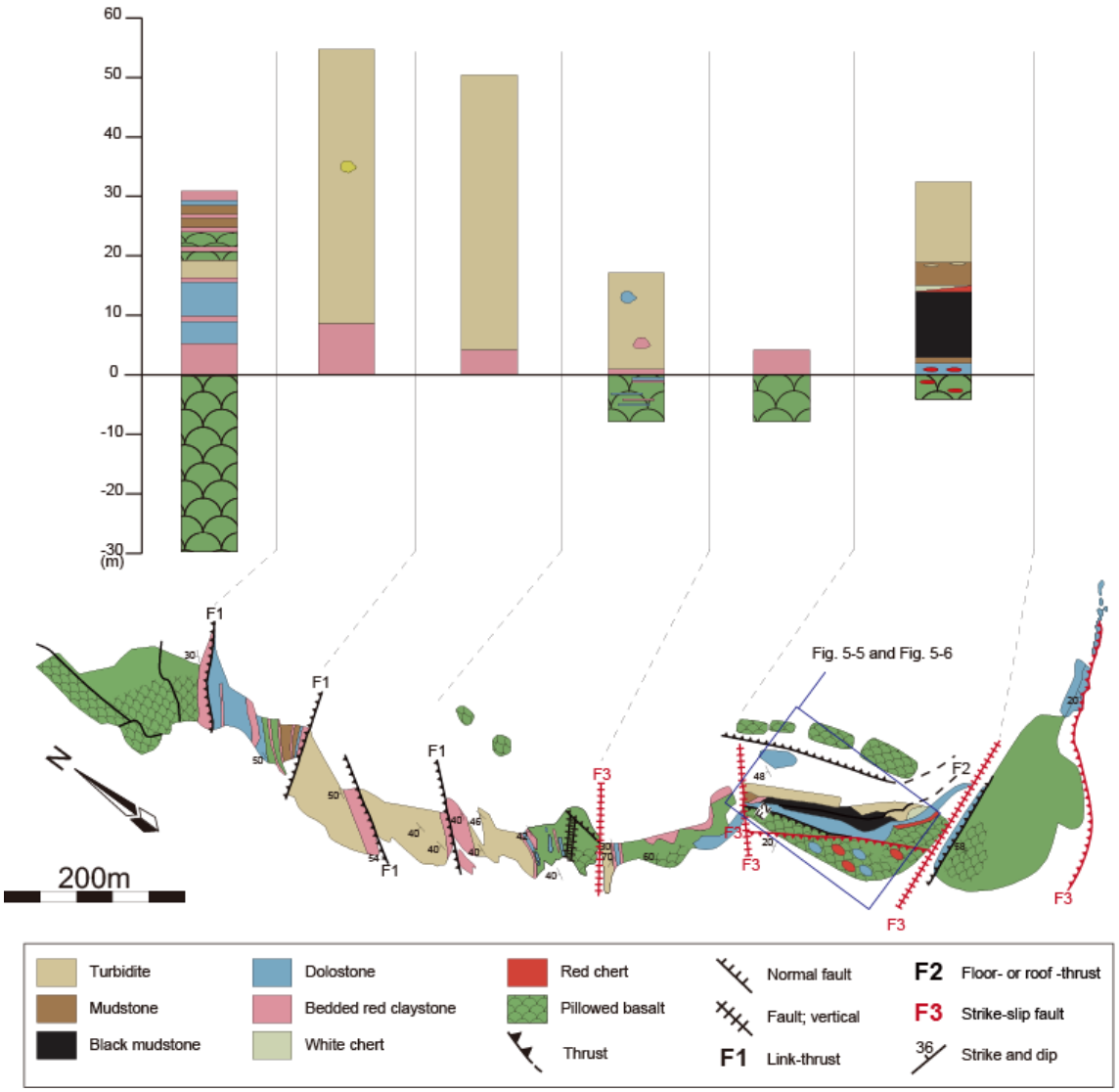

Fig. 5-4. Route map of Porth Felen, Lleyn, Wales, UK. Box indicates the position of the black mudstone outcrop. Position of Figure 5-4 is indicated by the red box in Fig. 5-3

5-3 Ocean plate stratigraphy in the Porth Felen

At Porth Felen, Lleyn, Wales, the OPS of the Gwna Group crops out. The OPS is composed of pillow basalts, black mudstone, hemipelagite, and turbidite in ascending order.

Along the coastline, a series of excellent outcrops are present. A series of layer-parallel faults are observed (Fig. 5-5, 6). Reconstructed complete column is

shown in Fig. 5-7.

I discovered an exposure of Marinoan Snowball Earth event in deep-sea sediments in Wales, UK. These deep-sea sediments are fragments of Neoproterozoic accretionary complex, often cut by layer-parallel thrusts, but still possible to reconstruct ocean plate stratigraphy. The reconstructed OPS shows that the stratigraphical bottom is MORB > 50 m which is overlain by red-claystones interlayered with a few cm thick red cherts 5 m, which in turn overlain by 5 m thick black mudstone layer. This is a layer extremely enriched carbon (ca. 6-10 wt%) with fine-grained pyrite, underlain by 10 m thick dolomitic carbonate with off-ridge basalt flows 7 m, capped by 5-10 m mafic-felsic trench turbidite with pebbles, presumably dropstone in origin.

In this outcrop, some ocean plate stratigraphy has been repeated by thrusts in duplexes; this combination and structural style are typical of accretionary complexes worldwide (Isozaki et al., 1990).

Black mudstone (ca. 7 m-thick) can be divided into more than four subunits (Fig. 5-7, 8, 9). (1) dark gray mudstone with thin light gray lamina, (2) gray siliceous claystone with thin dark-gray lamina, (3) thin-bedded black mudstone, and (4) alternation of black and gray mudstone. Pelagic to hemipelagic sedimentary sequence overlies the black mudstone bed (ca. 7 m-thick). In ascending order, greenish gray chert (1 m), greenish gray siliceous mudstone (2 m), greenish gray mudstone (1 m), greenish gray mudstone with sandstone pebble (1 m), and sandstone (> 5 m). Pebbles in the sandstone are possibly dropstone origin. It suggests that the sea-ice melting and drop stone occurred clearly after the black mudstone deposition.

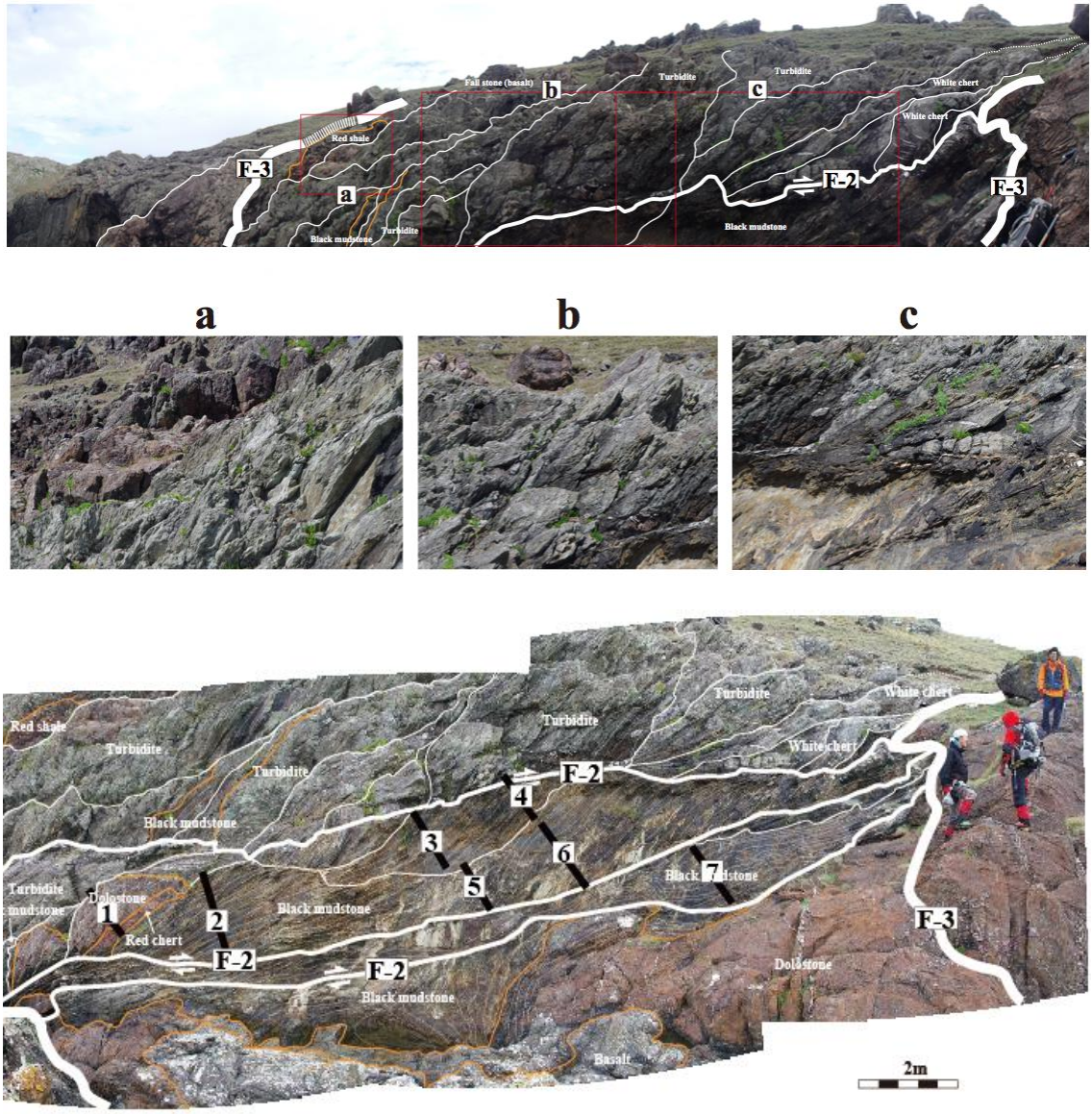

Fig. 5-5. Outcrop photo of the hanging wall with black mudstone at Porth Felen, Lleyn Peninsula, Wales. The duplex showing thrusts on bedding planes.

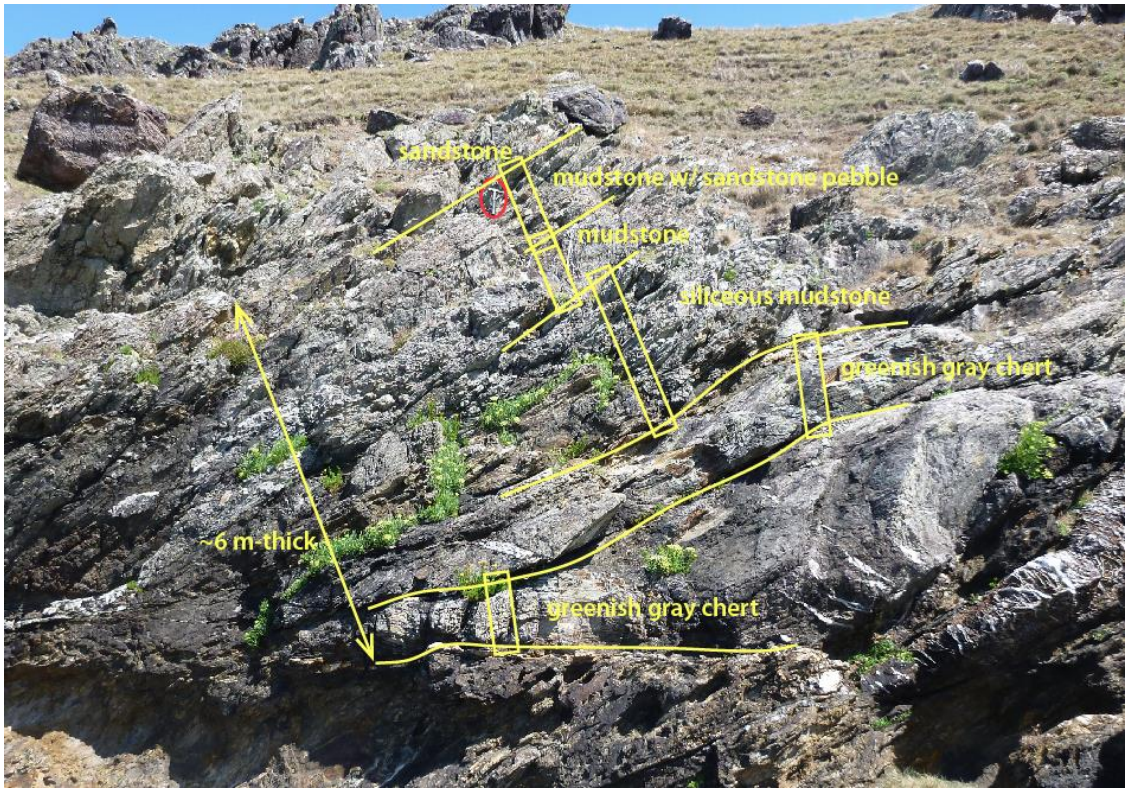

Fig. 5-6. Close-up photos of the outcrop at Porth Felen, Lleyn Peninsula, Wales. The boxes show the observed stratigraphic columns.

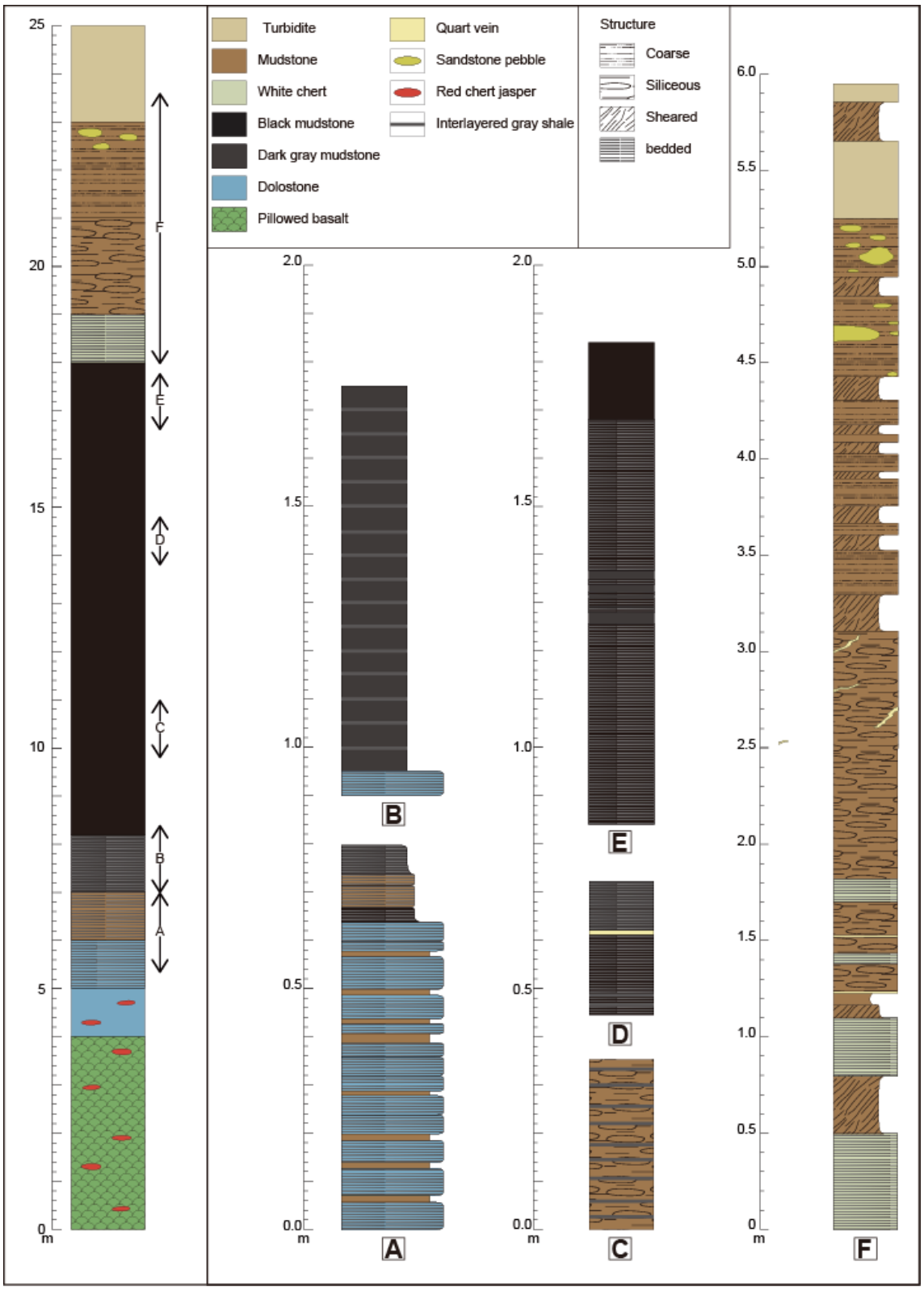

Fig. 5-7. Stratigraphic column of OPS at Porth Felen, Lleyn Peninsula, Wales.

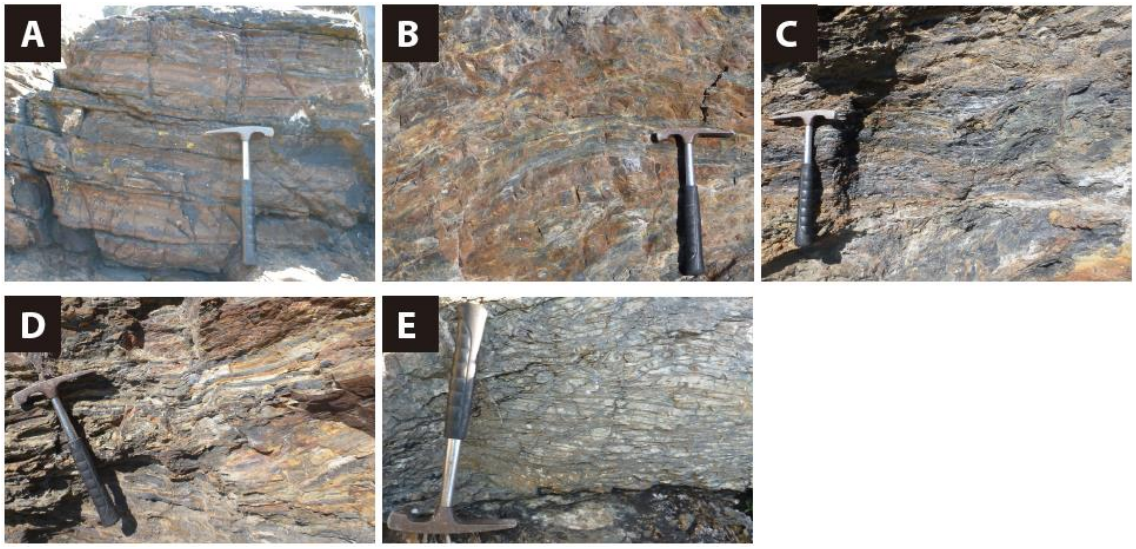

Fig. 5-8. Close-up photo of the outcrop of the Llyen Peninsula. A; uppermost part of the brownish bedded dolostone. B; lower part of the black mudstone, . C; middle part of the black mudstone, darkest and unclear bedding. D; upper part of the black mudstone, dark gray mudstone w/ gray layer. E; greenish gray siliceous mudstone.

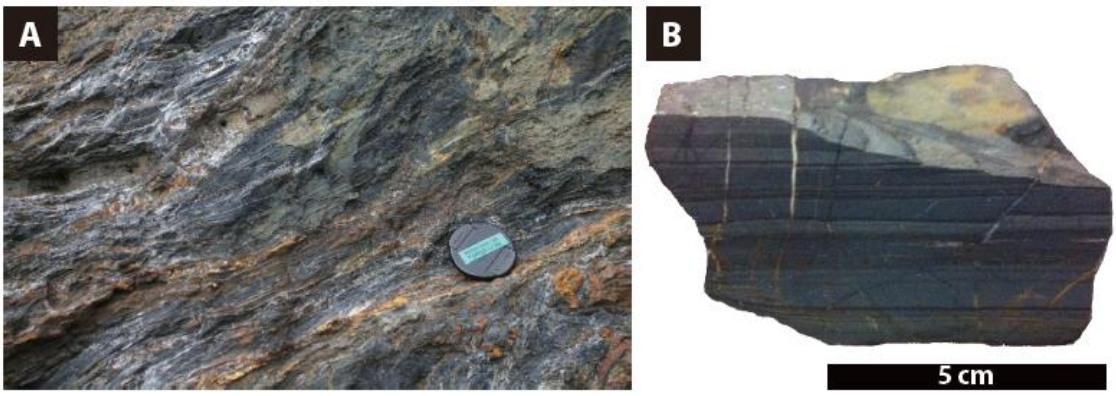

Fig. 5-9. Black mudstone intercalated with the deep-sea sediments in the OPS at Porth Felen, Llyen Peninsula, Wales. A; outcrop, B; slab photo. Note that the black mudstone is thinly laminated and contains pyrites, suggesting reducing depositional condition.

5-4 Zircon Chronology

Zircon crystals were separated from a sandy mudstone (LLY464) in the middle of the black mudstone bed in order to determine their radiometric ages. They were extracted using the mineral separation system at the Tokyo Institute of Technology, and mounted and polished in 8 mm epoxy discs. The zircons are variable in size, shape, and color; they are euhedral, subhedral, elliptical, and spindly. Average grain size is ~100 μm. More than 80 % of the zircons are red, and the others are pale white. I extracted zircons from each tuff sample and analyzed 10 grains for U-Pb isotopes. U-Pb analyses were performed on a laser ablation–inductively coupled plasma–mass spectrometer (LA-ICP-MS) at Kyoto University.

The results are shown in Table 5-1. The youngest zircon age of the sandy mudstone showed 637±13 Ma (Fig. 5-10).

Table 5-1. Analysed zircon from sandy mudstone (LLY464).

									Age(Ma)				
Analysis number	204Pb/206Pb	Uppm1	Th/U	207Pb/235U	2σ	206Pb/238U	2σ	207Pb/206Pb	2σ	207Pb/235U	2s abs	206Pb/238U	2s abs	207Pb/206Pb	2s abs	% U-Pb disc4
LLY464-1	0.000360	3226	1.68	5.139	± 0.378	0.2965	± 0.0051	0.1257	± 0.0045	1843	± 65	1674	± 26	2038	± 132	18
LLY464-2	0.000118	3761	1.13	2.603	± 0.194	0.2165	± 0.0038	0.0872	± 0.0032	1302	± 56	1263	± 20	1365	± 146	7
LLY464-3	0.000375	7099	1.04	1.690	± 0.125	0.1625	± 0.0028	0.0755	± 0.0027	1005	± 48	970	± 15	1081	± 152	10
LLY464-4	0.000000	1189	2.82	6.376	± 0.481	0.3694	± 0.0069	0.1252	± 0.0046	2029	± 69	2027	± 33	2031	± 135	0
LLY464-5	0.000000	1611	1.33	0.922	± 0.079	0.1038	± 0.0022	0.0644	± 0.0027	664	± 43	637	± 13	756	± 186	16
LLY464-6	0.000000	2747	1.90	2.268	± 0.240	0.2136	± 0.0036	0.0770	± 0.0040	1202	± 78	1248	± 19	1121	± 224	11
LLY464-7	0.000284	3793	3.37	5.061	± 0.528	0.3182	± 0.0051	0.1154	± 0.0059	1830	± 93	1781	± 25	1885	± 198	6
LLY464-8	0.000611	3476	0.77	4.063	± 0.426	0.2367	± 0.0039	0.1245	± 0.0064	1647	± 89	1370	± 20	2022	± 196	32
LLY464-9	0.000568	3150	0.83	4.692	± 0.491	0.2937	± 0.0048	0.1159	± 0.0060	1766	± 92	1660	± 24	1893	± 199	12
LLY464-10	0.000209	7763	3.15	1.472	± 0.154	0.1445	± 0.0023	0.0739	± 0.0038	919	± 65	870	± 13	1039	± 225	16

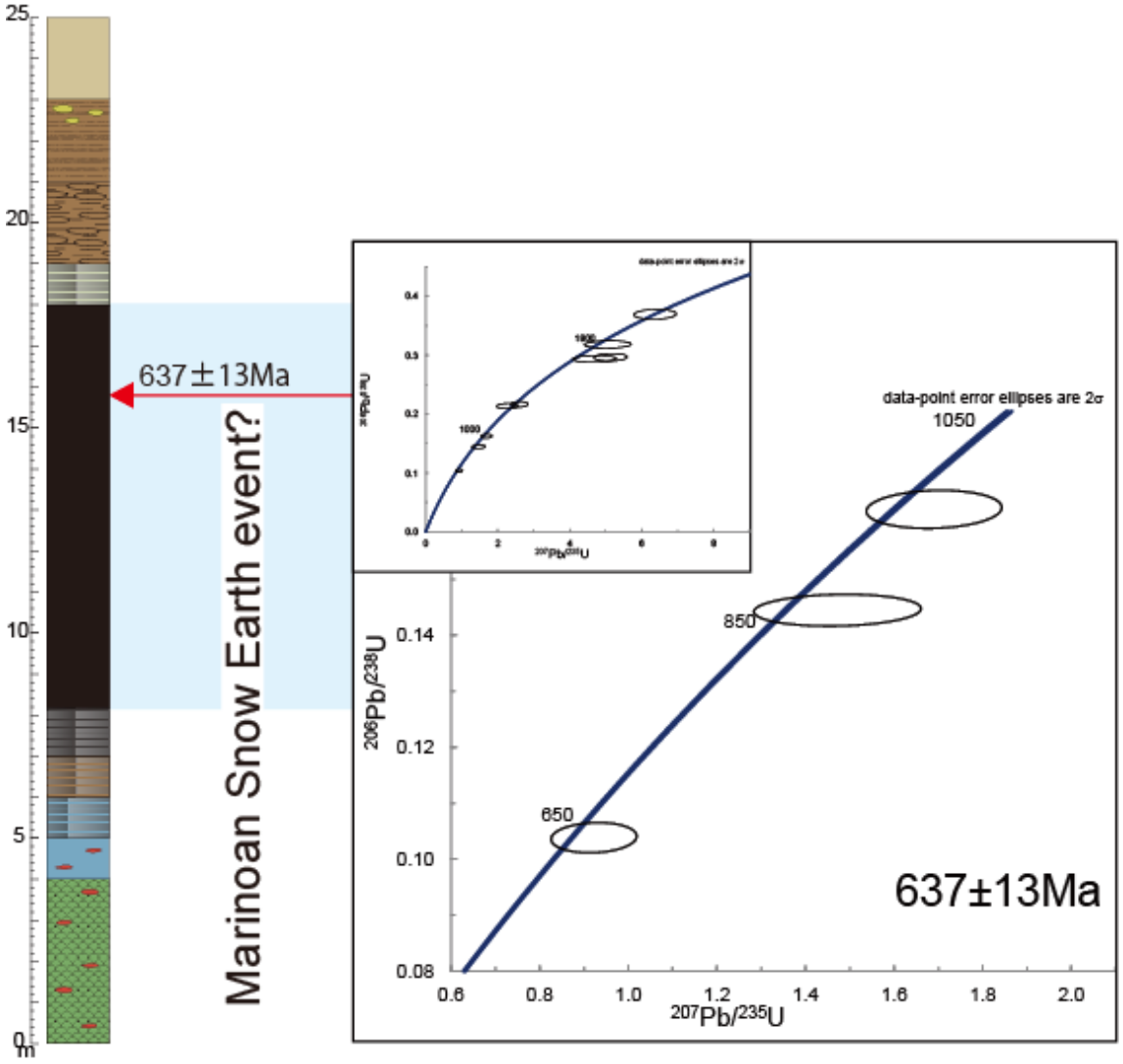

Fig. 5-10. Synthetic stratigraphic column of OPS at Porth Felen, Lleyn Peninsula, Wales. Concordia plot of in-situ U-Pb dates of zircons with LA-ICP-MS.

5-5 Discussion

The data of the Marinoan Snowball Earth has been limited only to shallow-sea sedimentary rocks such as in China. The geological evidence from the deep-sea is important because the deep-sea sediments of this interval are very rare in the world. Kawai et al. (2007, 2008) showed that the Gwna Group is accretionary complexes. There are hemipelagic mudstones at Llanddwyn island, Anglesey. The age constraint of zircon in the Llanddwyn OPS. The depositional site of the dropstones in Porth

Felen was likely near trench, because the black mudstone and hemipelagic siliceous mudstone have no dropstones (Fig. 5-11). Dropstones corresponding to the Gaskiers glaciation (ca. 580 Ma) are reported from Llanddwyn Island by Kawai et al. (2008).

Hoffman & Li (2009) reviewed the time constraints of the Marinoan Snowball Earth event.

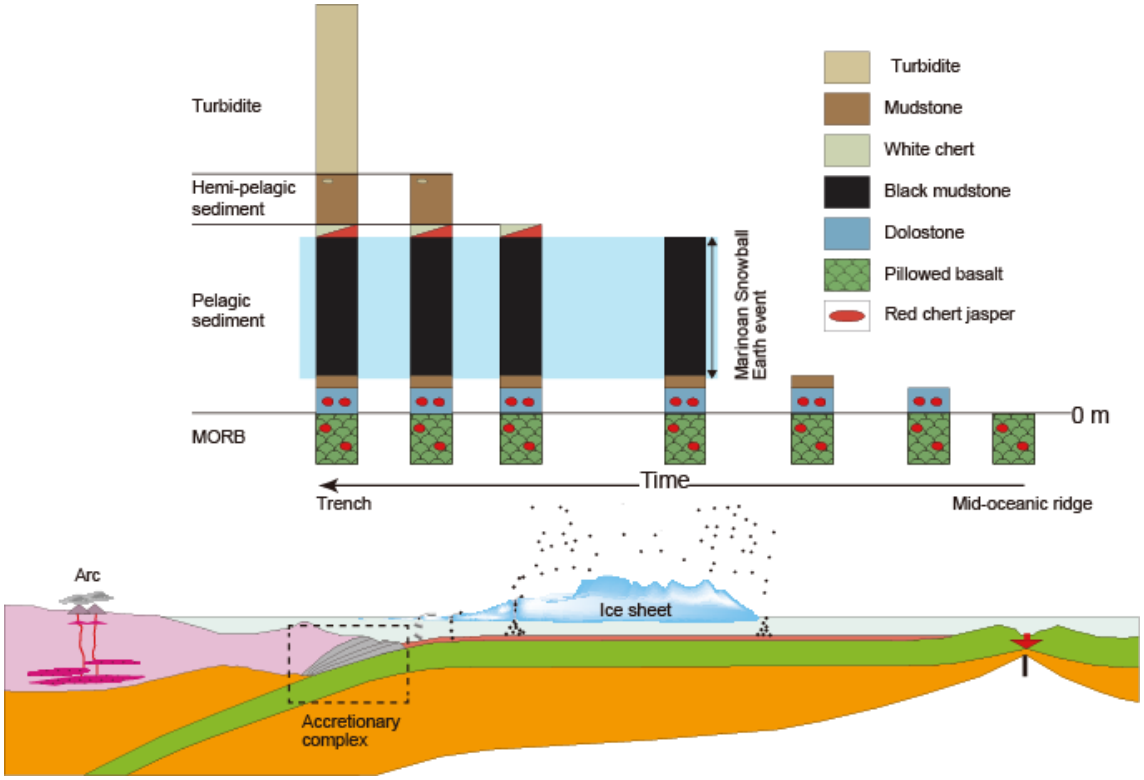

Fig. 5-11. Travel history of accreted oceanic fragments at Wales from MOR to trench. The deposition of the dropstones from the base of icebergs into pelagic mudstone on the sea floor.

5-5-1 Marinoan Snowball Earth and "Superanoxia"

The Phanerozoic deep ocean was regarded to have been oxic just like the modern ocean, except for some anoxic events, such as the P-T boundary Superanoxia (Isozaki, 1997) or Cretaceous Oceanic Anoxic Events (OAEs; Meyer & Kump, 2008). Those events are characterized by organic-rich black mudstones as evidences for the anoxic

depositional environments. For example, black claystones of the P-T boundary interval are intercalated between the red bedded cherts of the Permian and Triassic deep-sea setting; black shales of the Cretaceous OAE intervals are intercalated between the white limesones of the Cretaceous shallow-sea settings. The depositional mechanism for such kind of black shales is suggested as follows; (1) ocean stratification caused by weakening of ocean circulation resulted in oxygen-depletion in the deep ocean (ex. the P-T Superanoxia, OAE1a, and modern Black Sea); (2) enhanced upwelling caused by enforced ocean circulation resulted in the formation of oxygen-minimum zone in the continental slope (ex. OAE2, and modern off coast of Chile). In any case, anoxic environment is basically regarded as local; however, some studies of anoxic events (ex. OAE1a and OAE2) suggested that the whole global ocean including shallow-waters became anoxic.

This study recognized the black mudstone intercalated between the red cherts in Porth Felen for the first time. As the black mudstone occurs in OPS in AC and does not contain any terrigenous clastics, it is regarded to have been deposited on pelagic deep-sea floor in the Neoproterozoic. The occurrence of the black mudstone sandwiched by red chert is similar to the deep-sea chert sequence across the P-T boundary in Inuyama, Japan. This fact suggests that the ocean stratification and deep-sea anoxia in the Neoproterozoic caused the deposition of the black mudstone at Porth Felen; although further discussions for the depositional model based on geochemical proxies such as carbon isotope are needed. During the black mudstone deposition, the whole ocean including the shallow-marine environments was possibly turned into anoxic. The zircon data, 637±17 Ma, suggests that the black mudstone corresponds to the Marinoan Snowball Earth interval (655-635 Ma; Condon et al., 2005;

Fig. 5-12). Snowball Earth hypothesis (Kirschvink, 1992) is characterized by the ocean stagnation by the ice-sheet covering. The stagnation might cause oceanic anoxia, although there are debate it was truly frozen or partly.

Here I propose that the black mudstone at Porth Felen shows the global-scale oceanic anoxic event during the Marinoan Snowball Earth, and name this long-term (ca. 35 million years) catastrophic event the "Marinoan Superanoxia" in comparison to the Permo-Triassic Superanoxia. During the P-T Superanoxia across the P-T boundary, pelagic deep-sea sediments are represented by ca. 30 m-thick organic-rich black mudstone (e.g. Isozali, 1994). The P-T Superanoxia, is regarded as one of the cause of the largest mass extinction in the Phanerozoic. Likewise, the Marinoan Superanoxia led the organic carbon burial, black mudstone deposition, and might be a cause of the extinction in the Ediancaran that predate the Cambrian Explosion. The duration of the black mudstone deposition is comparable to, or much longer than, the P-T Superanoxia.

5-5-2 Significance of deep-sea sediments

The first oxidation of the deep ocean in the Earth's history is regarded to have occurred stepwise in the Neoproterozoic, coincident with the metazoan diversification (e.g. Anbar & Knoll, 2002; Canfield et al., 2007). In order to estimate the redox condition semi-quantitatively, geochemical and isotopic data of Neoproterozoic sedimentary rocks

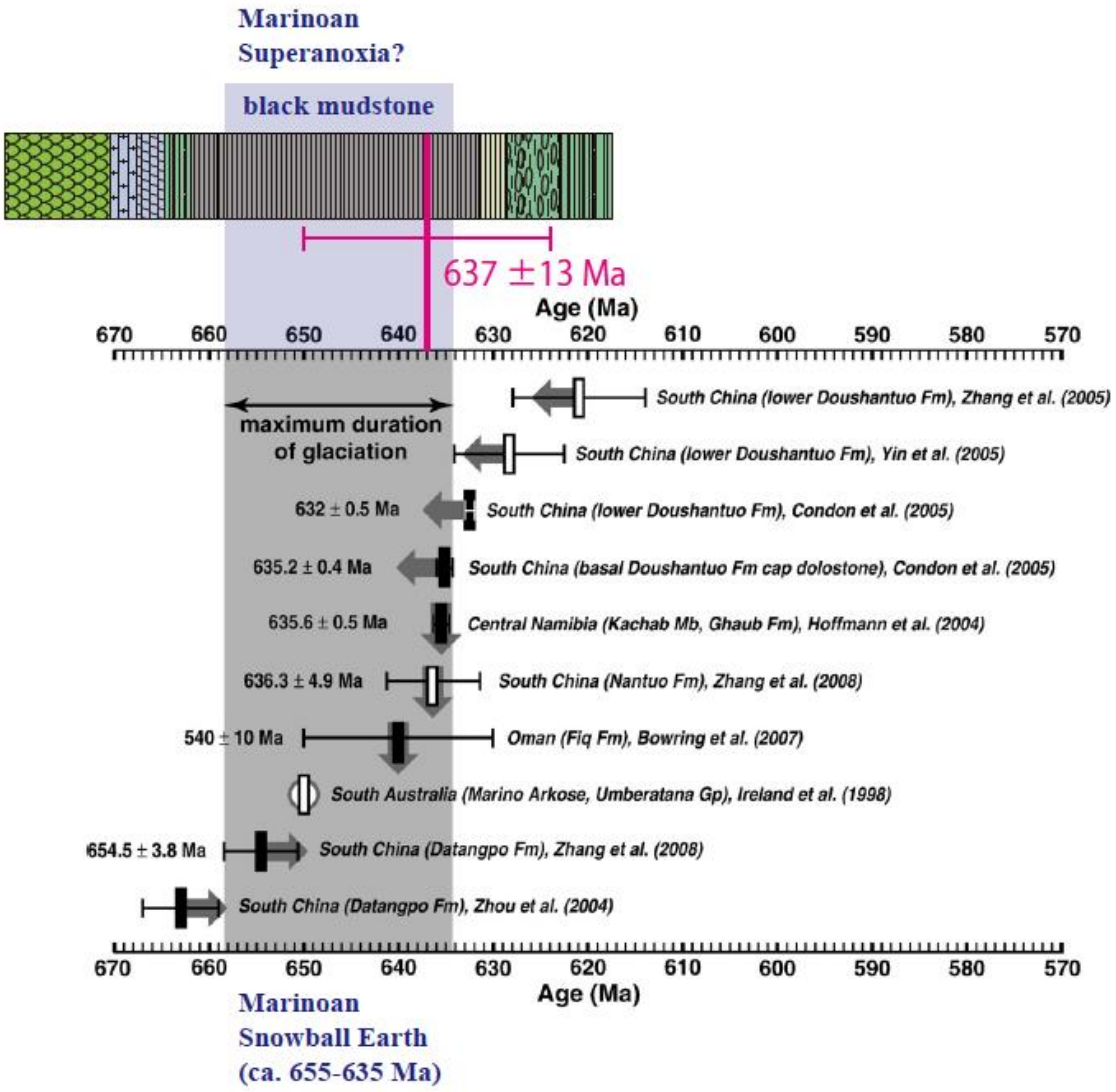

Fig. 5-12. Time correlation between OPS and the Snowball Earth event established in the other locality (modified from Hoffman & Li, 2009).

were analyzed by numerous studies; in particular, the parameters based on the chemical states of iron have been regarded as useful redox indicators (e.g., Canfield et al, 2007). It has been proposed that sulfidic deep-ocean persisted for a billion years of mid-Proterozoic, turned ferruginous in the late Neoproterozoic, and then turned oxygenated about 580 Ma (e.g., Canfield et al, 2007); however the precise process of the oxidation is still controversial.

The biggest problem is that most previous studies have investigated only epicontinental shallow-ocean sedimentary rocks and the mid-oceanic sediments have not been checked. It is because the ocean-floors older than 200 Ma have been lost by oceanic-plate subduction, and there are no sediments of the Proterozoic or Early Paleozoic ages in modern sea floor (Isozaki, 1994).

Pelagic deep-sea cherts in ancient accretionary complexes are essential to analyze past global deep-ocean, as shown in the previous studies of Paleozoic-Mesozoic boundary (e.g., Isozaki, 1994), because they are the only records of pelagic deep-sea environments older than 200 Ma and have better chance to record global signals than epicontinental sediments that are liable to be influenced by local fluctuations. Such cherts can be found solely in the accretionary orogenic belts exposed on land.

As the older cherts in accretionary complex have more chance to be suffered from metamorphism and/or alteration, the deep-sea cherts of the Neoproterozoic age are very rare. The pelagic deep-sea sediments in the studied area may be important window for checking the paleo deep-ocean environment.

Moreover, based on recent investigations, the effects of extra-terrestrial forcing on the Earth are estimated here through the measurement of the abundances of platinum group elements (PGE) in sediments. Pelagic sediments composed of interlayered shale and/or mudstones are optimal for PGE-abundance analysis because of their low sedimentation rate. By analyzing PGE and Ir abundance of pelagic sediments collected from the accretionary complex of Anglesy-Lleyn, we can see the existence of cosmogenic materials (Asanuma et al., 2013).

References

Asanuma, H., Sawaki, Y., Yokoyama, T., Maruyama, S., 2013, Detection of cosmogenic material in deep-sea sediments based on platinum group element (PGE) abundances. GSA Annual Meeting, no. 66-11.

Anbar, A.D. and Knoll, A.H., 2002, Proterozoic ocean chemistry and evolution: A bioinorganic bridge? *Science*, **297**, 1137-1142.

Barber, A.J., Max, M.D., 1979. A new look at the Mona Complex, Anglesey, North Wales. *J. Geol. Soc. Lond.*, 136, 407–432.

Canfield, D.E., Poulton, S.W. and Narbonne, G.M., 2007, Late-Neoproterozoic deep-ocean oxygenation and the rise of animal life. *Science*, **315**, 92-95.

Condon, D., Zhu, M., Bowring, S.A.,Wang,W., Yang, A., Jin, Y., 2005. U–Pb ages from the Neoproterozoic Doushantuo Formation, China. *Science*, 308, 95–98.

Dallmeyer, R.D. and Gibbons, W., 1987, The age of blueschist metamorphism on Anglesey, North Wales: evidence from $^{40}Ar/^{39}Ar$ mineral dates of the Penmynydd schists. *Jour. Geol. Soc., Lond.*, **144**, 843-850.

Greenly, E., 1919, *The geology of Anglesey.* Mem. Geol. Surv. Great Britain. HMSO, London, 980 pp.

Hoffman, P.F., Schrag, D.P., 2002, The snowball Earth hypothesis: testing the limits of global change. *Terra Nova*, 14, 129–155.

Hoffman, P.F., Li, Z.X., 2009, A palaeogeographic context for Neoproterozoic glaciation. *Palaeogeography, Palaeoclimatology, Palaeoecology*, 277,158–172.

Ishikawa, T., Ueno, Y., Komiya, T., Sawaki, Y., Han, J., Shu, D., Li, Y., Maruyama, S. and Yoshida, N., 2008, Carbon isotope chemostratigraphy of a Precambrian/Cambrian boundary section in the Three Gorge area, South China: Prominent global-scale isotope excursions just before the Cambrian Explosion. *Gondwana Research*, **14**, 193-208.

Isozaki, Y., Maruyama, S., Furuoka, F., 1990, Accreted oceanic materials in Japan. *Tectonophysics*, 181, 179-205.

Isozaki, Y., 1994, Superanoxia across the Permo-Triassic boundary: Record in accreted deep-sea pelagic chert in Japan. *Mem. Canad. Soc. Petrol. Geol.*, **17**, 805-812.

Kataoka, R., Ebisuzaki, T., Miyahara, H., Nimura, T., Tomida, T., Sato, T., Maruyama, S., 2013, The Nebula Winter: The united view of the snowball Earth,mass extinctions, and explosive evolution in the late Neoproterozoic and Cambrian periods. *Gondwana Research*, in press.

Kawai, T., Windley, B.F., Terabayashi, M., Yamamoto, H., Maruyama, S., Omori, S., Shibuya, T., Sawaki, Y. and Isozaki. Y., 2007, Geotectonic framework of the Blueschist Unit on Anglesey-Lleyn, UK, and its role in the development of a Neoproterozoic accretionary orogen. *Precambrian Res.*, **153**, 11-28.

Kawai, T., Windley, B.F., Terabayashi, M., Yamamoto, H., Isozaki, Y. and Maruyama, S., 2008, Neoproterozoic glaciation in the mid-oceanic realm: An example from hemi-pelagic mudstones on Llanddwyn Island, Anglesey, UK. *Gondwana Res.*, **14**, 105-114.

Kirschvink, J.L., 1992. Late Proterozoic low latitude glaciation: The Snowball Earth. pp. 51-52 in Schopf and Klein, eds., *The Proterozoic Biosphere: A Multidisciplinary Study.* Cambridge Univ. Press, Cambridge.

Maruyama, S., Sawaki, Y., Ebisuzaki, T., Ikoma, M., Omori, S., Komabayashi, T., 2014, Initiation of leaking Earth: An ultimate trigger of the Cambrian explosion. *Gondwana Research*, in press.

Meyer, K.M., Kump, L.R., 2008. Oceanic Euxinia in Earth History: Causes and Consequences. *Annual Review of Earth and Planetary Sciences* **36**: 251–288.

Sawaki, Y., Ohno, T., Fukushi, Y., Komiya, T., Ishikawa, T., Hirata, T. and Maruyama, S., 2008a. Sr isotope excursion across the Precambrian-Cambrian boundary in the Three Gorges area, South China. *Gondwana Research*, **14**, 134-147.

Shu, D., 2008, Cambrian explosion: Birth of tree of animals. *Gondwana Research*, 14, 219-240.

Shu, D., Isozaki, Y., Zhang, X., Han, J., Maruyama, S., 2014, Birth and early evolution of metazoans. *Gondwana Research*, in press.

Thorpe, R.S., 1972. Possible subduction zone origin for two Precambrian calc-alkaline plutonic complexes from southern Britain. Geol. Soc. Am. Bull. 83, 3663–3668.

Chapter 6 New chronological constraints for Cryogenian to Cambrian rocks in the Three Gorges, Weng'an and Chengjiang areas, South China

Abstract

The Neoproterozoic and Cambrian are two of the most dramatic periods in the history of the Earth, because large multi-cellular animals first appeared then in the so-called "Cambrian Explosion". To better understand this event, many paleontological and geochemical studies now focus on rocks in South China, because of the fossiliferous succession and good exposure. Since the recognition of the Yangtze Gorges and Chengjiang area as type localities of the Sinian (Ediacaran) and Meishucunian (Early Cambrian) Systems, both sections have been intensively investigated. In order to decipher the relationships between the evolution of life and surface environmental changes, it is necessary to acquire their paleontological, geochemical and geo-chronological constraints.

Geochronological data are fundamental for understanding the geological history, and this study presents new chronological constraints for the Cryogenian to Cambrian rocks in the Three Gorges, Weng'an and Chengjiang areas, South China. We discovered two tuff layers, one at the base of the Shuijingtuo Fm at Three Gorges and the other at the bottom of the Dahai Member in Chengjiang. In addition, we collected sandstones from Neoproterozoic strata in the Three Gorges, Chengjiang and Weng'an areas for provenance analysis. Zircons, separated from the tuff layers, provide new Nano-SIMS

U-Pb ages of 526.4 ± 5.4 Ma at the base of the Shuijingtuo Fm, and 523.9 ± 6.7 Ma at the bottom of the Dahai Member. The tuffaceous beds occur at an unconformity, and nodules are common in the Three Gorges, Meishucun and Taoying sections, indicating that major and relatively wide-scale volcanic and sedimentological events occurred at *ca.* 525 Ma. Moreover, carbonate carbon isotope chemostratigraphies at Morocco, Siberia, Three Gorges and Meishucun display different characteristics during the Tommotian. One possibility is that the South China Ocean was separated from an outer ocean at that time. Detrital zircons in sandstones indicate that paleo-hinterland of the Nanhua and Kangdian rift basins was geologically complex with the following age spectrum *ca.* 2.7, 1.8, 1.6, 1.0 and from 0.9 to 0.75 Ga. Despite the lack of the *ca.* 1.6 Ga rocks in the Yangtze and Cathaysia Blocks, these data are nevertheless interpreted to indicate derivation of the zircons from basement rocks in the Yangtze craton.

Keywords:

Tuff, zircon, U-Pb geochronology, LA-ICP-MS, nano-SIMS, South China.

6-1. Introduction

One of the most drastic events in the fossil record was the explosive diversification of metazoa in the Neoproterozoic and Cambrian (Fig. 6-1). The emergence of animals and subsequent evolution, as well as the origin of life and emergence of eukaryotes, were also key events in the evolution of life. Recent paleontological studies have clarified the emergence of multi-cellular animals, soft-bodied Ediacaran fauna and calcified metazoa in the Cyrogenian and Ediacaran (*e.g.* Xiao et al., 1998; Amthor et al., 2003; Brasier and Antcliffe, 2004). Thereafter, Cambrian-type shelly faunas and all present animal phyla had appeared by the early Cambrian (*e.g.* Bengston et al., 1991).

Studies concerning paleo-environment and evolution of life from the Neoproterozoic to the Cambrian have been conducted worldwide. Owing to the relatively good preservation of fossils and continuous successions, the Cryogenian-early Cambrian strata in South China also play an important role in exploring the relationships between evolution of life and paleo-environmental changes. Among them, the "Chengjiang Fauna" in the Maotianshan shale is composed of many kinds of important animal fossils and attracts increasing attention, because its depositional age is older than that of the "Burgess Fauna" in British Columbia (Shu et al., 1996). Therefore, many paleontological and geochemical studies have focused on the strata in South China. Present paleontological, geochemical and geo-chronological datasets are insufficient for detailed determination of surface environmental changes and their influence on biological activity and evolution. Previous studies concerning paleo-environment were based only on some proxies (at most, $\delta^{13}C_{carb}$, $\delta^{13}C_{org}$, $\delta^{18}O$,

$\delta^{34}S$ and $^{87}Sr/^{86}Sr$), and their time resolutions and continuities are insufficient. In addition, the exact antero-posterior relationships remain uncertain.

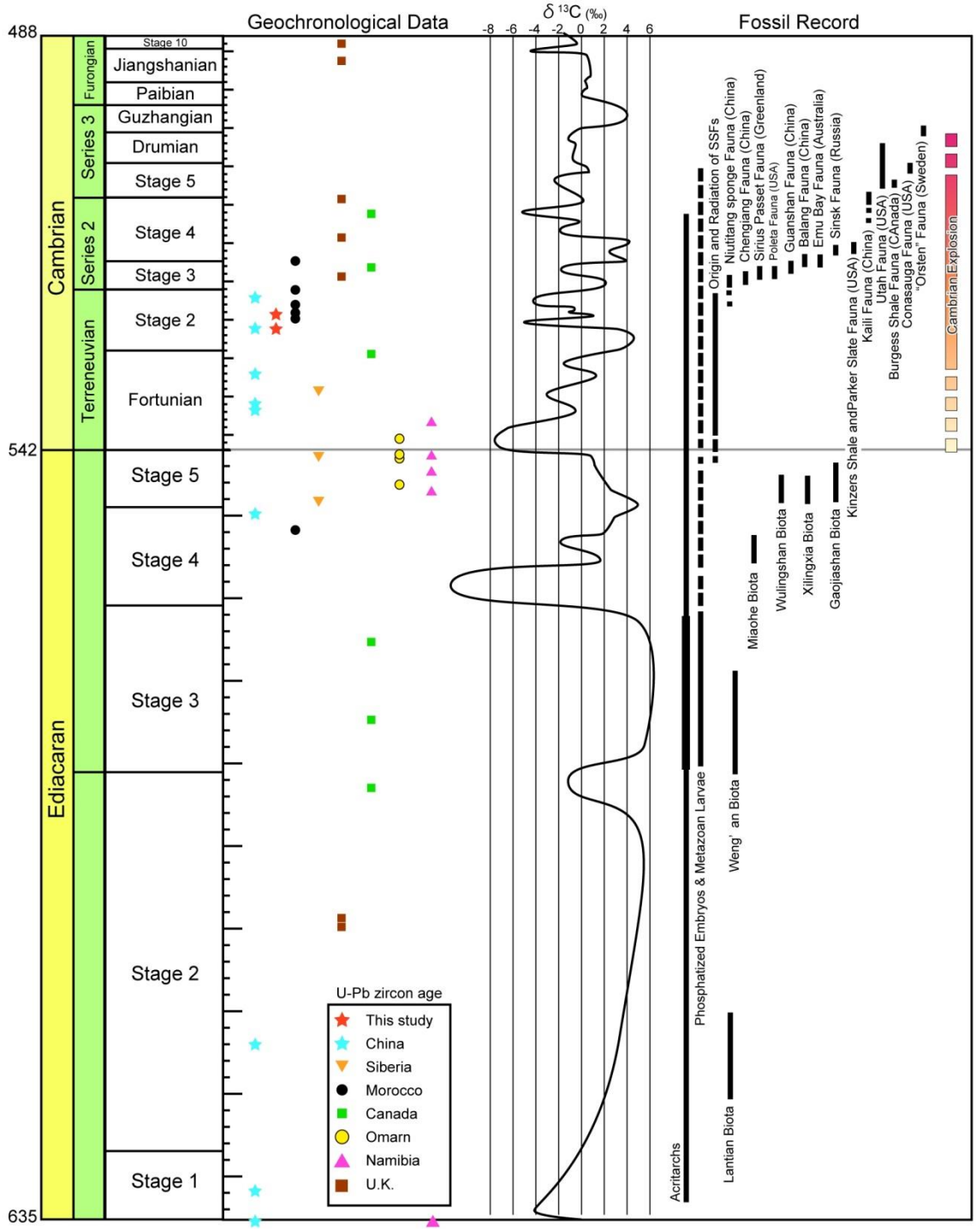

Figure 6-1. The emerging Standard Chronostratigraphic Framework for the Ediacaran and Cambrian System of South Cniha (modified after Babcock et al., 2005; Zhu et al., 2006), showing key biotas, bio-events and physico-chemical correlation signals with compilation of zircon U-Pb ages (modified

after Benus et al., 1988; Haliday et al., 1989; Bowring et al., 1993; 2003; 2007; Isachsen et al., 1994; Grotzinger et al., 1995; Landing et al., 1998; Amthor et al., 2003; Halliday et al., 1989; Dempster et al., 2002; Condon et al., 2005; Maloof et al., 2005, 2010: Zhu et al., 2009; Liu et al., 2009). The curve of $\delta^{13}C$ is a composite based on various published data sources (*e.g.* Peng et al., 2004; Zhu et al., 2004; Babcock et al., 2005; Maloof et al., 2005; 2010; Kouchinsky et al., 2005; Ishikawa et al., 2008).

We have conducted detailed geological surveys since 2004 and carried out on-land drilling at 22 sites in 5 regions (Fig. 6-2a). Three Gorges, Weng'an, Shiduping, Tianping and Chengjiang, in order to collect fresh and continuous rock specimens. Although quite continuous chemostratigraphies at intervals of centimeters are obtained ($\delta^{13}C_{carb}$, $\delta^{13}C_{org}$, $\delta^{18}O$; Ishikawa et al., 2008; 2013; Tahata et al., 2013: $\delta^{15}N$; Kikumoto et al., in this volume: $^{87}Sr/^{86}Sr$, $\delta^{88}Sr$; Ohno et al., 2008; Sawaki et al., 2008a; 2010: $\delta^{44/42}Ca$; Komiya et al., 2008; Sawaki et al., in this volume: phosphorus contents; Shimura et al., in this volume: REE contents; Komiya et al., 2008), existing age constraints are limited. The aim of this study is to refine the geochronology of the study area using igneous zircons extracted from tuffaceous beds in the Cambrian successions in the Three Gorges and Chengjiang regions (Fig. 6-3). Igneous zircons separated from these tuffaceous beds can be used for age dating. In addition, provenance analysis by detrital zircons has been recently introduced (*e.g.*, Rino et al., 2004, 2008; L. J. Wang et al., 2010, 2012). Generally speaking, sandstones contain many detrital zircons that can provide information about their source rocks. In this regard, studies of detrital zircons from the Yangtze block have focused on crustal evolution and have demonstrated the presence of distinctive age populations (Zhang et al., 2006a; Liu et al., 2008; L. J. Wang et al., 2010; 2012; 2013) that have application for interpreting our data.

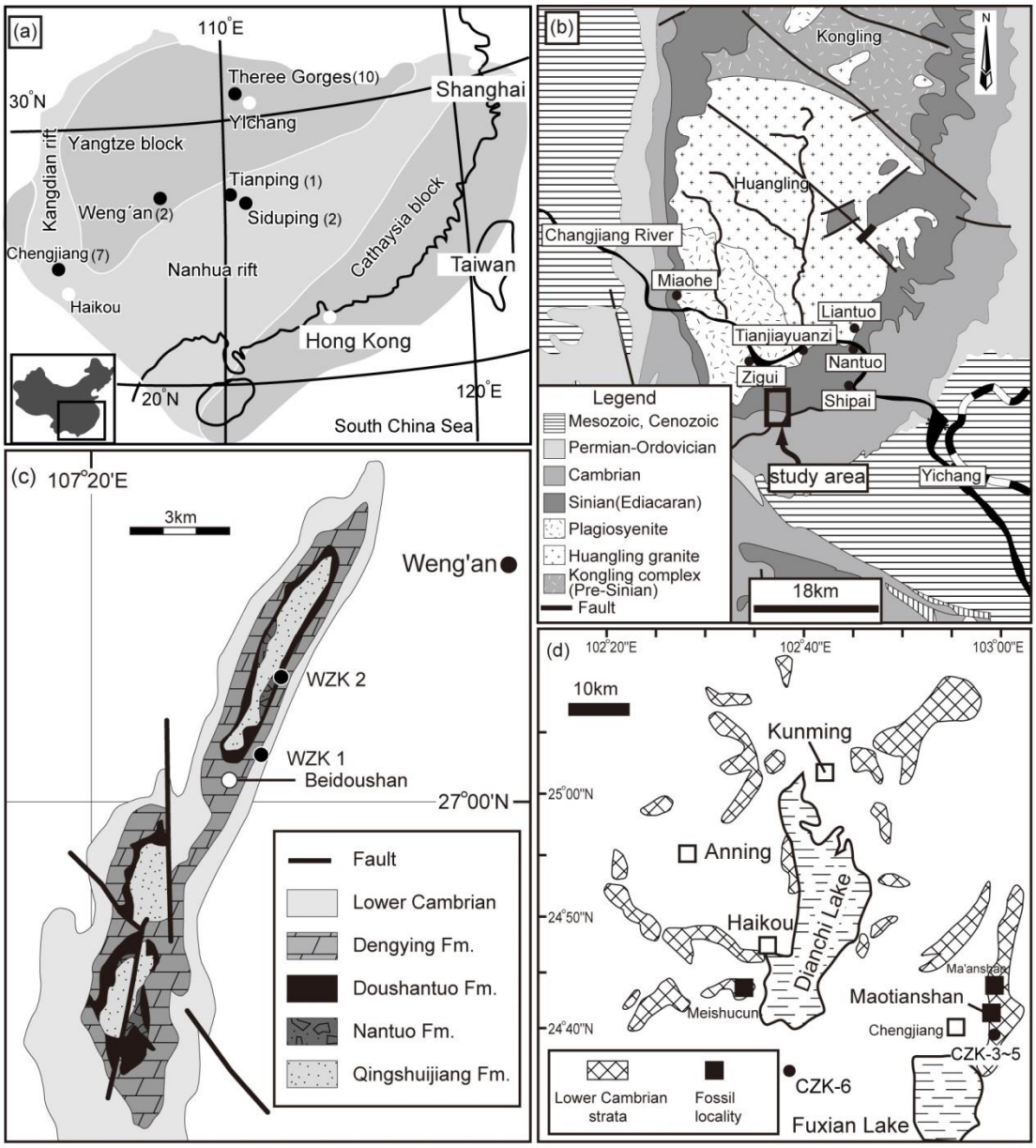

Figure 6-2. (a) Simplified paleogeographic map of the Yangtze Platform around 600 Ma (modified after Jiang et al., 2003). Large black circles indicate our geological survey areas. Numbers in parenthesis represent the numbers of drill-core samples collected by our group. (b) Geological map of the Three Gorges area, South China, showing our study area marked by a box along the Yangtze River. (c) Simplified geological map of the Weng'an area. Samples were collected in the Beidoushan area (modified after Komiya et al., 2008). (d) Very simplified geological map of Yunnan province, showing the distribution of Neoproterozoic to Cambrian strata (modified after Zhang et al., 2001). The Maotianshan section is located at the southeastern side of Dainchi Lake.

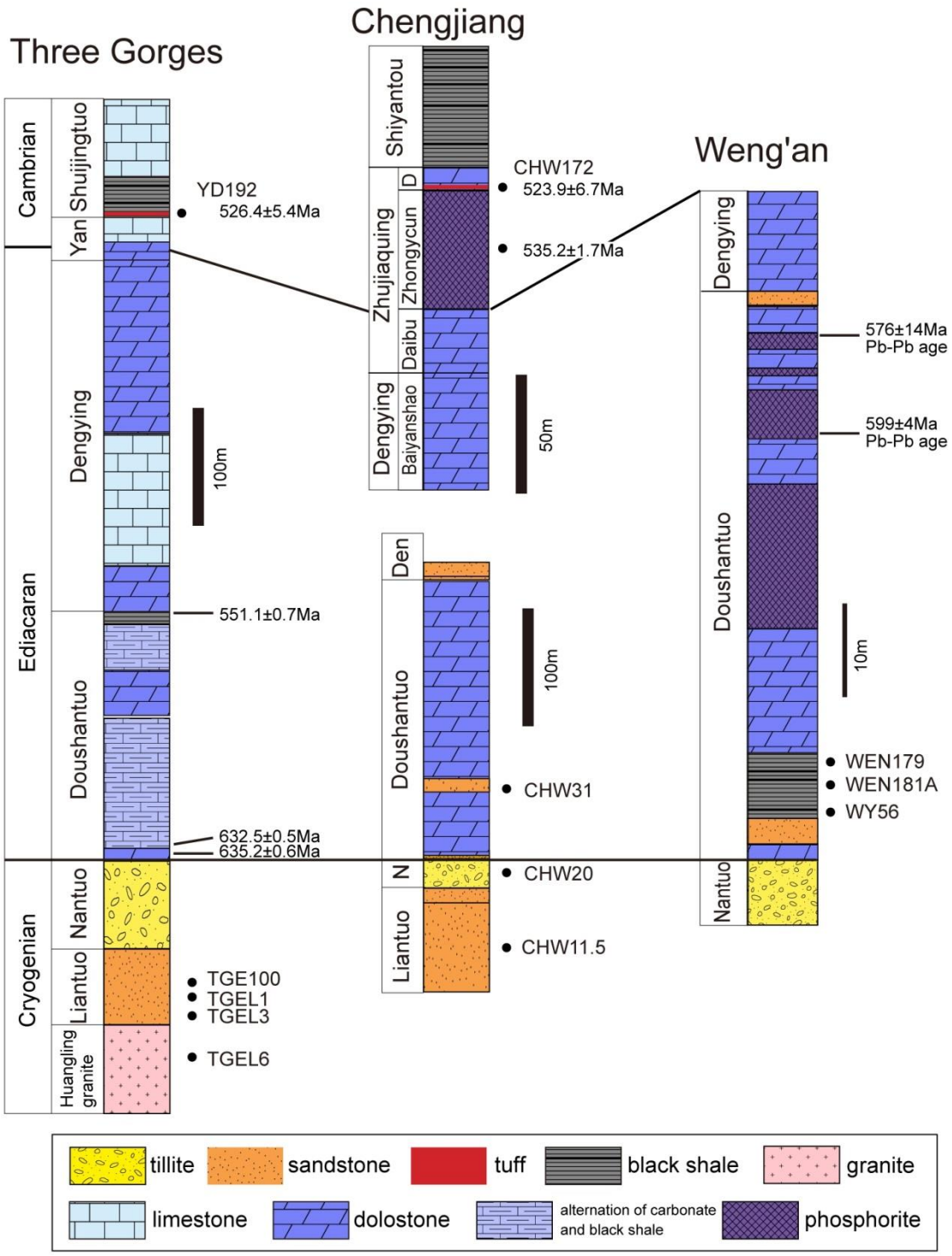

Figure 6-3. Simplified lithostratigraphic columns with chronological data in the Three Gorges, Chengjiang, Maotianshan and Weng'an areas, South China (age data from Barfod et al., 2002, Chen et al., 2004, Condon et al., 2005 and this study). Sample numbers represent stratigraphic positions in each column. N - Nantuo Fm, Den - Dengying Fm, D - Dahai member.

To further enhance knowledge of the geochronology of Cambrian successions in the Three Gorges and Chengjiang regions, we present new zircon U-Pb ages by LA-ICP-MS and Nano-SIMS from tuff beds in the Cambrian successions in the Three Gorges and Chengjiang regions. We will discuss the meaning of the new U-Pb ages, and compare carbon isotope ratios in South China, Siberia and Morocco based on the new data. In addition, we separated detrital zircons from sandstones in the Three Gorges, Weng'an and Chengjiang regions, which provide us information about the paleo-hinterland of the Nanhua and Kangdian rift basins (Fig. 6-2a).

6-2 Geology

Neoproterozoic to Cambrian strata are widely distributed in South China (Fig. 6-2a). These sedimentary rocks were deposited in a basin related to the rifting of the Yangtze and Cathaysia Blocks, amalgamated along the Jiangan orogen (X.H. Li et al., 2003b)The lower half of the strata comprises basaltic and rhyolitic volcanic rocks, carbonates, clastic sediments, black shales and tillites, which were deposited in the N-S and NE-SW trending Nanhua and Kangdian rift basins from *ca.* 800 Ma (X. H. Li et al., 2002). The upper half of the strata is composed of Ediacaran to Cambrian dolomitic limestone, dolostone, black shale, limestone, and mudstone, which were deposited on the southern margin of the Yangtze Block (*e.g.* the Yangtze Platform). All rock samples used for this study were collected at outcrop, aside from the drill core samples.

6-2-1 Three Gorges area

In the Three Gorge area in Hubei Province the Cryogenian to Cambrian strata were deposited on the Western Hubei platform. They occur around the dome of the

Huangling granite and Kongling Complex (Fig. 6-2b). The study section at Wuhe-Aijiahe is one of the best-known sections in the Three Gorge area (study area in Fig. 6-2b). The Cryogenian to early Cambrian section consists of six formations (Fm) in ascending order; Liantuo, Nantuo, Doushantuo, Dengying, Yanjiahe and Shuijingtuo (Fig. 6-3; *e.g.* Zhang, 1981; Zhao et al., 1985; Zhou and Xu, 1987; Chen, 1987; Zhao et al., 1988; Ding et al., 1996). The Liantuo Fm is about 400 m thick, and is composed of *ca.* 748 Ma sandstones (Ma et al., 1984). We collected red sandstones (Fig. 6-3; TGE100, TGEL3 and TGEL1) for provenance analyses. In addition, we collected a rock sample from the Huangling granite as TGEL6 for comparison with these sandstones. The Nantuo Fm comprises a 40 m thick tillite, which corresponds to the Marinoan glaciation (Hoffman and Schrag, 2002; Condon et al., 2005). The basal Doushantuo Fm is composed of a characteristic cap carbonate sequence (*e.g.* Jiang et al., 2003). The Middle and Upper parts of the Doushantuo Fm consist of dolostone and black shale. The age of the boundary between the Doushantuo and overlying Dengying formations is constrained by a zircon U-Pb age (551.7 ± 0.7 Ma; Condon et al., 2005; 555.2 ± 6.1 Ma; Zhang et al., 2005). The Dengying Fm is a thick carbonate sequence, and the overlying Yanjiahe Fm consists of dolomitic muddy limestone, calcareous black shale, and minor sandstone and chert (Fig. 6-4a). The boundary between the Yanjiahe Fm and overlying Shuijintuo Fm is a possible disconformity (Fig. 6-4b). The Shuijigntuo Fm mainly consists of black shale with many prominent carbonate nodules. We discovered a new tuff bed at the bottom of the Shuijigntuo Fm. The tuff layer (YD192) is pale brown to white and a few centimeters thick (Fig. 6-4c).

According to paleontological studies in this area (Chen, 1984; Qian, 1999), *Protohertzina anabarica* and *Anabarites trisulcatus* (Small Shelly Fossils (SSFs) Zone

1; Steiner et al., 2007), key fossils of the Nemakit-Daldynian stage, first appear at a horizon 11.7 m above the Dengying/Yanjiahe boundary, and Tommotian-type SSFs (*e.g. Aldanella*; SSFs Zone 3; Steiner et al., 2007) occur at 2.7 m below the Yanjiahe/Shuijingtuo boundary (Fig. 6-4a). Also, trilobites corresponding to the Atdabanian stage first appear in the upper part of the Shuijingtuo Fm (Ding et al., 1992; Zhu et al., 2003).

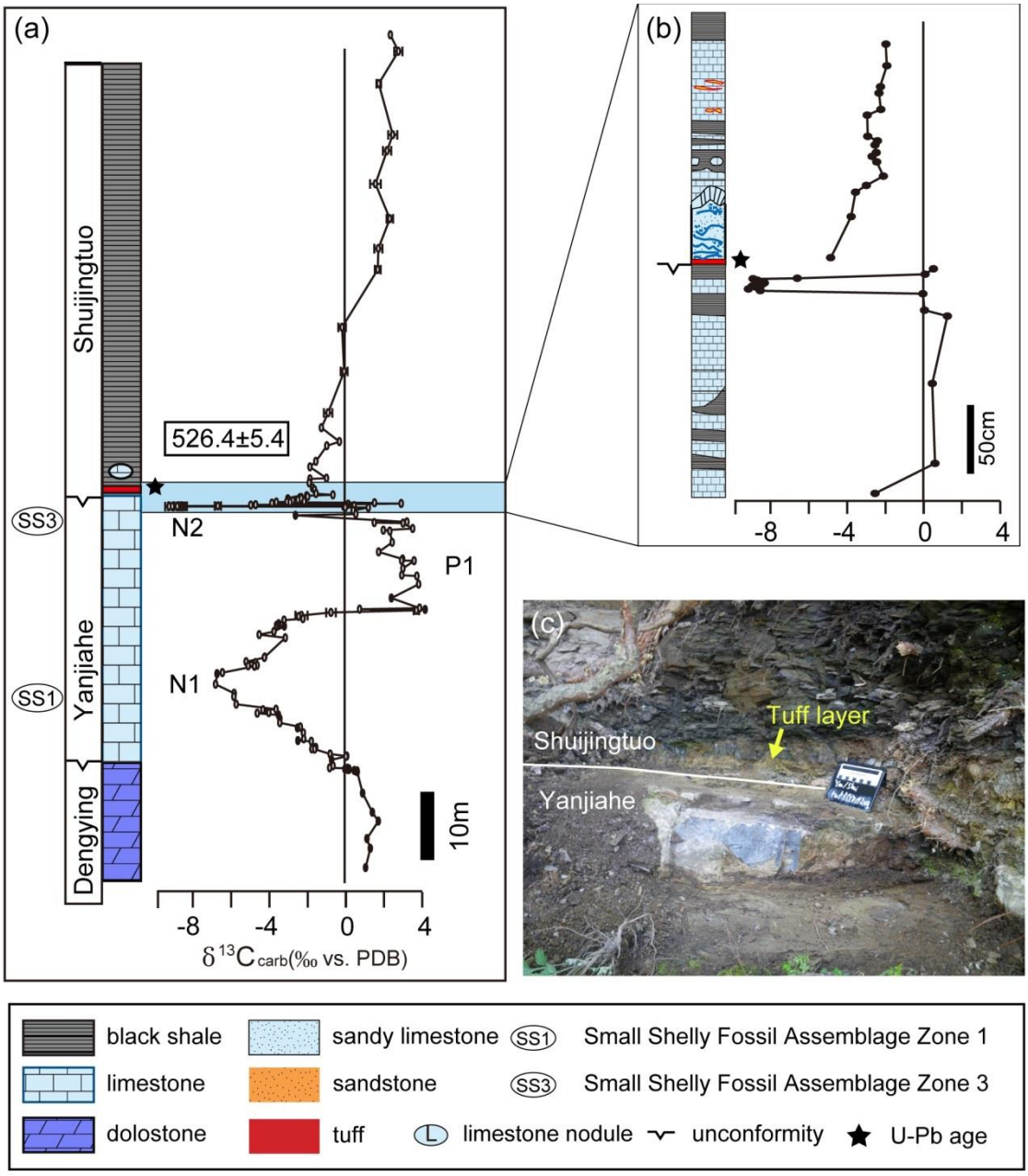

Figure 6-4. (a) Lithostratigraphic column, carbon isotope excursion and fossil zonation of small shelly fossils (SSFs) in the early Cambrian succession in the Three Gorges area. (b) Enlarged lithostratigraphic column and carbon isotope profile around the Yanjiahe/Shuijingtou Fms boundary. (c) Field photograph of tuff layer (YD192) at the base of the Shuijingtou Fm. Sketch book for scale is 10 cm long.

6-2-2 Weng'an area

The Neoproterozoic successions in the Weng'an area of the Guizhou Province (Fig. 6-2c) comprise the Nantuo, Doushantuo and Dengying formations in ascending order (Fig. 6-3). Importantly these rocks contain one of the oldest animal embryo and multicellular algal fossils yet discovered (*e.g.* Xiao et al., 1998) and the Weng'an is clearly one of the most famous fossil localities.

Regionally, the Doushantuo Fm overlies the older metamorphic Qingshuijiang Fm of the Banxi Group, and sporadically overlies the Marinoan Nantuo tillite (Yin et al., 2004; Zhou et al., 2004), and it underlies a thick dolostone layer of the Dengying Fm. The *ca.* 70 m thick Doushantuo Fm, which is relatively thin compared with those in other regions in South China (Fig. 6-3), is mainly composed of phosphorite, dolostone and black shale (Chen et al., 2004). We collected clastic sediments from the lower part of the Doushantuo Fm for provenance analyses (Fig. 6-3; WY56, WEN179 and WEN181A). Abundant fossils of animal embryos and multicellular algae were discovered in phosphorites in the upper Doushantuo Fm (Xiao et al., 1998), and a subaerial exposure surface was reported from the base of the upper Doushantuo Fm (Xue et al., 1998; Wang et al., 1998). Lu–Hf and Pb–Pb isochron ages from the upper part of the Doushantuo Fm yielded ages of 602 ± 43 Ma, 599 ± 4 Ma and 576 ± 14 Ma respectively (Fig. 6-3; Barfod et al., 2002; Chen et al., 2004).

The Dengying Fm is mainly composed of course-grained white dolostones. The

top of the Dengying Fm locally contains Cambrian-type SSFs, therefore, the Precambrian/Cambrian (PC/C) boundary is located in the succession (Wang et al., 1984).

2-3 Chengjiang area (Maotianshan)

The Chengjiang area in Eastern Yunnan Province lies on the southwestern margin of the Yangtze Platform (Fig. 6-2a), where the upper Cryogenian to lower Cambrian successions are well exposed (Fig. 6-2d). They contain abundant fossils, including “Chengjiang Fauna”, and thus were one of the candidates for a standard for the stratigraphic subdivision and correlation of the Lower Cambrian (Luo et al., 1984). The Maotianshan section in Chengjiang County is located on the northeastern side of Fuxian Lake, 35 km east of the Meishucun section, which is one of the well-studied sections of Chengjiang fossils (Fig. 6-2d). The Cryogenian to early Cambrian succession in the Chengjiang area consists of the Liantuo, Nantuo, Doushantuo, Dengying, Zhujiaquing and Shiyantou formations in ascending order (Fig. 6-3).

The Liantuo Fm is about 50 m thick and mainly consists of cross-laminated sandstone. The Doushantuo Fm rests conformably on tillite of the Nantuo Fm, and is mainly composed of dolostone, dolomitic sandstone and subordinate amount of black shales. We collected the clastic sediments from these three formations (Fig. 6-3; CHW11.5, CHW20 and CHW31) for provenance analyses. The Dengying Fm comprises massive dolostone and sandstone, and the upper part consists of limestone.

Thick phosphorite deposits around PC/C boundary are ubiquitous in the Chengjiang area. The base of the Zhujiaquing Fm contains various SSFs, which indicates that the PC/C boundary in this section located here (e.g. Siegmund 1997;

Steiner et al, 2007). The Zhujiaquing Fm consists of three members; Daibu, Zhongyicun and Dahai in ascending order (Fig. 6-3). The Daibu Member is characterized by dolostone. The Zhongyicun Member, *ca.* 50 m thick, is characterized by dolomitic phosphorite and sandstone. Dolostone in the Dahai Member is very thin, *ca.* 2 m thick. We newly identified an acidic tuff bed at the bottom of the Dahai member and collected the rock sample (Fig. 6-3; CHW172). The Shiyantou Fm is mainly composed of black shale, which contains many phosphoritic nodules at the bottom. The upper part of the Shiyantou Fm contains abundant animal fossils, the so-called "Chengjiang Fauna" (*e.g.* Shu et al., 1984).

2-4 Pre Cryogenian Rocks in the Yangtze craton

We briefly introduce the pre-Cryogenian rocks in the Yangtze craton. Outcrops of Archean and Paleoproterozoic crystalline basement are scarce in South China, the oldest being the Kongling complex near Yichang (Fig. 6-2b), which has 3.3-3.2 Ga and 3.0-2.8 Ga TTGs (Tonalite-Trondjhemite-Granodiorite) that have suffered from modification by *ca*. 2.75 Ga high-grade metamorphism, and 1.9-1.8 Ga granitic intrusive rocks (Qiu et al., 2000; Jiao et al., 2009; Gao et al., 2011; Zhang and Zheng, 2013). Another Paleoproterozoic rocks have been found in Houhe complex, which has about 2.1 Ga from gray gneiss (Ling 1996; Wu et al., 2012).

Other pre-Cryogenian rocks are commonly metamorphosed to greenschist facies. In spite of their widespread occurrence around the Yangtze craton, their ages and tectonic significance are generally poorly understood. They underwent tight folding and erosion prior to the deposition of young (< 820 Ma) volcaniclastic rocks. A prominent angular unconformity, found throughout much of South China, has been interpreted as a

consequence of the “Sibao Orogen” (Z. X. Li et al., 2003a), the timing and kinematics of which are also poorly constrained. The Tianli Schist in the southern margin of the Yangtze block has Ar-Ar ages of 1042 ± 7 Ma and 1015 ± 4 Ma (Z. X. Li et al., 2007). In the eastern Sibao Orogen arc volcanics in the Shuangxiwu have SHRIMP U-Pb zircon ages of 970-890 Ma (X. H. Li et al., 2009). A 970 Ma granite in the Gan-Wan arc/ophiolitic belt dates the period of subduction (W. X. Li and X. H. Li, 2003). Amphibole in blueschists at the same locality provides an Ar-Ar age of *ca.* 900 Ma (Xu et al., 1992). Thus the eastern segment of this orogen probably culminated at *ca.* 900 Ma.

In western Sibao Orogen there is a *ca.* 1000 Ma (SHRIMP U-Pb zircon) granitic gneiss in southern Sichuan province, and a 857 ± 13 Ma granodiorite in southern Sichuan that intrudes Mesoproterozoic rocks (X. H. Li et al., 2003a) constraining the younger age limit of the Sibao orogeny. A Sibao-age arc (> 900 Ma) also exists along the northern margin of the Yangtze craton (Ling et al., 2003). A number of Sibao-age syn-tectonic granitoids have recently been reported along the Sibao Orogen; their crystallization age range from *ca.* 1060 to 990 Ma (Liu et al., 2001; Chen et al., 2001; Z. X. Li et al., 2002).

There are a few minor *ca.* 860 Ma intrusive rocks in South China. *Ca.* 850-860 Ma magmatic zircons in younger pre- and syn-rift granites in some regions indicate the presence of *ca.* 850-860 Ma igneous rocks (H. W. Zhou et al., 2002; X. H. Li et al., 2003b, Z. X. Li et al., 2003b; X. H. Li et al., 2008; W. X. Li et al., 2010). Mafic to ultramafic intrusions are widespread in northern Guangxi in the southern Yangtze block, and their age is *ca.* 820 Ma (Zhao et al., 1994; Wingate et al., 1998; Z. X. Li et al., 1999; Sinclair, 2001; M. F. Zhou et al., 2002). But Neoproterozoic granitoids are also

widespread in the Yangtze block. U-Pb zircon analyses indicate that pre-rift granitoids formed synchronously at *ca.* 820 Ma, including the Huanling granite (819 ± 7 Ma) in Hubei, and the Eshan granite (819 ± 8 Ma) in central Yunnan (Ma et al., 1989; Roger and Calassou, 1997; X. H. Li et al., 2003b). The 810-750 Ma syn-rift intrusions and volcanic rocks within the Kangdian Rift were partly generated as the result of a mantle superplume beneath the Rodinia super-continent (Z. X. Li et al., 2003a).

6-3 Method

6-3-1 Sample preparation and cathodoluminescence images of zircons

We separated zircons from the tuff layers (YD192, CHW172) and sandstones. The zircons were extracted using a mineral separation system at the Tokyo Institute of Technology, and were then mounted on 10 mm epoxy discs. The zircons were polished until the midsections of the grains were exposed. Final polishing was performed with a 0.25 μm diamond paste. Cathodoluminescence (CL) images were obtained using a JEOL JSM-5310 scanning electron microprobe combined with an Oxford cathodoluminescence system at the Tokyo Institute of Technology. The detailed analytical method is described elsewhere (Iizuka et al., 2005, 2007). The zircons display various internal structures; oscillatory zonation, inherited cores, dull structures, mottled structure and overgrowths (Fig. 6-5). The internal structures are empirically used to identify the igneous origin and to evaluate the influence of alteration and late-stage thermal modification. The CL images show that *ca.* 30 % of zircons from the tuff beds have oscillatory rims and inherited cores with white dusty structures or dull structures and *ca.* 70 % of the zircons display no zonation or mottled structure. Although some magmatic zircons also display dull structures, metamorphic or re-crystallized zircons

commonly show these textures. In addition, many zircons contain mineral inclusions, which we checked under a microscope, and thus were able to avoid mineral inclusions during the U-Pb isotope analyses. We analyzed U-Pb ratios of the oscillatory rims to determine the igneous age of the individual grains from the tuffs and sandstones.

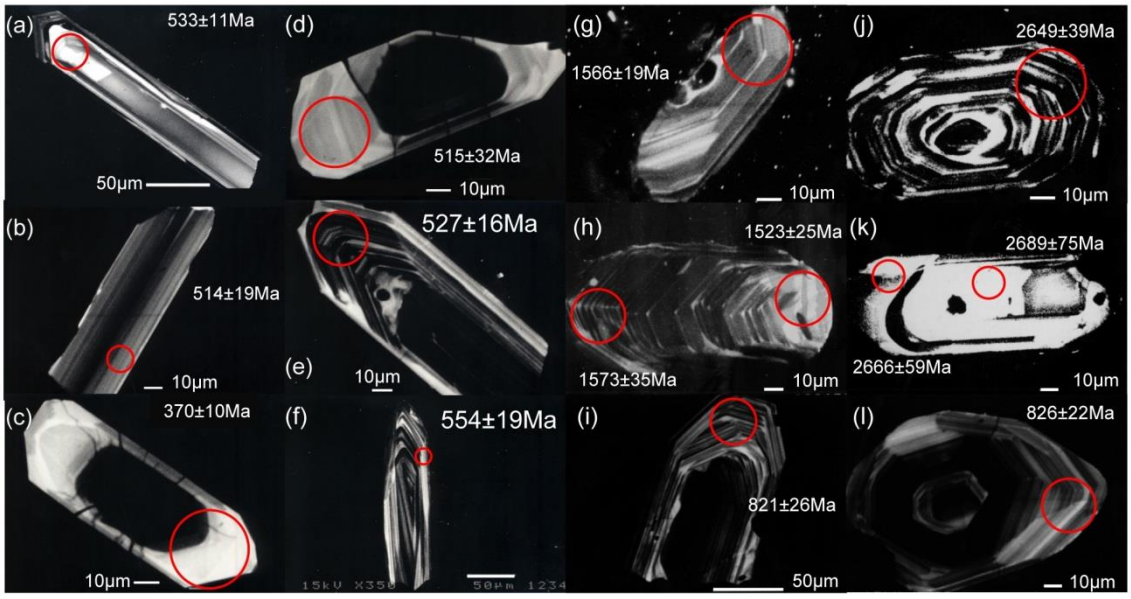

Figure 6-5. Cathodoluminescence images of zircons from tuff layers (a-d, YD192; e-f, CHW172) and sandstones (g CHW31; h and l, WEN181A; i, TGEL6, j and k, TGEL1), and ^{238}U-^{206}Pb ages determined with LA-ICP-MS. Red circles represent analytical spots.

6-3-2 Analytical methods with LA-ICP-MS and Nano-SIMS instruments

In-situ U-Pb analyses were performed with a LA-ICP-MS at Kyoto University, and with an ion microprobe (Cameca Nano-SIMS50) at the Ocean Research Institute of the University of Tokyo. The ICP-MS is a ThermoElemental VG PlasmaQuad 2, quadrupole-based ICP-MS equipped with an S-option interface (Hirata and Nesbitt 1995). The laser ablation is a MicroLas production (Gottingen, Germany) GeoLas 200CQ laser ablation system. Analytical uncertainties combine counting statistics and the reproducibility of the standard analyses (NIST 610 for $^{207}Pb/^{206}Pb$ and Nancy 91500

standard zircon for $^{206}Pb/^{238}U$), added in quadrature. The details of the analytical methods were reported elsewhere (Iizuka and Hirata, 2004; Rino et al., 2004; Iizuka et al., 2006, 2007). After measurements with the LA-ICP-MS, some zircons extracted from the tuff beds were also dated with the Cameca Nano-SIMS50 ion microprobe. The mounts were slightly polished with 0.25 μm diamond paste in order to remove zircon powder due to the laser ablation by ICP-MS. Then, the mounts were cleaned by ethanol and pure water, and coated with gold to dissipate any charge during the SIMS analysis. Using a critical illumination mode, a 5-8 nA mass filtered O- primary beam was used to sputter a spot with a diameter of 10-15 μm. Secondary positive ions were extracted for mass analysis by a high mass resolution method. Before the actual analysis, the sample surface was pre-sputtered 8 minutes, including tuning time. $^{28}Si^+$, $^{204}Pb^+$, $^{206}Pb^+$, $^{238}U^{16}O^+$ and $^{238}U^{16}O_2{}^+$ ions were measured simultaneously for 500 seconds in order to estimate the U-Pb age and U and Pb contents. The intensity of $^{28}Si^+$ ion was measured with a Faraday cup, while those of the other ions were measured with electron multiplier pulse counting detectors (EM#4: $^{204}Pb^+$, EM#4B: $^{206}Pb^+$, EM#5: $^{238}U^{16}O^+$, LD: $^{238}U^{16}O_2{}^+$). The entrance and exit slits (for Faraday cup, EM#1-EM#5, and LD) were set to about 40 μm and 50 μm, respectively. A mass resolution of 3500 at 1 % peak height was attained to separate $^{206}Pb^+$ from $^{176}Hf^{28}Si^+$ with adequate flat-topped peaks. $^{204}Pb^+$ beams are also discriminated from $^{178}Hf^{28}Si^+$ beams. A Pb sensitivity of 2.3 cps/nA O-/ppm was obtained. The difference in the sensitivity of EM#4 and EM#4B was calibrated, using a $^{208}Pb^+$ beam with magnet scanning, which was 1.012 ± 0.003 at the time of the analysis. The $^{206}Pb/^{238}U$ ratio of an unknown sample was estimated by the following empirical equation:

$$(^{206}Pb/^{238}U)_{sam} = (^{206}Pb^*/^{238}U)_{QCNG}$$

$\times(^{206}Pb/^{238}UO^{+})_{sam}/\{a(UO_2^{+}/UO^{+})^2_{sam} + b\}$

where subscripts of "sam" and "QCNG" indicate ratios of the unknown sample and a standard zircon. QGNG is a multi-crystal zircon standard from a Quartz–Gabbro–Norite–Gneiss from Cape Donnington, Eyre Peninsula, South Australia, whose U/Pb age by thermal ionization mass spectrometry (TIMS) is 1849.8 ± 1.1 Ma (Black et al., 2005). Constants "a" and "b" were estimated by repeated measurements of the standard. More detailed descriptions are given elsewhere (Takahata et al., 2008).

6-4 Results

6-4-1 Zircon U-Pb ages from the Cambrian tuff beds

All analytical data with LA-ICP-MS and nano-SIMS are summarized in Tables 1 and 2, respectively. The U-Pb Concordia diagrams ($^{207}Pb/^{235}U$ versus $^{206}Pb/^{238}U$) of zircons are presented in Figure 6-6. We monitored ^{204}Pb during the analyses by LA-ICP-MS and excluded zircons with detectable ^{204}Pb from Table 1, since the ^{204}Pb is not radioactive in origin. The ten zircons of YD192 plot off the concordia curve within analytical error, which is likely due to partial loss of Pb (Table 1). Six zircons plot on the concordia curve within analytical error represent the true igneous age of the tuff bed (Fig. 6-6a). The weighted mean $^{207}Pb/^{206}Pb$, $^{206}Pb/^{238}U$ and $^{207}Pb/^{235}U$ ages are 564.3 ± 150 Ma (MSWD = 2.0), 520 ± 10 Ma (MSWD = 1.9) and 526 ± 33 Ma (MSWD = 2.6), respectively. Also, the Concordia age is calculated as 520.3 ± 8.5 Ma (MSWD = 0.39) using the ISOPLOT program of Ludwing (1991).

Table 1
LA-ICP-MS U.Pb isotopic analytical data for zircons from tuff samples

Grein	Th (ppm)	U (ppm)	$^{206}Pb/^{238}U$ (2s)	$^{207}Pb/^{235}U$ (2s)	$^{207}Pb/^{206}Pb$ (2s)	Age (Ma) $^{206}Pb/^{238}U$ (2s)	$^{207}Pb/^{235}U$ (2s)	$^{207}Pb/^{206}Pb$ (2s)	Concordance
YD192-1	26	42	0.0832 ± 0.0054	0.713 ± 0.177	0.0622 ± 0.015	515 ± 32	547 ± 100	681 ± 530	0.94
YD192-2	109	158	0.0831 ± 0.0033	0.681 ± 0.089	0.0594 ± 0.007	514 ± 19	527 ± 52	582 ± 274	0.98
YD192-3	141	223	0.0856 ± 0.0028	0.786 ± 0.080	0.0666 ± 0.006	529 ± 17	589 ± 45	825 ± 202	0.90
YD192-4	756	433	0.0828 ± 0.0024	0.632 ± 0.054	0.0553 ± 0.004	513 ± 14	497 ± 33	424 ± 180	0.97
YD192-5	76	91	0.0826 ± 0.0018	0.650 ± 0.053	0.0570 ± 0.004	512 ± 10	508 ± 32	492 ± 173	0.99
YD192-6	245	291	0.0859 ± 0.0019	0.695 ± 0.050	0.0587 ± 0.004	531 ± 11	536 ± 30	556 ± 151	0.99
YD192-7	59	62	0.0647 ± 0.0039	1.072 ± 0.190	0.1202 ± 0.020	404 ± 24	740 ± 89	1959 ± 302	0.55
YD192-8	87	43	0.0504 ± 0.0040	0.551 ± 0.154	0.0792 ± 0.021	317 ± 24	446 ± 96	1177 ± 551	0.71
YD192-9	61	54	0.0581 ± 0.0029	0.771 ± 0.125	0.0962 ± 0.015	364 ± 17	580 ± 69	1552 ± 293	0.63
YD192-10	106	43	0.0555 ± 0.0042	0.777 ± 0.186	0.1016 ± 0.023	348 ± 25	584 ± 101	1654 ± 433	0.60
YD192-11	85	179	0.0458 ± 0.0021	0.489 ± 0.073	0.0774 ± 0.011	289 ± 13	404 ± 49	1132 ± 286	0.71
YD192-12	48	81	0.0571 ± 0.0032	0.604 ± 0.119	0.0768 ± 0.015	358 ± 20	480 ± 73	1116 ± 385	0.75
YD192-13	25	43	0.0712 ± 0.0048	1.198 ± 0.235	0.1221 ± 0.023	443 ± 29	800 ± 103	1987 ± 333	0.55
YD192-14	48	103	0.0455 ± 0.0012	0.385 ± 0.038	0.0614 ± 0.006	287 ± 7	331 ± 27	653 ± 205	0.87
YD192-15	84	55	0.0674 ± 0.0041	1.288 ± 0.215	0.1386 ± 0.022	421 ± 24	841 ± 91	2210 ± 273	0.50
YD192-16	43	81	0.0534 ± 0.0014	0.707 ± 0.057	0.0959 ± 0.007	336 ± 9	543 ± 33	1546 ± 143	0.62
CHW172-1	65	143	0.0898 ± 0.0033	0.808 ± 0.106	0.0653 ± 0.008	554 ± 19	601 ± 58	783 ± 266	0.92
CHW172-2	65	98	0.0837 ± 0.0037	0.806 ± 0.128	0.0698 ± 0.011	518 ± 22	600 ± 69	924 ± 316	0.86
CHW172-3	74	140	0.0867 ± 0.0032	0.771 ± 0.104	0.0644 ± 0.008	536 ± 19	580 ± 58	756 ± 276	0.92
CHW172-4	46	73	0.0862 ± 0.0032	0.721 ± 0.074	0.0607 ± 0.006	533 ± 19	551 ± 43	627 ± 207	0.97
CHW172-5	146	176	0.0830 ± 0.0026	0.716 ± 0.049	0.0626 ± 0.004	514 ± 16	548 ± 29	693 ± 129	0.94
CHW172-6	161	251	0.0851 ± 0.0027	0.715 ± 0.044	0.0609 ± 0.003	527 ± 16	548 ± 26	637 ± 112	0.96
CHW172-7	107	164	0.0874 ± 0.0017	0.747 ± 0.071	0.0620 ± 0.006	540 ± 10	567 ± 40	674 ± 199	0.95
CHW172-8	111	234	0.0861 ± 0.0027	0.754 ± 0.045	0.0635 ± 0.003	532 ± 16	571 ± 26	727 ± 109	0.93
CHW172-9	98	153	0.1440 ± 0.0044	1.249 ± 0.128	0.0629 ± 0.006	867 ± 25	823 ± 56	706 ± 209	0.95
CHW172-10	114	124	0.1413 ± 0.0047	1.305 ± 0.145	0.0670 ± 0.007	852 ± 27	848 ± 62	837 ± 223	1.00
CHW172-11	174	196	0.0950 ± 0.0031	0.700 ± 0.047	0.0534 ± 0.003	585 ± 18	539 ± 28	347 ± 134	0.91
CHW172-12	108	159	0.0843 ± 0.0019	0.774 ± 0.056	0.0666 ± 0.005	522 ± 11	582 ± 32	826 ± 145	0.90
CHW172-13	174	108	0.1253 ± 0.0041	1.462 ± 0.093	0.0846 ± 0.005	761 ± 23	915 ± 38	1307 ± 107	0.83
CHW172-14	130	146	0.0781 ± 0.0026	0.711 ± 0.053	0.0660 ± 0.004	485 ± 15	545 ± 31	806 ± 140	0.89
CHW172-15	240	291	0.0856 ± 0.0014	0.806 ± 0.043	0.0683 ± 0.003	529 ± 8	600 ± 24	878 ± 105	0.88
CHW172-16	47	64	0.1279 ± 0.0033	1.464 ± 0.125	0.0831 ± 0.007	776 ± 19	916 ± 50	1271 ± 159	0.85

Note: all errors are quoted at 2 s level.

Table 2
Nano-SIMS U-Pb isotopic analytical data for zircons from tuff samples

Sample	206Pb com (%)*	U (ppm)	206Pb/238U	2σ	206Pb-238U age (Ma)	2σ
YD192-1	1.7	50	0.0825	0.0029	511	17
YD192-2	0.5	157	0.0842	0.0028	521	17
YD192-3	0.6	55	0.0850	0.0020	526	12
YD192-4	0.4	187	0.0854	0.0018	528	11
YD192-5	0.3	95	0.0861	0.0017	532	10
YD192-6	1.1	197	0.0855	0.0097	529	58
CHW172-1	0.3	194	0.0830	0.0043	514	26
CHW172-2	0.3	121	0.0830	0.0025	514	15
CHW172-3	0.6	153	0.0835	0.0040	517	24
CHW172-4	1.6	103	0.0843	0.0046	522	27
CHW172-5	0.8	118	0.0851	0.0029	527	17
CHW172-6	0.8	85	0.0848	0.0037	525	22
CHW172-7	0.4	99	0.0857	0.0037	530	22
CHW172-8	0.6	149	0.0862	0.0045	533	27
CHW172-9	0.8	201	0.0869	0.0043	537	25
CHW172-10	0.3	303	0.0870	0.0044	538	26

Note: all errors are quoted at 2 s level.
*206Pb com (%)=206Pb common / 206Pb total

Although six zircons from CHW172 also plot off the concordia curve, the remaining eight zircons plot on the concordia curve within analytical error (Fig. 6-6c). On the other hand, the two zircons plot on a concordia curve around 850 Ma. These results possibly are due to contamination by inherited old zircons, despite our careful check of internal structures. Except for the two zircons, the weighted mean $^{207}Pb/^{206}Pb$,

$^{206}Pb/^{238}U$ and $^{207}Pb/^{235}U$ ages are 696 ± 56 Ma (MSWD = 0.71), 533 ± 9.8 Ma (MSWD = 2.2), and 561± 12 Ma (MSWD = 0.50), respectively. And the Concordia age determined by ISOPLOT is 536.6 ± 9.0 Ma (MSWD = 17).

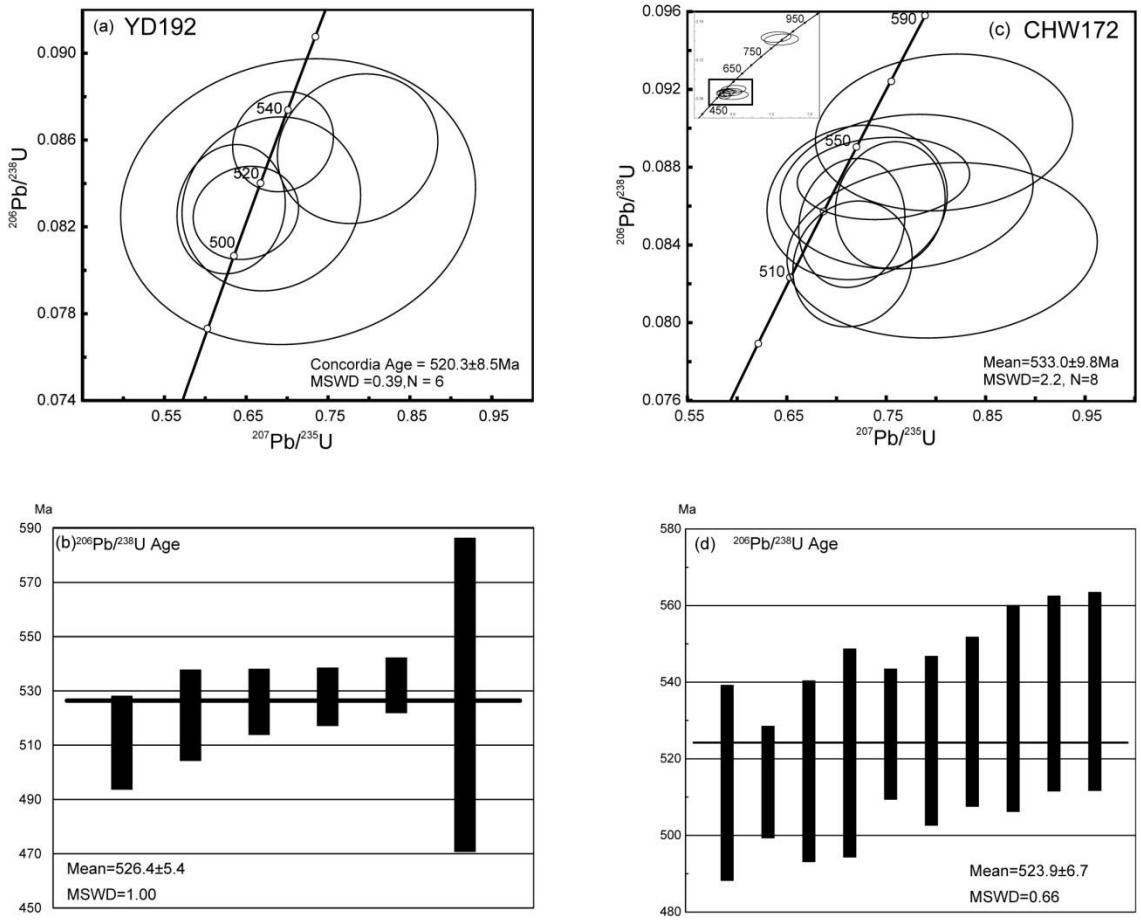

Figure 6-6. Concordia diagrams of in-situ U-Pb dates of zircons with LA-ICP-MS for (a) YD192 and (c) CHW172. These figures were illustrated using the ISOPLOT (Ludwig 1991). Error ellipses on individual spots are at 2σ level. Zircon U-Pb age distribution diagram based on the result of in-situ 238U-206Pb analyses with nano-SIMS for (b) YD192 and (d) CHW172. Central lines represent weighted mean averages of zircon 238U-206Pb ages.

Although Nano-SIMS is unsuitable to analyze both $^{238}U/^{206}Pb$ and $^{207}Pb/^{206}Pb$ at the same time, its merit is its spot size (7~15 μm), which is smaller than that of the LA-ICP-MS. This enables accurate and easy analysis of the rims of zircons. Therefore,

we evaluated the lead loss due to the thermal modifications using the results obtained by LA-ICP-MS and the concordia curve, and we determined the accurate depositional ages from results obtained by Nano-SIMS.

The analyses by Nano-SIMS for YD192 and CHW172 are shown in Figure 6-6b, d. The zircon U-Pb ages in both samples are close to 525 Ma. The weighted average ages of YD192 and CHW172 are 526.4 ± 5.4 Ma (N = 6, MSWD = 1.00), 523.9 ± 6.7 Ma (N = 10, MSWD = 0.66). We apply these ages as the best estimates of the depositional ages of YD 192 and CHW172.

6-4-2 Age spectrum of detrital zircon grains from the Cryogenian to Ediacaran sandstones

The results of U-Pb dating of detrital zircons from sandstones and igneous zircons from a granite by LA-ICP-MS are listed in Table 3-6, and the U-Pb Concordia diagrams ($^{207}Pb/^{235}U$ versus $^{206}Pb/^{238}U$) are presented in Figures 7-7 and 7-8. Most zircons from the sandstones are rounded and show oscillatory zoning under CL images (Fig. 6-5). Some zircons contain an inherited core. About half the zircons from sandstones at Weng'an are euhedral. No systematic differences of the CL images and shapes of zircons were detected in each age population.

The 24 igneous zircons from a granite (TGEL6) plot on a Concordia curve within 2σ error, and their ages range from 794 ± 27 to 893 ± 27 Ma (Fig. 6-7). Disconcordance of the remaining two zircons are more than 10 % (Table S1), indicating a possibility of Pb loss. The maxima in the frequency distribution peak at 810 and 860 Ma (Fig. 6-9). The weighted mean $^{207}Pb/^{206}Pb$, $^{206}Pb/^{238}U$ and $^{207}Pb/^{235}U$ ages are 848 ± 49 Ma (MSWD = 2.1), 836 ± 11 Ma (MSWD = 5.6), 836 ± 14 Ma (MSWD = 2.0),

respectively.

The 23 zircons separated from TGE100, TGEL1 and TGEL3 from the Liantuo Fm in the Three Gorges area show $^{206}Pb/^{238}U$ ages ranging from *ca.* 725 to 2800 Ma. Age spectra of these three sandstones are integrated and shown in Figure 6-9. The age spectrum shows a broad peak at *ca.* 800 Ma (Fig. 6-9). Although one of them plots off the concordia curve, the sandstones apparently include Archean zircon grains (*ca.* 2650 and 2800 Ma). Aside from these, a Paleoproterozoic age ($^{206}Pb/^{238}U$, *ca.* 1850 Ma) is also included. The youngest (725 ± 13 Ma) age constrains the maximum depositional age of the sandstone in the Liantuo Fm.

Table 3
LA-ICP-MS U.Pb isotopic analytical data for zircons from sandstone and granite samples in Three Gorges area

Grein	Th (ppm	U (ppm)	$^{206}Pb/^{238}U$ (2s)	$^{207}Pb/^{235}U$ (2s)	$^{207}Pb/^{206}Pb$ (2s)	Age (Ma) $^{206}Pb/^{238}U$ (2s)	$^{207}Pb/^{235}U$ (2s)	$^{207}Pb/^{206}Pb$ (2s)	Concordance
TGE6-1	139	103	0.133 ± 0.005	1.297 ± 0.108	0.071 ± 0.005	807 ± 30	844 ± 47	945 ± 143	0.96
TGE6-2	71	60	0.140 ± 0.006	1.178 ± 0.129	0.061 ± 0.006	847 ± 35	790 ± 58	634 ± 202	0.93
TGE6-3	16	21	0.135 ± 0.008	1.412 ± 0.235	0.076 ± 0.012	817 ± 46	894 ± 94	1089 ± 283	0.91
TGE6-4	44	43	0.131 ± 0.006	1.355 ± 0.163	0.075 ± 0.008	795 ± 36	870 ± 68	1066 ± 208	0.91
TGE6-5	91	124	0.132 ± 0.005	1.178 ± 0.094	0.065 ± 0.005	800 ± 29	790 ± 43	763 ± 140	0.99
TGE6-6	76	124	0.133 ± 0.005	1.287 ± 0.099	0.070 ± 0.005	805 ± 29	840 ± 43	932 ± 131	0.96
TGE6-7	166	130	0.144 ± 0.004	1.354 ± 0.095	0.068 ± 0.004	865 ± 21	869 ± 40	881 ± 131	0.99
TGE6-8	24	34	0.139 ± 0.006	1.315 ± 0.179	0.069 ± 0.009	840 ± 34	852 ± 76	885 ± 246	0.99
TGE6-9	99	143	0.138 ± 0.003	1.299 ± 0.089	0.068 ± 0.004	834 ± 19	845 ± 39	875 ± 126	0.99
TGE6-10	59	51	0.131 ± 0.005	1.287 ± 0.146	0.071 ± 0.008	794 ± 27	840 ± 63	965 ± 204	0.94
TGE6-11	54	108	0.142 ± 0.004	1.249 ± 0.099	0.064 ± 0.005	858 ± 22	823 ± 44	730 ± 151	0.96
TGE6-12	42	47	0.137 ± 0.005	1.197 ± 0.145	0.063 ± 0.007	827 ± 29	799 ± 65	723 ± 228	0.97
TGE6-13	84	93	0.136 ± 0.005	1.225 ± 0.113	0.065 ± 0.006	824 ± 28	812 ± 50	777 ± 170	0.98
TGE6-14	141	118	0.132 ± 0.003	1.177 ± 0.088	0.065 ± 0.005	800 ± 16	790 ± 40	760 ± 144	0.99
TGE6-15	76	146	0.134 ± 0.003	1.277 ± 0.083	0.069 ± 0.004	812 ± 16	836 ± 36	898 ± 123	0.97
TGE6-16	68	115	0.145 ± 0.003	1.317 ± 0.094	0.066 ± 0.005	870 ± 17	853 ± 41	809 ± 138	0.98
TGE6-17	35	44	0.137 ± 0.005	1.236 ± 0.141	0.066 ± 0.007	825 ± 27	817 ± 62	795 ± 213	0.99
TGE6-18	104	145	0.142 ± 0.003	1.308 ± 0.082	0.067 ± 0.004	855 ± 17	849 ± 35	833 ± 118	0.99
TGE6-19	133	96	0.143 ± 0.003	1.249 ± 0.097	0.063 ± 0.005	860 ± 20	823 ± 43	723 ± 149	0.95
TGE6-20	43	48	0.149 ± 0.005	1.304 ± 0.139	0.064 ± 0.006	893 ± 27	847 ± 60	729 ± 202	0.95
TGE6-21	19	34	0.141 ± 0.005	1.473 ± 0.179	0.076 ± 0.009	848 ± 31	919 ± 71	1095 ± 215	0.92
TGE6-22	109	99	0.135 ± 0.003	1.158 ± 0.092	0.062 ± 0.005	815 ± 19	781 ± 42	685 ± 154	0.96
TGE6-23	60	56	0.140 ± 0.004	1.475 ± 0.139	0.076 ± 0.007	845 ± 24	920 ± 56	1106 ± 169	0.92
TGE6-24	95	119	0.142 ± 0.003	1.332 ± 0.091	0.068 ± 0.004	856 ± 18	860 ± 39	869 ± 128	1.00
TGE6-25	28	31	0.142 ± 0.007	1.695 ± 0.217	0.087 ± 0.010	853 ± 41	1007 ± 79	1358 ± 210	0.85
TGE6-26	37	43	0.127 ± 0.006	1.357 ± 0.164	0.077 ± 0.009	772 ± 35	871 ± 68	1131 ± 206	0.89
TGE100-1	237	185	0.135 ± 0.004	1.219 ± 0.116	0.065 ± 0.006	816 ± 23	809 ± 52	790 ± 179	0.99
TGE100-2	156	141	0.136 ± 0.005	1.306 ± 0.137	0.070 ± 0.007	822 ± 26	849 ± 59	919 ± 192	0.97
TGE100-3	304	176	0.131 ± 0.004	1.215 ± 0.118	0.068 ± 0.006	791 ± 23	808 ± 53	854 ± 180	0.98
TGE100-4	85	60	0.134 ± 0.006	1.209 ± 0.199	0.065 ± 0.010	810 ± 35	805 ± 88	790 ± 300	0.99
TGE100-5	396	445	0.129 ± 0.003	1.280 ± 0.079	0.072 ± 0.004	784 ± 18	837 ± 35	980 ± 112	0.94
TGEL1-1	74	46	0.518 ± 0.018	13.201 ± 0.898	0.185 ± 0.011	2689 ± 75	2694 ± 62	2698 ± 94	1.00
TGEL1-2	58	146	0.542 ± 0.012	13.630 ± 0.539	0.182 ± 0.006	2792 ± 50	2724 ± 37	2674 ± 54	0.98
TGEL1-3	80	45	0.331 ± 0.013	5.213 ± 0.519	0.114 ± 0.010	1842 ± 62	1855 ± 81	1869 ± 157	0.99
TGEL1-4	632	323	0.508 ± 0.009	14.269 ± 0.408	0.204 ± 0.004	2649 ± 39	2768 ± 27	2856 ± 35	0.96
TGEL1-5	84	118	0.130 ± 0.004	1.150 ± 0.141	0.064 ± 0.008	788 ± 26	777 ± 65	746 ± 231	0.99
TGEL3-1	123	154	0.131 ± 0.003	1.161 ± 0.110	0.064 ± 0.006	796 ± 19	783 ± 50	744 ± 182	0.98
TGEL3-2	228	170	0.131 ± 0.003	1.223 ± 0.108	0.068 ± 0.006	796 ± 19	811 ± 48	855 ± 166	0.98
TGEL3-3	108	77	0.143 ± 0.005	1.355 ± 0.169	0.069 ± 0.008	864 ± 28	870 ± 70	884 ± 230	0.99
TGEL3-4	79	121	0.159 ± 0.004	1.523 ± 0.143	0.069 ± 0.006	953 ± 24	940 ± 56	909 ± 175	0.99
TGEL3-5	166	121	0.124 ± 0.004	1.103 ± 0.121	0.065 ± 0.007	752 ± 21	755 ± 57	763 ± 208	1.00
TGEL3-6	108	122	0.133 ± 0.004	1.227 ± 0.127	0.067 ± 0.007	805 ± 22	813 ± 56	834 ± 195	0.99
TGEL3-7	14	29	0.155 ± 0.004	1.538 ± 0.278	0.072 ± 0.013	930 ± 25	946 ± 106	982 ± 326	0.98
TGEL3-8	103	94	0.129 ± 0.003	1.208 ± 0.137	0.068 ± 0.008	781 ± 15	804 ± 61	868 ± 216	0.97
TGEL3-9	36	61	0.143 ± 0.003	1.365 ± 0.181	0.069 ± 0.009	863 ± 18	874 ± 75	902 ± 248	0.99
TGEL3-10	295	133	0.119 ± 0.002	1.129 ± 0.112	0.069 ± 0.007	725 ± 13	767 ± 52	890 ± 189	0.95
TGEL3-11	161	248	0.135 ± 0.002	1.266 ± 0.088	0.068 ± 0.005	816 ± 12	831 ± 38	870 ± 133	0.98
TGEL3-12	39	53	0.127 ± 0.003	1.120 ± 0.174	0.064 ± 0.010	772 ± 18	763 ± 80	737 ± 296	0.99
TGEL3-13	424	315	0.146 ± 0.002	1.344 ± 0.080	0.067 ± 0.004	876 ± 12	865 ± 34	835 ± 117	0.99

Note: all errors are quoted at 2 s level.

Table 4
LA-ICP-MS U-Pb isotopic analytical data for zircons from sandstone samples in Weng'an area

Grein	Th (ppm)	U (ppm)	$^{206}Pb/^{238}U$ (2s)	$^{207}Pb/^{235}U$ (2s)	$^{207}Pb/^{206}Pb$ (2s)	Age (Ma)			Concordance
						$^{206}Pb/^{238}U$ (2s)	$^{207}Pb/^{235}U$ (2s)	$^{207}Pb/^{206}Pb$ (2s)	
WEN179-1	187	172	0.132 ± 0.006	1.202 ± 0.066	0.066 ± 0.002	800 ± 32	802 ± 30	808 ± 72	1.00
WEN179-2	60	60	0.134 ± 0.004	1.252 ± 0.074	0.068 ± 0.004	810 ± 20	824 ± 33	863 ± 109	0.98
WEN179-3	124	178	0.136 ± 0.004	1.253 ± 0.056	0.067 ± 0.002	820 ± 25	825 ± 25	839 ± 64	0.99
WEN179-4	149	219	0.136 ± 0.004	1.244 ± 0.053	0.066 ± 0.002	823 ± 25	821 ± 24	814 ± 58	1.00
WEN179-5	126	85	0.136 ± 0.003	1.279 ± 0.065	0.068 ± 0.003	823 ± 20	836 ± 28	871 ± 91	0.98
WEN179-6	70	69	0.137 ± 0.004	1.240 ± 0.069	0.066 ± 0.003	825 ± 20	819 ± 31	801 ± 103	0.99
WEN179-7	234	365	0.126 ± 0.005	1.189 ± 0.058	0.068 ± 0.002	766 ± 30	795 ± 26	879 ± 50	0.96
WEN179-8	56	27	0.125 ± 0.004	1.226 ± 0.104	0.071 ± 0.006	758 ± 23	813 ± 46	965 ± 161	0.93
WEN179-9	113	141	0.144 ± 0.005	1.359 ± 0.063	0.068 ± 0.002	867 ± 27	871 ± 27	882 ± 68	1.00
WEN179-10	113	106	0.134 ± 0.006	1.340 ± 0.080	0.073 ± 0.003	810 ± 33	863 ± 34	1002 ± 84	0.94
WEN179-11	47	30	0.115 ± 0.004	1.129 ± 0.097	0.071 ± 0.005	705 ± 26	767 ± 45	954 ± 158	0.92
WEN179-12	357	65	0.077 ± 0.004	0.842 ± 0.068	0.079 ± 0.005	479 ± 21	620 ± 37	1176 ± 132	0.77
WEN181A-1	166	154	0.141 ± 0.004	1.266 ± 0.129	0.065 ± 0.006	848 ± 22	831 ± 56	784 ± 193	0.98
WEN181A-2	393	445	0.132 ± 0.002	1.214 ± 0.075	0.067 ± 0.004	797 ± 14	807 ± 34	834 ± 118	0.99
WEN181A-3	74	156	0.139 ± 0.004	1.284 ± 0.129	0.067 ± 0.006	841 ± 22	838 ± 56	833 ± 189	1.00
WEN181A-4	414	271	0.139 ± 0.003	1.293 ± 0.099	0.067 ± 0.005	840 ± 17	843 ± 43	849 ± 145	1.00
WEN181A-5	227	248	0.266 ± 0.005	3.551 ± 0.179	0.097 ± 0.005	1523 ± 25	1539 ± 39	1561 ± 85	0.99
WEN181A-6	113	116	0.276 ± 0.007	3.650 ± 0.263	0.096 ± 0.006	1573 ± 35	1561 ± 56	1544 ± 121	0.99
WEN181A-7	240	178	0.142 ± 0.004	1.317 ± 0.123	0.067 ± 0.006	855 ± 21	853 ± 52	849 ± 175	1.00
WEN181A-8	104	190	0.137 ± 0.004	1.342 ± 0.120	0.071 ± 0.006	829 ± 20	864 ± 51	954 ± 166	0.96
WEN181A-9	243	127	0.128 ± 0.004	1.158 ± 0.077	0.066 ± 0.004	775 ± 22	781 ± 36	798 ± 119	0.99
WEN181A-10	422	294	0.119 ± 0.003	1.049 ± 0.052	0.064 ± 0.003	725 ± 19	728 ± 25	739 ± 84	1.00
WEN181A-11	48	112	0.181 ± 0.005	1.868 ± 0.109	0.075 ± 0.004	1070 ± 29	1070 ± 38	1069 ± 97	1.00
WEN181A-12	58	139	0.178 ± 0.005	1.836 ± 0.099	0.075 ± 0.003	1057 ± 28	1059 ± 35	1062 ± 88	1.00
WEN181A-13	48	50	0.135 ± 0.006	1.212 ± 0.127	0.065 ± 0.006	814 ± 32	806 ± 57	784 ± 190	0.99
WEN181A-14	35	46	0.135 ± 0.006	1.285 ± 0.136	0.069 ± 0.007	817 ± 32	839 ± 59	898 ± 188	0.97
WEN181A-15	150	113	0.133 ± 0.005	1.132 ± 0.085	0.062 ± 0.004	807 ± 28	769 ± 40	660 ± 135	0.95
WEN181A-16	198	148	0.295 ± 0.005	4.132 ± 0.151	0.102 ± 0.003	1667 ± 25	1661 ± 29	1652 ± 59	1.00
WEN181A-17	232	276	0.133 ± 0.002	1.218 ± 0.056	0.067 ± 0.003	803 ± 13	809 ± 25	825 ± 86	0.99
WEN181A-18	168	244	0.137 ± 0.002	1.206 ± 0.058	0.064 ± 0.003	828 ± 13	803 ± 27	734 ± 93	0.97
WEN181A-19	642	299	0.128 ± 0.002	1.170 ± 0.052	0.066 ± 0.003	778 ± 12	786 ± 24	811 ± 84	0.99
WEN181A-20	635	291	0.130 ± 0.002	1.133 ± 0.052	0.063 ± 0.003	786 ± 12	769 ± 24	722 ± 88	0.98
WEN181A-21	88	149	0.143 ± 0.003	1.366 ± 0.079	0.069 ± 0.004	863 ± 16	875 ± 33	905 ± 108	0.99
WEN181A-22	464	228	0.116 ± 0.002	1.056 ± 0.055	0.066 ± 0.003	707 ± 12	732 ± 27	810 ± 102	0.97
WEN181A-23	162	173	0.135 ± 0.003	1.222 ± 0.068	0.066 ± 0.004	814 ± 14	811 ± 31	802 ± 109	1.00
WEN181A-24	149	200	0.138 ± 0.002	1.249 ± 0.064	0.066 ± 0.003	834 ± 14	823 ± 29	793 ± 100	0.99
WEN181A-25	82	97	0.231 ± 0.005	2.933 ± 0.153	0.092 ± 0.004	1340 ± 25	1390 ± 39	1468 ± 89	0.96
WEN181A-26	109	134	0.129 ± 0.003	1.109 ± 0.076	0.062 ± 0.004	781 ± 16	758 ± 36	688 ± 134	0.97
WEN181A-27	160	144	0.126 ± 0.003	1.139 ± 0.075	0.065 ± 0.004	766 ± 15	772 ± 35	790 ± 126	0.99
WEN181A-28	83	183	0.135 ± 0.003	1.234 ± 0.070	0.066 ± 0.004	817 ± 15	816 ± 31	812 ± 108	1.00
WEN181A-29	95	169	0.138 ± 0.003	1.300 ± 0.075	0.068 ± 0.004	832 ± 15	846 ± 32	882 ± 108	0.98
WEN181A-30	290	299	0.133 ± 0.002	1.228 ± 0.056	0.067 ± 0.003	803 ± 13	814 ± 25	842 ± 85	0.99
WEN181A-31	403	348	0.133 ± 0.002	1.225 ± 0.052	0.067 ± 0.003	802 ± 12	812 ± 23	839 ± 79	0.99
WEN181A-32	401	204	0.127 ± 0.003	1.160 ± 0.068	0.066 ± 0.004	768 ± 14	782 ± 31	821 ± 111	0.98
WEN181A-33	353	190	0.128 ± 0.003	1.159 ± 0.070	0.065 ± 0.004	779 ± 15	782 ± 32	789 ± 116	1.00
WEN181A-34	150	149	0.281 ± 0.006	3.806 ± 0.121	0.098 ± 0.002	1594 ± 32	1594 ± 25	1594 ± 41	1.00
WEN181A-35	120	117	0.129 ± 0.003	1.173 ± 0.058	0.066 ± 0.003	780 ± 18	788 ± 27	811 ± 87	0.99
WEN181A-36	133	142	0.130 ± 0.003	1.186 ± 0.054	0.066 ± 0.003	790 ± 18	794 ± 25	807 ± 79	0.99
WEN181A-37	131	384	0.131 ± 0.003	1.187 ± 0.039	0.066 ± 0.002	794 ± 17	795 ± 18	796 ± 50	1.00
WEN181A-38	228	386	0.128 ± 0.001	1.169 ± 0.030	0.066 ± 0.002	776 ± 8	786 ± 14	814 ± 48	0.99
WEN181A-39	242	260	0.129 ± 0.002	1.154 ± 0.035	0.065 ± 0.002	784 ± 9	779 ± 16	767 ± 58	0.99
WEN181A-40	178	332	0.131 ± 0.001	1.215 ± 0.033	0.067 ± 0.002	793 ± 8	808 ± 15	847 ± 50	0.98
WEN181A-41	61	58	0.136 ± 0.002	1.191 ± 0.071	0.063 ± 0.004	823 ± 14	796 ± 33	722 ± 117	0.97
WEN181A-42	132	122	0.137 ± 0.002	1.259 ± 0.050	0.066 ± 0.003	830 ± 9	827 ± 22	819 ± 77	1.00
WEN181A-43	292	230	0.130 ± 0.001	1.181 ± 0.036	0.066 ± 0.002	790 ± 7	792 ± 16	797 ± 59	1.00
WEN181A-44	50	48	0.131 ± 0.002	1.218 ± 0.078	0.067 ± 0.004	794 ± 13	809 ± 35	850 ± 123	0.98
WY56-1	56	59	0.133 ± 0.003	1.260 ± 0.076	0.069 ± 0.004	803 ± 19	828 ± 34	895 ± 113	0.97
WY56-2	207	202	0.134 ± 0.003	1.257 ± 0.052	0.068 ± 0.002	813 ± 19	826 ± 23	861 ± 68	0.98
WY56-3	161	218	0.142 ± 0.005	1.314 ± 0.057	0.067 ± 0.002	855 ± 26	852 ± 25	844 ± 60	1.00
WY56-4	136	243	0.143 ± 0.003	1.332 ± 0.051	0.068 ± 0.002	859 ± 19	860 ± 22	861 ± 63	1.00
WY56-5	47	55	0.137 ± 0.004	1.295 ± 0.088	0.069 ± 0.004	826 ± 22	843 ± 38	890 ± 128	0.98
WY56-6	138	251	0.141 ± 0.003	1.272 ± 0.049	0.066 ± 0.002	849 ± 20	834 ± 22	793 ± 62	0.98
WY56-7	216	244	0.134 ± 0.003	1.220 ± 0.048	0.066 ± 0.002	813 ± 19	810 ± 22	801 ± 64	1.00
WY56-8	61	105	0.133 ± 0.005	1.269 ± 0.068	0.069 ± 0.003	806 ± 26	832 ± 30	900 ± 87	0.97
WY56-9	135	141	0.142 ± 0.003	1.293 ± 0.053	0.066 ± 0.002	854 ± 18	842 ± 23	811 ± 73	0.99
WY56-10	191	261	0.134 ± 0.003	1.260 ± 0.048	0.068 ± 0.002	809 ± 18	828 ± 21	878 ± 62	0.98
WY56-11	143	85	0.128 ± 0.004	1.157 ± 0.068	0.065 ± 0.003	778 ± 20	780 ± 31	788 ± 109	1.00
WY56-12	118	81	0.136 ± 0.005	1.148 ± 0.069	0.061 ± 0.003	821 ± 26	777 ± 32	650 ± 107	0.94
WY56-13	76	124	0.134 ± 0.003	1.172 ± 0.059	0.063 ± 0.003	813 ± 19	787 ± 27	717 ± 93	0.97
WY56-14	79	121	0.136 ± 0.005	1.190 ± 0.062	0.063 ± 0.003	823 ± 26	796 ± 28	721 ± 86	0.97
WY56-15	109	107	0.140 ± 0.003	1.239 ± 0.058	0.064 ± 0.003	846 ± 18	819 ± 26	744 ± 86	0.97
WY56-16	142	230	0.164 ± 0.005	1.546 ± 0.064	0.068 ± 0.002	980 ± 29	949 ± 25	878 ± 54	0.97
WY56-17	106	97	0.150 ± 0.004	1.351 ± 0.071	0.066 ± 0.003	898 ± 22	868 ± 30	791 ± 95	0.97
WY56-18	498	433	0.120 ± 0.003	1.107 ± 0.038	0.067 ± 0.002	729 ± 16	757 ± 18	840 ± 53	0.96
WY56-19	190	334	0.123 ± 0.003	1.153 ± 0.042	0.068 ± 0.002	747 ± 17	779 ± 20	871 ± 56	0.96
WY56-20	264	220	0.139 ± 0.005	1.400 ± 0.060	0.073 ± 0.002	838 ± 26	889 ± 25	1018 ± 56	0.94
WY56-21	165	139	0.133 ± 0.003	1.347 ± 0.055	0.073 ± 0.003	807 ± 17	866 ± 24	1020 ± 70	0.93
WY56-22	87	93	0.131 ± 0.003	1.370 ± 0.074	0.076 ± 0.004	793 ± 19	876 ± 31	1094 ± 94	0.90
WY56-23	61	63	0.135 ± 0.004	1.445 ± 0.089	0.078 ± 0.004	815 ± 21	908 ± 36	1140 ± 110	0.90
WY56-24	55	41	0.121 ± 0.004	1.255 ± 0.098	0.075 ± 0.005	739 ± 22	825 ± 43	1067 ± 144	0.89

Table 5
LA-ICP-MS U-Pb isotopic analytical data for zircons fromsandstone samples in Chengjiang area

Grein	Th (ppn	U (ppm)	$^{206}Pb/^{238}U$ (2s)	$^{207}Pb/^{235}U$ (2s)	$^{207}Pb/^{206}Pb$ (2s)	Age (Ma) $^{206}Pb/^{238}U$ (2s)	$^{207}Pb/^{235}U$ (2s)	$^{207}Pb/^{206}Pb$ (2s)	Concordance
CHW31-1	347	232	0.137 ± 0.002	1.324 ± 0.040	0.070 ± 0.002	828 ± 11	856 ± 17	929 ± 54	0.97
CHW31-2	360	299	0.134 ± 0.002	1.213 ± 0.034	0.066 ± 0.002	812 ± 11	807 ± 16	791 ± 51	0.99
CHW31-3	434	261	0.245 ± 0.003	3.405 ± 0.073	0.101 ± 0.002	1414 ± 18	1505 ± 17	1637 ± 31	0.94
CHW31-4	447	362	0.279 ± 0.004	3.722 ± 0.072	0.097 ± 0.001	1586 ± 19	1576 ± 15	1563 ± 26	0.99
CHW20-1	239	242	0.135 ± 0.004	1.283 ± 0.100	0.069 ± 0.005	818 ± 25	838 ± 43	893 ± 139	0.98
CHW20-2	97	164	0.138 ± 0.005	1.264 ± 0.118	0.066 ± 0.006	836 ± 27	830 ± 51	812 ± 171	0.99
CHW20-3	143	130	0.129 ± 0.005	1.216 ± 0.128	0.068 ± 0.007	784 ± 28	808 ± 57	875 ± 192	0.97
CHW20-4	88	121	0.128 ± 0.005	1.195 ± 0.132	0.068 ± 0.007	776 ± 28	798 ± 59	860 ± 200	0.97
CHW20-5	267	229	0.130 ± 0.004	1.191 ± 0.098	0.067 ± 0.005	785 ± 24	796 ± 44	827 ± 149	0.99
CHW20-6	120	146	0.131 ± 0.005	1.209 ± 0.121	0.067 ± 0.006	792 ± 27	805 ± 54	840 ± 183	0.98
CHW20-7	102	194	0.133 ± 0.005	1.218 ± 0.107	0.067 ± 0.005	803 ± 26	809 ± 48	824 ± 161	0.99
CHW20-8	235	234	0.131 ± 0.004	1.169 ± 0.093	0.065 ± 0.005	793 ± 20	786 ± 42	767 ± 149	0.99
CHW20-9	242	287	0.125 ± 0.003	1.135 ± 0.083	0.066 ± 0.004	760 ± 19	770 ± 39	800 ± 136	0.99
CHW20-10	146	127	0.130 ± 0.004	1.189 ± 0.125	0.066 ± 0.007	787 ± 24	795 ± 57	820 ± 196	0.99
CHW20-11	523	149	0.122 ± 0.004	1.181 ± 0.116	0.070 ± 0.007	743 ± 22	792 ± 53	931 ± 180	0.94
CHW11.5-1	212	202	0.124 ± 0.003	1.088 ± 0.030	0.064 ± 0.002	754 ± 31	748 ± 29	730 ± 72	0.99
CHW11.5-2	134	72	0.125 ± 0.001	1.115 ± 0.030	0.065 ± 0.003	757 ± 12	761 ± 28	773 ± 107	0.99
CHW11.5-3	267	151	0.128 ± 0.001	1.184 ± 0.022	0.067 ± 0.002	778 ± 9	793 ± 20	835 ± 72	0.98
CHW11.5-4	349	311	0.129 ± 0.001	1.187 ± 0.019	0.067 ± 0.002	783 ± 16	794 ± 18	827 ± 51	0.99
CHW11.5-5	373	229	0.130 ± 0.001	1.196 ± 0.021	0.067 ± 0.002	787 ± 16	799 ± 20	833 ± 59	0.98
CHW11.5-6	95	70	0.132 ± 0.001	1.213 ± 0.032	0.067 ± 0.003	797 ± 12	806 ± 29	833 ± 104	0.99
CHW11.5-7	234	213	0.132 ± 0.003	1.240 ± 0.033	0.068 ± 0.002	799 ± 33	819 ± 30	872 ± 65	0.98
CHW11.5-8	99	101	0.133 ± 0.002	1.228 ± 0.029	0.067 ± 0.003	805 ± 18	813 ± 26	836 ± 87	0.99
CHW11.5-9	265	254	0.133 ± 0.001	1.198 ± 0.019	0.065 ± 0.002	806 ± 14	800 ± 18	781 ± 56	0.99
CHW11.5-10	246	262	0.134 ± 0.001	1.226 ± 0.017	0.066 ± 0.002	811 ± 8	813 ± 16	816 ± 54	1.00
CHW11.5-11	334	173	0.135 ± 0.002	1.279 ± 0.026	0.069 ± 0.002	815 ± 20	836 ± 23	892 ± 64	0.97
CHW11.5-12	104	122	0.136 ± 0.001	1.294 ± 0.027	0.069 ± 0.003	819 ± 14	843 ± 24	906 ± 77	0.97
CHW11.5-13	118	82	0.130 ± 0.002	1.241 ± 0.033	0.069 ± 0.003	789 ± 21	819 ± 30	903 ± 94	0.96
CHW11.5-14	95	189	0.120 ± 0.003	1.080 ± 0.031	0.065 ± 0.002	733 ± 31	744 ± 29	777 ± 75	0.99
CHW11.5-15	87	182	0.126 ± 0.003	1.195 ± 0.033	0.069 ± 0.002	766 ± 32	798 ± 30	888 ± 71	0.96
CHW11.5-16	175	76	0.123 ± 0.003	1.164 ± 0.044	0.068 ± 0.003	751 ± 39	784 ± 40	880 ± 106	0.96
CHW11.5-17	180	67	0.123 ± 0.003	1.219 ± 0.047	0.072 ± 0.004	750 ± 39	809 ± 42	975 ± 109	0.93
CHW11.5-18	96	61	0.135 ± 0.004	1.368 ± 0.053	0.074 ± 0.004	816 ± 43	875 ± 44	1029 ± 107	0.93
CHW11.5-19	160	133	0.140 ± 0.003	1.338 ± 0.039	0.069 ± 0.003	845 ± 35	863 ± 33	907 ± 78	0.98
CHW11.5-20	153	116	0.146 ± 0.001	1.395 ± 0.029	0.069 ± 0.002	881 ± 16	887 ± 24	902 ± 75	0.99
CHW11.5-21	96	87	0.148 ± 0.002	1.345 ± 0.034	0.066 ± 0.003	887 ± 23	865 ± 29	810 ± 89	0.97
CHW11.5-22	247	160	0.157 ± 0.001	1.552 ± 0.027	0.072 ± 0.002	939 ± 16	951 ± 21	979 ± 60	0.99
CHW11.5-23	204	66	0.141 ± 0.002	1.447 ± 0.037	0.075 ± 0.003	849 ± 17	909 ± 31	1056 ± 95	0.93
CHW11.5-24	137	166	0.129 ± 0.002	1.248 ± 0.026	0.070 ± 0.002	781 ± 19	823 ± 23	937 ± 66	0.95
CHW11.5-25	147	125	0.128 ± 0.001	1.282 ± 0.028	0.072 ± 0.003	779 ± 17	838 ± 24	996 ± 75	0.93
CHW11.5-26	88	56	0.150 ± 0.002	1.686 ± 0.044	0.081 ± 0.004	903 ± 19	1003 ± 33	1229 ± 93	0.90
CHW11.5-27	289	352	0.105 ± 0.002	1.048 ± 0.027	0.072 ± 0.002	645 ± 27	728 ± 26	993 ± 54	0.89
CHW11.5-28	148	36	0.135 ± 0.001	1.575 ± 0.051	0.085 ± 0.005	814 ± 16	960 ± 39	1312 ± 119	0.85

The 79 zircons separated from WEN179, WEN181A and WY56 of the Doushantuo Fm in the Weng'an area have $^{206}Pb/^{238}U$ ages ranging from *ca.* 713 to 1667 Ma. Age spectra of these three sandstones are also integrated (Fig. 6-9); the age spectrum shows a large peak around 800 Ma. Some Mesoproterozoic zircons, from *ca.* 1050 Ma to 1660 Ma, are included. The youngest $^{206}Pb/^{238}U$ age is *ca.* 713 Ma, indicating an upper depositional age-limit of the Doushantuo Fm (Fig. 6-9).

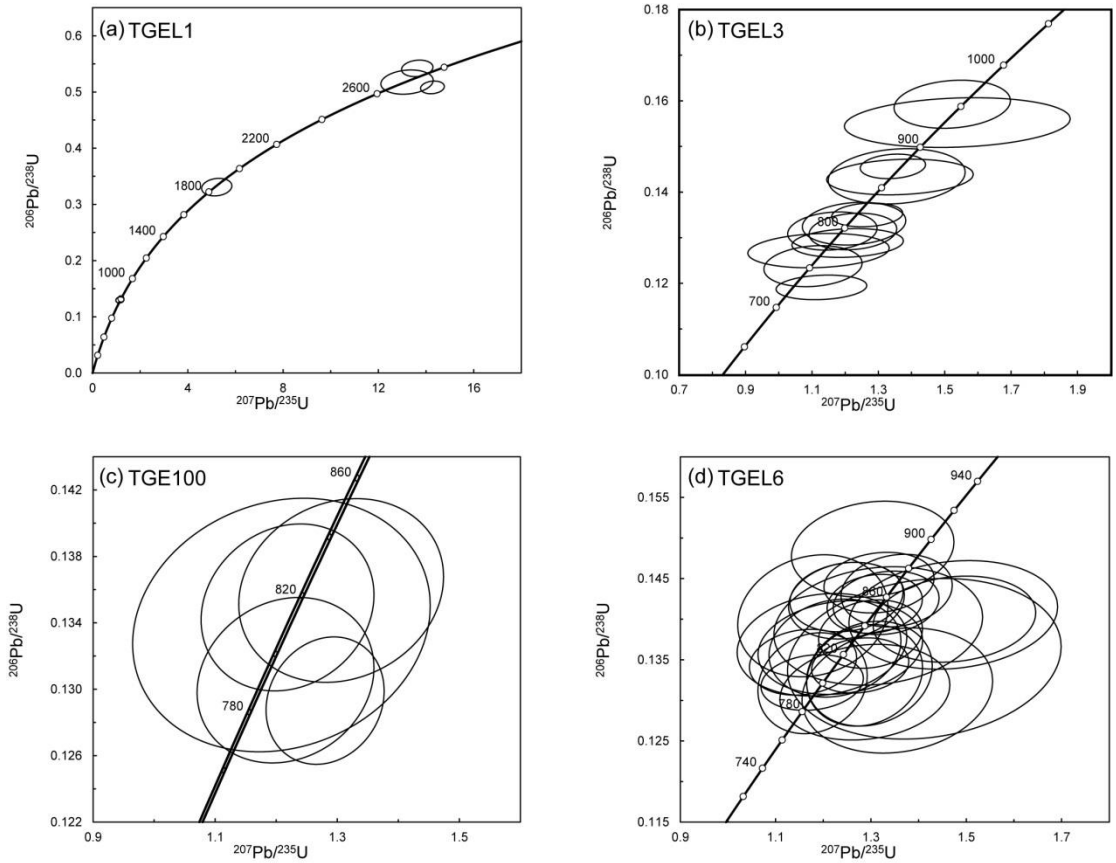

Figure 6-7. Concordia plots of in situ U-Pb dates of zircons with LA-ICP-MS from (a-c) sandstones in the Liantuo Fm (TGEL1, TGEL3 and TGE100) and (d) the Huangling granite (TGEL6) in the Three Gorges area.

The range of $^{206}Pb/^{238}U$ ages from the CHW11.5, Liantuo Fm in Chengjiang area, is between 733 ± 31 and 939 ± 16 Ma (Fig. 6-10). The maximum in the frequency distribution occurs at *ca.* 800 Ma. The 11 zircons separated from CHW20 in Nantuo Fm in Chengjiang area show a monotonous peak at *ca.* 800 Ma (Fig. 6-10), and their ages ranging from 743 ± 22 to 836 ± 27 Ma. In spite of only 4 analyses, sandstone of CHW31 from the Doushantuo Fm in the Chengjiang area includes Neoproterozoic (*ca.* 820 Ma) to Mesoproterozoic zircon grains, but the grain with a $^{206}Pb/^{238}U$ age of 1410 Ma is discordant (Fig. 6-8 and 7-10).

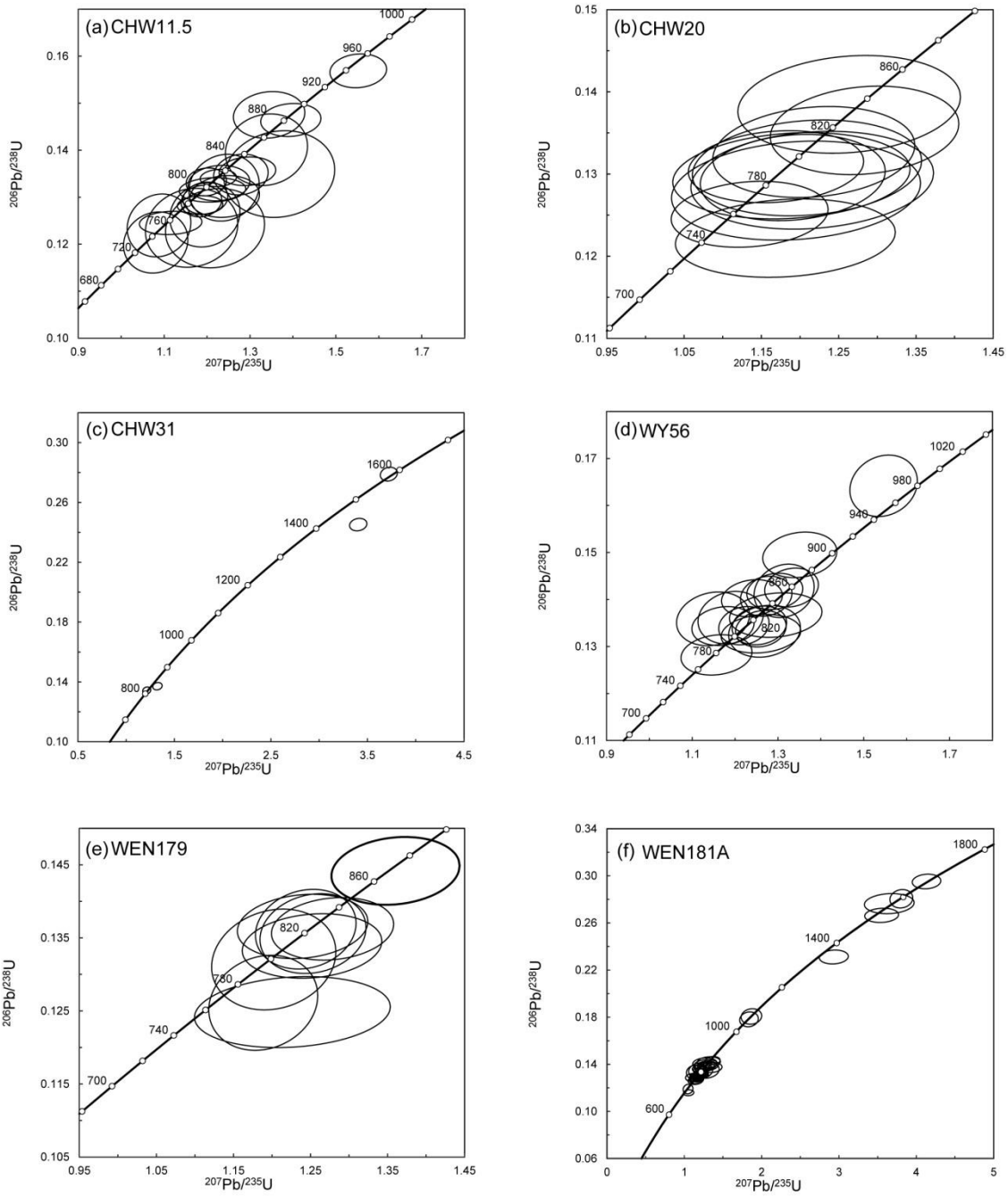

Figure 6-8. Concordia plots of in situ U-Pb dates of zircons with LA-ICP-MS from (a-c) sandstones collected in the Chengjiang area (CHW11.5, CHW20 and CHW31) and (d-f) sandstones collected in the Weng'an area (WY56, WEN179 and WEN181A).

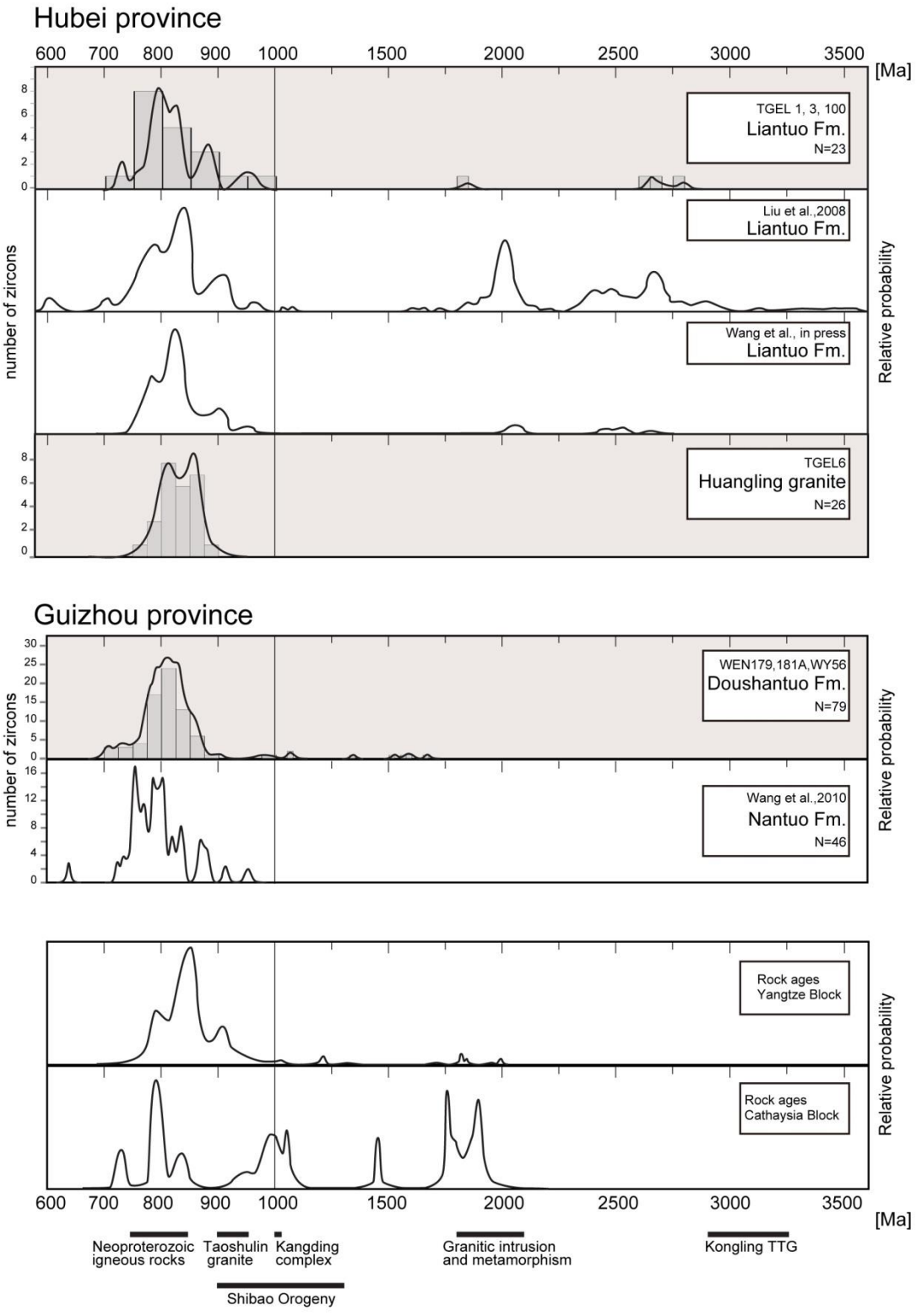

Figure 6-9. Age spectra of detrital zircon grains from Cryogenian to Ediacaran sandstones in Three Gorges and Weng'an areas, showing secular changes in provenance that shed terrigenous clastics to the Nanhua rift basin. For comparison, results from previous studies are also shown (Liu et al., 2008;

Wang et al., 2010, in press). Note there are large peaks around 800 Ma in all the sandstones. Very old (>1750 Ma) zircon grains are included only in sandstone in the Three Gorges area (TGEL1) and originated from the Kongling complex and Paleo-proterozoic granitic intrusions, close to the Three Gorges area.

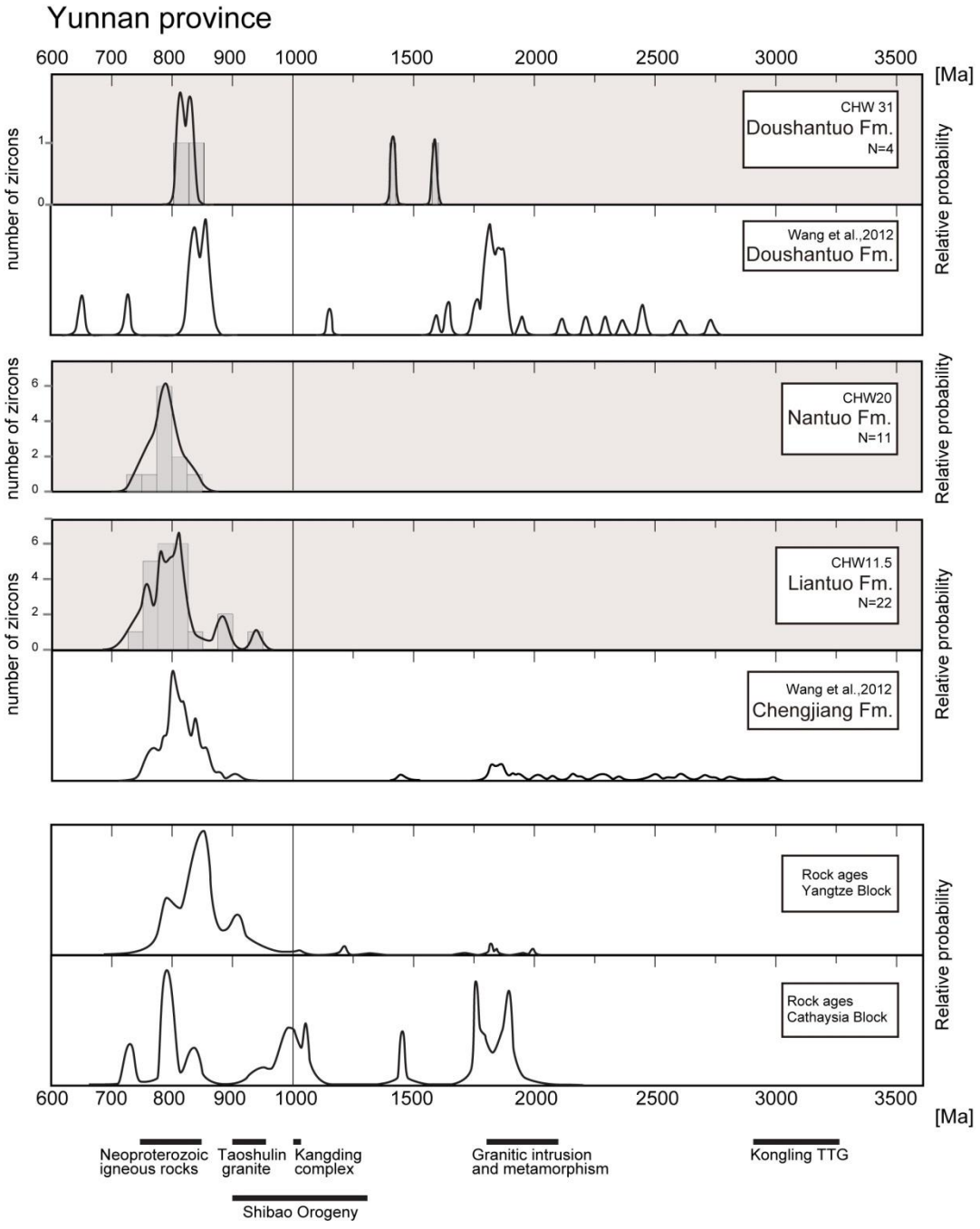

Figure 6-10. Age spectrum of detrital zircon grains from Cryogenian to Ediacaran sandstones in the Chengjiang region, Yunnan Province. As is the case in Three

Gorges and Weng'an, there are large peaks around 800 Ma in sandstones in the Chengjiang region. Mid-proterozoic (ca. 1600 Ma) zircon grains are also included in sandstone from the Doushantuo Fm (CHW31), but their source rocks have yet not been discovered in the Yangtze craton.

6-5 Discussion

6-5-1 Chronological constraints from tuff beds

While the succession in the Three Gorges area contains many fossils, the sedimentary ages, especially in the early Cambrian, are not fully constrained because of the absence of radiometric ages. The PC/C boundary in South China is defined by the first emergence of the Nemakit-Daldynian type SSFs (Zone 1; *e.g.* Qian, 1999; Steiner et al., 2007), and the age of the boundary is determined by zircon U-Pb analyses from tuff layers in Oman and set to *ca.* 542 Ma (*e.g.* Brasier et al., 1994; Amthor et al., 2003). The PC/C boundary in Oman is defined by the demise of *Cloudina* and a large negative $\delta^{13}C_{carb}$ anomaly. In the Three Gorges area, a large negative $\delta^{13}C_{carb}$ anomaly is also recorded in almost the same horizon as the first appearance of the Nemakit-Daldynian-type SSFs (N1 in Fig. 6-4a; Ishikawa et al., 2008). Therefore, the succession with the large negative $\delta^{13}C_{carb}$ anomaly in the Yanjiahe Fm should have been deposited at about 542 Ma. The first appearance of Tommotian-type SSFs (Zone 3; Steiner et al., 2007), 2.7 m below the Yanjiahe/Shuijingtuo formations, is another milestone (Fig. 6-4a). The time of the first appearance of Tommotian-type SSFs is not fully constrained. Zircons separated from a basal conglomerate in Siberia have U-Pb ages of 534.6 ± 0.5 Ma (Fig. 6-11; Bowring et al., 1993), which provides only a maximum depositional age for the appearance of Tommotian-type SSFs.

This study presents the first direct age constraint on the early Cambrian succession in the Three Gorges area. The age is 526.4 ± 5.4 Ma at the bottom of the

Shuijingtuo Fm (Fig. 6-4a, b), and is not so different from the time of the start of the Tommotian (< 534.6 ± 0.5 Ma). Therefore, the duration of the hiatus at the boundary of the Yanjiahe/Shuijingtuo formations is minor. In addition, this age constraint is consistent with fossil records (Fig. 6-11). Black limestone in the uppermost Shuijingtuo Fm contains trilobites (Zhu et al., 2003), which indicates an Atdabanian age (*ca.* 521 Ma; Stage 3 in Fig. 6-1).

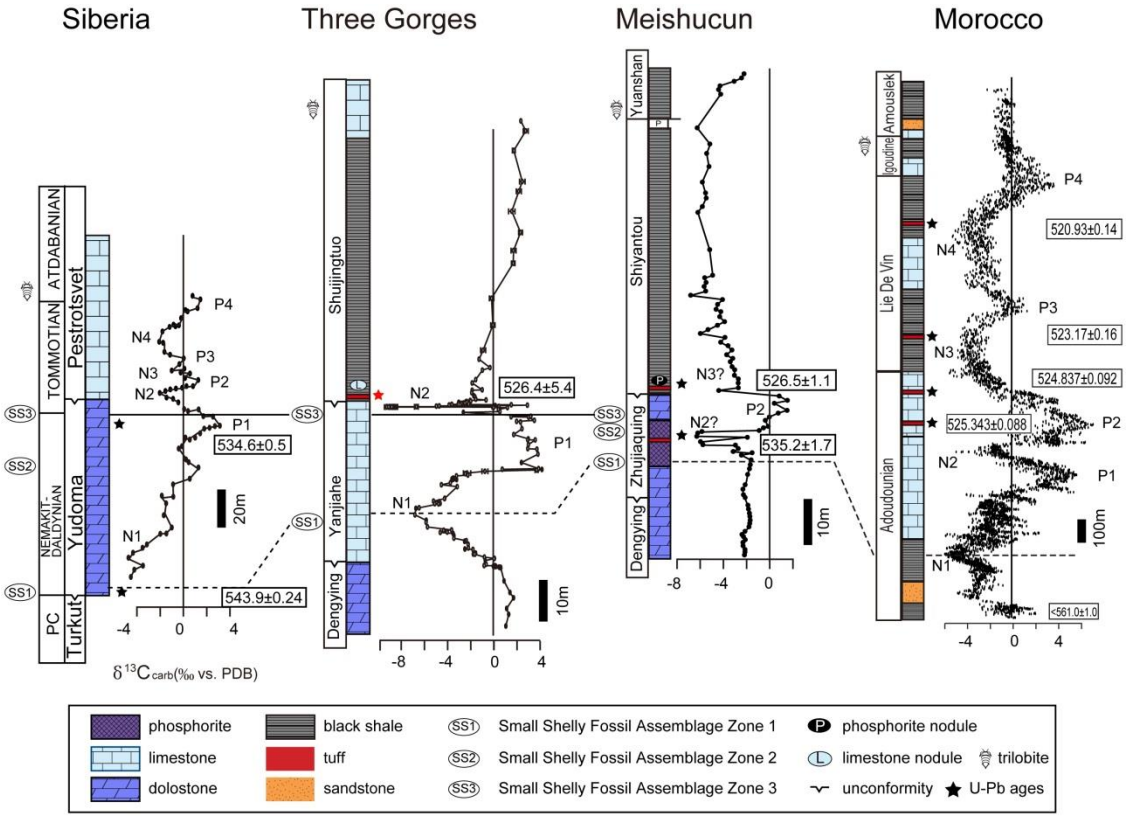

Figure 6-11. Comparison of lithostratigraphic columns, chemostratigraphies (carbon isotope ratios), SSFs bio-zonation and absolute zircon U-Pb ages in the Siberia, Three Gorges, Meishucun and Morocco areas (Brasier et al., 1994; Bowring et al., 1993; Ishikawa et al., 2008; Brasier et al., 1990; Zhu et al., 2009; Maloof et al., 2005, 2010; Compston et al., 2008). The Precambrian/Cambrian boundary is defined by the first appearance of SSFs (bottom of Zone 1). Numbers in squares represent zircon U-Pb ages from tuff beds. Red star represents the position of the tuff layer analyzed in this study. PC – Precambrian.

We will now review and summarize the chronological data from the Maotianshan area, Yunnan Province. In this section, the PC/C boundary is also defined by the first appearance of the SSFs (SSFs assemblage zone 1) and its boundary is within the basal Daibu Member of the Zhujiaquing Fm (Fig. 6-3). There is no age constraint on the succession in the Maotianshan area, but some previous workers provided radiometric ages of a bed in the Meishucun area (Fig. 6-11). The lithostratigraphies of these two areas are very similar. Phosphorite sequences in the Zhongyicun Member are present in both areas. At Meishucun there is a tuff layer within a phosphorite bed of the Zhongyicun Member, which gave a U-Pb zircon age of 535.2 ± 1.7 Ma (Fig. 6-11; *e.g.* Sawaki et al., 2008b; Zhu et al., 2009). Richly diverse assemblages of micro-molluscs and SSFs occur above this tuff layer, and these assemblages correspond to SSFs assemblage zone 3 (Steiner et al., 2007). This study presents a new age constraint of 523.9 ± 6.7 Ma for the bottom of the Dahai Member in Maotianshan. These two age constraints from tuff beds indicate that the beginning of the Tommotian age (Stage 2) is between about 535 and 524 Ma, which is consistent with the Siberian data (Fig. 6-11). Recently, a new chronological constraint (526 ± 1.1 Ma) was provided for the basal Shiyantou Fm at Meishucun, East Yunnan (Fig. 6-11; Compston et al., 2008). The Shiyantou succession and the overlying Yu'anshan formations contain trilobites and the "Chengjiang Fauna". This *ca.* 526 Ma date constrains the maximum depositional age for the appearance of these faunas. In the Taoying section, Guizhou province, a tuff at the bottom of the Niutitang Fm has a zircon U-Pb age of 522.7 ± 4.9 Ma (X. Wang et al., 2012). This tuff underlies a sequence with phosphorite nodules, similar to the Meishucun section. Tuffaceous beds in the Three Gorges, Meishucun and Taoying areas have similar sedimentological configurations, including an underlying unconformity

and overlying nodule-rich layers. Therefore, these tuffaceous beds were probably deposited during the same volcanic event. In addition, unconformities in the early Tommotian are preserved globally, indicating in many successions a global regression (Ripperdan, 1994).

6-5-2 Comparison of carbon isotope excursions

Carbonate carbon isotope chemostratigraphy has been used to compare successions in different regions as a role of blind dating (*e.g.* Melezhik et al., 2001), because there are so few U-Pb age data in the early Cambrian. However, it is ambiguous whether the carbon isotope ratios in all regions are always similar. In general, there are fossils in mainly "shallow" marine sediments, which hold the possibility of isolation from an outer ocean depending on sea-level changes. Under such a local condition, carbon isotope ratios of the isolated regions may be different from those globally. Moreover, some unconformities are reported from the Cambrian successions in several regions, which makes comparison difficult because of the deficient chemostratigraphies (*e.g.*, Ishikawa et al., 2008). In the light of all the evidence, we will discuss and compare carbon isotope excursions in the regions; Siberia, Three Gorges, Meishucun and Morocco (Fig. 6-11). The Meishucun section is the Early Cambrian type locality of South China, and it is important for study of this period.

The Keys Succession in Morroco lacks SSFs. But carbonate carbon isotope ratios are most abundant and continuous (Maloof et al., 2005; 2010). The depositional age of this succession is well constrained by zircon U-Pb analyses, with respect to the later Early Cambrian (Fig. 6-11). There are more than 4 negative isotope anomalies during the early Cambrian. The first negative anomaly decreases to -6 ‰ (N1 in Fig.

6-11). A large negative isotope anomaly around PC/C boundary is characteristic globally (*e.g.* Figs. 7-5 and 7-6 in Ishikawa et al., 2008), and the N1 negative anomaly in Morocco also corresponds to it. However, such a large negative isotope anomaly is not recorded in the Meishucun section (Fig. 6-11), which indicates a different depositional setting in Meishucun at the beginning of the Cambrian. A second bold negative anomaly (N2) occurred at *ca.* 535 Ma, and this is common feature in Siberia, Morocco, Three Gorges and Meishucun. On the other hand, carbon isotope excursions above N2 display quite different aspects. Between N2 and the first appearance of trilobites, there are 2, 0, 1 and 2 negative isotope anomalies in Siberia, Three Gorges, Meishucun and Morocco, respectively (Fig. 6-11). If the first appearances of trilobites in these regions were almost simultaneous, this difference indicates an absence of an anomaly by hiatus or different depositional (possibly local) environments in each region. A basal Tommotian unconformity exists in various areas, such as Siberia, South China and Mongolia (Ripperdan, 1994). This unconformity indicates that global regression occurred in the early Tommotian. On the other hand, if the differences of the $\delta^{13}C_{carb}$ indicate different depositional environments, we must consider the individual environment of each region.

6-5-3 Provenance of sediments in the Nanhua and Kangdian rift basins

An age spectrum of detrital zircon from a sandstone can provide information about ancient provenance. We separated detrital zircons from 9 Cryogenian and Ediacaran sandstones in the Three Gorges, Weng'an and Chengjiang areas, and obtained 5 age spectra (Figs. 7-9 and 7-10). Previous workers reported pre-Cryogenian igneous

and metamorphic rocks in the Yangtze craton, including gneiss (-3.3 Ga; Gao et al., 2011) and trondhjemitic rocks in the Kongling complex (2.95-2.9 Ga; Qiu et al., 2000; Zhang et al., 2006b), 2.1-1.8 Ga granitic intrusions and metamorphic rocks (Qiu et al., 2000; Xiong et al., 2009; Zhen and Zhang 2007), igneous rocks associated with the Sibao Orogen (around 1.0 Ga), granitic gneiss in the Kangding Complex (1.0 Ga; X. H. Li et al., 2002), and igneous and metamorphic rocks associated with pre-rift and syn-rift magmatism (0.86-0.75 Ga; Figs. 7-9 and 7-10; e.g. Zhao and Zhou, 2009a, b; Pei et al., 2009; Zhao and Zhou, 2007; Z. X. Li et al., 2003b).

Detrital zircons in all the sandstones analyzed in this and previous studies have peaks at 900-750 Ma (Figs. 7-9 and 7-10; Liu et al., 2008; L. J. Wang et al., 2010; 2012; in press). Neoproterozoic pre-rift and syn-rift granitoids are widespread in the Yangtze Block, and their igneous ages overlap the prominent peaks in sandstones at 900-750 Ma (Ma et al., 1989; Roger and Calassou, 1997; X. H. Li, 1999; X. H. Li et al., 2003b; Z. X. Li et al., 2003a). We also collected a sample from the Huangling granite, one of the pre-rift granitoids, as TGEL6, which yielded a weighted mean $^{206}Pb/^{238}U$ age of 836 ± 11 Ma (MSWD = 5.6). The Huangling granite is overlain by a Cryogenian succession in the Three Gorges area (Figs. 7-2b and 7-3) and is one of the provenances of the overlying sandstone in the Liantuo Fm (Fig. 6-9). Sandstones of TGEL3, WY56 and CHW11.5 have zircons ranging from 1.0 to 0.9 Ga (Table S1, S2 and S3 in Supplementary Information). Sibao Orogeny-associated rocks are distributed widespread in the Yangtze craton (section 2.4.; Fig. 6-9), and the 1.0 to 0.9 Ga zircon grains in sandstones possibly originated from these igneous and metamorphic rocks.

Although some Archean zircons were reported from sandstones in the Chengjiang area by L. J. Wang et al. (2012), our data provide no Archean-age zircons (Fig. 6-10).

This can possibly be attributed to the deficit of analyzed zircons in this study. On the other hand, we obtained Archean and Paleoproterozoic populations (2.67-2.85, 1.85 Ga) from sandstones of the Liantuo Fm in the Three Gorges area. Previous studies also have reported detrital zircons of Archean and Paleoproterozoic age (Liu et al., 2008; L. J. Wang et al., in press). The 2.95-2.90 Ga Kongling trondhjemitic rocks that experienced *ca.* 2.75 Ga high-grade metamorphism and 1.9-1.8 Ga granitic intrusions are present in the Three Gorges area (Qiu et al., 2000), and these old igneous rocks are possibly the origin of the Archean and Paleoproterozoic zircons in the Liantuo Fm.

Sandstones from the Doushantuo Fm in Weng'an and CHW31 from the Doushantuo Fm in Chengjiang have zircons with an age of *ca.* 1.5-1.6 Ga (Figs, 7-5, 7-9, 7-10). Wang and others (2010) also analyzed U-Pb ratios in detrital zircons from the Nantuo Fm in the Fanjingshan area in Guihou Province. Despite the difference of stratigraphic unit, they have not reported the *ca.* 1.5-1.6 Ga age (Fig. 6-9). On the other hand, Wang and others (2012) reported *ca*. 1.5 Ga detrital zircons from the Doushantuo Fm in the Kunming area, Yunnan province (Fig. 6-10). *Ca*. 1.5 Ga zircons in this study are rounded in shape and show oscillatory zoning, these features were also observed by previous workers (L. J. Wang et al., 2010). In addition, *ca*. 1.5 Ga detrital zircons occur in Tianli Schists in the southwest of the Yangtze block (X. H. Li et al., 2008) and in sediments in the Kunyang Group in the southeast of the Yangtze Block (Zhou et al., 2009). Although previous studies have not reported any igneous and metamorphic events at that time in the Yangtze and Cathaysia Blocks, the possibility that Mesoproterozoic basement had existed and/or is now covered by younger sediments was suggested by L. J. Wang et al. (2010). Moreover, in Kangdian region, Zhao and Zhou (2011) obtained a U-Pb age of 1681 ± 13 Ma from a volcanic rock in the

Dahogchuan Group and 1659 ± 16 Ma for a dolerite dyke cutting the Group. These data would indicated that Mesoproterozoic basement made at ca. 1.6 Ga.

6-6 Conclusions

(1) We discovered a tuff layer at the base of the Shuijingtuo Fm in the Three Gorges area, and another tuff layer in the Zhujiaquing Fm in the Chengjiang area, South China.

(2) We separated zircons from the tuff layers and acquired new U-Pb ages of 526.4 ± 5.4 Ma at the base of the Shuijingtuo Fm in the Three Gorges area, and 523.9 ± 6.7 Ma at the base of the Dahai Member of the Zhujiaquing Fm in the Chengjiang area.

(3) Tuffaceous beds accompanied by unconformities and nodules are common in the Three Gorges, Meishucun and Taoying sections, indicating major volcanic and sedimentary events at *ca.* 525 Ma.

(4) Carbonate carbon isotope chemostratigraphies have different characteristics in strata in Morocco, Siberia, Three Gorges and Meishucun during the second half of the early Cambrian. One possibility is that the ocean in South China was separated from an outer ocean during the Tommotian.

(5) U-Pb ratios of detrital zircons extracted from sandstones in Three Gorges, Weng'an and Chengjiang areas yield *ca*. 1.5 Ga ages. These are the first reported Mesoproterozoic zircons from sandstones in Doushantuo Fm in Weng'an. They suggest the existence of unexposed Mesoproterozoic basement rocks of the Yangtze Block.

Acknowledgements

This work was financially supported by the Sino-Japan Cooperative Program on "Evolution of Early Life and Environments from Snowball to the Phanerozoic Earth: Records in S. China" and partly supported by the National Natural Science Foundation of China (Grant Nos. 40332016 and 40602003), the National "973" Project (Grant No. 2006CB806401) and the Program for Chengjiang Scholars and Innovative Research Team in University (PCSIRT) in China. This work was partly supported by grants "Secular variation of seawater composition (No. 16740284)", and "Coevolution of surface environment and solid earth from the Neoproterozoic Snowball Earth to Cambrian explosion events (No. 18740318)" from the Ministry of Education, Culture, Sports, Science and Technology, Japan.

We thank Dr. Takaomi Yokoyama for technical assistance (ICP-MS) in data acquisition at Kyoto University. The comments of Prof. Pat Eriksson and an anonymous reviewer significantly improved this manuscript. We also appreciate Prof. Brian F. Windley and Prof. Kenneth Collerson correcting English grammar of this manuscript.

References

Amthor, J. E., Grotzinger, J. P., Schröder, S., Bowring, S. A., Ramezani, J., Martin, M. W., Matter, A., 2003. Extinction of Cloudina and Namacalathus at the Precambrian–Cambrian boundary in Oman. Geology, 31, 431-434.

Babcock, L. E., Peng, S. C., Geyer, G., Shergold, J. H., 2005. Changing perspectives on Cambrian chronostratigraphy and progress toward subdivision of the Cambrian System. Geosciences Journal, 9, 101-106.

Barfod, G. H., Albarede, F., Knoll, A. H., Xiao, S., Telouk, P., Frei, R., Baker, J., 2002. New Lu–Hf and Pb–Pb age constraints on the earliest animal fossils. Earth and Planetary Science Letters, 201, 203-212.

Bengston, S., Farmer, M., Runneger, B., 1991. The Proterozoic-Early Cambrian evolution of metaphytes and metazoans. The Proterozoic Biosphere: A Multidisciplinary Study. Chapter 8, Oxford university press, 425-462.

Benus, A. P., 1988. Small Shelly Fossils and the Precambrian- Cambrian Boundary, Trace Fossils, (eds. E. Landing, G. M. Narbonne, P. Myrow, New York State Museum and Geological Survey Bulletin, Albany, NY, 1988), 463, 8-9.

Black, L. P., Kamo, S. L., Williams, I. S., Mundil, R., Davis, D. W., Korsch, R. J., Foudoulis, C., 2003. The application of SHRIMP to Phanerozoic geochronology; a critical appraisal of four zircon standards. Chemical Geology, 200, 171-188.

Bowring, S. A., Grotzinger, J. P., Isachsen, C. E., Knoll, A. H., Pelechaty, S. M. Kolosov, P., 1993. Calibrating rates of Early Cambrian evolution. Science, 261, 1293-1298.

Bowring, S. A., Myrow, P., Landing, E., Ramezani, J., Grotzinger, J. P., 2003. Geochronological constraints on terminal Neoproterozoic events and the rise of metazoans. European Geophysical Union Annual Meeting, Nice 2003. Geophysical Research Abstracts, 5, 13219.

Brasier, M. D., Magaritz, M., Corfield, R., Luo, H., Wu, X., Ouyang, L., Jiang, Z., Hamadi, B., He, T., Frazier, A.G., 1990. The carbon- and oxygen-isotopic record of the Precambrian-Cambrian boundary interval in China and Iran and their correlation. Geological Magazine, 127, 319-332.

Brasier, M. D., Cowie, J. Taylor, M., 1994. Decision on the Precambrian-Cambrian boundary stratotype. Episodes, 17, 3-8.

Brasier, M. D., McCarron, G., Tucker, R., Leather, J., Allen, P. Shields, G., 2000. New U-Pb zircon dates for the Neoproterozoic Ghubrah glaciation and for the top of the Huqf Supergroup, Oman. Geology, 28, 175-178.

Brasier, M., Antcliffe, J., 2004. PALEOBIOLOGY: Decoding the Ediacaran Enigma. Science, 305, 1115-1117.

Chen, D. F., Dong, W. Q., Zhu, B. Q., Chen, X. P., 2004. Pb–Pb ages of Neoproterozoic Doushantuo phosphorites in South China: constraints on early metazoan evolution and glaciation events.

Precambrian Research, 132, 123-132.

Chen, J. Y., Bottjer, D. J., Oliveri, P., Dornbos, S. Q., Gao, F., Ruffins, S., Chi, H., Li C. W., Davidson, E. H., 2004. Small bilaterian fossils from 40 to 55 million years before the Cambrian. Science, 305, 218-222.

Chen, P., 1984. Discovery of Lower Cambrian small shelly fossils from Jijiapo, Yichang West Hubei and its significance. Professional papers of Stratigraphy and Palaeontology, 13, 49-66.

Chen, P., 1987. The Sinian System. In: Wang, X. (Ed.), Stratigraphic excursion guidebook in the Yangtze Gorge Area. Yichang Institute of Geology and Mineral Resources, Chinese Academy of Geological Sciences. Geological Publishing House, Beijing, China, pp. 2-7.

Chen, Z. Q., Li, W. H., Guo, L., 2001. Granite of Proterozoic eon founded in Northeast Guangdong. Guangdong Geol., 16, 16-21 (in Chinese with English abstract).

Compston W, Zhang Z, Cooper J. A., Ma, G.G., Jenkins, R.J.F., 2008. Further SHRIMP geochronology on the early Cambrian of south China. American Journal of Science, 308, 399-420.

Condon, D., Zhu, M., Bowring, S., Wang, W., Yang, A., Jin, Y., 2005. U-Pb Ages from the Neoproterozoic Doushantuo Formation, China. Science, 308, 95-98.

Dempster, T. J., Rogers, G., Tanner, P.W.G., Bluck, B.J., Muir, R.J., Redwood, S.D., Ireland, T.R., Paterson, B.A., 2002. Timing of deposition, orogenesis and glaciation within the Dalradian rocks of Scotland: constraints from U-Pb zircon ages. Journal of the Geological Society, London, 159, 83-94.

Ding, L., Li, Y., Chen, H., 1992. Discovery of Micrhystridium regulare from Sinian–Cambrian boundary strata in Yichang, Hubei, and its stratigraphic significance. Acta Palaeontologica Sinica, 9, 303-309.

Ding, L., Li, Y., Hu, X., Xiao, Y., Su, C., Huang, J., 1996. Sinian Miaohe Biota of China. Geological Publishing House, Beijing.

Gao S., Yang, J., Zhou, L., Lj, M., Hu, Z. C., Guo, J. L., Yuan, H. L., Gong, H. J., Xiao, G. Q., Wei, J. Q., 2011. Age and growth of the Archean Kongling terrain, South China, with emphasis on 3.3 Ga granitoid gneisses. American Journal of Science, 311, 153-182.

Grotzinger, J. P., Bowring, S. A., Saylor, B. Z. Kaufman, A. J., 1995. Biostratigraphic and geochronologic constraints on early animal evolution. Science, 270, 598-604.

Halliday, A. N., Graham, C. M., Aftalion, M., Dymoke, P., 1989. The depositional age of the Dalradian Supergroup: U.Pb and Sm.Nd isotopic studies of the Tayvallich Volcanics, Scotland. Journal of the Geological Society, London, 146, 3-6.

Hirata, T. and Nesbitt, R. W., 1995. U-Pb isotope geochronology of zircons: evaluation of the laser probe inductively coupled plasma-mass spectrometry technique: Geochimica Cosmochimica Acta, 59, 2491-2500.

Hoffman, P. F. and Schlag, D. P., 2002. The snowball Earth hypothesis: testing the limits of global

change. Terra Nova, 14, 129-155.

Hsu, K.J., Oberhansli, H., Gao, J.Y., Shu, S., Haihong, C., Krahenbuhl, U., 1985. 'Strangelove ocean' before the Cambrian Explosion. Nature, 316, 809-811.

Iizuka, T. and Hirata, T., 2004. Simultaneous determinations of U-Pb age and REE abundances for zircons using ArF excimer laser ablation-ICPMS. Geochemical Journal, 38, 229-241.

Iizuka, T., Hirata, T., Komiya, T., Rino, S., Katayama, I., Motoki,A., Maruyama, S., 2005. U-Pb and Lu-Hf isotope systematics of zircons from the Mississippi River sand: Implications for reworking and growth of continental crust. Geology, 33, 485-488.

Iizuka, T., Horie, K., Komiya, T., Maruyama, S., Hirata, T., Hidaka, H., Windley, B.F., 2006. Occurrence of a 4.2 Gyr old zircon in the Acasta Gneiss Complex of northwestern Canada. Geology, 34, 245-248.

Iizuka, T., Komiya, T., Maruyama, S., 2007. 1 The Early Archean Acasta Gneiss Complex: geological, geochronological and isotopic studies and implications for early crustal evolution. Earth's oldest rocks, Elsevire, 15, 127-147.

Isachsen, C. E., Bowring, S. A., Landing, E., Samson, S. D., 1994. New constraint on the division of Cambrian time. Geology, 22, 496-498.

Ishikawa, T., Ueno, Y., Komiya, T., Sawaki, Y., Shu, D., Li, Y., Maruyama, S., Han, J., 2008. C-isotope chemostratigraphy of a PC/C boundary section, Three Gorge area, South China: Basal-Tommotian regression and Cambrian Explosion. Gondwana Research, 14, 193-208.

Ishikawa,T., Ueno, Y., Shu, D., Li, Y., Han, J., Guo, J., Yoshida, N., Komiya, T., 2013. Irreversible change of the oceanic carbon cycle in the earliest Cambrian: High-resolution organic and inorganic carbon chemostratigraphy in the Three Gorges area, South China. Precambrian Research, 225, 190-208.

Jiang, G.-Q., Kennedy, M. J., Christie-Blick, N., 2003. Stable isotopic evidence for methane seeps in Neoproterozoic. Nature, 426, 822-826.

Jiang, S. Y., Pi, D H.., Heubeck, C., Frimmel, H., Liu, Y. P, Deng, H. L., Ling, H. F., Yang, J. H.,2009. Early Cambrian ocean anoxia in South China. Nature, 459, E5-E6.

Jiao, W. F., Wu, Y. B., Yang, S. H., Peng, M., Wang, J., 2009. The oldest basement rock in the Yangtze Craton revealed by zircon U-Pb age and Hf isotope composition. Science in China Series D: Earth Sciences, 52, 1393-1399.

Khomentovsky, V. and Karlova, G., 1993. Biostratigraphy of the Vendian-Cambrian beds and the lower Cambrian boundary in Siberia. Geological Magazine 130, 29-45.

Kikumoto, K., Tahata, M., Nishizawa, M., Sawaki, Y., Maruyama, S., Shu, D., Han, J., Komiya, T., Takai, K., Ueno, Y., in this volume. Nitrogen isotope chemostratigraphy of the Ediacaran to Early Cambrian platform sequence in the Three Gorges, South China. Gondwana Research.

Kirschvink, J., 1992. Late Proterozoic low-latitude global glaciation: the snowball earth. In: The

Proterozoic Biosphere, 51-52. Cambridge University Press, Cambridge.

Knoll, A.H., Grotzinger, J.P., Kaufman, A.J. Kolosov, P., 1995. Integrated approaches to terminal Proterozoic stratigraphy: an example from the Olenek Uplift, northeastern Siberia. Precambrian Research, 73, 251-270.

Komiya, T., Suga, A., Han, J., Guo, J., Yamamoto, S., Hirata, T., Li, Y., 2008. Ca isotopic compositions of dolomite, phosphorite and the oldesr animal embryo fossils from the Neoproterozoic in Weng'an, South China. Gondwana Research, 14, 209-218.

Kouchinsky, A., Bengtson, S., Pavlov, V., Runnegar, B., Torssander, P., Young, E., Ziegler, K., 2007. Carbon isotope stratigraphy of the Precambrian–Cambrian Sukharikha River section, northwestern Siberian platform. Geological magazine, 144, 1-10

Landing, E., 1994. Precambrian-Cambrian boundary global stratotype ratified and a new perspective of Cambrian time. Geology, 22, 179-182.

Landing, E., Bowring, S., Davidek, K., Westrop, S., Geyer, G., and Heldmaier, W. 1998. Duration of the Early Cambrian: U–Pb ages of volcanic ashes from Avalon and Gondwana. Canadian Journal of Earth Science, 35, 329-338.

Li, X. H., Li, Z. X., Zhou, H., Liu, Y., Kinny, P. D., 2002. U–Pb zircon geochronology, geochemistry and Nd isotopic study of Neoproterozoic bimodal volcanic rocks in the Kangdian Rift of South China: implications for the initial rifting of Rodinia. Precambrian Research, 113, 135-154.

Li, X. H., Li, Z. X., Zhou, H. W., Liu, Y., Liang, X., Li, W., 2003a. SHRIMP U-Pb zircon age, geochemistry and Nd isotope of the Guandaoshan pluton in SW Sichuan: Petrogenesis and tectonic significance. Science in China Series D 46 (Suppl.), 73-83.

Li, X. H., Li, Z. X., Ge, W., Zhou, H., Li, W., Liu, Y., Wingate, M. T. D., 2003b. Neoproterozoic granitoids in South China: crustal melting above a mantle plume at ca. 825 Ma? Precambrian Research, 122, 45-83.

Li, X. H., Li, W. X., Li, Z. X., Liu, Y., 2008. 850-790 Ma bimodal volcanic and intrusive rocks in northern Zhejiang, South China: a major episode of continental rift magmatism during the breakup of Rodinia. Lithos, 102, 341-357.

Li, X. H., Li, W. X., Li, Z. X., Lo, C. H., Wang, J., Ye, M. F., Yang, Y. H., 2009. Amalgamation between the Yangtze and Cathaysia Blocks in South China: constraints from SHRIMP U-Pb zircon ages, geochemistry and Nd-Hf isotopes of the Shuangxiwu volcanic rocks. Precambrian Research, 174, 117-128.

Li, W. X., Li, X. H., 2003. Adakitic granites within the NE Jiangxi ophiolites, South China: geochemical and Nd isotopic evidence, Precambrian Research, 122, 29-44.

Li, W. X., Li, X. H., Li Z. X., 2010. Ca. 850 Ma bimodal volcanic rocks in Northeastern Jiangxi Province, South China: Initial extension during the breakup of Rodinia? American Journal of science, 310, 951-980.

Li, Z. X., 1998. Tectonic evolution of the major East Asian lithospheric blocks since mid-Proterozoic - a synthesis. In: Martin, F.J., Chung, S.-L., Lo, C.-H., Lee, T.-Y. ŽEds.., Mantle Dynamics and Plate Interactions in East Asia. AGU Geodynamics Series, vol. 27. Am. Geophys. Un., Washington, DC, 221-243.

Li, Z. X., Li, X. H., Zhou, H. W., Kinny, P. D., 2002. Grenvillian continental collision in south China: New SHRIMP U-Pb zircon results and implications for the configuration of Rodinia. Geology, 30, 163-166.

Li, Z. X., Wang, J., Li, X. H., Zhang, S., 2003a. From Sibao orogenesis to Nanhua rifting: Late Precambrian tectonic history of Eastern South China—an overview and field guide. IGCP 440 South China Field Symposium 9–18 October, 2003, China. Geological Publishing House, Beijing

Li, Z. X., Li, X. H., Kinny, P. D., Wang, J., Zhang, S., Zhou, H., 2003b. Geochronology of Neoproterozoic syn-rift magmatism in the Yangtze Craton, South China and correlations with other continents: evidence for a mantle superplume that broke up Rodinia. Precambrian Research, 122, 85-109.

Li, Z. X., Wartho, J. A., Occhipinti, S., Zhang, C. L., Li, X. H., Wang, J., Bao, C. M., 2007. Early history of the eastern Sibao Orogen (South China) during the assembly of Rodinia: new mica 40Ar/39Ar dating and SHRIMP U-Pb detrital zircon provenance constraints. Precambrian Research, 159, 79-94.

Ling,W.L., 1996. Isotopic geochronology and crustal growth of Proterozoic basement along the Norhtern margin of Yangtze Craton: I. Houhe Group and Xixiang Group. Earth Science —rJournal of China University of Geocscinences 21, 491–494.

Ling, W., Gao, S., Zhang, B., Li, H., Liu, Y., Cheng, J., 2003. Neoproterozoic tectonic evolution of the northwestern Yangtze craton, South China: implications for amalgamation and break-up of the Rodinia Supercontinent. Precambrian Research, 122, 111-140.

Liu, B. X., Liu, C. G., Qiu, Y. Q., 2001. The Pb-Pb isotopic ages and geological significance of gneissic granite in Hezi, Jiangxi. Volcano. Min. Res., 22, 264-268 (in Chinese with English abstract).

Liu, X. M., Gao, S., Diwu, C. R., Ling, W. L., 2008. Precambrian crustal growth of Yangtze Craton as revealed by detrital zircon studies. American Journal of Science, 308, 421-468.

Liu, P. J., Yin, C. Y., Gao, L. Z., Tang, F., Chen, S. M., 2009. New material of microfossils from the Ediacaran Doushantuo Formation in the Zhangcunping area, Yichang, Hubei Province and its zircon SHRIMP U-Pb age. Chinese Science Bulletin, 54, 1058-1064.

Ludwig, K. 1991. Isoplot-a plotting and regression program for radiogenic isotope data. Technical report, US Geological Survey.

Luo, H., Jiang, Z., Wu, X., Song, X., Ouyang, L., Xing, Y., Liu, G., Zhang, S., Tao, Y., 1984. Sinian-Cambrian boundary stratotype section at Meishucun, Jinning, Yunnan, China. People's publishing House, Yunnan, China, Kunming, 179 pp.

Maloof, A. C., Schrag, D. P., Crowley, J. L., Bowring, S. A., 2005. An expanded record of Early Cambrian carbon cycling from the Anti-Atlas Margin, Morocco. Canadian Journal of Earth Sciences, 42, 2195-2216.

Ma, G., Li, H., Zhang, Z., 1984. An investigation of the age limits of the Sinian System in South China. Bulletin of the Yichang Institute of Geology and Mineral Resources, 8, 1-29.

Ma, G., Zhang, Z., Li, H., Chen, P., Huang, Z., 1989. A geochronostratigraphical study of the Sinian System in Yangtze Platform. Bull. Yichang Inst. Geol. Miner. Res., 14, 83-124 (in Chinese with extended English abstract).

Maloof, A. C., Ramezani J., Bowring, S. A., Fike D. A., Porter S. M., Mazouad M., 2010. Constraints on early Cambrian carbon cycling from the duration of the Nemakit-Daldynian–Tommotian boundary δ13C shift, Morocco. Geology, 38, 623-626.

Melezhik, V. A., Gorokhov, L. M., Kuznetsov, A. B., Fallick, A. E., 2001. Chemostratigraphy of Neoproterozoic carbonates: implications for `blind dating'. Terra Nova, 13, 1-11

Narbonne, G.M., 2005. The Ediacara biota: Neoproterozoic origin of animals and their ecosystems. Annual Reviews in Earth Planetary Sciences, 33, 421-442.

Pei, X. Z., Li, Z. C., Ding, S. P., Li, R. B., Feng, J. Y., Sun, Y., Zhang, Y. F., Liu, Z. Q., 2009. Neoproterozoic Jiaoziding peraluminous granite in the northwestern margin of Yangtze Block: zircon SHRIMP U-Pb age and geochemistry and their tectonic significance. Earth Science Frontier, 16, 231-249.

Peng, S. C., Babcock, L. E., Geyer, G., Moczydlowska, M., 2006. Nomenclature of Cambrian epochs and series based on GSSPs-comments on an alternative proposal by Rowland and Hicks. Episodes, 29, 130-132.

Qian, Y., 1999. Taxonomy and Biostratigraphy of Small Shelly Fossils in China. Scientific Publishing House, Beijing.

Qiu. Y. M., Gao, S., McNaughton, N. J., Groves, D. I., Ling, W., 2000. First evidence of >3.2 Ga continental crust in the Yangtze craton of South China and its implications for Archean crustal evolution and Phanerozoic tectonics. Geology, 28, 11-14.

Ripperdan, R. L., 1994. Global variations in carbon isotope composition during the latest Neoproterozoic and earliest Cambrian. Annual Review in Earth Planetary Sciences, 22, 385-417.

Rino, S., Komiya, T., Windley, B.F., Katayama, I., Motoki, A., Hirata, T., 2004. Major episodic increases of continental crustal growth determined from zircon ages of river sands; implications for mantle overturns in the Early Precambrian. Physics of Earth and Planetary Interiors, 146, 369-394.

Rino, S., Kon, Y., Sato, W., Maruyama, S., Santosh, M., Zhao, D., 2008. The Grenvillian and Pan-African orogens: World's largest orogenies through geologic time, and their implications on the origin of superplume. Gondwana Research, 14, 51-72.

Roger, F., Calassou, S., 1997. U-Pb geochronology on zircon and isotopic geochemistry (Pb, Sr and Nd)

of the basement in the Songpan-Garze fold belt (China). C. R. Acad. Sci. Ser., 324, 819-826.

Rozanov, A. Y., Missarzhevsky, V. V., Volkova, N. A., Voronova, L. G., Krylov, I. N., Keller, B. M., Korolyuk, I. K., Lendzion, K., Michniak, R., Pychova, N. G., Sidorov, A. D., 1969. The Tommotian Stage and the Cambrian lower boundary problem. Trudy Geological Institute, 206, Nauka, Moskow, 1-380.

Sawaki, Y., Ohno, T., Fukushi, Y., Komiya, T., Ishikawa, T., Hirata, T.,Maruyama, S., 2008a. Sr isotope excursion across Precambrian–Cambrian boundary, in Three Gorge area, South China. Gondwana Research, 14, 134-147.

Sawaki Y, Nishizawa M, Suo T, Komiya, T., Hirata, T., Takahata, N., Sano, Y., Han, J., Kon, Y., Maruyama, S., 2008b. Internal structures and U-Pb ages of zircons from a tuff layer in the Meishucunian formation, Yunnan Province, South China. Gondwana Research, 14, 148-158.

Sawaki, Y., Ohno, T., Tahata, M., Komiya, T., Hirata, T., Maruyama, S., Windley, B. F., Han, J., Shu, D. and Li, Y., 2010. The Ediacaran radiogenic Sr isotope excursion in the Doushantuo Formation in the Three Gorges area, South China. Precambrian Research, 176, 46-64.

Sawaki, Y., Tahata, M., Ohno, T., Komiya, T., Hirata, T., Maruyama, S., Han, J., Shu, D., in this volume. The anomalous Ca cycle in the Ediacaran ocean: evidence from Ca isotopes preserved in carbonates in the Three Gorges area, South China. Gondwana Research.

Shimura, T., Kon, Y., Sawaki, Y., Hirata, T., Han, J., Shu, D., Komiya, T., in this volume. In-situ analyses of phosphorus contents of carbonate minerals: Reconstruction of phosphorus contents of seawater from the Ediacaran to early Cambrian. Gondwana Research.

Siegmud, H., 1997. The Ocruranus-Eohalobia group of small shelly fossils from the Lower Cambrian of Yunnan. Lethaia, 30, 285-291.

Sinclair, J. A., 2001. Petrology, geochemistry, and geochronology of the "Yanbian ophiolite suite", South China: implications for the western extension of the Sibao Orogen. Honours thesis, The University of Western Australia, Perth, 69 pp.

Steiner, M., Li, G., Qian, Y., Zhu, M. Erdtmann, B. D., 2007. Neoproterozoic to early Cambrian small shelly fossil assemblages and a revised biostratigraphic correlation of the Yangtze Platform (China). Palaeogeography Palaeoclimatology Palaeoecology, 254, 67-99.

Takahata, N., Tsutsumi, Y., Sano, Y., 2008. Ion microprobe U-Pb dating of zircon with a 15 micrometer spatial resolution using NanoSIMS. Gondwana Research, 14, 587-596.

Tahata, M., Ueno, Y., Ishikawa, T., Sawaki, Y., Murakami, Y., Han, J., Shu, D., Li, Y., Guo, J., Yoshida, N., Komiya, T., 2013. Carbon and oxygen isotope chemostratigraphies of the Yangtze platform, South China: Decoding temperature and environmental changes through the Ediacaran. Gondwana Research, 23, 333-353.

Wang, L. G., Qiu, Y.M., McNaughton, N. J., Groves, D. I., Luo, Z. K., Huang, J. Z., Miao, L. C., Liu, Y.K.., 1998. Constraints on crustal evolution and gold metallogeny in the Northwestern Jiaodong

Peninsula, China, from SHRIMP U-Pb zircon studies of granitoids. Ore Geology Reviews 13, 275-291.

Wang, L. J., Griffin, W. L., Yu, J. H., O'Reilly, S. Y., 2010. Precambrian crustal evolution of the Yangtze Block tracked by detrital zircons from Neoproterozoic sedimentary rocks. Precambrian Research, 177, 131-144.

Wang, L. J., Yu, J. H., Griffin, W. L., O'Reilly, S. Y., 2012. Early crustal evolution in the western Yangtze Block: evidence from U–Pb and Lu–Hf isotopes on detrital zircons from sedimentary rocks. Precambrian Research, 222-223, 368-385.

Wang, L. J., Griffin, W. L., Yu, J. H., O'Reilly, S. Y., 2013. U–Pb and Lu–Hf isotopes in detrital zircon from Neoproterozoic sedimentary rocks in the northern Yangtze Block: Implications for Precambrian crustal evolution. Gondwana Research, 23, 1261-1272.

Wang, X., Shi, X., Jiang, G., Zhang, W., 2012. New U–Pb age from the basal Niutitang Formation in South China: Implications for diachronous development and condensation of stratigraphic units across the Yangtze platform at the Ediacaran–Cambrian transition. Journal of Asian Earth Sciences, 48, 1-8.

Wang, X. F., Bernd, D. E., Chen, X. H., Mao, X. D., 1998. Integrated sequence-, bio- and chemostratigraphy of the terminal Proterozoic to Lowermost Cambrian "black rock series" from central South China. Episodes, 21, 178-189.

Wang, Y., Yin, G., Zheng, S., Zhu, S., Chen,Y., Luo, Q., Wamg, F., Qian, Y., 1984. The upper Precambrian and Sinian-Cambrian Boundary in Guizhou. Te people's Publishing House of Guizhou, Guiyang. 170 pp.

Wingate, M. T. D., Campbell, I. H., Compston, W., Gibson, G. M., 1998. Ion microprobe U-Pb ages for Neoproterozoic-basaltic magmatism in south-central Australia and implications for the breakup of Rodinia. Precambrian Research, 87, 135-159.

Wu, Y., Gao, S., Zhang, H., Zheng, J., Liu, X., Wang, H., Gong, H., Zhou, L., Yuan, H., 2012. Geochemistry and zircon U–Pb geochronology of Paleoproterozoic arc related granitoid in the Northwestern Yangtze Block and its geological implications. Precambrian Research 200–203, 26–37.

Xiao, S., Zhang, Y. Knoll, A. H., 1998. Three-dimensional preservation of algae and animal embryos in a Neoproterozoic phosphorite. Nature, 391, 553-558.

Xiao, S., Yuan, X. Knoll, A. H., 2000. Eumetazoan fossils in terminal Proterozoic phosphorites? PNAS, 97, 13684-13689.

Xu, B., Guo, L., Shi, Y., 1992. Proterozoic terranes and multiphase collision orogens in the Anhui-Zhejiang-Jiangxi areas. Geological Publishing House, Beijing, 112 pp. (in Chinese with English abstract).

Xu, L. G., Lehmann, B., Mao, J. W., Qu, W. J., Du, A. D., 2011. Re-Os age of polymetallic

Ni-Mo-PGE-Au mineralization in early Cambrian black shales of South China - a reassessment. Economic Geology, 106, 511-522.

Yin, C., Tang, F., Liu, Y., Gao, L., Liu, P., Xing, Y., Yang, Z., Wan, Y., Wang, Z., 2005. U-Pb zircon age from the base of the Ediacaran Doushantuo Formation in the Yangtze Gorges, South China: constraint on the age of Marinoan glaciation. Episodes, 28, 48-49.

Zhang, S., Jiang, G., Zhang, J., Song, B., Kennedy, M.J., Christie-Blick, N., 2005. U-Pb sensitive high-resolution ion microprobe ages from the Doushantuo Formation in South China: Constraints on late Neoproterozoic glaciations. Geology, 33, 473-476.

Zhang, X., Shu, D., Li, Y., Han, J., 2001. New sites of Chengjiang fossils: crucial windows on the Cambrian explosion. Journal of the Geological Society, London, 158, 211-218.

Zhang, Z., 1981. Precambrian microfossils from the Sinian of South China. Nature, 289, 792-793.

Zhang, S.-B., Zheng, Y.-F., Wu, Y.-B., Zhao, Z.-F., Gao, S., Wu, F.-Y., 2006a. Zircon U–Pb age and Hf isotope evidence for 3.8 Ga crustal remnant and episodic reworking of Archean crust in South China. Earth and Planetary Science Letters, 252, 56-71.

Zhang, S. B., Zheng, Y. F., Wu, Y. B., Zhao, Z. F., Gao, S., Wu, F. Y., 2006b. Zircon isotope evidence for ≥3.5 Ga continental crust in the Yangtze craton of China. Precambrian Research, 146, 16-34.

Zhang, S. B., Zheng, Y. F., 2013. Formation and evolution of Precambrian continental lithosphere in South China. Gondwana Research, 23, 121-1260.

Zhao, J. H., Zhou, M. F., 2007. Geochemistry of Neoproterozoic mafic intrusions in the Panzhihua district (Sichuan Province, SW China): implications for subduction-related metasomatism in the upper mantle. Precambrian Research, 152, 27-47.

Zhao, J. H., Zhou, M. F., 2009a. Secular evolution of the Neoproterozoic lithospheric mantle underneath the northern margin of the Yangtze Block, South China. Lithos, 107, 152-168.

Zhao, J. H., Zhou, M. F., 2009b. Melting of newly formed mafic crust for the formation of Neoproterozoic I-type granite in the Hannan region, South China. Journal of Geology, 117, 54-70.

Zhao, J. X., Malcolm, M. T., Korsch, R. J., 1994. Characterisation of a plume-related 800 Ma magmatic event and its implications for basin formation in central-southern Australia. Earth and Planetary Sciences, Letters, 121, 349-367.Zhao, X.-F., Zhou, M.-F., 2011. Fe–Cu deposits in the Kangdian region, SW China: a Proterozoic IOCG (iron-oxide–copper–gold)metallogenic province. Mineralium Deposita, 1–17.

Zhao, Z., Xing, Y., Ma, G., Chen, Y., 1985. Biostratigraphy of The Yangtze Gorge area, Sinian. Geological Publishing House, Beijing.

Zhao, Z., Xing, Y., Ding, Q., Liu, G., Zhao, Y., Zhang, S., Meng, X., Yin, C., Ning, B., Han, P., 1988. The Sinian System of Hubei. China University of Geosciences Press, Wuhan.

Zhou, J.C., Wang, X.L., Qiu, J.S., 2009. Geochronology of Neoproterozoic mafic rocks and sandstones from northeastern Guizhou, South China: coeval arc magmatism and sedimentation. Precambrian

Research, 170, 27–42.

Zhou, T., Xu, G., 1987. The Cambrian System. In:Wang, X. (Ed.), Stratigraphic Excursion Guidebook in the Yangtze Gorge Area. Yichang Institute of Geology and Mineral Resources, Chinese Academy of Geological Sciences. Geological Publishing House, Beijing, China, pp. 8-13.

Zhou, H. W., Li, X. H., Wang, H. R., Li, J., Li, H. M., 2002. U-Pb zircon geochronology of basic volcanic rocks within the Yingyangguan Group in Hezhou, Guangxi, and its tectonic implications. Geological Review 48 (suppl.), 22-25 (in Chinese with English abstract).

Zhou, M. F., Kennedy, A. K., Sun, M., Malpas, J., Lesher, C. M., 2002. Neoproterozoic arc-related mafic intrusions along the Northern Margin of South China: implications for the accretion of Rodinia. The Journal of Geology 110, 611-618.

Zhou, M., Luo, T., Li, Z., Zhao, H., Long, H., Yang, Y., 2008. SHRIMP U–Pb zircon age of tuff at the bottom of the Lower Cambrian Niutitang Formation, Zunyi, South China. Chinese Science Bulletin, 53, 576-583.

Zhu, M., Li, G., Zhang, J.M., Steiner, M., Yang, A.H., Li, G.X., Erdtmann, B.D., 2003. Sinian-Cambrian stratigraphic framework for shallow- to deep-water environments of the Yangtze Platform: an integrated approach. Progress in Natural Science, 13, 951-960.

Zhu, M.Y., Zhang, J.M., Steiner, M., 2003. Sinian–Cambrian stratigraphic framework for-shallow- to deep-water environments of the Yangtze Platform: an integrated approach. Proceedings of the National Academy and Sciences, 13, 951-960.

Zhu, M.Y., Babcock, L. E., Peng, S. C., 2006. Advances in Cambrian stratigraphy and paleontology: Integrating correlation techniques, paleobiology, taphonomy and paleoenvironmental reconstruction. Palaeoworld, 15, 217-222

Zhu, R. X., Li, X. H., Hou, X. G., Pan, Y. X., Wamg, F., Deng, C. L., He H. Y., 2009. SIMS U-Pb zircon age of a tuff layer in the Meishucun section, Yunnan, southwest China: Constraint on the age of the Precambrian-Cambrian boundary. Science in China Series D: Earth Sciences, 52, 1385-1392.

Acknowledgement

I would like to express my sincere gratitude to my supervisor Prof. Shigenori Maruyama (Tokyo Institute of Technology). He gave me the best advice, useful discussion and selfless supports throughout six years. I also thank him for giving me opportunities to join the geological survey in Scotland, Wales and South China during 2008-2013, and for teaching me many aspects of the Earth science.

I thank Dr. Shinji Yamamoto, Dr. Kazumasa Aoki (The University of Tokyo), Dr. Yusuke Sawaki, Dr. Tomohiko Sato, Takuya Saito, Kazue Suzuki, Wataru Fujisaki, Tatsuyuki Arai, Hisashi Asanuma and Hikaru Sawada for supporting field research. I also thank Prof. Brian F. Windley (The University of Leicester, UK) who organized the geological survey in Scotland and provided me the critical comments and improved my immature English expressions.

As to sample analyses, I wish to thank Dr. Yoshiaki Kon (LA-ICP-MS), Dr. Takaomi Yokoyama, Satoki Okabayashi (MC-ICP-MS), Prof. Yuji Sano, Prof. Naoto Takahata and Dr. Manabu Nishizawa (nano-SIMS) for assisting and discussing in the acquisition of analytical data. Almost all isotopic data in this work were analyzed by LA-ICP-MS regulated by Prof. Takafumi Hirata (Kyoto University).

I am grateful to a secretary of Maruyama laboratory, Ms. Shio Watanabe. She always helped my daily college life in various aspects. I also thank the secretaries of the Earth and Planetary Science for their kindness: Mrs. Kei Kudo, Mrs. Yuko Imamura, Mrs. Noriko Asakawa, Mrs. Momoko Takeyama, Mrs. Satsuki Sekiguchi.

I express my appreciation to Prof. Shigenori Maruyama, Prof. Hideo Tsunakawa, Prof. Yasuo Ogawa, Prof. Tetsuya Yokoyama and Prof. Yuichiro Ueno for acceptance to become reviewers of my thesis.

I also wish to thank other members of the Maruyama-Hirose-Ueno Laboratory: Prof. Kei Hirose, Dr. Tetsuya Komabayashi, Dr. Kenji Kawai, Dr. Shigehiko Tateno, Dr. Takahiro Aze, Dr. Kenji Ohta, Dr. Masafumi Saitoh, Dr. Haruka Ozawa, Dr. Emiko Sugimura, Dr. Kazumi Yoshiya, Ryuichi Nomura, Hitoshi Gomi, Fumihiro Matsuura, Kazue Suzuki, Saori Imada, Konomi Suda, Ryohei Suzuki, Kaoru Mishima, Shin-nosuke Aoyama, Yoshiaki Endo, Chie Kato, Fumiya Tomiyasu, Tetsuya Kawamura, Yuko Mori, Hidemasa Yoshida, Tsubasa Hirai and Yuki Murakami for discussion, assistance and encouragement.

Some studies in this thesis were performed using a research fellowship of the Japan Society for the Promotion of Science for Young Scientists.

Finally, I would like to thank my parents, Yoshifumi Okada and Makiko Okada for financial support and continuous encouragement.